UNIVERSITÀ DEGLI STUDI DI PARMA

FACOLTÀ DI SCIENZE MATEMATICHE FISICHE E NATURALI

DOTTORATO IN
SCIENZA E TECNOLOGIA DEI MATERIALI INNOVATIVI
XXII Ciclo

ORGANIC CHROMOPHORES FOR ADVANCED APPLICATIONS: MODELS AND SPECTROSCOPY

Tutors:
Prof. Anna Painelli
Prof. Francesca Terenziani

Coordinatore:
Prof. Anna Painelli

Candidato:
Dr. Cristina Sissa

Contents

List of Abbreviations

CT	charge transfer
D/A	electron donor/acceptor
NLO	nonlinear optics
PES	potential energy surface
EA	electroabsorption
OPA	one-photon absorption
TPA	two-photon absorption
TPEF	two-photon excited fluorescence
GM	Göppert-Mayer units (1GM=$10^{-50}\cdot$ cm $^{4}\cdot$ s $\cdot$ photon^{-1})
mf	mean field
SA	self assembled
$\mathcal{D}/\mathcal{A}$	energy donor/acceptor
ET	energy transfer
RET	resonance energy transfer

Introduction: materials and phenomena

The recent impressive developments in the fields of organic electronics and photonics has been driven by the synthesis of smart molecular materials. Smart molecular materials are in demand not only for the development of new electronic and photonic devices [1, 2, 3] but also for a wealth of other applications including, to cite a few, drug delivery [4], in vivo optical microscopy [5], microfabrication [6, 7, 8], photodynamic therapy [9, 10, 11]. From a different perspective, fundamental biological processes involve functional molecules, as nicely demonstrated by the light harvesting complexes exploited in the photosynthetic process [12, 13]. A thorough understanding of these processes will unveil some fundamental mechanism of life, offering at the same time important clues for the optimal engineering of molecular-based devices [14].

Functional materials respond in a qualitatively different way to different inputs: nonlinear responses to external stimuli (including light, electrical fields, chemical concentration, pressure, etc.) are an obvious prerequisite for smart behavior [3, 15, 16, 17, 18]. Delocalized electrons represent a powerful source of nonlinearity: materials based on π-conjugated molecules and polymers combine functional behavior with low cost, low weight and mechanical flexibility. Their properties can be fine-tuned by chemical synthesis, opening perspectives that are not possible in the more traditional field of silicon-based material. π-conjugated molecules and polymers then

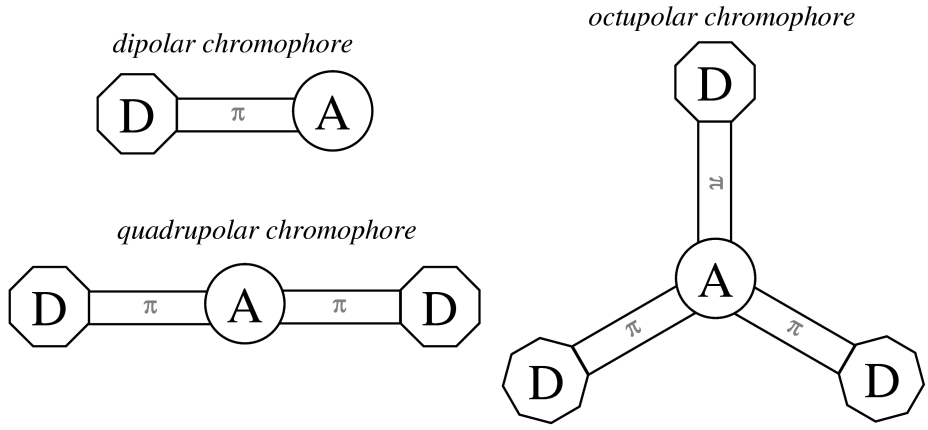

Figure 1: *Sketch of charge-transfer chromophores of different structure and dimensionality.*

represent one of the most promising families of molecular materials for advanced applications in photonics and electronics [15, 19, 20, 21].

In this thesis we focus attention on a family of conjugated molecules called charge-transfer (CT) chromophores. CT chromophores are constituted by electron-donor (D) and electron-acceptor (A) groups, linked by conjugated chains to form molecules of different symmetry and dimensionality, as exemplified in Figure 1. In the simplest structure, a D group is linked to an A group to give a linear dipolar DA chromophore. In so-called quadrupolar chromophores, instead, two D (or A) groups are linked to an A (or D) group to give linear structures [22]. In so-called octupolar chromophores a planar structure is formed linking three A (or D) groups to a central D (or A) group [23].

CT-chromophores find interesting applications in the fields of nonlinear optics [18, 24, 25, 26, 27, 28, 29], and molecular electronics [1, 30]. They also represent interesting model systems to investigate electron-transfer processes [31, 32, 33, 34, 35, 36] and show quite impressive solvatochromic properties [23, 37, 38, 39]. The low-energy physics of CT chromophores is governed

by charge-resonance between D and A groups and their optical spectra and properties are dominated by charge-transfer transitions. This makes CT chromophores particularly interesting from our perspective. In fact their behavior can be described in terms of comparatively simple models that just account for the few relevant degrees of freedom [23, 38, 39]. These essential-state models offer a general rationalization of optical spectra and properties of different families of CT dyes, leading to the definition of reliable structure-properties relationships as required to guide the chemical synthesis. Essential-state models are semiempirical, and model parameters have to be extracted from the analysis of selected spectroscopic data. But, once parameters for a specific chromophore are obtained, one gains access to a reliable and predictive description of its linear and nonlinear spectral properties, including non-trivial environmental effects.

In the first part (Sections 1.2 and 1.3) of this thesis we shortly introduce the two- and three-state models already developed in the host laboratory to describe dipolar and quadrupolar chromophores. In Section 1.4 we describe in detail the four-state model developed in this work for octupolar chromophores. The power of the essential-state approach is demonstrated by an extension of the two-state model to account for the enhancement of the two-photon intensity of a terpyridine-based DA chromophore upon complexation on a metallic center [40] (work in collaboration with the groups of Prof. D. Roberto, Milano, Italy, and Prof. C. Ferrante, Padova, Italy) as well as in a combined study of two related families of polar and octupolar chromophores, in collaboration with Prof. M. Blanchard-Desce (Rennes, France).

A thorough understanding of the intriguing physics of CT chromophores requires their full spectroscopic characterization. Essential-state models allow for the calculation of linear and nonlinear spectra of polar and multipolar chromophores accounting for molecular vibrations and for polar solvation, making possible a detailed analysis of the spectral position, intensity, and shape of the bands [23, 38, 39]. These non-trivial calculations were already

developed in the host laboratory for linear spectra [23, 38, 40, 39], for Raman [41] and two-photon absorption spectra [23, 39, 40]. In Chapter 2 we develop in detail the calculation of electroabsorption (EA) spectra. We demonstrate that the analysis of EA spectra can offer invaluable information on the location of dark states, not accessible in linear spectroscopy [42]. In the same Chapter, we describe two spectroscopic techniques that have become available thanks to the acquisition of a liquid-cell cryostat. In particular, we discuss fluorescence thermochromism and low-temperature fluorescence anisotropy measurements. The last technique turned out extremely informative for planar octupolar chromophores. The complex behavior of fluorescence anisotropy spectra can only be understood if the interaction of electrons with symmetry-lowering fluctuations of molecular vibrations and of polar solvation fields are carefully described.

The hyper-polarizable nature of CT-chromophores makes these systems extremely responsive to environmental perturbations. This is very well evident in polar solvation effects, that range from symmetry breaking in the excited states of multipolar chromophores, to subtle symmetry-lowering effects in fluorescence anisotropy spectra, and to unconventional broadening phenomena in Raman spectra. Even more dramatic effects are expected when different CT chromophores mutually interact via electrostatic forces. Collective and cooperative effects were predicted in clusters of polar or multipolar chromophores [43, 44] that result in large perturbation of linear and nonlinear spectral properties, cooperative amplification or suppression of nonlinear optical (NLO) responses [17, 45], and in bistability induced by electrostatic interactions in clusters of dipolar chromophores [43, 44, 46, 47].

In the developed approach, the molecular (hyper)polarizability is fully and self-consistently accounted for, so that the properties of interacting chromophores can be predicted starting from the knowledge of easily accessible properties of the isolated chromophore (for example in solution). Environment-independent parameters can be safely exported from the isolated chromophore to clusters or multichromophores, where the chromophor-

es interact via electrostatic forces. This bottom-up theoretical approach mimics the synthetic route from the molecular to the supramolecular level. In Chapter 3 this bottom-up modeling strategy is applied to two families of materials. In the first example we investigate the evolution of the spectral properties of a zwitterionic DA chromophore when going from the solvated chromophore to a solvated dimer and to a self-assembled film of (properly functionalized) chromophores on gold (in collaboration with Prof. A. Abbotto, Milano-Bicocca, Italy). The second example applies to a quadrupolar chromophore and to its dimers in solution (in collaboration with Prof. A. Abbotto, Milano-Bicocca, Italy, and Prof. C. Ferrante, Padova, Italy) [48]. In both cases the bottom up strategy works very well and allows to rationalize the effects of interchromophore interactions.

The same interchromophore electrostatic interactions affecting optical spectra of clusters of chromophores are responsible for energy transfer in heterochromophoric systems. Energy transfer is an extremely interesting process that lies at the hearth of light-harvesting in biological systems [12, 13] and whose careful exploitation can lead to important improvements in the hot fields of photovoltaics [14, 49] and organic-light emitting devices [50]. While the results presented here are somewhat preliminary, we are able to use the machinery developed so far to investigate energy transfer in heterochromophoric systems. In particular, we rationalize the energy-transfer phenomenon observed in a triad composed of a quadrupolar dye, acting as an energy-donor, and of two polar dyes, acting as energy-acceptors (in collaboration with Prof. M. Blanchard-Desce, Rennes, France). Moreover, in the standard treatments of energy transfer, interchromophore interactions are usually described in the point-dipole approximation. Within our approach we can relax this approximation without loss of generality and we obtain the exciting result that new channels to energy transfer, strictly forbidden in the point-dipole approximation, open up with similar (or even larger) efficiency as for allowed channels in the point-dipole approximation. Work is in progress to experimentally verify this important result, which has been con-

firmed by quantum chemical calculations performed in collaboration with the group of Prof. S. Pati, JNCASR Bangalore, India.

The work developed in this thesis represents an important step forward towards the understanding of charge- and energy-transfer phenomena. The theoretical work, combined with experimental investigation, allowed to obtain very interesting and promising results concerning the spectral properties of CT-chromophores. Moreover, the robustness of the modeling strategy is demonstrated by the rationalization of spectroscopic (linear and non-linear) phenomenology of several classes of isolated and interacting CT-chromophores.

Chapter 1

(Multi)polar chromophores in solution: essential-state models

1.1 Introduction

Essential-state models offer an efficient theoretical tools to investigate optical properties of π-conjugated molecules exhibiting charge-transfer (CT) transitions at low energy. These molecules are constituted by electron-donor (D) and electron-acceptor (A) groups, linked by conjugated π-bridges. The low-energy physics of these dyes is governed by the charge resonance between the D and A moieties. Chemists describe these molecules as resonating between different structures: we will define the basis states of our model as corresponding to these resonating forms.

In the 50's Mulliken proposed a two-state model to describe the optical spectra of charge-transfer complexes in solution [51]. The same model is at the heart of the Marcus-Hush [31, 34] theory of electron transfer. Ouder and Chemla in the 70's applied the same model to investigate nonlinear optical properties for π-conjugated D-A molecules [52]. Starting from these pioneering works, essential-state models have been extended to account for

electron-phonon coupling [53] and environment effects, such as polar solvation [54] and interchromophoric interactions [43, 44, 47, 48]. The efficiency of the technique is proved by the excellent agreement with the optical (linear and nonlinear) experimental properties [38, 41, 39, 23].

Essential-state models are semi-empirical approaches. They offer a simplified view of complex phenomena, trying to disentangle the relevant essential physics of the phenomena at hand. As typical of semiempirical approaches, the model parameters are extracted from experiments. The power of this approach lies in its simplicity and in the limited number of parameters. At the same time, it is able to reproduce the main optical characteristics of different kinds of CT dyes. Moreover, the parameters that describe a single molecule in solution can be transferred to clusters of molecules, as described in the last Chapter: this bottom-up approach offers a powerful strategy to model fairly complex systems.

In this Chapter the models for isolated (multi)polar chromophores in solution are presented. The first and the second sections of this Chapter are dedicated to an overview of the work about the two- and three-state model for dipolar and quadrupolar chromophores, respectively, already developed in the host laboratory. Both models are applied to experimental systems to investigate their linear and nonlinear optical spectra. The last section is devoted to the four-state model, that we developed to understand optical spectra of octupolar chromophores. All models are validated via an extensive comparison with experimental data.

1.2 Two-state model for dipolar chromophores

Push-pull chromophores are a class of asymmetric molecules constituted by an electron donor (D) and an electron acceptor group (A) connected by an unsaturated bridge. The intrinsic structure of push-pull dyes allows the displacement of electrons upon excitation from the D-moiety to the A-moiety (charge-transfer transition). The presence of a low-lying transition

makes these molecules highly polarizable, and hence interesting for nonlinear optical (NLO) applications.

A two-state description is well suited for push-pull chromophores. Following a model proposed by Mulliken in the 50's, the neutral and zwitterionic resonance structures, $DA \leftrightarrow D^+A^-$, are chosen as the two basis wavefunctions [51, 53, 54]. The energy gap between the two basis states is 2η (Figure 1.1), while the mixing element is $-\sqrt{2}t$. The following equations describe the electronic Hamiltonian and its two eigenstates:

$$\mathcal{H} = 2\eta\hat{\rho} - \sqrt{2}t\hat{\sigma} = \begin{pmatrix} 0 & -\sqrt{2}t \\ -\sqrt{2}t & 2\eta \end{pmatrix} \tag{1.1}$$

$$\begin{aligned} |g\rangle &= \sqrt{1-\rho}|DA\rangle + \sqrt{\rho}|D^+A^-\rangle \\ |c\rangle &= \sqrt{\rho}|DA\rangle - \sqrt{1-\rho}|D^+A^-\rangle \end{aligned} \tag{1.2}$$

The operator $\hat{\rho}$ is called ionicity and its expectation value in the ground state, ρ, measures the weight of the zwitterionic state in the ground state, and defines the ground state polarity. ρ is a function of the $\eta/\sqrt{2}t$ ratio:

$$\rho = \frac{1}{2}\left(1 - \frac{\eta}{\sqrt{\eta^2 + 2t^2}}\right) \tag{1.3}$$

Push-pull chromophores are classified as neutral when $\rho < 0.5$, zwitterionic when $\rho > 0.5$. The $\rho = 0.5$ case describes a system where the two basis states, DA and D^+A^-, have exactly the same energy (the so-called cyanine limit) [24].

To investigate spectral properties, it is necessary to define the dipole moment operator. The contribution to the dipole moment of the D^+A^- state is largely dominant with respect to all other terms, that, as originally suggested by Mulliken [51], can be neglected. The dipole moment operator therefore is:

$$\hat{\mu} = \mu_0\hat{\rho} \tag{1.4}$$

where μ_0 is the dipole moment of the D^+A^- state. The main spectroscopic quantities relevant to the CT transition can be expressed in terms of ρ:

$$\mu_{gc} = \mu_0\sqrt{\rho(1-\rho)} \tag{1.5}$$

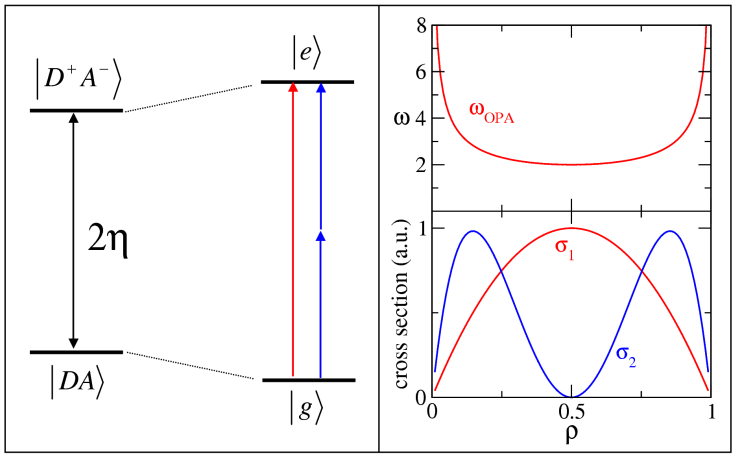

Figure 1.1: *Left panel: a sketch of the two-state model. Right panel: on the top the ρ dependence of the transition frequency is shown. Bottom panel shows the ρ dependence of the OPA (σ_1) and TPA (σ_2) intensities ($\sqrt{2}t = 1$)*

$$\hbar\omega_{gc} = \frac{\sqrt{2}t}{\sqrt{\rho(1-\rho)}} \tag{1.6}$$

$$\mu_g = \mu_0\rho \tag{1.7}$$

$$\mu_c = \mu_0(1-\rho) \tag{1.8}$$

where μ_{gc} is the transition dipole moment, $\hbar\omega_{gc}$ is the transition energy and μ_g and μ_c are the dipole moments of the ground and the excited state, respectively. From these equations it is evident that η (or ρ), $\sqrt{2}t$ and μ_0 can be extracted from experimental data. The right Panel of Figure 1.1 shows the ρ dependence of the transition frequency and the one-photon and two-photon absorption cross sections.

Molecular vibrations play an important role in the definition of linear and nonlinear spectral properties of CT chromophores, and the detailed analysis of the effects of electron-phonon coupling is a subject of research since many years [53, 55, 56, 57, 58, 59, 60]. The simplest way to approach the problem of molecular vibrations is to introduce a single effective vibrational coordinate

to account for the relaxation of the molecular following the charge transfer. In an adiabatic picture, the potential energy surface (PES) relative to the ground and the excited states have different minima (or in other words, the equilibrium geometry of the molecule changes from the ground to the excited state), and the displacement of the two PES is related to the electron-phonon coupling. The vibrational Hamiltonian can be expressed as follows (Holstein coupling):

$$\mathcal{H}_v = -\sqrt{2\omega_v} g \hat{q}\hat{\rho} + \frac{1}{2}(\omega_v^2 \hat{q}^2 + \hat{p}^2) \tag{1.9}$$

where $g = \sqrt{\omega_v \epsilon_v}$ is the electron-phonon coupling constant, ω_v is the frequency of the vibration, and ϵ_v is the vibrational relaxation energy, that corresponds to the small polaron binding energy of the Holstein model, as shown in Figure 1.2. $\hat{q}$ and $\hat{p}$ are the position and momentum operator of the harmonic oscillator ($\hbar = 1$):

$$\hat{q} = (a^+ + a)\sqrt{\frac{1}{2\omega_v}} \tag{1.10}$$

$$\hat{p} = (a^+ - a)\sqrt{\frac{2}{\omega_v}} \tag{1.11}$$

where a and a^+ are the phonon annihilation and creation operators, respectively.

The coupled electron-vibration problem can be solved in the adiabatic approximation [38]. Here however we describe an exact non-adiabatic diagonalization of the problem. The procedure is simple: we write the total Hamiltonian $\mathcal{H} = \mathcal{H}_{el} + \mathcal{H}_v$ on the basis obtained as the direct product of the two electronic states times the eigenstates of the harmonic oscillator described by the second term of the right-hand side of Equation 1.9. The infinite vibrational basis is truncated at the first M states, leading to a 2M×2M Hamiltonian matrix that can be diagonalized numerically. Of course large enough M are chosen so that the properties of interest are unaffected by a further increase of M. Typical results are shown for M=10. The parameters of the model, ω_v and ϵ_v, are extracted directly from the experiment: the

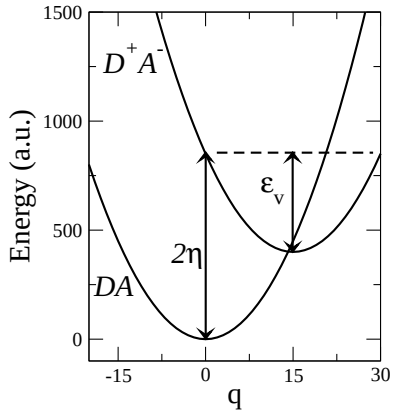

Figure 1.2: *The vibrational relaxation energy ϵ_v describes the energy gained by the system upon relaxation along the vibrational coordinate q*

frequency of the vibration is read from the spectra if vibronic transitions are resolved, while ϵ_v is chosen to best fit absorption and emission bands.

Absorption and fluorescence spectra of push-pull dipolar chromophores are solvatochromic: the position and the shape of the bands are strongly affected by the polarity of the medium [37]. The origin of this behavior is related to the ability of polar molecules to polarize the medium. To account for solvation effects, the reaction-field approach was followed [54, 61]. The electronic component of the reaction field, related to the deformation of the electronic charge distribution in the solvent molecules surrounding the polar solute, corresponds to a fast motion with respect to the relevant degrees of freedom of the solute. It therefore enters the model with a renormalization of the model parameters that, in the simplest approximation, acquire a dependence on the solvent refractive index [54, 62, 63]. The orientational component of the reaction field instead accounts for the reorientation of polar solvent molecules around the polar solute. This component of the reaction field then applies only to polar solvents and represents a slow motion. In the hypothesis that the solvent responds linearly to an applied electric field, the orientational reaction field is proportional to the dipole moment ($\langle\mu\rangle$)

of the solute molecule:

$$F_{or} = r_{or}\langle\mu\rangle \tag{1.12}$$

In principle r_{or} is related to the solute cavity, and to the refractive index and dielectric constant of the medium, but we extract it as a semiempirical parameter. Assuming that the solvent behaves as an elastic medium, the Hamiltonian relevant to polar solvation is:

$$\mathcal{H}_{or} = -F_{or}\hat{\mu} + \frac{F_{or}^2}{2r_{or}} \tag{1.13}$$

In this picture, polar solvation plays the same role as a vibrational coordinate that is treated adiabatically because its dynamic is very slow compared to the vibrational one (the kinetic energy is neglected). The solvation relaxation energy, $\epsilon_{or} = r_{or}\mu_0^2/2$, has the same meaning as ϵ_v for vibrations. ϵ_{or} is fixed to reproduce the solvatochromism: the only requirement is that it increases with solvent polarity. Polar solvation decreases the energy separation of the basis states in a neutral molecule ($\eta > 0$, $\rho < 0.5$), so that the molecule shows a positive solvatochromic behavior both in absorption and fluorescence. On the contrary, zwitterionic molecules show a negative solvatochromism (increasing the polarity of the solvent the bands in absorption and in fluorescence shift to the blue), because the energy gap between the states DA and D^+A^- increases with the solvent polarity (remember that in this case $\eta < 0$ and $\rho > 0.5$). Molecules having $\rho = 0.5$ are expected to be non-solvatochromic.

Polar solvation is also responsible for inhomogeneous broadening in optical spectra of DA chromophores [38, 41, 61]. From experimental data it is evident that in apolar solvents vibronic bands are often resolved, while in polar solvents, the vibronic structure is smeared out. The origin of this behavior is related to the presence of disorder in the system, caused by a thermal distribution of the orientational component of the reaction field around its equilibrium value. Inhomogeneous broadening strongly depends on temperature, as discussed in the next chapter.

Thermal fluctuations are included in our model imposing a Boltzmann

distribution of the reaction field [38, 61]: the total Hamiltonian ($\mathcal{H} = \mathcal{H}_{el} + \mathcal{H}_v + \mathcal{H}_{or}$) is diagonalized for fixed values of the reaction field, and each configuration is weighted for the Boltzmann probability. Of course the distribution is different for absorption and fluorescence: in the first case the solvent feels the field generated by the the ground state dipole and the distribution has to be calculated based on the ground-state energy; for fluorescence, the solvent relaxes after excitation, and the distribution has to be calculated based on the relaxed excited-state energy. For details about the calculation of spectra, see Appendix A.

The features described above are the main ingredients needed to model the spectral properties of push-pull chromophores. The strength of the two-state model stays in its simplicity, but this simple model, extended to account for molecular vibrations and solvation, captures the fundamental physics of the system, and reproduces the main spectral properties, as it has been demonstrated for many push-pull chromophores [38, 40, 41, 61]. Moreover, in contrast with other semi-empirical models, the number of parameters is limited: six solvent-independent parameters have to be fixed (η, $\sqrt{2}t$, μ_0, ϵ_v, ω_v and the intrinsic linewidth of the vibronic transition Γ) and only one parameter ϵ_{or} changes with the polarity of the solvent.

1.2.1 Comparison with experiment: the case study of a terpyridine-based ligand and the related Zn-complex

The two-state model was the starting point for the detailed study of a terpyridine-based ligand **T**, a push-pull chromophore where the terpyridine group acts as an electron-donor, while the amino group plays the role of an electron-acceptor, and the related complex **[ZnT]** (Figure 1.3). Both the molecule and the complex where synthesized by the group of Prof. D. Roberto of the University of Milano (Italy), while nonlinear characterization (two-photon absorption) was performed by the group of Prof. C. Ferrante of the University of Padova (Italy). [40]

Linear spectra were collected in our laboratory using a Lambda650 Perkin-

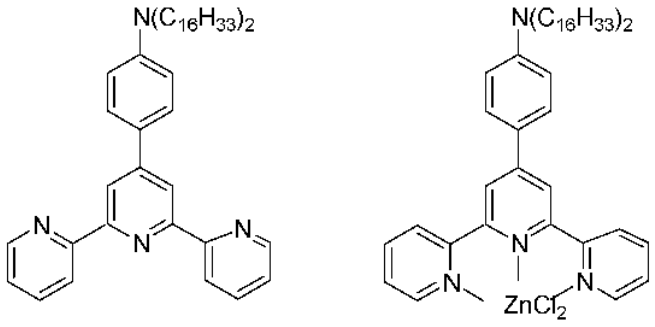

Figure 1.3: *Chemical structure of ligand* ***T*** *and of complex* ***[ZnT]****.*

Elmer instrument for absorption, and a Jobin-Yvon FluoroMax3 fluorometer for emission. For molar extinction coefficient measurements the Lambert-Beer law was verified. The experimental procedures adopted for quantum yield and TPA measurements are explained in detail in Appendices B and C, respectively. One-photon absorption (OPA) and fluorescence spectra were collected in cyclohexane (CH), toluene and dichloromethane.

Experimental spectra of the ligand **T** are shown in panels a (linear spectra) and b (TPA spectrum) of Figure 1.4 and summarized in Table 1.1. **T** hardly dissolves in CH, and in the resulting OPA spectrum a very weak band appears in the low-energy region that can be assigned to the complexation of **T** with traces of metallic ions in solution. To overcome this problem, the fluorescence excitation spectrum is shown in Figure 1.4. As expected for dipolar DA chromophores, **T** shows a very intense and weakly solvatochromic absorption band in the low-energy spectral region. Fluorescence spectra instead strongly shift towards the red when increasing the polarity of the solvent: this behavior is typical of largely neutral molecules. The TPA band exactly overlaps the linear absorption band, as expected for non-symmetric molecules. The two-state model presented in the previous section applies very well to the **T**-dye, as demonstrated by the calculated spectra shown in panels c and d of Figure 1.4, The spectra have been obtained with

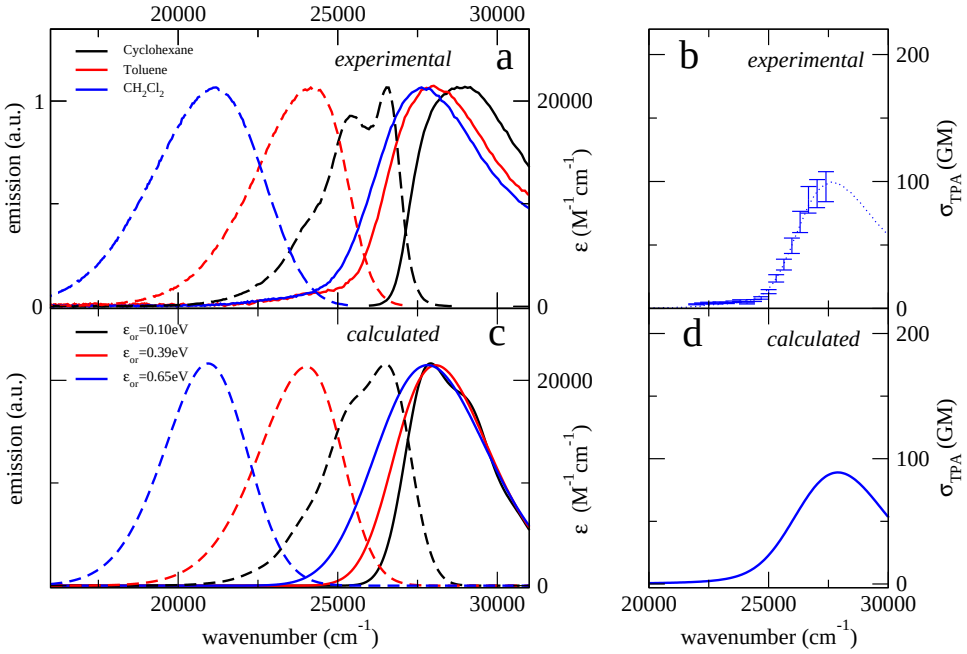

Figure 1.4: *Top panels: experimental spectra of* $\boldsymbol{T}$*. Panel a: continuous and dashed lines refer to absorption and fluorescence, respectively. The black continuous line actually shows the fluorescence excitation spectrum (in arbitrary units). The molar extinction coefficient was measured in* CH_2Cl_2 *and spectra collected in other solvents are normalized to this value. Panel c: TPA spectrum in Göppert-Mayer (symbols and errors bars) and OPA spectrum (arbitrary units, dotted line) collected in* CH_2Cl_2*. Bottom panels: Spectra calculated for* $\boldsymbol{T}$ *by the two-state model using the parameters reported in Table 1.2*

Table 1.1: *Experimental data for* $\boldsymbol{T}$ *in cyclohexane, toluene and dichloromethane.*

Solvents	λ_{abs}/nm^a (ϵ/M^{-1}cm^{-1})^a	λ_{fluo}/nm^a (Φ_{fluo})^b	λ_{TPA}/nm^a (σ_2/GM)^a
Cyclohexane	348	377	
Toluene	358	413	
Dichloromethane	362 (21300±500)	474 (0.27±0.03)	730 (96±12)

[a]All data refer to the band maxima.

[b]Fluorescence quantum yield, error ±10%

standard: Fluorescein in NaOH 0.1M, $\phi = 0.9$.

Table 1.2: *The two-state model parameters for* $\boldsymbol{T}$.

η/eV	$\sqrt{2}t$/eV	μ_0/D	ϵ_v/eV	ω_v/eV	Γ/eV	ϵ_{or}/eV
1.54	0.95	20.5	0.20	0.17	0.065	0.10 (cyclohexane)
						0.39 (toluene)
						0.62 (dichloromethane)

the model parameters listed in Table 1.2 (for details about the calculation of linear and two-photon spectra cf Appendix A). The results are excellent: not only transition energies, but also the evolution of the band shape with solvent polarity are well reproduced, both in absorption and emission. The TPA spectrum is also reproduced quantitatively with the same parameters: in particular we notice that both the molar extinction coefficient of OPA and the TPA cross section are in good agreement with the experimental data. We underline that six parameters of the model (η, $\sqrt{2}t$, μ_0, ϵ_v, ω_v and the intrinsic linewidth of the vibronic transition, Γ) are solvent-independent, while only one (ϵ_{or}) changes according to solvent polarity.

An extension of the two-state model to account for a virtual state

The complexation of **T** with the $ZnCl_2$ group has interesting consequences in optical spectra, as seen in Figure 1.5 (Table 1.3 summarizes experimental data). Absorption and fluorescence spectra are red-shifted with respect to the ligand, the molar extinction coefficient increases by a factor $\sim$1.2 while the cross section of two-photon absorption increases by a factor of $\sim$2 with respect to **T** [40]. Upon complexation with the Lewis acid $ZnCl_2$, the acceptor strength of the terpyridine group increases. As a consequence, in a two-state picture, the energy gap between the two states DA and D^+A^- decreases. The decrease of η can justify both the red-shift of the spectra, and the small increase of the molar extinction coefficient, but it cannot rationalize at the same time the sizable increase of the TPA response by a factor of 2. In a two-state model that properly reproduces the OPA intensity, the maximum increase of the TPA cross section is about 1.2. The reason of the failure of the two-state model for **[ZnT]** has to be ascribed to the presence of a higher-energy state, that contributes to the TPA response, while barely affecting the low-energy state involved in OPA.

In an essential-state picture, **[ZnT]** is modeled as DAA_v, where A_v is a virtual acceptor, that mimics the $ZnCl_2$ group. The three resonating structures $DAA_v \leftrightarrow D^+A^-A_v \leftrightarrow D^+AA_v^-$ define the basis states of a three-

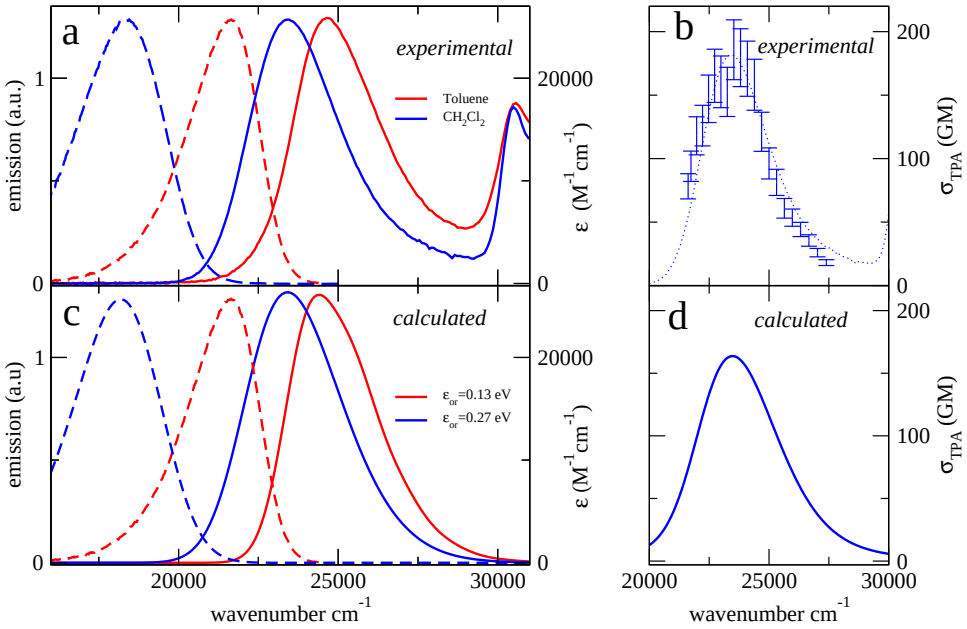

Figure 1.5: *Top panels: experimental spectra of* ***[ZnT]****. Panel a: continuous and dashed lines refer to absorption and fluorescence. The molar extinction coefficient was measured in* CH_2Cl_2 *and spectra collected in other solvents are normalized to this value. Panel c: TPA spectrum in GM (symbols and error bars) and OPA spectrum (arbitrary units, dotted line) collected in* CH_2Cl_2*. Bottom panels: Spectra calculated for* ***[ZnT]*** *by the three-state model using the parameters reported in Table 1.4*

Table 1.3: *Experimental data for **[ZnT]** toluene and dichloromethane.*

Solvent	λ_{abs}/nm^a (ϵ/M^{-1}cm^{-1})^a	λ_{fluo}/nm^a (Φ_{fluo})^b	λ_{TPA}/nm^a (σ_2/GM)^a
Toluene	405	463	
Dichloromethane	427 (25700±400)	549 (0.48±0.05)	847 (186±24)

[a]All data refer to the band maxima.

[b]Fluorescence quantum yield, error ±10%

standard: Fluorescein in NaOH 0.1M, $\phi = 0.9$.

state model. In agreement with the two-state model, the states DAA_v and $D^+A^-A_v$ are separated in energy by 2η and the mixing element is $-\sqrt{2}t$. The energy gap between $D^+A^-A_v$ and $D^+AA_v^-$ is $2(\chi - \eta)$, and they are mixed by $-\sqrt{2}t'$, as sketched in Figure 1.6. $D^+AA_v^-$ is a virtual high-energy state ($\chi \gg \eta$), that, being not directly coupled with the neutral state DAA_v, slightly affects the ground state. On the other hand, $D^+AA_v^-$ significantly contributes to the first excited state, leading to a sizeable increase of the dipole moment of the first excited state, and hence of $\Delta\mu = \mu_c - \mu_g$. As explained in detail in Appendix A, the OPA intensity is proportional to the squared transition dipole moment (μ_{gc}^2) between the ground state and the excited state, that is barely affected by the presence of the virtual state. On the other hand, the TPA cross section is proportional to $\Delta\mu^2\mu_{gc}^2$, so that a sizeable increase of the TPA response is expected as a result of complexation, as experimentally observed.

Before starting the detailed analysis of the **[ZnT]** complex, the role of the virtual state on the intensity of OPA and TPA is discussed more in detail. Color maps in Figure 1.7 show the OPA (top panel) and the TPA intensities (bottom panel) calculated as a function of η (half the energy gap between DAA_v and $D^+A^-A_v$) and of $\chi - \eta$ (half the energy gap between $D^+A^-A_v$ and $D^+AA_v^-$, Figure 1.6). Both the mixing elements are set to 1

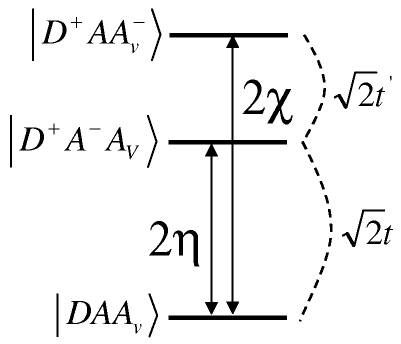

Figure 1.6: *The three basis states for **[ZnT]***

($\sqrt{2}t = \sqrt{2}t' = 1$) and the dipole moment of $D^+AA_v^-$ is set to $2\mu_0$, twice the dipole moment of $D^+A^-A_v$. For $\chi - \eta \gg \sqrt{2}t'$ the virtual state becomes irrelevant, and one regains the two-state model results. In particular for small values of η, $\rho \to 0.5$ and according to Equation 1.5 the transition dipole moment is very high, so that the OPA intensity is also high. Increasing η, the system becomes more neutral, ρ decreases, and OPA decreases as well. Anyway, the presence of the virtual excited state never affects the OPA intensity significantly. On the contrary, the TPA intensity strongly depends on the energy of the virtual state, and, as shown in the bottom panel of Figure 1.7, it increases when the virtual excited states approaches the first excited state. These predictions suggest that the three-state model can indeed explain the experimental observations.

For a more detailed modeling of the complex [**ZnT**], molecular vibrations and polar solvation are introduced, along the same lines as previously discussed for the two-state model. Only one effective molecular coordinate is coupled to the electronic transition, with frequency ω_v and relaxation energy ϵ_v. The reaction-field approach is followed to account for polar solvation.

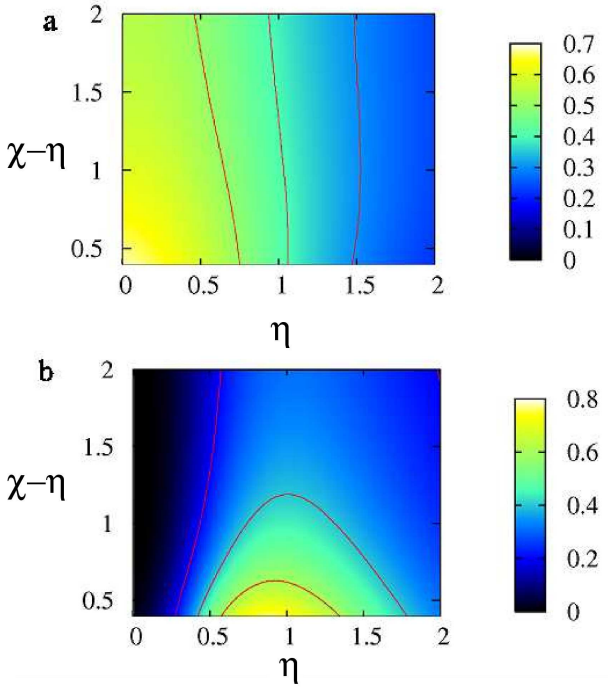

Figure 1.7: *The color maps (arbitrary units) show the maximum OPA (top panel) and TPA (bottom panel) intensities calculated as function of* η *and* $\chi - \eta$ *for the electronic three-state model with* $\sqrt{2}t = \sqrt{2}t' = 1$ *and setting the dipole moment of the third basis state* ($D^+AA_v^-$) *to* $2\mu_0$. *The red contour lines mark the equispaced levels, with increments 0.1 and 0.2 in the top and bottom panel, respectively.*

Table 1.4: *The three-state model parameters for **[ZnT]**: the molecular parameters relevant to the **T** ligand ($\sqrt{2}t$, η, μ_0, ω_v, ϵ_v and Γ) are rigidly transferred from the two-state model (Table1.2) and are not listed here.*

χ/eV	$\sqrt{2}t'$/eV	μ_0'/D	$\alpha\mu_0$/D	ϵ_{or}/eV
2.28	0.77	8.6	36.9	0.13 (toluene)
				0.27 (dichloromethane)

The three-state Hamiltonian is:

$$\mathcal{H} = \begin{pmatrix} -\mu' F_{or} & -\sqrt{2}t & 0 \\ -\sqrt{2}t & 2\eta - \tilde{q} - (\mu' + \mu_0)F_{or} & -\sqrt{2}t' \\ 0 & -\sqrt{2}t' & 2\chi - \tilde{q} - (\mu' + \alpha\mu_0)F_{or} \end{pmatrix} \quad (1.14)$$

where $\tilde{q} = \omega_v\sqrt{2\epsilon_v}q$. Again we treat F_{or} as a classical variable. For fixed F_{or} the $\mathcal{H}$ in Equation 1.14 defines a coupled electron-vibration problem that is numerically diagonalized on a non-adiabatic basis. The spectra are calculated as described in Appendix A, and results for different F_{or} are summed up weighted according to the relevant Boltzmann distribution. The parameters allowing to best reproduce experimental spectra are listed in Table 1.4: $\sqrt{2}t$, η, μ_0, ω_v, ϵ_v and Γ are kept fixed to the values relevant to the two-state model for **T**. μ' accounts for the permanent dipole of the group $ZnCl_2$: it does not affect OPA and TPA intensity, while it is responsible for a larger solvatochromism of the bands. The last parameter introduced is α, that defines the dipole moment $\alpha\mu_0$ of the $D^+AA_v^-$ state (for physical reasons $\alpha > 0$). Solvent relaxation energies are smaller than those reported for T, a fact that can be rationalized in terms of the smaller dimension of the solute cavity for **T** than for **[ZnT]**. Calculated spectra are reported in the bottom panels of Figure 1.5. The agreement with experimental data is very good: band shapes, transition energies and intensities (molar extinction coefficients and the TPA cross section) are well reproduced.

The proposed analysis follows a step-by-step approach, similar to the

bottom-up approach recently proposed for clusters of molecules [43, 47]. The ligand **T** is a push-pull chromophore, and its spectral behavior is well rationalized in terms of a two-state model, that allows to fix solvent-independent molecular parameters. The red-shift of absorption and fluorescence bands observed upon complexation can be understood in terms of an increase of the acceptor strength, according to the so-called inductive effect. But the increase of the acceptor strength alone cannot rationalize at the same time the observed small increase of the molar extinction coefficient, and the sizeable increase of the TPA cross section. To understand the observed enhancement of TPA intensity a more refined analysis of excited states proves necessary. The $ZnCl_2$ group behaves as a virtual acceptor A_v. Therefore a third virtual state must be included in the model, corresponding to the $D^+AA_v^-$ basis state. This state is a virtual state in the sense that it marginally affects the ground state and the linear spectral properties. The virtual state enters with sizeable weight in the first excited state, leading to an increase of the dipole moment of the first excited state, and hence to an amplification of the TPA response. The mechanism is general, and can be extended to different systems: attaching a virtual acceptor to a push-pull chromophore is expected to sizeably increase the TPA response.

1.3 The three-state model for quadrupolar chromophores

One of the most effective strategies to improve the TPA response is to increase the complexity of the molecular structure, moving from dipolar DA structures to branched systems, such as quadrupolar $D-\pi-A-\pi-D$ (or equivalently $A-\pi-D-\pi-A$) and octupolar chromophores (cf Section 1.4) [64, 65, 66, 67]. The increasing interest for more complex systems, and at the same time the interesting phenomena related to symmetry breaking, encouraged the development of appropriate essential-state models for branched systems. [39, 68]

The three-state model for quadrupolar dyes is a natural extension of the two-state model for dipolar dyes presented in the previous section. The three resonating structures, DAD, D^+A^-D and DA^-D^+ are taken as the basis states. The two charge-separated states D^+A^-D and DA^-D^+ are degenerate, and 2η is the energy gap between them and the neutral state DAD, while $-\sqrt{2}t$ represents the mixing with DAD. Exploiting symmetry, D^+A^-D and DA^-D^+ can be combined in a symmetric (*gerade*) and an antisymmetric (*ungerade*) state (left panel of Figure 1.8). The symmetrized basis wavefunctions are:

$$|N\rangle = |DAD\rangle \tag{1.15}$$

$$|Z_+\rangle = \frac{1}{\sqrt{2}}(|D^+A^-D\rangle + |DA^-D^+\rangle) \tag{1.16}$$

$$|Z_-\rangle = \frac{1}{\sqrt{2}}(|D^+A^-D\rangle - |DA^-D^+\rangle) \tag{1.17}$$

On the symmetrized basis, the following operators are conveniently defined:

$$\hat{\rho} = \begin{pmatrix} 0 & 0 & 0 \\ 0 & 1 & 0 \\ 0 & 0 & 1 \end{pmatrix} \tag{1.18}$$

$$\hat{\delta} = \begin{pmatrix} 0 & 0 & 0 \\ 0 & 0 & 1 \\ 0 & 1 & 0 \end{pmatrix} \tag{1.19}$$

$$\hat{\sigma} = \begin{pmatrix} 0 & 1 & 0 \\ 1 & 0 & 0 \\ 0 & 0 & 0 \end{pmatrix} \tag{1.20}$$

$\hat{\rho}$ and $\hat{\delta}$ define the charge distribution of the molecule: $\hat{\rho}$ measures the average charge on the central site A (equal to the sum of the two external charges), while $\hat{\delta}$ represents the unbalanced charge on the two external sites. $\hat{\sigma}$ is the mixing operator (only the two *gerade* states are mixed). The elec-

tronic Hamiltonian, written on the symmetrized basis, is:

$$\mathcal{H} = 2\eta\hat{\rho} - \sqrt{2}t\hat{\sigma} = \begin{pmatrix} 0 & -\sqrt{2}t & 0 \\ -\sqrt{2}t & 2\eta & 0 \\ 0 & 0 & 2\eta \end{pmatrix} \tag{1.21}$$

The diagonalization of the Hamiltonian leads to the ground state $|g\rangle$ and two excited states $|c\rangle$ and $|e\rangle$:

$$\begin{aligned} |g\rangle &= \sqrt{1-\rho}|N\rangle + \sqrt{\rho}|Z_+\rangle \\ |c\rangle &= |Z_-\rangle \\ |e\rangle &= \sqrt{\rho}|N\rangle - \sqrt{1-\rho}|Z_+\rangle \end{aligned} \tag{1.22}$$

where $|Z_-\rangle$ does not mix with the other basis states because of its different parity.

Following the same approximation adopted for dipolar dyes, we assume that the only non-negligible contributions to the dipole moment come from the D^+A^-D and DA^-D^+ states, that have the same dipole moment μ_0 aligned along the axis of the molecule, with opposite direction. The dipole moment operator on the symmetrized basis is:

$$\hat{\mu} = \mu_0\hat{\delta} \tag{1.23}$$

The expectation value of $\hat{\rho}$ in the ground state, ρ, measures the weight of the zwitterionic state $|Z_+\rangle$, or equivalently it defines the amount of charge separation in the ground state, and therefore the quadrupolar moment of the molecule. ρ is a function of the η/t ratio:

$$\rho = \frac{1}{2}\left(1 - \frac{\eta}{\sqrt{\eta^2 + 4t^2}}\right) \tag{1.24}$$

Transition dipole moments and transition frequencies, i.e. the relevant quantities for spectroscopy, can be expressed in terms of ρ:

$$\hbar\omega_{gc} = 2t\sqrt{\frac{1-\rho}{\rho}}, \quad \mu_{gc} = \mu_0\sqrt{\rho} \tag{1.25}$$

$$\hbar\omega_{ge} = 2t\sqrt{\frac{1}{\rho(1-\rho)}}, \quad \mu_{ge} = 0 \tag{1.26}$$

$$\hbar\omega_{ce} = 2t\sqrt{\frac{\rho}{(1-\rho)}}, \quad \mu_{ce} = -\mu_0\sqrt{1-\rho} \tag{1.27}$$

Figure 1.8 summarizes the electronic three-state model for quadrupolar chromophores. The transition towards the $|c\rangle$ state is OPA allowed, while the even $|e\rangle$ state is a dark state ($\mu_{ge} = 0$), but TPA allowed. For large values of η, the ground state is largely neutral ($\rho \to 0$), and the OPA and TPA transitions become degenerate. When $\eta = 0$, ρ is 0.5, and the $|g\rangle \to |e\rangle$ transition, TPA allowed, is located exactly at twice the energy of the $|g\rangle \to |c\rangle$ transition. The last notable case is when $\rho \to 1$: the energy of the OPA transition vanishes and the $|g\rangle$ and $|c\rangle$ states become degenerate. The intensity of the OPA transition increases linearly with ρ. The TPA intensity increases when ρ approaches 0.5 due to pre-resonance with the OPA state.

The coupling between electronic and vibrational degrees of freedom is related to the different geometry of the neutral and zwitterionic states, as for dipolar chromophores. In quadrupolar molecules at least two equivalent molecular vibrations must be introduced, one for each branch of the molecule. The two coordinates have the same vibrational frequency ω_v and the same relaxation energy ϵ_v measuring the gain of energy when the molecule is allowed to relax upon excitation along each molecular arm. The vibrational Hamiltonian reads:

$$\mathcal{H}_v = -\sqrt{2\epsilon_v}\omega_v\hat{q}_1\hat{\rho}_1 - \sqrt{2\epsilon_v}\omega_v\hat{q}_2\hat{\rho}_2 + \frac{1}{2}(\omega_v^2\hat{q}_1^2 + \hat{p}_1^2) + \frac{1}{2}(\omega_v^2\hat{q}_2^2 + \hat{p}_2^2) \tag{1.28}$$

The operators $\hat{q}_i$ and $\hat{p}_i$ represents the coordinate and the momentum of the two vibrations, while $\hat{\rho}_i$ is the ionicity relative to each branch.

Exploiting symmetry, the two molecular coordinates can be combined to get a symmetric ($q_+ = (q_1 + q_2)/\sqrt{2}$) and an antisymmetric ($q_- = (q_1 -$

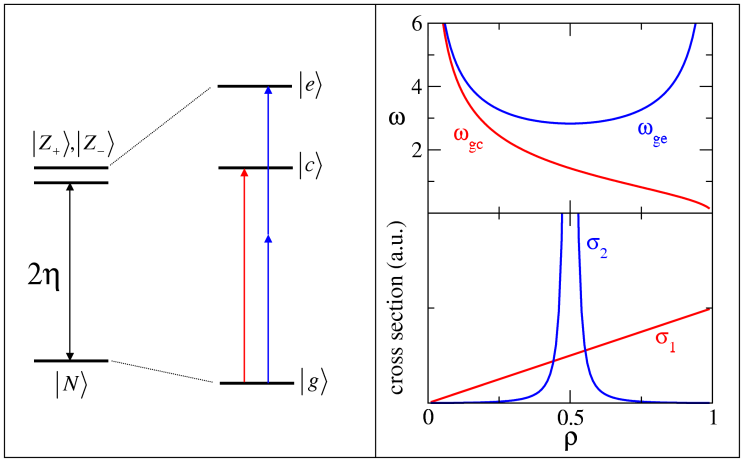

Figure 1.8: *Left Panel: sketch of the three state model for quadrupolar dyes. Right Panel: at the top the ρ dependence of transition frequencies relevant to the $|g\rangle \rightarrow |c\rangle$ transition (OPA allowed) and the $|g\rangle \rightarrow |e\rangle$ transition (TPA allowed). At the bottom the ρ dependence of OPA (σ_1) and TPA (σ_2) intensities.*

$q_2)/\sqrt{2}$) coordinate, and the relevant Hamiltonian reads:

$$\mathcal{H}_v = -\sqrt{\epsilon_v}\omega_v \hat{q}_+ \hat{\rho} - \sqrt{\epsilon_v}\omega_v \hat{q}_- \hat{\delta} + \frac{1}{2}(\omega^2 \hat{q}_+^2 + \hat{p}_+^2) + \frac{1}{2}(\omega^2 \hat{q}_-^2 + \hat{p}_-^2) \quad (1.29)$$

The symmetric coordinate $\hat{q}_+$ is coupled to the ionicity operator $\hat{\rho}$, and thus mixes the two symmetric states $|N\rangle$ and $|Z_+\rangle$: the q_+ mode drives a symmetric displacement of the charge. On the contrary, $\hat{q}_-$ is coupled to the antisymmetric operator $\hat{\delta}$, which mixes $|Z_-\rangle$ with $|Z_+\rangle$: this vibrational mode drives an unbalance of the charge distribution in the molecule, and is responsible for interesting symmetry breaking phenomena, with important consequences on the spectral behavior of molecules. [39]

The investigation of symmetry breaking starts from the analysis of the potential energy surfaces (PES) of the system. The PES are defined in the adiabatic approximation as the (q_-, q_+)-dependent energies of the electronic eigenstates. Examples of the calculated PES are shown as inset in Figure 1.9. Stable states with respect to symmetry breaking are characterized by a single minimum located at $q_- = 0$ and $q_+ = \sqrt{\epsilon_v}\langle\hat{\rho}\rangle/\omega$ (where $\langle\hat{\rho}\rangle$ indicates the expectation value of $\hat{\rho}$ in the relevant state). Unstable states show a double minimum at $q_- = \pm\sqrt{\epsilon_v}\rho/\omega$ (the position $q_- = 0$ corresponds to a saddle point of the PES), that define two equivalent equilibrium positions. When the system localizes in one of the two minima, the symmetry of the charge distribution breaks down, and the state becomes polar, because of the unbalanced distribution of charge.

Figure 1.9 shows the phase diagram proposed for quadrupolar chromophores. The lines in the diagram mark the values of ρ and ϵ_v for which the PES of the ground state (rightmost line) or the PES of the first excited state (leftmost line) have zero curvature along the q_- coordinate, while the q_+ coordinate is fixed at its equilibrium value for the ground state. Three different regions in the phase diagram can be recognized. Class I describes dyes with small ρ and high enough ϵ_v as to break the symmetry of the first excited state, which presents two equivalent minima. The ground state and the second excited state of molecules belonging to class I are non-polar, while the broken-symmetry OPA excited state is dipolar. In chromophores

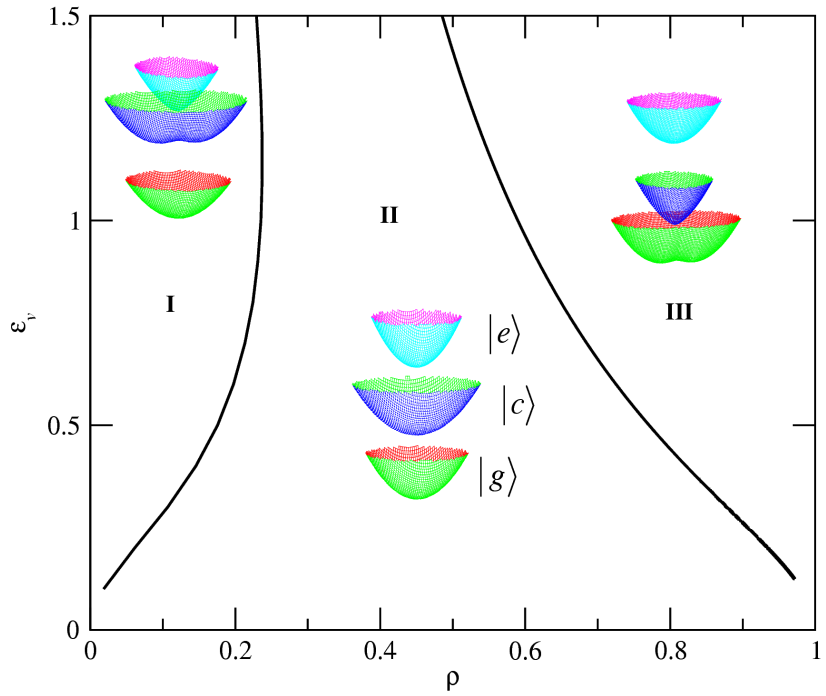

Figure 1.9: *Phase diagram for quadrupolar chromophores, describing the stability of different states (according to the PES sketched in each region) as a function of* ρ *and* ϵ_v*, in units of* $\sqrt{2}t$*. Region I: stable ground state and bistable first excited state; Region II: all PES have a single minimum; Region III: bistable ground state.*

of class II, symmetry is preserved for all the three eigenstates. The last class (III) of chromophores is characterized by a symmetry breaking of the ground state: in this case the ground state is dipolar, while both the excited states are non-polar.

One of the major problems related to symmetry breaking is to distinguish between true symmetry breaking, characterized by a localization of the excitation in one of the two equivalent minima, and false symmetry breaking, where the system switches very fast (tunnels) between the two minima. This problem is naturally overcome by relaxing the adiabatic approximation: we diagonalize the coupled electronic-vibrational problem on the non-adiabatic basis. The dimension of the Hamiltonian matrix is now $3M^2$, where M is the dimension of the truncated phonon basis.

Symmetry breaking gives rise to important consequences in the spectral properties of quadrupolar molecules. The presence of polar states, originated by symmetry breaking in the first excited state or in the ground state, leads to solvatochromic behavior: fluorescence solvatochromism is expected for molecules with a dipolar relaxed excited state (class I), while absorption solvatochromism is predicted when symmetry breaking occurs in the ground state (class III)

Polar solvation is included in the model in the reaction-field approach, along the same lines discussed in the previous section for dipolar chromophores (Equations 1.13, 1.23). As before, ϵ_{or} is an empirical parameter that describes the solvation relaxation energy, and increases with solvent polarity. Solvation becomes relevant when one of the states of the system is polar, and stabilizes one of the two equivalent minima of the broken-symmetry state. Since F_{or} is coupled to the same dipolar operator $\hat{\delta}$ as q_- (the driving force of symmetry breaking), polar solvation not only cooperates to break the symmetry of the molecule, but can induce symmetry breaking also in chromophores of class II. In other words, the total relaxation energy $\epsilon_v + \epsilon_{or}$ is the key quantity to guide the symmetry breaking process, and as a consequence systems with low ϵ_v that do not undergo symmetry breaking

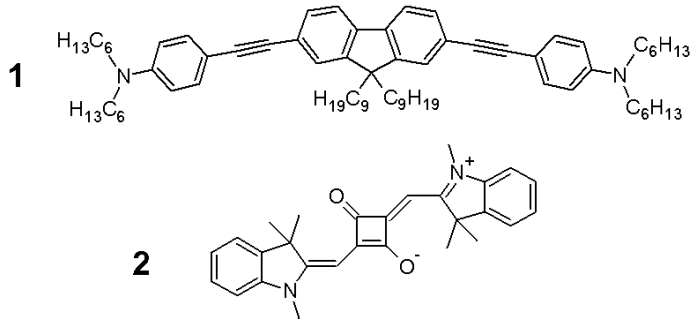

Figure 1.10: *Molecular structures of compounds **1** and **2**.*

in non-polar solvents, can break the symmetry for high values of ϵ_{or}, i.e. in polar solvents.

Keeping in mind that absorption is a vertical process that preserves the symmetry of the ground state, we do not expect absorption solvatochromism in dyes of either class I or class II. On the contrary, shifts induced by the polarity of the solvent are expected in fluorescence spectra of class I dyes. Fluorescence in fact comes from a relaxed state, where the excitation is localized on one of the two molecular arms. The localization makes the state polar, and therefore sensitive to solvent polarity.

Inhomogeneous broadening is also included in the model: all calculated spectra are averaged over the solvation coordinate weighted for the Boltzmann distribution in the relevant state. Appendix A describes relevant computational details.

1.3.1 Comparison with experiment: symmetry-breaking and symmetry-preserving systems

As typical examples of quadrupolar chromophores, we now discuss the two dyes in Figure 1.10. Compound **1** is constituted by a weak electron-acceptor group, fluorene, linked through a π-bridge to the two amino groups that act

as electron donors, while compound **2** is a squaraine-based chromophore. This work was developed in the host laboratory some years ago (cf Ref. [39]). Here we briefly summarize the main results, that will be the basis of the discussion in Chapter 2 about low-temperature spectra of compound compound **1** and a squaraine-based chromophore similar to compound **2**.

Absorption and fluorescence spectra of compound **1** in different solvents and the TPA spectrum in toluene are shown in the top panels of Figure 1.11. Absorption spectra are only marginally affected by solvent polarity: only some broadening of the bands is observed upon increasing the solvent polarity. On the contrary, fluorescence is strongly solvatochromic: increasing the solvent polarity from toluene to acetonitrile, the emission band moves to the red by ~ 3700 cm^{-1}. Experimental results suggest the presence of symmetry breaking in the OPA state. Indeed the observed solvatochromism of the fluorescence emission can be rationalized only in terms of a polar excited state, whose energy is stabilized by increasing the solvent polarity. On the contrary, absorption is non-solvatochromic because of the nonpolar character of the ground state.

Calculated spectra are presented in the bottom panels of Figure 1.11 (model parameters can be found in Ref. [39]). The model is able to reproduce the main features of the spectra. In low-polarity solvents, the vibronic structure is resolved, and the progressive broadening observed increasing the polarity. The agreement between experimental and calculated fluorescence spectra is remarkable: not only the position of the bands is well reproduced, but also the evolution of bandshapes (in particular the evolution of Franck-Condon progression) are well reproduced. The calculated lack of mirror-image symmetry between absorption and fluorescence spectra is in agreement with experimental data and is related to the fact that for a transition between single- and double-minimum states the Franck-Condon factor can be very different in absorption and fluorescence. All these results come naturally from the model. However the model does not reproduce the small Stokes shift observed in apolar solvents. This discrepancy could be

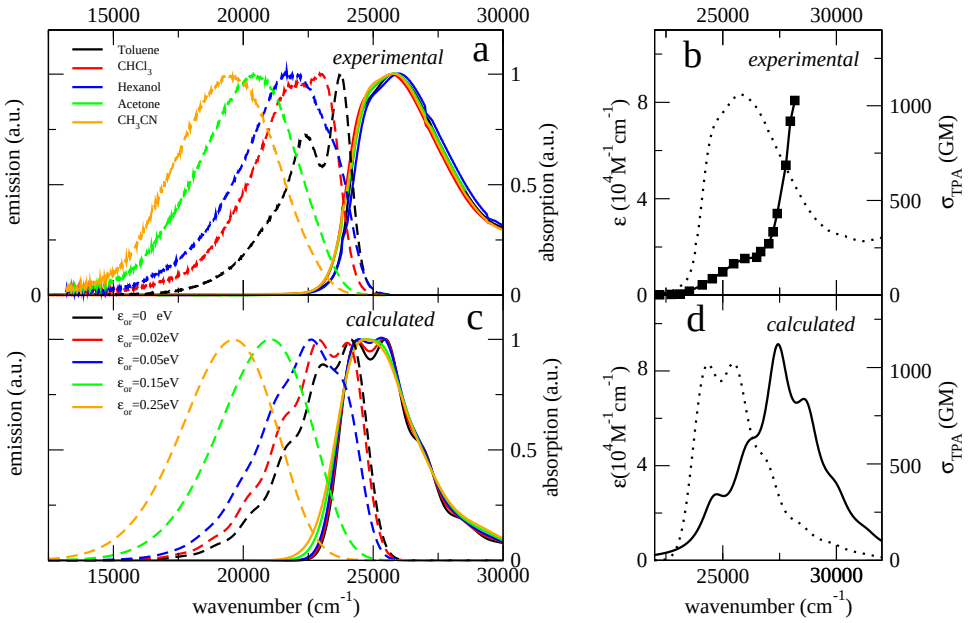

Figure 1.11: *Top panels: experimental spectra of compound* ***1****. Panel a: continuous and dashed lines refer to absorption and fluorescence spectra in different solvents (see legend). Panel b: TPA spectrum (symbols in Göppert-Mayer units) and OPA spectrum (dotted line) collected in toluene. Bottom panels: spectra calculated spectra by the three-state model using the parameters reported in Ref. [39].*

cured introducing some conformational or torsional degrees of freedom, but such a fine modeling is now beyond our aim. The TPA spectrum, in the experimentally accessible region, is quantitatively reproduced. The transition towards the odd c-state is forbidden by symmetry. However, the coupling between the electronic degrees of freedom and the vibrational antisymmetric coordinate q_-, makes the transition weakly allowed. This vibronic mechanism explains the shoulder observed in the TPA spectrum in the region of the OPA transition frequency.

Figure 1.12 shows linear and TPA spectra of compound **2**. Squaraine-based dyes are widely studied in the literature for their high two-photon response, due to pre-resonance effects with the OPA transition (cf Figure 1.8) [69, 70, 71]. Spectral properties are qualitatively different with respect to compound **1**. Neither absorption nor fluorescence spectra are significantly affected by solvent polarity, neither in terms of the position of the bands, nor in terms of inhomogeneous broadening. The small solvatochromic shifts observed in linear spectra can be ascribed to the different refractive index of the solvents. Limitations in the experimental setup (cf Appendix C) do not allow to access the TPA maximum, which was fixed between 700 and 800 nm according to literature data available for similar compounds [72, 73].

From the OPA and TPA frequencies, chromophore **2** turns out as a highly quadrupolar one, with $\rho \sim 0.4$. The weak vibronic structure of linear spectra reflects a low vibrational relaxation energy: ϵ_v is estimated around 0.16 eV. The ρ and ϵ_v values locate compound **2** into class II of the phase diagram of quadrupolar chromophores (Figure 1.9), so that in this system symmetry is preserved in the ground state and in the excited states. All states stay nonpolar irrespective of the solvent polarity. Further parameters of the model are listed Ref. [39]. Panels c and d in Figure 1.12 show the calculated spectra. We underline that, in spite of their qualitatively different spectroscopic behavior, the three state model satisfactorily reproduces the linear and nonlinear optical spectra of both class I and class II molecules.

In conclusion, in this section we have described the three-state model for

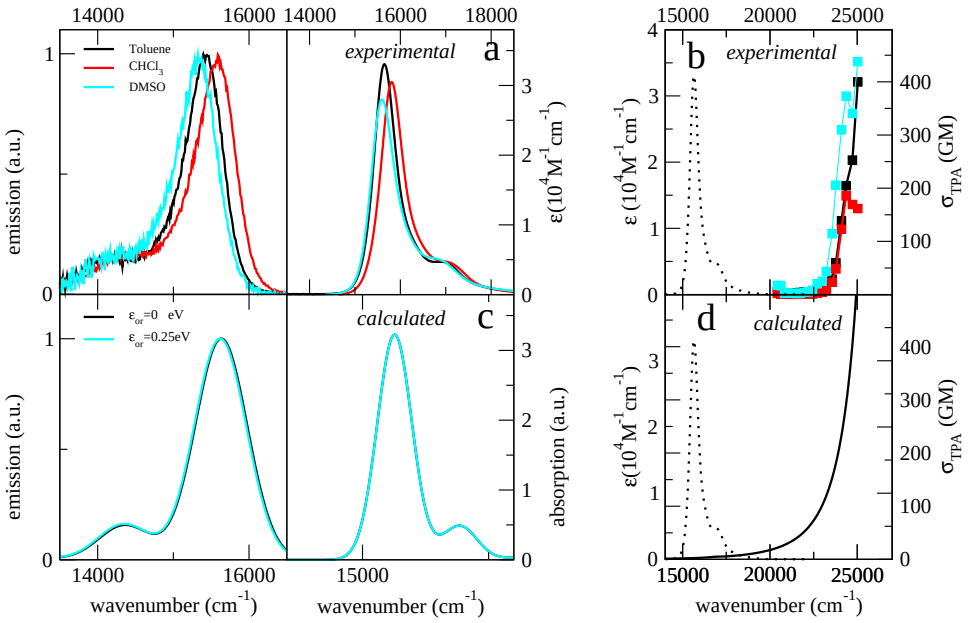

Figure 1.12: *Top panels: experimental spectra of compound* **2**. *Panel a: fluorescence and absorption spectra in solvents of increasing polarity (see legend). Panel b: TPA spectrum (symbols, in GM units) in solvents of increasing polarity. The OPA spectrum in toluene (dotted line) is reported for comparison. Bottom panels: Spectra calculated by the three-state model using the parameters reported in Ref. [39].*

quadrupolar molecules, extended to account for coupling with vibrational degrees of freedom and solvation effects. The phenomenon of symmetry breaking was discussed in detail. Symmetry breaking is induced by relaxation processes (of the solvation and vibrational coordinates), and is associated, for dyes belonging to class I, to the localization of the excitation in one of the two arms of the quadrupole, while for class III chromophores to an unbalanced distribution of charge in the ground state. Localization/delocalization of excitation is a major issue in the study of branched structures, starting from quadrupolar (or octupolar) chromophores up to all-conjugated dendrimers [74, 75]. Multipolar systems are currently studied also as model systems for energy transfer, a basic process in energy/light-harvesting systems [74]. Of course symmetry breaking has important implications in spectral properties, such as fluorescence solvatochromism. To confirm the validity of the model, results on two different chromophores were reported: the first one is a symmetry-breaking system of class I, while in the second one symmetry is preserved for all the states (class II). For both dyes the model works well, and is able to reproduce the main features of linear and nonlinear spectra. Examples of quadrupolar chromophores belonging to class III are probably constituted by cyanine dyes, which will be the subject of future investigation. The discussed model offers the basis to develop guidelines for the synthesis of chromophores with sought properties, and can be quite easily extended to more complicated structures, such as octupoles, that are the subject of the next section.

1.4 The four-state model for octupolar chromophores

In the last section of this chapter the discussion is focused on octupolar chromophores, a very interesting class of molecules, with several applications in the field of NLO [26, 76, 77, 78]. Octupolar chromophores are branched molecules, constituted by an electron-donor D (or electron-acceptor A) cen-

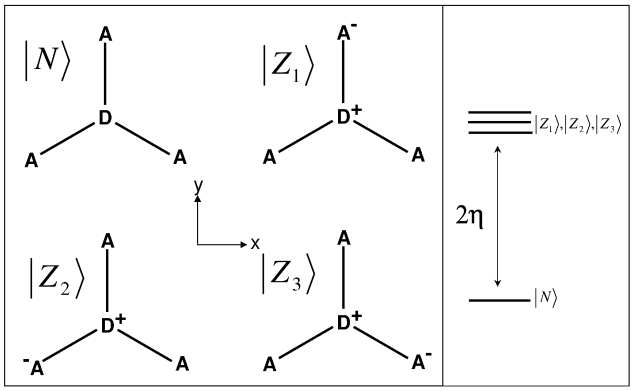

Figure 1.13: *The four resonating structures, corresponding to the the four basis state of the model, for DA_3 octupolar chromophores (similar structures apply to AD_3 dyes, with interchanged D and A sites).*

tral core, linked in a C_3 symmetry to three electron acceptors A (or electron donor D) through π-bridges. The symmetry of these molecules ensures interesting and non-trivial properties. DA_3 (or AD_3) systems show a low-energy CT transition, very high TPA response and significant second-order nonlinear optical response.

From the theoretical point of view, two different approaches have been described in literature. According to the excitonic model, the octupolar dye is described in terms of three dipolar DA dyes, interacting only via electrostatic forces, and the charge transfer between the three branches is neglected [26, 68]. This model allows to qualitatively understand the properties of octupolar dyes, starting from the corresponding dipoles, but a quantitative description of the spectra is difficult to obtain. On the other hand, the essential-state model offers a valid and efficient alternative: it describes the octupolar system in terms of four states, corresponding to the four resonance structures, and fully describes the charge-resonance process [23].

The development of the four-state model follows the same lines described in the Sections 1.2, 1.3 for the two-state model for dipoles and the three-

state model for quadrupoles, respectively. The four resonance structures are chosen as the basis wavefunctions of the problem: $|N\rangle$ is the neutral state, separated by an energy gap 2η from the three degenerate zwitterionic states ($|Z_1\rangle$, $|Z_2\rangle$ and $|Z_3\rangle$) (Figure 1.13). $|N\rangle$ is mixed with $|Z_i\rangle$ states by the matrix element $-\sqrt{2}t$. On the chosen basis set, the following operators are conveniently defined:

$$\hat{\rho} = \begin{pmatrix} 0 & 0 & 0 & 0 \\ 0 & 1 & 0 & 0 \\ 0 & 0 & 1 & 0 \\ 0 & 0 & 0 & 1 \end{pmatrix} \tag{1.30}$$

$$\hat{\sigma} = \begin{pmatrix} 0 & 1 & 1 & 1 \\ 1 & 0 & 0 & 0 \\ 1 & 0 & 0 & 0 \\ 1 & 0 & 0 & 0 \end{pmatrix} \tag{1.31}$$

$$\hat{\delta}_1 = \begin{pmatrix} 0 & 0 & 0 & 0 \\ 0 & 2 & 0 & 0 \\ 0 & 0 & -1 & 0 \\ 0 & 0 & 0 & -1 \end{pmatrix} \tag{1.32}$$

$$\hat{\delta}_2 = \begin{pmatrix} 0 & 0 & 0 & 0 \\ 0 & 0 & 0 & 0 \\ 0 & 0 & 1 & 0 \\ 0 & 0 & 0 & -1 \end{pmatrix} \tag{1.33}$$

The operators $\hat{\rho}$, $\hat{\delta}_1$ and $\hat{\delta}_2$ define the charge distribution within the molecule: $\hat{\rho}$ measures the symmetric displacement of charge along the three branches, while $\hat{\delta}_1$ and $\hat{\delta}_2$ measure the unbalanced charges on the three external sites.

The electronic Hamiltonian reads:

$$\mathcal{H}_{el} = 2\eta\hat{\rho} - \sqrt{2}t\hat{\sigma} \tag{1.34}$$

Two dipole moments operators are defined, along the x- and y-direction:

$$\begin{aligned} \hat{\mu}_x &= \frac{1}{2}\mu_0\hat{\delta}_1 \\ \hat{\mu}_y &= \frac{\sqrt{3}}{2}\mu_0\hat{\delta}_2 \end{aligned} \tag{1.35}$$

where μ_0 is the dipole moment of the D^+A^- branch.

The basis wavefunctions are conveniently combined exploiting the C_3 symmetry. Accordingly, we find two totally-symmetric (A-type) wavefunctions, $|A_1\rangle = |N\rangle$ and $|A_2\rangle = 1/\sqrt{3}(|Z_1\rangle + |Z_2\rangle + |Z_3\rangle)$, and two degenerate (E-symmetry) states, $|E_1\rangle = 1/\sqrt{6}(2|Z_1\rangle - |Z_2\rangle - |Z_3\rangle)$ and $|E_2\rangle = 1/\sqrt{2}(|Z_2\rangle - |Z_3\rangle)$. On this basis, the Hamiltonian mixes the A-symmetry states, while the two E-states stay unmixed. The eigenstates are:

$$\begin{aligned} |g\rangle &= \sqrt{1-\rho}|A_1\rangle + \sqrt{\rho}|A_2\rangle \\ |c_1\rangle &= |E_1\rangle \\ |c_2\rangle &= |E_2\rangle \\ |e\rangle &= \sqrt{\rho}|A_1\rangle - \sqrt{1-\rho}|A_2\rangle \end{aligned} \tag{1.36}$$

where ρ is the ground-state expectation value of the operator $\hat{\rho}$ (Equation 1.30), and represents the weight of the zwitterionic states in the ground state. In other words, ρ contains the information relevant to the octupolar character of the molecule: dyes with low ρ have a low octupolar moment, while on the contrary, when ρ is high, the octupolar character is strong. ρ is fixed by the model parameters η and $\sqrt{2}t$ as follows:

$$\rho = \frac{1}{2}\left(1 - \frac{\eta}{\sqrt{\eta^2 + 6t^2}}\right) \tag{1.37}$$

Transition wavelengths and transition dipole moments, i.e. the key quantities for spectroscopy, can be expressed in terms of ρ as follows:

$$\hbar\omega_{gc_1} = \hbar\omega_{gc_2} = \sqrt{6}t\sqrt{\frac{1-\rho}{\rho}} \tag{1.38}$$

$$\hbar\omega_{ge} = \sqrt{6}t\sqrt{\frac{1}{\rho(1-\rho)}} \tag{1.39}$$

$$\hbar\omega_{c_1e} = \hbar\omega_{c_2e} = \sqrt{6}t\sqrt{\frac{\rho}{1-\rho}} \tag{1.40}$$

$$\mu^x_{gc_1} = \mu^y_{gc_2} = \mu_0\sqrt{\frac{\rho}{2}}; \quad \mu^y_{gc_1} = \mu^x_{gc_2} = 0 \tag{1.41}$$

$$\mu^x_{ge} = \mu^y_{ge} = 0 \tag{1.42}$$

$$\mu^x_{c_1e} = \mu^y_{c_2e} = -\mu_0\sqrt{\frac{1-\rho}{2}}; \quad \mu^y_{c_1e} = \mu^x_{c_2e} = 0 \tag{1.43}$$

$$\mu^x_{c_1c_1} = \mu^x_{c_2c_2} = \mu^y_{c_1c_2} = \frac{1}{2}\mu_0; \quad \mu^y_{c_1c_1} = \mu^y_{c_2c_2} = \mu^x_{c_1c_2} = 0 \tag{1.44}$$

With the specific choice of the reference system shown in Figure 1.13, all transition dipole moments in Equations 1.41, 1.42, 1.43, 1.44 point along the x or the y direction. The permanent dipole moments of $|g\rangle$ and $|e\rangle$ are both zero, while $|c_1\rangle$ and $|c_2\rangle$ have non-vanishing components along x. The OPA transition from the ground state $|g\rangle$ is allowed towards both $|c_1\rangle$ and $|c_2\rangle$, while $|e\rangle$ is a dark state (the transition is allowed by two-photon absorption). Moreover the two $|c\rangle$ states are two-photon allowed, but with a weaker intensity than the $|e\rangle$ state. Figure 1.14 summarizes the spectroscopic behavior of octupolar molecules. Specifically in the right panels we show the TPA cross sections towards the $|c\rangle$ and $|e\rangle$ states as functions of ρ.

The electronic model is now extended to account for molecular vibrations. For dipoles only one vibration along the molecular axis was considered (Equation 1.9), while for quadrupoles two vibrations relevant to the two molecular branches were taken into account (Equation 1.28). For octupoles, three vibrational degrees of freedom (q_1, q_2, q_3) one for each molecular arms, have to be introduced. The three molecular coordinates are equivalent by symmetry: they are characterized by the same frequency ω_v and the same relaxation energy ϵ_v. The last parameter describes the energy gained by the system upon relaxation of the i-th branch after charge transfer along the same branch. The symmetry adapted vibrational coordinates are:

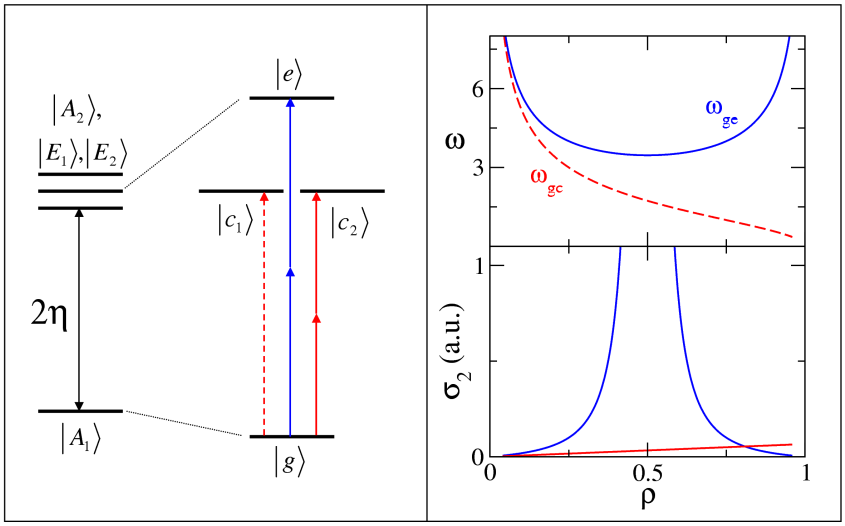

Figure 1.14: *Four-state model for octupolar chromophores on the symmetrized basis. The neutral $|A_1\rangle$ state and the three zwitterionic states, $|A_2\rangle$, $|E_1\rangle$ and $|E_2\rangle$, are separated by an energy gap 2η. $-\sqrt{2}t$ mixes the two totally symmetric states to give the ground state $|g\rangle$, and the excited state $|e\rangle$, which is active in TPA (full blue arrows). The two E-symmetry states stay unmixed and correspond to the two one-photon active (dotted red arrow) $|c_1\rangle$ and $|c_2\rangle$ states, that are weakly two-photon allowed (full red arrows). The top graph on the right panel shows the ρ-dependence of the transition frequencies to the states $|c\rangle$ and $|e\rangle$ (units with $\sqrt{2}t = 1$); the bottom graph shows the TPA cross sections evaluated on the maximum for the two TPA transition towards $|c\rangle$ (red) and $|e\rangle$ (blue) states.*

$$\hat{q}_A = \frac{1}{\sqrt{3}}(\hat{q}_1 + \hat{q}_2 + \hat{q}_3) \tag{1.45}$$

$$\hat{q}_{E_1} = \frac{1}{\sqrt{6}}(2\hat{q}_1 - \hat{q}_2 - \hat{q}_3) \tag{1.46}$$

$$\hat{q}_{E_2} = \frac{1}{\sqrt{2}}(\hat{q}_2 - \hat{q}_3) \tag{1.47}$$

where $\hat{q}_A$ describes a totally symmetric deformation, while $\hat{q}_{E_1}$ and $\hat{q}_{E_2}$ have E-symmetry.

The vibrational Hamiltonian reads:

$$\mathcal{H}_v = -\sqrt{\frac{2\epsilon_v}{3}}\omega_v \hat{q}_A \hat{\rho} - \sqrt{\frac{\epsilon_v}{3}}\omega_v \hat{q}_{E_1}\hat{\delta}_1 - \sqrt{\epsilon_v}\omega_v \hat{q}_{E_2}\hat{\delta}_2 \tag{1.48}$$
$$\frac{1}{2}(\omega_v^2\hat{q}_A^2 + \hat{p}_A^2) + \frac{1}{2}(\omega_v^2\hat{q}_{E_1}^2 + \hat{p}_{E_1}^2) + \frac{1}{2}(\omega_v^2\hat{q}_{E_2}^2 + \hat{p}_{E_2}^2)$$

where the operators $\hat{p}_A$, $\hat{p}_{E_1}$ and $\hat{p}_{E_2}$ represent the conjugate momenta of the relevant vibrational coordinate. The symmetrized vibrations couple to the electronic operators according to their symmetry: $\hat{q}_A$ is coupled to $\hat{\rho}$, and modulates the symmetric charge transfer from the central core to the peripheral groups. Instead, $\hat{q}_{E_1}$ and $\hat{q}_{E_2}$ are coupled with the operators $\hat{\delta}_1$ and $\hat{\delta}_2$ (see Equations 1.32, 1.33): vibrations along these coordinates mix states of different symmetry and lead to an unbalanced distribution of charge on the three peripheral groups.

In the adiabatic approximation the kinetic energy of the vibrational coordinates is neglected. In this approximation the energy of each electronic state depends on the vibrational coordinates, defining the corresponding potential energy surfaces (PES). Along these lines we construct for octupolar chromophores the phase diagram shown in the left panel of Figure 1.15. Specifically, in this Figure the PES are shown as functions of the two E-symmetry coordinates, q_{E_1} and q_{E_2}, while the totally symmetric coordinate q_A is kept at its equilibrium value ($q_A^{eq} = 2\epsilon_v\langle\hat{\rho}\rangle/\sqrt{3}$). The specific feature of PES relevant to octupolar dyes is the exact degeneracy of the two OPA states ($|c_1\rangle$ and $|c_2\rangle$) at the origin ($q_{E_1} = q_{E_2} = 0$). Any perturbation of the system removes their degeneracy, lowering the symmetry of the system. The right

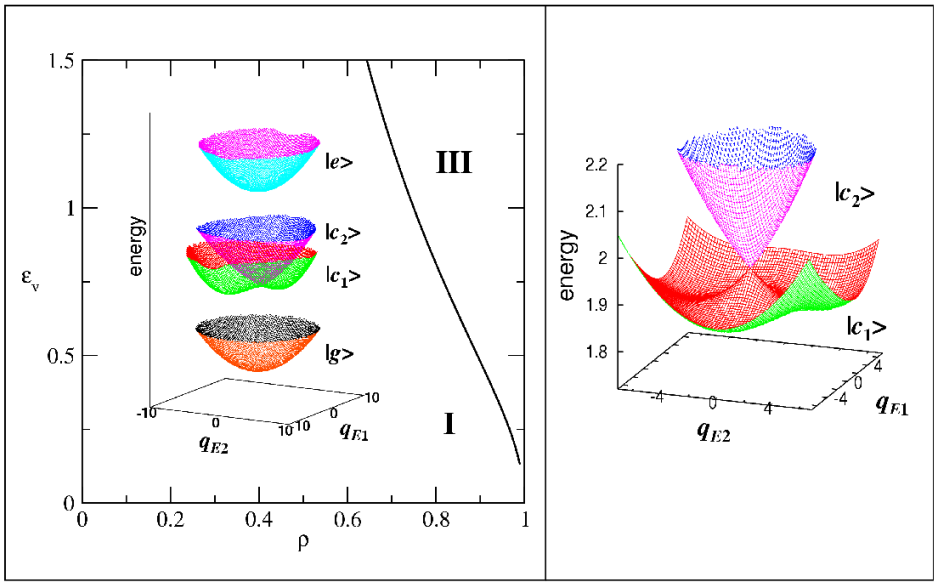

Figure 1.15: *Left Panel: Phase diagram for octupolar chromophores as a function of ρ, the octupolar character, and ϵ_v, the vibrational relaxation energy (in units of $\sqrt{2}t$). Region I corresponds to stable $|g\rangle$ and $|e\rangle$ states, and multistable $|c_1\rangle$ state, as shown in the inset. In region III both the ground and the $|c_1\rangle$ states are multistable. Right Panel: Magnification of the conical intersection between the two PES relevant to $|c_1\rangle$ and $|c_2\rangle$ shown in the left panel.*

panel of Figure 1.15 shows more clearly what explained before: the PES relevant to the states $|c_1\rangle$ and $|c_2\rangle$ show a conical-intersection structure, the two states being degenerate only at the position corresponding to the origin of the coordinate system. The lowest-energy PES shows three equivalent minima, along the three molecular branches. Octupolar chromophores present a multistable $|c_1\rangle$ state for any value of ρ and ϵ_v, so that this state always has a broken-symmetry character. The behavior of octupoles remarkably differs from that of quadrupoles, where symmetry breaking in the ground state or in the first excited state is conditional, i.e. it is observed only for specific values of the parameters ρ and ϵ_v. In quadrupoles, a large region of the phase diagram is occupied by class II chromophores, that do not undergo symmetry breaking in any electronic state. In octupolar chromophores class II is not present: symmetry-preserving octupoles do not exist.

For high values of ρ and ϵ_v not only the OPA but also the ground state become multistable, and in analogy with quadrupolar dyes, this is the region of class III dyes (Figure 1.15). Notice that for octupolar dyes of class I the $|c_1\rangle$ state is multistable, and for class III dyes the ground state $|g\rangle$ and the first excited state $|c_1\rangle$ are both multistables (while for class III quadrupoles only the ground state was characterized by a multiple-minima PES). Class I chromophores occupy a wide part of the phase diagram of Figure 1.15. Examples of class III octupolar chromophores were not identified in the literature, probably because of their intrinsic instability. In fact as ρ approaches the value of 1, the ground state becomes almost degenerate with the two $|c\rangle$ states, giving an almost threefold-degenerate multistable ground state.

As for quadrupolar chromophores, also for octupolar systems care has to be taken to discriminate between true and false symmetry breaking. When the excitation on the first excited state localizes in one of the three minima, the system undergoes a true symmetry breaking. On the contrary, if the excitation tunnels between the three minima, a false symmetry breaking is in action. The height of the barrier between the three minima (that is

connected to the strength of the electron-phonon coupling, i.e. ϵ_v) and the vibrational frequency of the phonons, ω_v, are the key parameters determining a true or false symmetry breaking: for large values of ϵ_v and small values of ω_v the system undergoes a true symmetry breaking. For the calculation of spectral properties, we adopted the non-adiabatic approach that naturally applies to both regimes. Symmetry breaking plays a main role in spectral properties, because it induces a dipolar character of the first excited (OPA allowed) state (notice that for class III dyes a polar ground state is also expected), corresponding to the localization of the excitation on one of the three branches.

We now turn attention to polar solvation. The ground state of chromophores belonging to class I is nonpolar, and OPA is expected not to be solvatochromic. In fact, absorption is a vertical process and, as the ground state preserves the symmetry, absorption does not shift with solvent polarity. Experimental results confirm this prediction. On the contrary, fluorescence spectra are strongly solvatochromic: fluorescence spectra of octupolar dyes, always red-shift upon increasing the solvent polarity. This is exactly the same behavior observed for quadrupolar dyes of class I. Also in this case the pronounced solvatochromism is ascribed to the presence of a relaxed dipolar excited state, whose energy is stabilized in polar solvents.

Polar solvation is included in the model following the reaction-field approach already presented for dipoles and quadrupoles. The solvent is treated as an elastic continuum medium, that responds linearly to local perturbations. The Hamiltonian relevant to solvation reads:

$$\mathcal{H}_v = -\hat{\mu}_x F_x^{or} - \hat{\mu}_y F_y^{or} + \frac{\mu_0^2}{4\epsilon_{or}}[(F_x^{or})^2 + (F_y^{or})^2] \tag{1.49}$$

where F_x^{or} and F_y^{or} are the two components of the reaction field, coupled to the x and y components of the dipole moment operator, respectively. The last term describes the elastic energy spent by the solvent to sustain the reaction field. The dynamics of polar solvation are very slow compared to

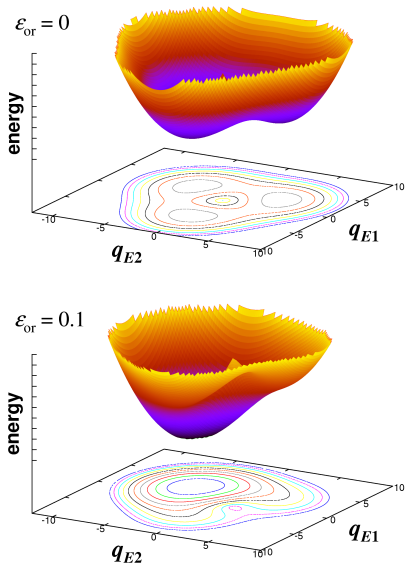

Figure 1.16: *Potential energy surfaces and isopotential lines relevant to the relaxed* $|c_1\rangle$ *state calculated along the two non symmetrical vibrational coordinates* q_{E_1} *and* q_{E_2} *in the case of an apolar solvent (top panel,* $\epsilon_{or} = 0$*) and a polar solvent (bottom panel,* $\epsilon_{or} = 0.1$*). The two components of the reaction field,* F_x^{or} *and* F_y^{or} *are fixed to their equilibrium value for the* $|c_1\rangle$ *state.*

both electronic and vibrational motions: F^{or} can be considered a classical variable. ϵ_{or} represents the solvent relaxation energy, or in other words, the energy gained by the system upon solvent relaxation; it increases with solvent polarity. The effects of polar solvation on the first excited state are shown in Figure 1.16 that shows PES calculated fixing q_A and $F^{or}_{x,y}$ at their equilibrium value for the $|c_1\rangle$ state. In the upper panel the PES was calculated for $\epsilon_{or} = 0$, i.e. in a non-polar solvent. Three equivalent minima are found in $|c_1\rangle$ state. The lower panel shows the same PES calculated for the same dye in a slightly polar solvent ($\epsilon_{or} = 0.1$). The interaction with the solvent leads to the stabilization of one of the three minima: in polar solvents the excitation localizes in one of the three molecular branches upon relaxation along the solvation coordinate. As a consequence, the symmetry of the charge distribution breaks down, the state becomes polar, and symmetry breaking comes into action. The consequences of symmetry breaking are evident in emission spectra. In octupolar chromophores, fluorescence comes from a relaxed dipolar excited state, which is stabilized by polar solvents. A red shift of emission is expected when the polarity of the solvent increases, and this is confirmed by experiments, as discussed in the next section.

Inhomogeneous broadening is included in the calculation of spectra, averaging over the reaction field according to the relevant Boltzmann distribution. For details about the calculation of spectra, see Appendix A.

1.4.1 From dipolar to octupolar chromophores: essential-state models at work

In this section the experimental and theoretical study of the series of compounds in Figure 1.17 is presented. Compounds **D1** and **D2** are dipolar dyes, constituted by the same electron-donor moiety, the triphenylamine group, and two different electron-acceptor groups: the dicyano-vinyl acceptor group of **D2** is stronger than the aldehyde acceptor group of **D1**. **O1** and **O2** are the corresponding octupolar compounds. **D1**, **D2** and **O1** were synthesized by the group of Prof. Mireille Blanchard-Desce of University of

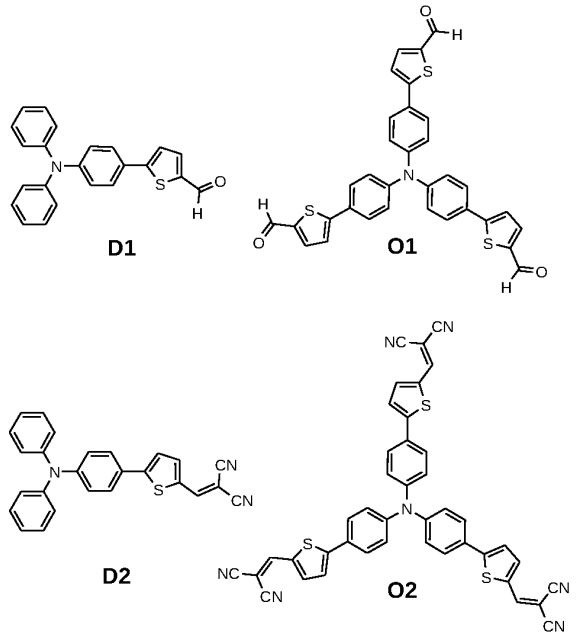

Figure 1.17: *Molecular structures of compounds **D1**, **O1** and **D2**, **O2**.*

Rennes 1 (France), while **O2** was purchased by Aldrich, and used without further purification. A detailed investigation of the linear spectra of the four compounds was performed in different solvents (spectra grade, obtained by Aldrich). The TPA cross section of all compounds was measured in $CHCl_3$.

Absorption spectra were collected on a Jasco V-570 spectrophotometer, on solutions about $\sim 10^{-5}$M. Molar extinction coefficients were measured in $CHCl_3$ on solutions of different concentrations to test the Lambert-Beer law. Fluorescence spectra were collected on an Edinburgh Instruments Fluorometer (FLS 920) and details about fluorescence quantum yield measurements are reported in Appendix B. The lifetime values were obtained from the reconvolution fit analysis of the decay profiles with the F900 analysis software, and each fit was judged by the reduced χ^2 value. TPA cross sections

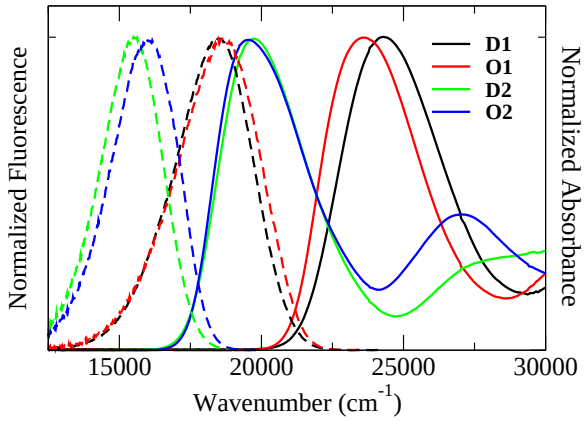

Figure 1.18: *Absorption (full lines) and fluorescence (dashed lines) spectra of **D1**, **O1** and **D2**, **O2** in $CHCl_3$.*

were measured by the investigation of the two-photon excited fluorescence in $\sim 10^{-4}$ solutions. For details about TPEF measurements see Appendix C.

Experimental absorption and fluorescence spectra in $CHCl_3$ are shown in Figure 1.18, while Table 1.5 summarizes experimental results in a few solvents. Absorption bands of **D1** and **O1** in $CHCl_3$ are located in the violet region of the visible spectrum. The absorption band of the octupolar compound is weakly red-shifted. Fluorescence spectra of the two compounds overlay, and they are in the blue-green spectral region. Absorption bands of **D2** and **O2** show a sizeable red-shift with respect to **D1** and **O1**, because of the stronger electron-acceptor character of the dicyano-vinyl groups with respect to the aldehyde group. Emission spectra are located in the yellow-orange region, with the **D2** spectrum slightly red-shifted with respect to **O2**. Molar extinction coefficients of octupolar molecules are roughly three times higher than those of the corresponding dipoles. The high values of molar extinction coefficients are typical of CT-molecules. Fluorescence quantum yields are remarkably high, especially in low-polarity solvents. The loss of fluorescence quantum yield in polar solvents is associated to the red shift of

Table 1.5: *Experimental data of compounds **D1**, **O1**, **D2** and **O2** in different solvent. **D2** and **O2** are not stable in DMSO.*

Compound	λ_{abs}/nm[a] (ϵ/M^{-1}cm^{-}1)[a]	λ_{fluo}/nm[a]	ϕ[b] (τ/ns)[c]
Toluene			
D1	401	472	0.89
O1	417	471	0.68
D2	495	578	0.10
O2	500	562	0.25
Chloroform			
D1	411 (28000)	541	0.82 (4.0)
O1	423 (63500)	536	0.63 (4.1)
D2	508 (36900)	644	0.43 (2.6)
O2	512 (93300)	625	0.44 (2.2)
Dichloromethane			
D1	421	551	0.83
O1	421	550	0.62
D2	501	677	0.34
O2	510	660	0.30
Dimethyl sulfoxide			
D1	409	593	0.1
O1	428	613	0.25

[a]All data refer to band maxima.

[b]Fluorescence quantum yield, error ±10%

standard: Fluorescein in NaOH 0.1M, $\phi = 0.9$.

[c]Fluorescence lifetime.

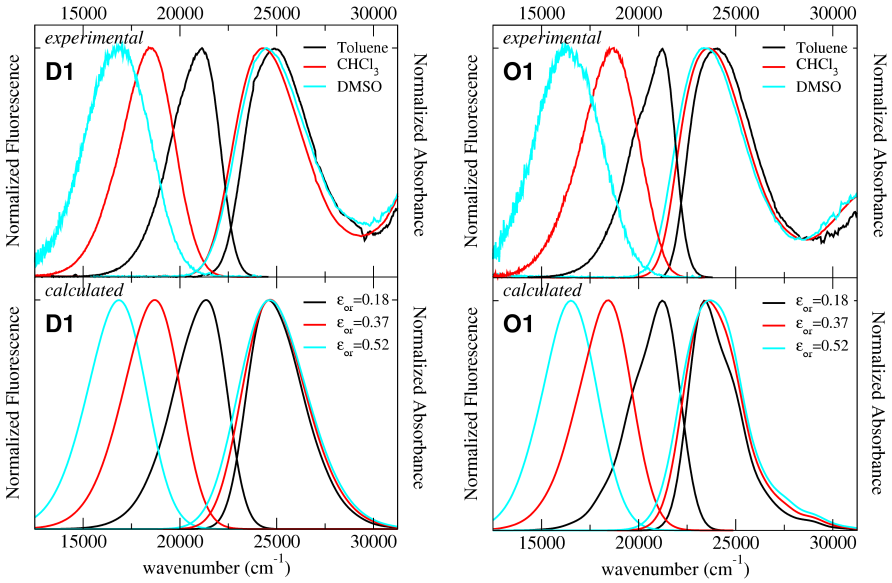

Figure 1.19: *Top panels: experimental absorption and fluorescence spectra of* ***D1*** *(left) and* ***O1*** *(right) in solvent of different polarity. Bottom panels: calculated absorption and fluorescence spectra of* ***D1*** *(left) and* ***O1*** *(right) for different values of the solvent relaxation energy* ϵ_{or}*. Parameters for calculation are given in Table 1.6.*

the bands (fluorescence intensity is proportional to the third power of the frequency).

Top panels of Figures 1.19 and 1.20 show emission and fluorescence spectra of the four compounds in different solvents. Absorption spectra are barely affected by solvent polarity, and the small shifts observed in absorption is ascribed to the different refractive indexes of the solvents. Fluorescence solvatochromism is prominent, for all compounds: increasing the polarity of the solvent, spectra shift to the red. This solvatochromic behavior is well understood for dipolar compounds, where the excited state, in an essential-state picture, is dominated by the charge-separated D^+A^-

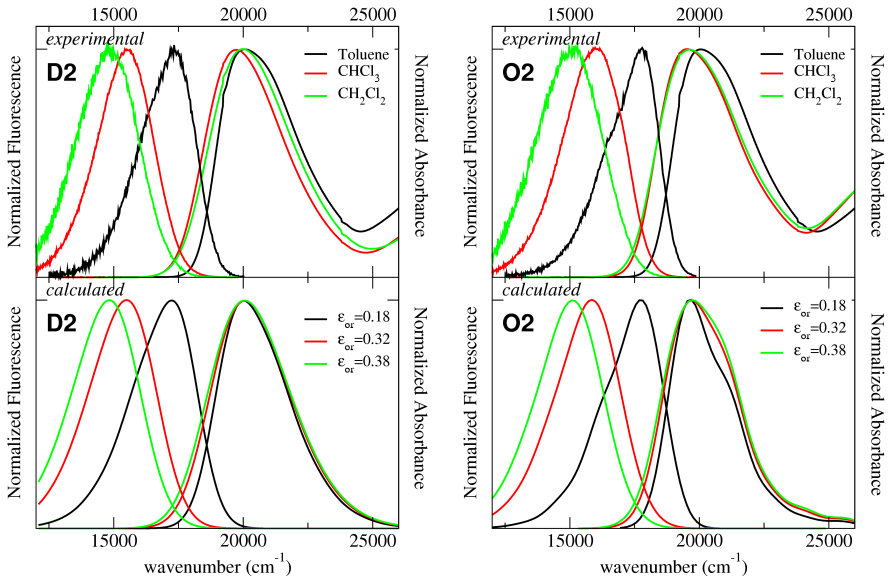

Figure 1.20: *Top panels: experimental absorption and fluorescence spectra of* ***D2*** *(left) and* ***O2*** *(right) in solvent of different polarity. Bottom panels: calculated absorption and fluorescence spectra of* ***D2*** *(left) and* ***O2*** *(right) for different values of the solvent relaxation energy* ϵ_{or}*. Parameters for calculation are given in Table 1.6.*

state. On the other hand, the strong solvatochromism observed in octupoles is associated to symmetry-breaking phenomena, as discussed in the previous section. In fact only a dipolar excited state can justify such a large solvatochromism. As already discussed, the dipolar excited state is originated by the localization of the excitation in one of the three arms of the molecule.

TPA spectra in $CHCl_3$ are shown in Figure 1.21. Different measurements were performed, with different filters to remove laser light, and different references according to the excitation wavelength. Results obtained with different filters, well agree in the region of spectral overlap. On the contrary, results obtained using different references, i.e. Fluorescein, as measured by Xu and Webb (XW) [79], and Styryl-9M, as measured by Drobizhev et al. (MDR) [80], show big discrepancies in the 900-1000nm region. The disagreement is relevant only for **D2** and **O2**, because the central part of the band is involved. For the dipolar compounds, a perfect overlap of the TPA band with the OPA band is expected: indeed this is observed for **D1**. Instead for **D2** two peaks appear in the TPA band, and this behavior is ascribed to an experimental artifact. In particular the XW reference probably leads to a overestimated TPA response, while the MDR reference underestimates the TPA response. Anyway, to overcome the problem we average over all measurements: a Gaussian fit of the averaged bands is presented in Figure 1.21.

As already discussed in the previous section, octupolar compounds show two TPA bands. The weaker band overlaps the OPA band (both the $|c_{1,2}\rangle$ states are TP allowed), while the more intense band is at higher energy and corresponds to the $|g\rangle \rightarrow |e\rangle$ transition. Top panels of Figure 1.22 show the comparison between TPA spectra of the dipoles and the corresponding octupoles. TPA spectra of octupolar compounds were divided by 3, so that Figure 1.22 shows the TPA response per branch. For both the pairs **D1**/**O1** and **D2**/**O2** the TPA intensity normalized per branch increases in the octupolar compound. In particular the TPA intensity of the band corresponding to the transition towards $|c_{1,2}\rangle$ is weaker in the octupolar

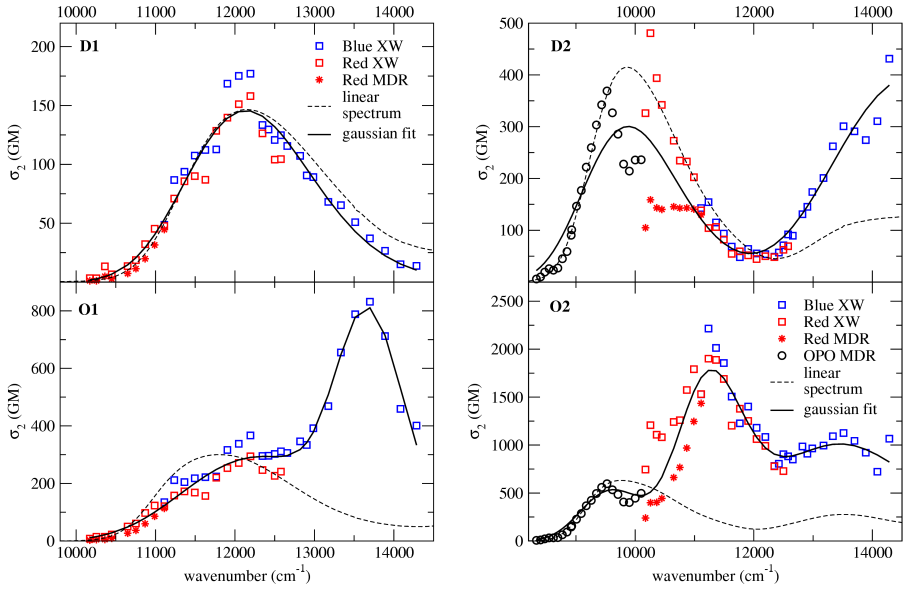

Figure 1.21: *Two-photon absorption cross section of the four compounds in chloroform. Squares report data obtained using Xu and Webb's data (XW) [79] for Fluorescein as a reference. Blue and red symbols correspond to the use of a blue and red filter, respectively. Stars report data obtained using Drobizhev's data (MDR) [80] for Styryl-9M as a reference, and red filter. Circles report data obtained with the OPO (optical parametric oscillator). The full black lines show the (multi)Gaussian fits of the mean σ_2 values. Dashed lines show rescaled linear absorption spectra (at the double of the transition energy)*

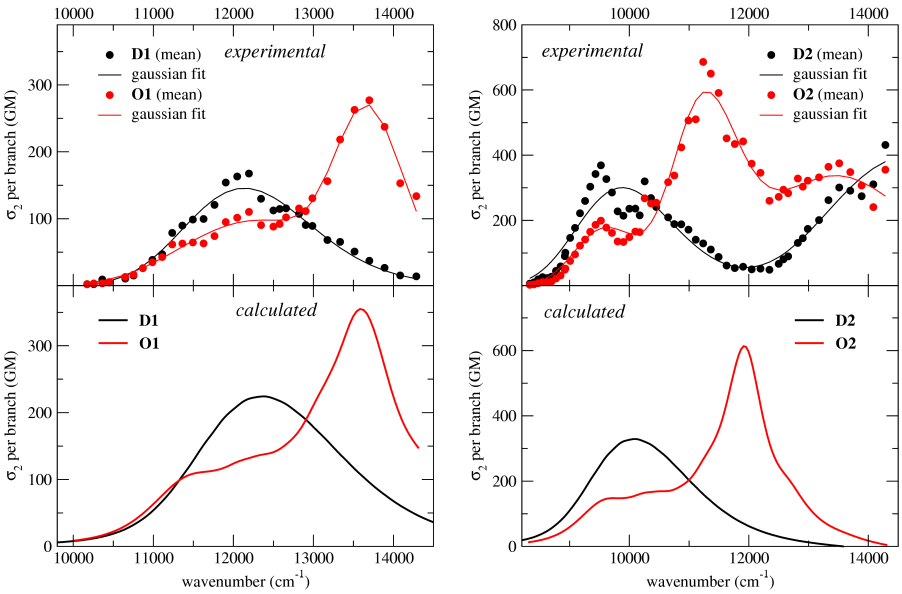

Figure 1.22: *Top panels: comparison of TPA cross section of dipolar and octupolar (per branch) chromophores in chloroform. Circles represents the mean values of the different sets of measurements, while the continuous lines are the corresponding (multi)Gaussian fit. Bottom panels: calculated TPA spectra, using parameters reported in Table 1.6.*

dyes, while the intensity of the higher-energy band, corresponding to the transition towards the $|e\rangle$-state, is sizeably higher.

Bottom panels of Figures 1.19, 1.20 and 1.22 show the calculated spectra. Dipolar compounds were modeled adopting the two-state description presented in the first section of this chapter, while the four-state model was adopted for octupolar compounds. Table 1.6 reports the parameters chosen for calculations. Moving from dipoles to octupoles, all the parameters are kept fixed, but the energy separation between the basis state 2η. In fact $\sqrt{2}t$, the mixing element between the basis states, is related to the π-conjugated bridge, that is the same in dipoles and octupoles. Similarly, we keep constant

Table 1.6: *The four-state model parameters for compound **D1**, **O1**, **D2** and **O2**.*

Compound	η/eV	$\sqrt{2}t$/eV	μ_0/D	ϵ_v/eV	ω_v/eV	Γ/eV
D1	1.48	0.55	36	0.16	0.18	0.07
O1	1.36	0.55	36	0.16	0.18	0.07
D2	1.18	0.55	36	0.16	0.18	0.07
O2	1.1	0.55	36	0.16	0.18	0.07

all the parameters concerning electron-phonon coupling (i.e. ω_v and ϵ_v), as well as Γ. μ_0 is the same because the length of the dipole D^+A^- is exactly the same in dipolar and octupolar dyes. ϵ_{or} is related to the dimension of the cavity that the solute occupies (and of course to the dielectric constant and the refractive index of the solvent). Because fluorescence comes from a broken-symmetry state, and the excitation is localized on a single branch of the molecule, so that the effective size of the emitting part is the same as for the dipole, we keep ϵ_{or} constant (for the same solvent) for dipolar and octupolar molecules. The proposed model gives excellent results, both for linear and nonlinear spectra. The main spectral properties are well reproduced by essential-state models: in particular we well reproduce fluorescence solvatochromism, the OPA and TPA band shapes and intensities [23].

The power of the essential-state models becomes evident moving from the aldehydes compounds to the compounds with the dicyano-vinyl groups: also in this case all the parameters of the model are kept fixed but η. The energy separation for both the dipole and the octupole are lower than the corresponding molecules with the aldehyde group, because the electron-acceptor strength is noticeably higher. A slight change in ϵ_{or} is justified by the different dimensions of the acceptor groups. All the other parameters remain fixed for the considerations proposed before. Also in this case the results of modeling are impressively good.

This result is a proof of the robustness of the essential-state approach in the description of (multi)polar chromophores of different charge-distribution symmetry. In fact, five parameters ($\sqrt{2}t, \omega_v, \epsilon_v, \Gamma, \mu_0$) are kept fixed, and only η changes (according to physical considerations) from one molecule to the other, plus ϵ_{or}, the parameter related to the solvent relaxation energy. Using these parameters not only the linear spectral properties in different solvents are well-reproduced for all compounds, but also the TPA reponse. The pertinence of the modeling is not confined to OPA and TPA spectra, but it can be exploited for many different properties, like electroabsorption, nonlinear polarizabilities or anisotropy, without any further modification of the parameters.

1.5 Conclusion

In this Chapter theoretical methods based on the essential-state strategy were presented. The models apply to CT molecules of different symmetry. Electronic models are extended to take into account the role of molecular vibrations and polar solvation. The first section briefly reviewed the two-state model. Then we presented the work developed in this thesis to describe a terpyridine based ligand and its complex on Zn. The two-state model that successfully describes the ligand must be extended to account for the active role of the metal in order to understand the observed amplification of the TPA intensity upon complexation.

The second section reviewed model and results for quadrupolar chromophores. The symmetry-breaking phenomenon was discussed in detail.

In the last section the work developed in this thesis on the four-state model for octupolar molecules was presented. Symmetry-breaking phenomena and their implications on optical spectra are discussed in detail. To complete the discussion, the linear and nonlinear spectra of two of dipole/octupole pairs were investigated.

Essential-state models work very well, for all the three different classes of

molecules, reproducing in a quantitative way not only linear spectra, but also nonlinear responses. The models requires a limited number of parameters: for each molecule six parameters are kept fix ($\sqrt{2}t, \omega_v, \epsilon_v, \Gamma, \mu_0$), while only one parameter is changed according to the polarity of the solvent. Even more interestingly, the same parameters can be exported, without any further modification, to calculate different properties, such as hyperpolarizabilities, electroabsorption or anisotropy (cf next Chapter).

Chapter 2

(Multi)polar chromophores in solution: some advanced spectroscopic tools

2.1 Introduction

In this Chapter three advanced spectroscopic tools are discussed: electroabsorption, low-temperature excitation and emission spectra, and fluorescence anisotropy. The discussion is focused on spectra of charge-transfer dyes. For these systems in fact these spectroscopic techniques provide very useful information.

Electroabsorption measures the difference between the absorption spectrum in the presence and in the absence of a static electric field. In this Chapter theoretical calculations of electroabsorption spectra of (multi)polar dyes are presented. The essential-state approach is compared with the commonly adopted approach developed by Liptay.

Excitation and emission spectra of dipolar, quadrupolar and octupolar dyes were collected at different temperatures ranging from 77K to 300K. The aim of the work is to investigate inhomogeneous broadening, that clearly depends on temperature. Moreover low-temperature measurements set the

basis for fluorescence anisotropy, discussed in Section 2.4.

Fluorescence anisotropy measures the fluorescence intensity exciting with polarized light, and detecting emission through an analyzer. Fluorescence anisotropy in frozen solutions provides information about the angle between the absorption and fluorescence transition dipole moments. Anisotropy is particularly interesting for non linear molecules, such as octupoles. Experimental results are discussed with reference to spectra calculated using essential-state models.

2.2 Electroabsorption spectra of (multi)polar chromophores: beyond the Liptay formulation

Electroabsorption (EA) is a widespread experimental technique, that measures the effects of a static electric field on the linear absorption spectrum. [81, 82, 83]. Johannes Stark in the first decade of 1900 discovered the splitting of spectral lines of atoms in the presence of an applied electric field. Applications of the EA technique to chemically and biologically interesting systems started in the 70s [82]. EA spectroscopy is a straightforward tool to investigate excited states and physical properties related to charge-transfer phenomena. In particular, the interaction between the applied external field with the molecules in the sample perturbs the absorption spectra, so that some molecular properties, not accessible in linear spectroscopy can be addressed.

EA spectra measure a third-order nonlinear response $\chi^{(3)} = (-\omega; \omega, 0, 0)$, where one of the applied electric fields has a vanishing frequency. The early work of Liptay on EA set the basis for understanding EA spectra in solution [84, 85]. The EA response is related to the changes in the dipole moment ($\Delta\mu$) and in the polarizability ($\Delta\alpha$) of the molecule upon absorption, and to the transition dipole moment. The Liptay formulation was developed for polar dyes in frozen solutions, showing a well-separated electronic excitation and in the absence of vibronic structure. Liptay demonstrated that

EA spectra can be modeled as a linear combination of the linear absorption spectrum and of its first and second derivatives [84, 85]. This approach was successfully applied not only to many molecular systems, even in the presence of structured bands [82, 86, 87] but also to mixed-valence complexes [35, 81, 88, 89, 90] and quantum dots [91]. EA was measured also on polymeric films [83, 92, 93] and molecular crystal [94, 95]. In general, the Liptay approach becomes dangerous if dark states (i.e. forbidden states in absorption) are not far in energy from the allowed linear transition [15, 96, 97, 98]. Forbidden states appear in highly symmetric systems, such as quadrupolar and octupolar chromophores, as discussed in Chapter 1 [42]. EA spectra of quadrupolar and octupolar dyes may offer important information on dark states that are not accessible by linear spectroscopy. The Liptay approach is not suitable for these systems, and new treatments need to be developed to extract reliable molecular properties and parameters from EA.

In this section, the essential-state models presented in the previous chapter are applied to describe EA spectra of dipolar, quadrupolar and octupolar chromophores [42, 99]. As expected, we regain the Liptay result for dipolar dyes, while new relations are found for quadrupolar and octupolar chromophores. The first part of this section develops the electronic problem, while interactions with slow degrees of freedom are introduced in the last part.

2.2.1 The electronic problem: a perturbative approach to EA spectra

Dipolar dyes

The two-state model for dipolar dyes presented in section 1.2 is now applied to the calculation of EA spectra ($EA(\omega)$). The EA spectrum is defined as the difference between the linear spectrum in the presence ($S(\omega, F)$) and in absence ($S(\omega)$) of a static electric field (F). For a frozen solution of dipolar DA dyes in which chromophores are randomly oriented, the linear contribution in F averages to zero, and only the quadratic contribution

survives [81]:

$$EA(\omega) = \frac{S(\omega, F) - S(\omega)}{F^2} \tag{2.1}$$

The two-state model allows to directly calculate the exact EA response introducing F in the Hamiltonian of the system as follows:

$$\mathcal{H} = \begin{pmatrix} 0 & -\sqrt{2}t \\ -\sqrt{2}t & 2\eta - \mu_0 F \end{pmatrix} \tag{2.2}$$

The problem is treated as for linear absorption spectra, and the EA spectrum is numerically calculated with Equation 2.1.

Keeping in mind that the main purpose of EA measurements is to derive some specific molecular properties, such as the mesomeric dipole moment, $\Delta\mu$, and the variation of the linear polarizability $\Delta\alpha$ upon absorption, we followed a perturbative approach to isolate the different contributions to $EA(\omega)$. Perturbation theory up to the second order in F leads to an exact analytical expression for EA, that coincides with the result first obtained by Liptay [84, 85]:

$$EA(\omega) = AS(\omega) + \omega B \frac{d}{d\omega}\left(\frac{S(\omega)}{\omega}\right) + \omega C \frac{d^2}{d\omega^2}\left(\frac{S(\omega)}{\omega}\right) \tag{2.3}$$

The EA signal has three contributions coming from the the linear spectrum, its first and second derivatives. The three coefficients are related to the molecular properties as follows:

$$A = 3M\left(\frac{3\Delta\mu_{g,c}^2 - 4\mu_{gc}^2}{\omega_{gc}^2}\right) \tag{2.4}$$

$$B = 3M\left(\frac{2\Delta\mu_{g,c}^2 - 2\mu_{gc}^2}{\omega_{gc}}\right) = 3M\left(\frac{2\Delta\mu_{g,c}^2}{\omega_{gc}} + \frac{1}{2}\Delta\alpha_{g,c}\right) \tag{2.5}$$

$$C = \frac{3}{2}M\Delta\mu_{g,c}^2 \tag{2.6}$$

where $|g\rangle$ and $|c\rangle$ refer to the ground and the excited states of Equation 1.3; ω_{gc} is the transition frequency of Equation 1.6 and $\Delta\mu_{gc} = \mu_g - \mu_c$ is the difference between the permanent dipole moments of the states, reported in Equations 1.7, 1.8 . $\Delta\alpha_{gc} = \alpha_g - \alpha_c$ is the change of the linear polarizability

upon photoexcitation, and according to the sum-over-state expression, it can be expressed in terms of ω_{gc} and μ_{gc} as follows [100]:

$$\Delta\alpha_{gc} = 2\frac{\mu_{gc}^2}{\omega_{gc}} \tag{2.7}$$

M is a numerical factor accounting for orientational averaging. For linear molecules $M = 1/5$ $(1/15)$ when the oscillating electric field is polarized parallel (perpendicular) to F. The analysis of EA spectra of dipolar dyes implies a fitting procedure, to extract the coefficients A, B and C, from which the molecular parameters are finally obtained.

Quadrupolar Dyes

The three-state model for quadrupolar chromophores was presented in Section 1.3 [39]. Quadrupolar molecules are characterized by the presence of a dark (one-photon forbidden) state $|e\rangle$ (Equation 1.22), that significantly influences the EA spectrum. The perturbative approach, already proposed for dipolar dyes, can be used for quadrupolar chromophores as well [42]. Because of the presence of a dark state, the expression for the EA signal obtained for quadrupolar dyes has a new term $T(\omega)$, with no counterpart in the expression for dipolar chromophores. Moreover, the prefactor of the second-derivative term, C in Equation 2.3, exactly vanishes in quadrupolar dyes: C is in fact proportional to the mesomeric dipole moment, which is zero in quadrupolar dyes. The EA expression for quadrupolar dyes is the following:

$$EA(\omega) = AS(\omega) + \omega B\frac{d}{d\omega}\left(\frac{S(\omega)}{\omega}\right) + D\omega T(\omega) \tag{2.8}$$

The last term comes from the one-photon forbidden $|g\rangle \rightarrow |e\rangle$ transition, which becomes allowed due to the presence of the static electric field. $T(\omega)$ does not have a counterpart in the linear absorption spectrum: it represents a normalized band shape function (that we arbitrarily set equal to a Lorentzian in the calculation of spectra) at the frequency of the $|g\rangle \rightarrow |e\rangle$

transition. The prefactors A, B and D are related to molecular properties:

$$A = 3M\left(-4\frac{\mu_{gc}^2}{\omega_{gc}^2} - \frac{\mu_{ce}^2}{\omega_{ce}^2} + 2\frac{\mu_{ce}^2}{\omega_{ce}\omega_{gc}} + 2\frac{\mu_{ce}^2}{\omega_{ge}\omega_{gc}}\right) \tag{2.9}$$

$$B = 3M\frac{\Delta\alpha_{g,c}}{2} \tag{2.10}$$

$$D = MK\mu_{ce}^2\mu_{gc}^2\left(\frac{1}{\omega_{gc}} - \frac{1}{\omega_{ce}}\right)^2 \tag{2.11}$$

A is a cumbersome linear combination of dipole moments and energies, while B exactly coincides with the Liptay result for molecules with vanishing mesomeric dipole moment. Finally, D involves the $|c\rangle \rightarrow |e\rangle$ transition dipole moment and frequency. K is the dimensional factor that transforms the dimensionless normalized band shape $T(\omega)$ into an absorbance.

Estimating molecular properties from EA spectra of quadrupolar dyes is more complicated than for dipolar dyes. In fact, for dipoles, the EA spectrum is a combination of the linear spectrum and its derivatives, i.e. of experimentally accessible quantities. For quadrupolar dyes the fitting procedure is not straightforward because the $T(\omega)$ term has no experimental counterpart. The spectral region of $T(\omega)$ can be inferred from the TPA spectrum, but the band shape relevant to EA is unknown.

The analysis of EA spectra of quadrupolar dyes is however particularly interesting, because it offers information on dark states not accessible by OPA. On the other hand, the analysis is hindered by the appearance of features that cannot be related to the linear spectrum or its derivatives, and the actual possibility to obtain reliable information on the properties of quadrupolar molecules from EA spectra critically depends on the energy gap between the two excited states $|c\rangle$ and $|e\rangle$, and hence on the quadrupolar character ρ of the molecule (cf Equation 1.24).

Chromophores with a low quadrupolar character ($\rho \rightarrow 0$) have almost degenerate OPA and TPA transition (see Figure 1.8), so that in EA spectra the features related to the absorption spectrum $S(\omega)$ and to $T(\omega)$ overlap, hindering the analysis of the spectra. Figure 2.1 shows the spectra calculated for the largely neutral quadrupolar chromophore **1** presented in Section

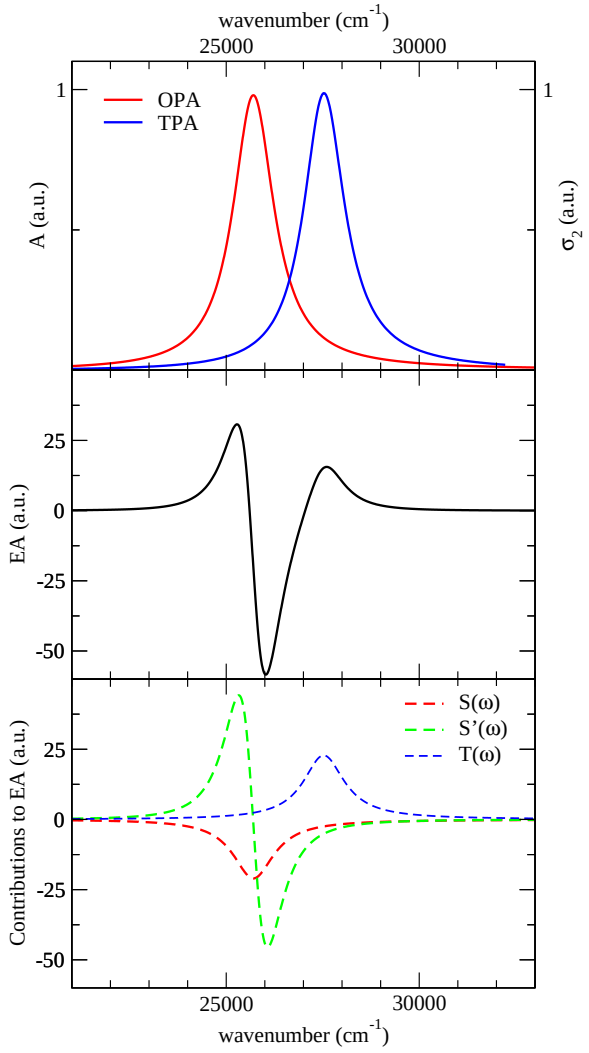

Figure 2.1: *Optical spectra calculated for a largely neutral quadrupolar dye with* $\rho \sim 0.07$ *(*$\eta = 1.48eV$*,* $\sqrt{2}t = 0.6eV$*). Spectra are calculated imposing a Lorentzian lineshape for the absorption process with* $\Gamma = 0.08eV$ *(half width at half maximum). All spectra are in arbitrary units: absolute intensities of linear and third-order (EA and TPA) processes scale with* μ_0^2 *and* μ_0^4*, respectively. Top panel: one- and two-photon absorption spectra versus the transition energy (twice the absorbed photon energy for TPA). Middle panel: EA spectrum. Bottom panel: the different contributions to EA.*

1.3.1. At this stage, we considered neither the electron-phonon coupling nor the solvent degrees of freedom, so that we tuned the parameter η to reproduce the estimated $\rho \sim 0.07$ value. The top panel of Figure 2.1 shows the OPA and TPA spectra, both reported as functions of the transition energy (for TPA twice the energy of the absorbed photon). OPA and TPA bands are not far in energy, as expected for a largely neutral quadrupolar dye. The middle panel of Figure 2.1 shows the EA spectrum. The contributions from $S(\omega)$ and its first derivative $S'(\omega)$ partially overlap with the $T(\omega)$ contribution (the three contributions are shown separately in the bottom panel of Figure 2.1). Discriminating among the different contributions is almost impossible, and, even worst, the overall EA spectrum closely resembles a typical EA spectrum with a large second-derivative contribution. Applying the Liptay procedure to this molecule would lead to a spurious second-derivative contribution suggesting a sizeable value of $\Delta\mu$, that instead exactly vanishes by symmetry.

Increasing ρ the situation improves. Figure 2.2 shows the results calculated for chromophore **2** of Ref. [39], with $\rho = 0.13$. Again η was tuned to get $\rho \sim 0.13$ in the absence of vibrational and solvation degrees of freedom. In this case OPA and TPA show a minor overlap, and the contribution from $T(\omega)$ is well separated from the contribution of $S(\omega)$ and its first derivative $S'(\omega)$. A fit of the EA spectrum in the OPA region can follow the standard procedure, of course neglecting contributions from the second-derivative on the basis of symmetry considerations. The results from the fit lead to reliable information on the molecular properties, and specifically on the change of polarizability upon excitation ($\Delta\alpha$). Moreover the second peak at higher energy gives information on the spectral position of the dark state.

A further increase of the value of ρ to 0.4, corresponding to chromophore **2** of Section 1.3.1, moves the energy of the TPA state to almost twice the energy of the OPA state (Figure 2.3). Under these conditions, the standard fitting procedure in the OPA region is possible, obviously neglecting the contribution from the second-derivative of the linear spectrum. In this case,

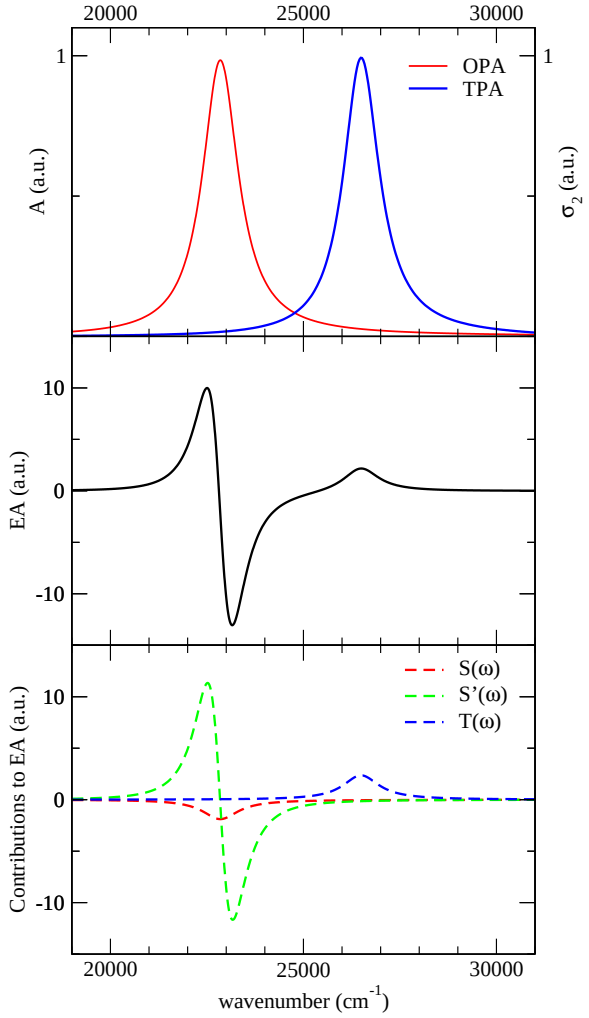

Figure 2.2: *Same as Figure 2.1, but for a quadrupolar dye with* $\rho \sim 0.13$ *(*$\eta = 1.24eV$, $\sqrt{2}t = 0.8eV$*). Spectra are calculated imposing a Lorentzian lineshape for the absorption process with* $\Gamma = 0.07eV$ *(half width at half maximum).*

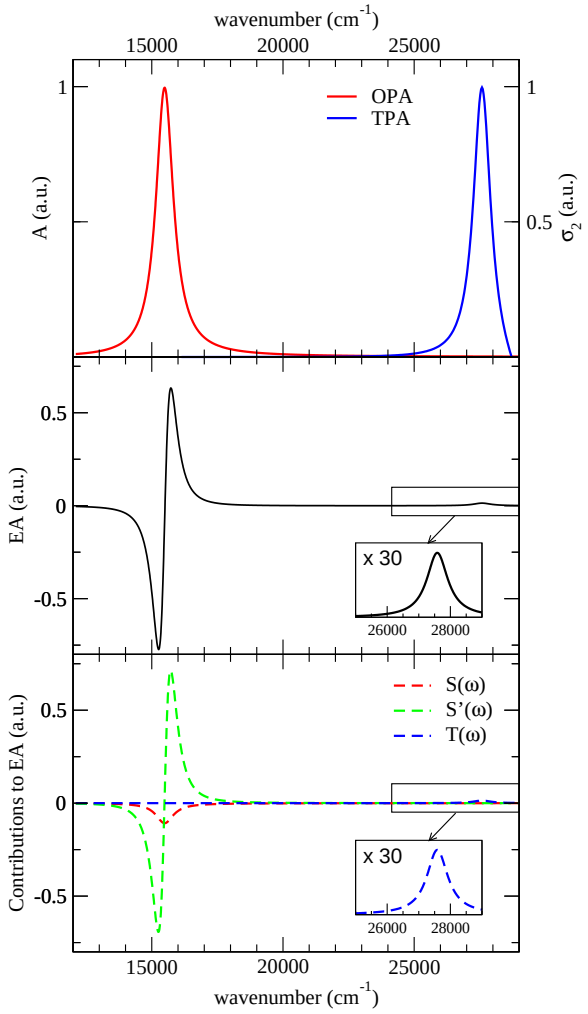

Figure 2.3: *Same as Figure 2.1, but for a quadrupolar dye with* $\rho \sim 0.4$ *(*$\eta = 0.21eV$, $\sqrt{2}t = 1.2eV$*) and* $\Gamma = 0.05eV$.

however, the intensity of $T(\omega)$ becomes extremely weak, so that retrieving information on the position of the dark state is difficult.

Octupolar dyes

Octupolar chromophores are described in terms of the four-state model presented in Section 1.4 [23]. The presence of a dark state (the $|e\rangle$-state of Equation 1.36) suggests that, as for quadrupolar chromophores, a D-like contribution shall appear in the EA signal. On the other hand, the allowed $|c\rangle$-states have permanent dipole moments (Equation 1.44), even if the ground state is non-dipolar by symmetry. Therefore a contribution from the second derivative of the linear spectrum is expected. The perturbative treatment of the static electric field leads to the same EA expression as reported for DA dyes in Equation 2.3, but with an additional term, equal to the last term in the right-hand side of Equation 2.8, as follows

$$EA(\omega) = AS(\omega) + \omega B \frac{d}{d\omega}\left(\frac{S(\omega)}{\omega}\right) + \omega C \frac{d^2}{d\omega^2}\left(\frac{S(\omega)}{\omega}\right) + D\omega T(\omega) \quad (2.12)$$

The four $A - D$ coefficients are related to molecular properties via the following expressions, that refer to an experiment where the oscillating field is polarized parallel to the direction of the static field:

$$A = \frac{4}{5}\left(-4\frac{\mu_{gc_1}^2}{\omega_{gc_1}^2} - \frac{\mu_{c_1e}^2}{\omega_{c_1e}^2} + 2\frac{\mu_{c_1e}^2}{\omega_{c_1e}\omega_{gc_1}} + 2\frac{\mu_{c_1e}^2}{\omega_{ge}\omega_{gc_1}} + 3\frac{\mu_{c_1c_1}^2}{\omega_{gc_1}^2}\right) \quad (2.13)$$

$$B = \frac{4}{5}\left(\frac{\mu_{c_1e}^2}{\omega_{c_1e}} - 2\frac{\mu_{gc_1}^2}{\omega_{gc_1}} + 2\frac{\mu_{c_1c_1}^2}{\omega_{gc_1}}\right) = \frac{4}{5}\left(\frac{1}{2}\Delta\alpha_{c_1,g}^{(xx)} + 2\frac{\mu_{c_1c_1}^2}{\omega_{gc_1}}\right) \quad (2.14)$$

$$C = \frac{2}{5}\mu_{c_1c_1}^2 = \frac{2}{5}\mu_{c_1c_2}^2 \quad (2.15)$$

$$D = \frac{8}{15}\mu_{c_1e}^2\mu_{gc_1}^2 K\left(\frac{1}{\omega_{gc_1}} - \frac{1}{\omega_{c_1e}}\right)^2 \quad (2.16)$$

As for quadrupolar dyes, A is a complicated expression, from which it is difficult to extract specific information about molecular properties. B contains information about the change in molecular polarizability, as well as the dipole moment of the excited state (remember that the dipole moment

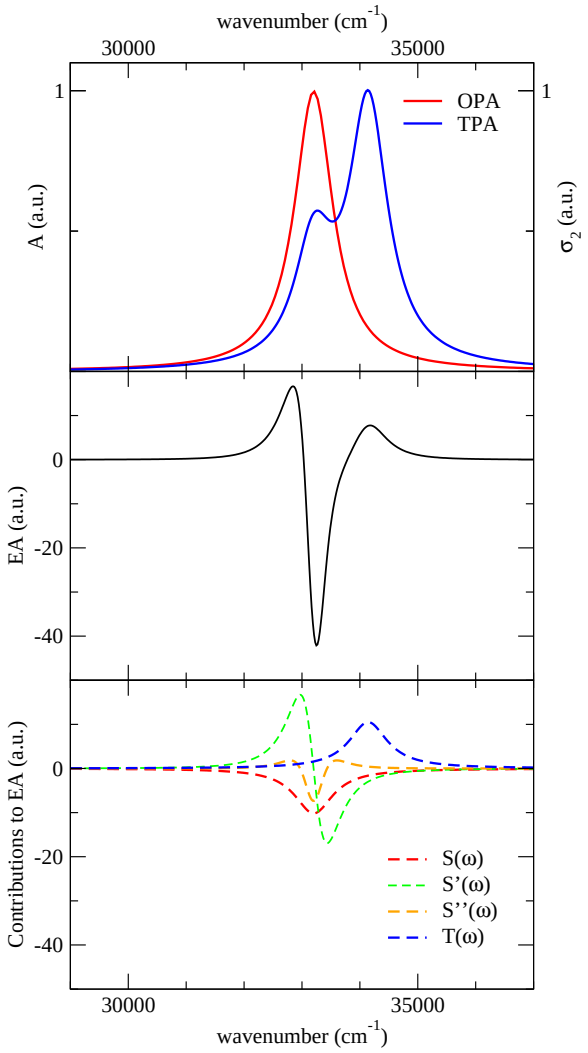

Figure 2.4: *Results for a largely neutral octupolar dye with* $\rho \sim 0.03$ *(*$\eta = 2.0eV$, $\sqrt{2}t = 0.4eV$*) and* $\Gamma = 0.1eV$*. Top panel: one- and two-photon absorption spectra versus transition energy (twice the absorbed photon energy for TPA). Middle panel: EA spectrum. Bottom panel: the different contributions to EA.*

of the ground state vanishes by symmetry, so that the mesomeric dipole moment coincide with $\mu_{c_1c_1}$). C is directly related to the permanent dipole moment of the OPA allowed state, $\mu_{c_1c_1}$, that coincides with the transition dipole moment between the two degenerate $|c_1\rangle$ and $|c_2\rangle$ excited states. K is the dimensional factor that transforms the dimensionless normalized band shape $T(\omega)$ into an absorbance. In principle, as for dipolar DA dyes, information on the excited-state dipole moment and on the variation of the molecular polarizability upon photoexcitation can be obtained from B and C. However, as for quadrupolar dyes, the fit of the EA spectrum as a sum of the linear spectrum and of its derivative becomes much more complicated than for dipolar dyes, if the dark state is close in energy to the allowed state. In fact in this case the field-induced absorption feature $T(\omega)$ overlaps the $S(\omega)$ feature in $EA(\omega)$.

Figure 2.4 exemplifies the situation for a largely neutral octupolar chromophore ($\rho = 0.03$). The top panel shows OPA and TPA transitions. TPA clearly shows two bands, because in octupolar chromophores, as discussed in section 1.4 and sketched in Figure 1.14, all the excited states are accessible via two-photon absorption. The low degree of charge transfer character ($\rho \sim 0.03$) of this system makes the two $|c\rangle$-states very close in energy to the one-photon forbidden state. As a consequence, the EA spectrum shown in the middle panel of Figure 2.4, resembles a second-derivative shape. The bottom panel shows the four different contributions to $EA(\omega)$: despite the shape of the spectrum, the second derivative gives only a weak contribution to the signal, while $T(\omega)$ is responsible for the higher energy part of the $EA(\omega)$ spectrum. A fit of $EA(\omega)$ not accounting for the dark-state contribution for this kind of molecules would lead to unreliable information on molecular properties.

2.2.2 EA spectrum as a third-order nonlinear response

The EA spectrum can also be calculated as a third-order susceptibility $\chi^{(3)}$:

$$EA(\omega) \propto Im\left[\chi^{(3)}_{IJKL}(-\omega;\omega,0,0)\right] \propto Im\left[\langle\gamma(-\omega;\omega,0,0)\rangle_{IJKL}\right] \qquad (2.17)$$

where $\langle\gamma(-\omega;\omega,0,0)\rangle_{IJKL}$ is the $IJKL$ component of the second hyperpolarizability γ tensor ($IJKL$ indices run on laboratory axis), which can be obtained from the γ_{ijkl} components ($ijkl$ run on the axis of the molecular reference system) through an average over all the possible orientations. For linear (dipolar and quadrupolar) molecules γ_{xxxx} is the only non vanishing component, so that the orientational average simply leads to the proportional factor M of Equations 2.4, 2.5, 2.6 and 2.9, 2.10, 2.11. For octupolar chromophores, $\langle\gamma(-\omega;\omega,0,0)\rangle_{XXXX} = 8/15\gamma_{xxxx}$ [101].

Quite surprisingly, EA spectra calculated according to Equation 2.17 using the standard sum-over-state (SOS) [100] expression for $\gamma_{xxxx}(-\omega;\omega,0,0)$ do not coincide with spectra calculated either from perturbative expansion, or as the difference between spectra in the presence and in the absence of the static electric field. The deviations are small but sizeable, as showed in Figure 2.5. In the SOS expression for γ_{xxxx} there are denominators containing sum and/or differences of the transition frequencies Ω_{eg} and the frequency of the applied fields, ω_i. The transition frequencies enter as complex quantities, $\Omega_{eg} = \omega_{eg} - i\Gamma_e$, where ω_{eg} is the real transition frequency and Γ_e is the inverse lifetime of the excited state e. In the EA spectrum one of the applied electric field is static, with vanishing frequency. To regain the exact EA response, the expression for γ_{xxxx} must be modified to enter the real transition frequencies (infinite lifetimes, $\Gamma_e \to 0$) in all the $\Omega_{eg} \pm \omega_i$ when $\omega_i = 0$. The expression for the γ_{xxxx} contribution to EA then reads as follows (non resonant terms are omitted):

$$\gamma_{xxxx}(-\omega;\omega,0,0) = \frac{2}{\hbar^3}\sum_{lmn}\langle g|\mu_x|l\rangle\langle l|\bar{\mu}_x|m\rangle\langle m|\bar{\mu}_x|n\rangle\langle n|\mu_x|g\rangle$$
$$\left[\frac{1}{(\Omega_{lg}-\omega)(\Omega_{mg}-\omega)(\Omega_{ng}-\omega)} + \frac{1}{(\Omega_{mg}-\omega)(\Omega_{ng}-\omega)\omega_{lg}} + \right.$$
$$\frac{1}{(\Omega_{lg}-\omega)(\Omega_{mg}-\omega)\omega_{ng}} + \frac{1}{(\Omega_{mg}-\omega)\omega_{ng}\omega_{lg}} +$$
$$\left.\frac{1}{(\Omega_{lg}-\omega)\omega_{mg}\omega_{ng}} + \frac{1}{(\Omega_{ng}-\omega)\omega_{mg}\omega_{lg}}\right] -$$

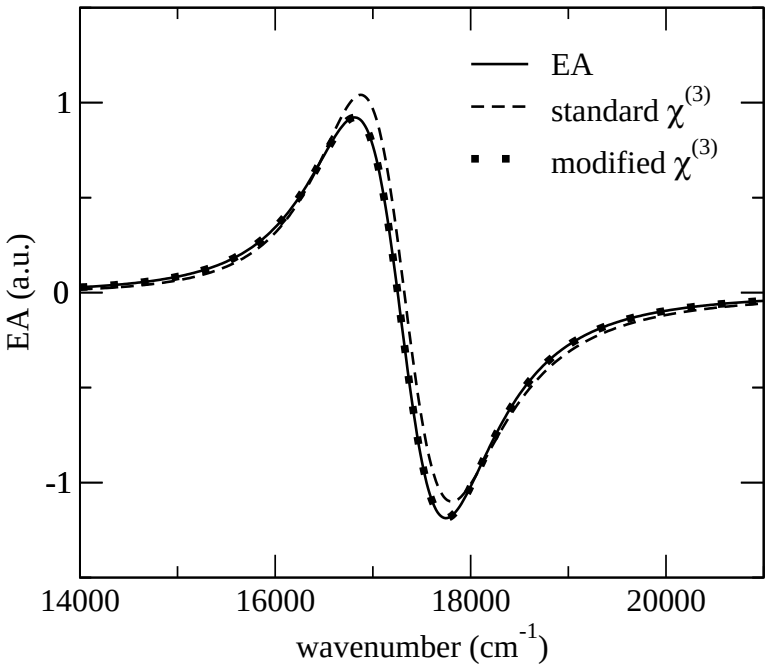

Figure 2.5: *EA spectrum for a quadrupolar dye with* $\rho = 0.34$ *(*$\eta = 0.4eV$*,* $\sqrt{2}t = 1.2eV$ *and* $\Gamma = 0.1eV$*). Full line: the exact EA spectrum obtained from the perturbative expansion or, equivalently, as the difference between linear spectra in the presence and in the absence of an applied field , divided by the squared amplitude of the field. Dashed line: EA spectrum calculated according to the standard expression for* $\gamma(-\omega;\omega,0,0)$*, i.e., incorrectly using complex transition frequencies (finite damping factors) for the* $\Omega_{eg}\pm\omega_i$ *terms in the denominators with* $\omega_i = 0$*. Dotted line: result corresponding to the modified* $\gamma(-\omega;\omega,0,0)$ *expression, according to Equation 2.18.*

$$\frac{2}{\hbar^3}\sum_{mn}\langle g|\mu_x|m\rangle\langle m|\bar{\mu}_x|g\rangle\langle g|\bar{\mu}_x|n\rangle\langle n|\mu_x|g\rangle$$
$$\left[\frac{1}{(\Omega_{mg}-\omega)(\Omega_{ng}-\omega)\omega_{mg}-\omega}+\frac{1}{(\Omega_{ng}-\omega)\omega_{ng}\omega_{mg}}+\right.$$
$$\frac{1}{(\Omega_{mg}-\omega)^2\omega_{ng}}+\frac{1}{(\Omega_{mg}-\omega)\omega_{ng}^2}+$$
$$\left.\frac{1}{(\Omega_{ng}-\omega)\omega_{mg}\omega_{ng}}+\frac{1}{(\Omega_{ng}-\omega)\omega_{mg}\omega_{ng}}\right] \tag{2.18}$$

EA spectra calculated with this expression coincide with spectra obtained via the perturbative expression discussed in the the previous section, and hence with the spectra calculated according to Equation 2.1, as shown in Figure 2.5.

2.2.3 Interaction with slow degrees of freedom: exact electroabsorption spectra of multipolar dyes in solution

Electronic spectra of organic chromophores usually show a vibronic structure due to the coupling between electronic and vibrational degrees of freedom. Moreover, the interaction between the electronic charge distribution and the slow orientational degrees of freedom of polar solvents leads to inhomogeneous broadening effects. Electron-phonon coupling and solvation effects are responsible for symmetry-breaking phenomena, recently recognized for excited states of multipolar dyes in polar solvents [23, 39].

As first discussed by Liptay, the analytical expression for EA spectra of polar dyes in Equation 2.3 does not apply in the presence of coupled vibrations, nor for inhomogeneously broadened bands [84, 85]. However, the Liptay expression is commonly adopted in the assumption that molecular properties (transition and permanent dipole moments) are approximately the same for all the transitions that contribute to the observed band.

Essential-state models presented in the previous chapter can account for vibrational degrees of freedom and polar solvation effects. In the presence of electron-phonon coupling and solvation, the perturbative treatment described before becomes too complex to obtain closed expressions for EA.

However EA spectra can be calculated from the F-dependent linear spectrum, according to Equation 2.1. Alternatively, EA spectra can be obtained from $\chi^{(3)}$, according to Equations 2.17 and 2.18. These equations also apply in the presence of vibronic coupling, provided that the sums in Equation 2.18 run over all vibrational and vibronic states [60]. Extending the same treatment to account for polar solvation is more delicate because local-field corrections to the static field must be explicitly taken into account [102]. The calculation of EA spectra of dipolar, quadrupolar and octupolar dyes, accounting for electron-phonon coupling and polar solvation, leads to results that can be directly compared with experimental data. Here, we explicitly discuss two model cases, relevant to a quadrupolar and an octupolar dye. Figure 2.6 presents the optical spectra calculated for the quadrupolar dye studied in Ref. [39] (chromophore **2**, $\rho \sim 0.13$). The calculated optical properties, in the absence of electron-phonon coupling and polar solvation, were presented in Figure 2.2, where, because of the lack of vibronic structure and inhomogeneous broadening, OPA and TPA bands were narrow, and hence hardly overlapped. The coupling to molecular vibrations leads to the wider and partially overlapping bands in Figure 2.6, whose vibronic structure is smeared as a result of inhomogeneous broadening. Moreover, because of the presence of antisymmetric vibrations, OPA (TPA) states with an odd-occupation number of antisymmetric phonons become TPA (OPA) allowed via an Herzberg-Teller coupling mechanism, that further increases the spectral overlap between OPA and TPA features. The EA spectrum in Figure 2.6 extends over a large spectral range, including both OPA and TPA regions. As expected, the shape of the EA spectrum is complex and difficult to reproduce using the standard Liptay formulation in terms of $S(\omega)$ and its derivative, as shown by the fit of in the middle panel of Figure 2.6. Specifically, the Liptay approach fails in the high-frequency region, where the contribution from the dark state is dominant. In any case, as shown in the bottom panel of Figure 2.6, a fit *à la* Liptay, would suggest a very large contribution from the second-derivative term, which should correspond to

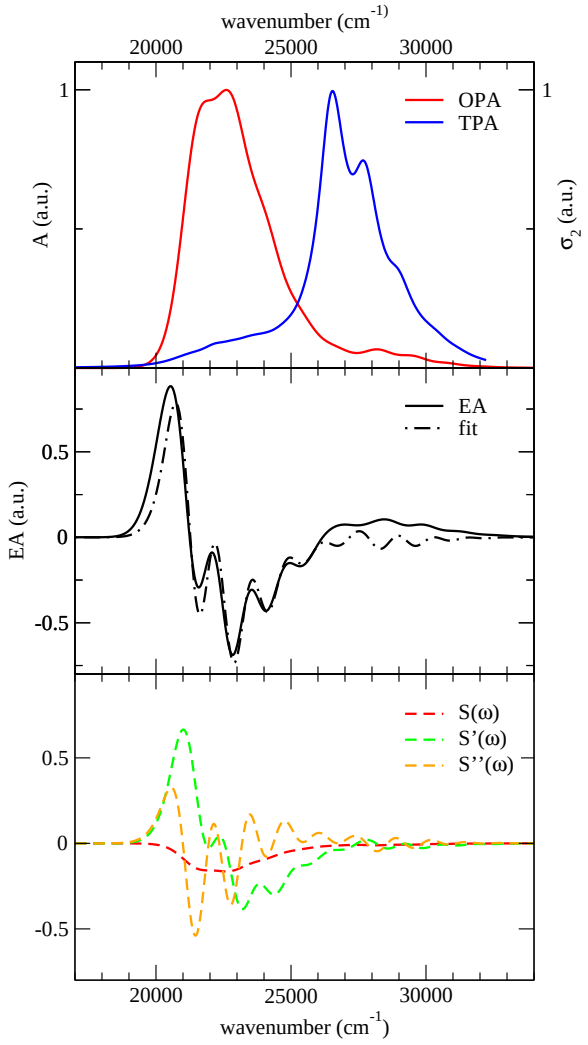

Figure 2.6: *Optical spectra of a quadrupolar dye with* $\rho = 0.13$*, corresponding to compound* ***2*** *in Ref. [39]. Results refer to a polar solvent, acetonitrile, with* $\epsilon_{or} = 0.25eV$*. Top panel: linear absorption (red line) and TPA (blue line). Middle panel: a comparison between the exact EA spectrum (full line) and its best fit (dot-dashed lines) obtained in terms of a linear combination of the OPA spectrum and its first and second derivatives. Bottom panel: decomposition of the best fit into its different contributions.*

a large $\Delta\mu$ value. This is a spurious result, because $\Delta\mu$ vanishes for centrosymmetric quadrupolar dyes.

Figure 2.7 shows the results relevant relevant to the largely neutral octupolar dye of Ref [23], with $\rho = 0.11$. In this case a fit *à la* Liptay does not reproduce the EA spectrum, not even in the OPA region. Indeed OPA and TPA bands strongly overlap, hindering the simple analysis based on the linear spectrum and its derivatives. The large spectral overlap is due to the low energy gap between the two degenerate $|c_1\rangle$ and $|c_2\rangle$ states, and the $|e\rangle$ state, and is further amplified by the fact that both types of excited states are active in the TPA process. The OPA and TPA states are strongly mixed by the electric field, and a reliable analysis of EA spectrum cannot neglect the $T(\omega)$ contribution.

In conclusion, in this section we discussed EA spectra of (multi)polar dyes. EA is a nonlinear spectroscopic technique, that offers complementary information with respect to linear absorption spectra. For polar dyes, it may offer valuable information on the excited-state dipole moment and polarizability. For more complex (symmetric) dyes, with quadrupolar and octupolar structures, it can also give important information about dark states. The Liptay approach, based on the fit of EA spectra with the linear absorption spectrum and its derivatives, hardly applies to quadrupolar and octupolar chromophores, because of the presence of dark states, often lying in close proximity of OPA allowed states. Here we propose an alternative approach to EA spectroscopy, based on essential-state models. Essential-state models are simple and tractable models for (multi)polar dyes that account for molecular vibrations and polar solvation. However, even with these simple models, closed expression for EA cannot be obtained, and one must resort to numerical solutions. Essential-state models allow to extract molecular parameters from linear spectra (absorption and fluorescence), that can be used to calculate nonlinear responses, such as EA or TPA spectra. Once a reliable set of parameters is obtained for the molecule under investigation, it is possible to evaluate several molecular properties, included the mesomeric

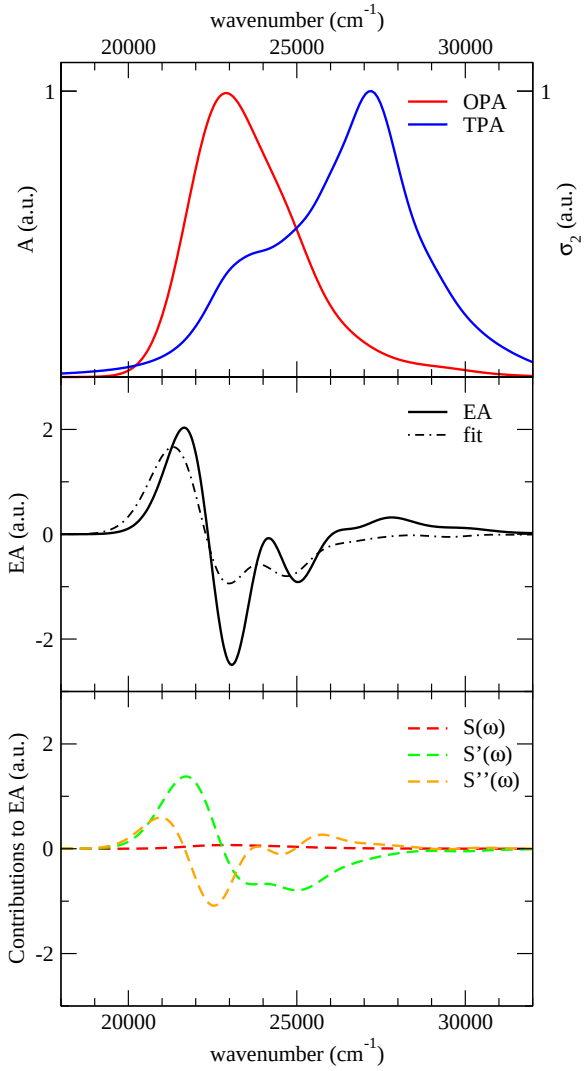

Figure 2.7: *Optical spectra of an octupolar dye with* $\rho = 0.11$*, corresponding to the compound* ***3b*** *in Ref. [23]. Results refer to toluene as the solvent, modeled by* $\epsilon_{or} = 0.2eV$*. Top panel: linear absorption (red line) and TPA (blue line). Middle panel: a comparison between the exact EA spectrum (full line) and its best fit (dot-dashed line), obtained according to the standard Liptay approach, in terms of a linear combination of the OPA spectrum and its first and second derivatives. Bottom panel: decomposition of the best fit into its different contributions.*

dipole moment and the change in polarizability upon photoexcitation.

2.3 Thermochromism of (multi)polar dyes in solution

Thermochromism is the phenomenon connected to the change of colour (or more generally of spectral properties) that some materials exhibit upon variation of the temperature. Liquid crystals and leuco dyes are examples of thermochromic materials with wide technological applications [103, 104, 105].

Here we focus the discussion on low-temperature spectroscopic measurements on solution of CT dyes. The technique was recently applied to investigate the nature of excited states of quadrupolar dyes [106, 107], and is also adopted to investigate the properties of the solvents, especially at low temperature [108, 109].

From our point of view, low-temperature measurements give hints about two phenomena related to solvation of CT-dyes: inhomogeneous broadening and symmetry breaking. As previously discussed, molecules of polar solvents arrange according to the electric field created by the polar solute (remember that for symmetric quadrupolar or octupolar molecules, the ground state is nonpolar by symmetry, while excited states become polar in the presence of symmetry-breaking phenomena), originating the so-called reaction field. Inhomogeneous broadening is related to the disorder of the system caused by a thermal distribution of the orientational component of the reaction field around its equilibrium value. Being governed by thermal fluctuations, inhomogeneous broadening is affected by temperature.

Symmetry breaking in quadrupolar and octupolar dyes is a solvation-assisted process, as discussed in Sections 1.3 and 1.4. If the temperature is sufficiently low to immobilize the solvent molecules (glass or solid transition, depending on the solvent and the cooling speed), the relaxation of the solvent around the excited solute molecule is hindered and symmetry-breaking is

suppressed.

Moreover, low-temperature measurements in glassy solvents set the basis for emission and excitation anisotropy, discussed in the next Section.

Here we present the experimental set-up for low-temperature measurements (Section 2.3.1), and experimental spectra of dipolar, quadrupolar and octupolar chromophores (Section 2.3.2).

2.3.1 Experimental setup

Experimental measurements at low temperature were performed using the liquid-nitrogen cooled cryostat OptistatDN (Oxford Instruments), equipped with the temperature controller ITC601 (speed of cooling $\sim 20°C$/minute).

Figure 2.8 shows a schematic diagram of the OptistatDN cryostat. Liquid nitrogen is stored in a reservoir, that surrounds the central sample access tube, but is thermally isolated from it. Liquid nitrogen is supplied to the sample space heat exchanger through a capillary tube. The flow of liquid nitrogen is aided by gravity, but the flow rate is controlled by the exhaust valve at the top of the sample space. A platinum resistor and heater are fitted to the sample space heat exchanger and a temperature controller is used to supply the required amount of heat to balance the cooling power and set the required temperature.

The sample is positioned inside the window block, which is just below the sample space heat exchanger, and three quartz windows give optical access to the sample. The sample chamber is pumped with a rotatory pump, to evacuate air and especially water vapour, and the sample space is filled with dry helium, that, thanks to its good thermal conductivity, ensures good heat exchange to the sample. The reservoir and sample space are thermally isolated from the room temperature surroundings by the outer vacuum chamber (OVC). This space is pumped to a high vacuum before the cryostat is cooled down, and the vacuum is maintained by a small sorption pump fitted to the reservoir. This continuously pumps the residual gases from the OVC to maintain good thermal isolation. A heater has been fitted

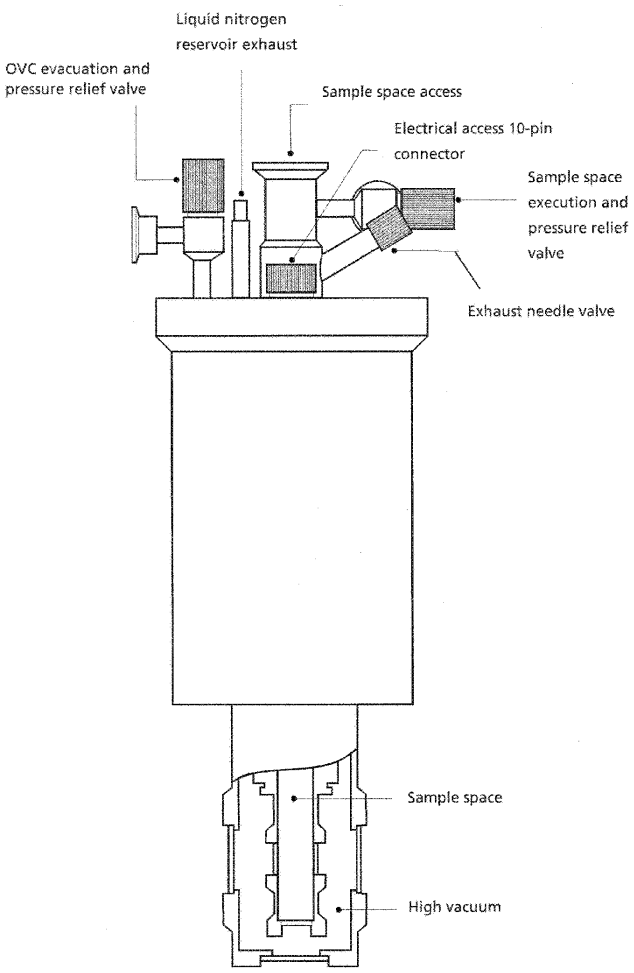

Figure 2.8: *Schematic diagram of the OptistatDN cryostat.*

Table 2.1: *Glass-transition temperatures for different solvents.*

Solvent	$T_g(K)$	storage
2Me-THF	91	under molecular sieves for 1 night
Propylene Glycol	210	taken from the bottle without any further purification
EPA	77	taken from the bottle without any further purification

to the sorb, and this is used to drive the absorbed gases out of the activated charcoal when the system is at room temperature [110].

Special cells of quartz for cryogenic applications have been used. They are constituted by a single piece, because glue usually has a different coefficient of thermal expansion with respect to quartz, what can cause the breaking of the cell. Alternatively, the faces of the cells have to be sealed with special glues for cryogenics.

All measurements are performed on diluted solution, with absorbance < 0.1 ($\sim 10^{-6}$M), to avoid inner filter effects. Particular attention is paid to the choice of solvents for measurements at low temperature. Solvents that show a glass transition (instead of the more common crystallization transition) are preferred, both to avoid light scattering and because glassy solvents are strictly required for anisotropy measurements, as it will be discussed later. Many solvents are reported in the literature to have a glass transition, but the glass transition strongly depends on the cooling speed. Using the cryostat described previously, we were able to obtain glasses from 2-methyltetrahydrofuran (2Me-THF), propylene glycol and EPA mixture (ethylether : isopentane : ethanol (5 : 5 : 2)). In Table 2.1 the glass-transition temperatures and the storage conditions of solvents are listed.

Properties of solvents, such as the refractive index and the dielectric constant, strongly depend on temperature. In particular, for all organic solvents, the refractive index increases when temperature decreases [111]. The dielectric constant increases as well when temperature decreases, so that solvents become more polar when decreasing the temperature. Some empirical relations are available. For example, in THF, the dielectric constant is reported to change with temperature as follows [112]:

$$\epsilon(T) = -1.5 + \frac{2650}{T(K)} \tag{2.19}$$

In the next section, fluorescence and fluorescence excitation spectra of dipolar, quadrupolar and octupolar compounds in 2Me-THF at different temperatures are discussed. 2Me-THF at room temperature is a solvent of intermediate polarity, with dielectric constant $\epsilon = 6.97$. The whole series of measurements where performed at 77K, i.e. when the solvent is a transparent glass, and from 150K to 300K (liquid solvent) at intervals of 30K. The range of temperature between 77K and 150K was not explored, because 2Me-THF crystallizes at 137K. Approaching the temperature of crystallization is dangerous because we observed that glass to crystal transitions often results in the cell breaking.

2.3.2 Experimental results and discussion

Dipolar Chromophores

We start the discussion with a well-known dipolar dye, Nile Red [NR], obtained from Aldrich. Panel a of Figure 2.9 shows the molecular structure of NR and spectra at different temperatures in 2Me-THF, while Table 2.2 summarizes the experimental results. NR is a neutral donor-acceptor chromophore with a medium dipolar character ($\rho \sim 0.2$) [38]. Ref. [38] reports solvatochromic data of NR at room temperature: as expected for dipolar chromophores with $\rho < 0.5$, both absorption and fluorescence spectra of NR shift to red when the solvent polarity increases. The Stokes shift is small in apolar solvent, and increases with the solvent polarity.

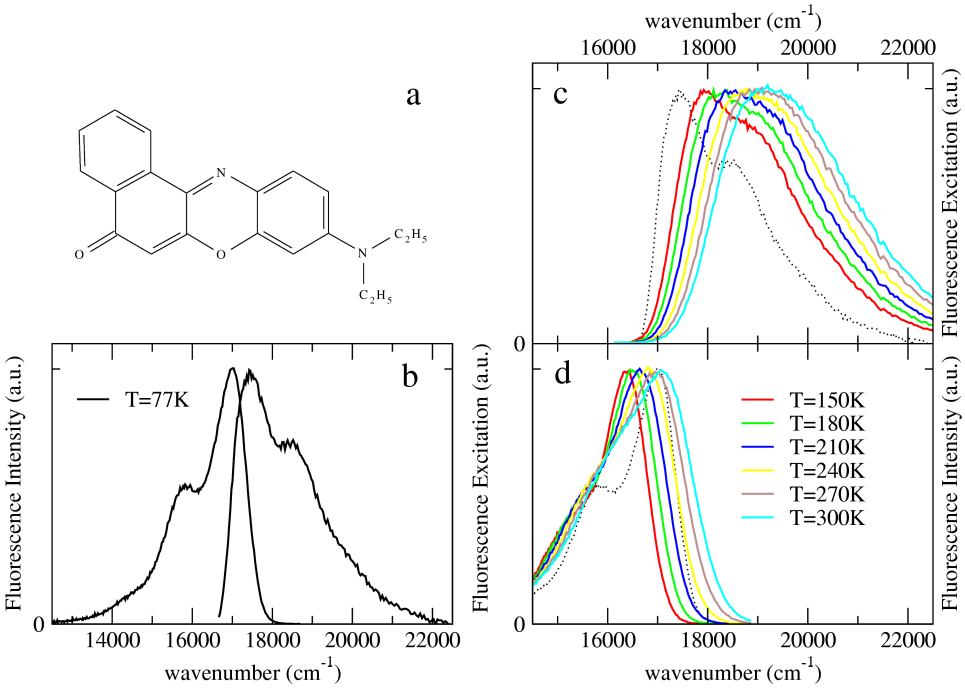

Figure 2.9: *Thermochromic study of Nile Red. Panel a: molecular structure of NR. Panel b: excitation and emission spectra spectra at 77K in 2Me-THF (glassy solvent). Panels c and d: excitation and emission spectra in 2Me-THF at different temperatures, from 150K to 300K (liquid solvent).*

Table 2.2: *Experimental data about the thermochromic study of Nile Red. Wavelenghts correspond to the maximum of excitation and emission spectra. In the last column the Stokes shift is reported.*

T(K)	λ_{exc}/nm	λ_{fluo}/nm	Stokes shift (cm^{-1})
77	574	588	414
150	557	611	1587
180	550	606	1680
210	542	600	1784
240	535	595	1885
270	525	590	2098
300	521	586	2129

Spectra at room temperature (T=300K) in 2Me-THF are reported in Panels b and c of Figure 2.9 (light-blue lines). Both absorption and excitation bands are broad, while the Stokes shift is about 2100 cm^{-1}, as reported in Table 2.2. Panel b of Figure 2.9 shows spectra at 77K, when the solution is a glassy matrix. Both emission and excitation bands are narrower than at room temperature, with partly resolved vibronic structure, and the two spectra are almost mirror images. Moreover, the Stokes shift is largely reduced with respect to the room temperature spectra, and the 0-0 transitions (where 0 stays for the vibronic state) relevant to the emission and excitation processes partly overlap.

Thermal fluctuations are reduced when lowering T and the resulting reduction of inhomogeneous broadening, is responsible for the appearance of the vibronic structure at low temperature, and the consequent more resolved bands. As described in the previous chapter, inhomogeneous broadening plays a main role in determining the band-shape of spectra. Polar solvent molecules align themselves according to the electric field generated by the solute. Inhomogeneous broadening originates from thermal fluctuations of

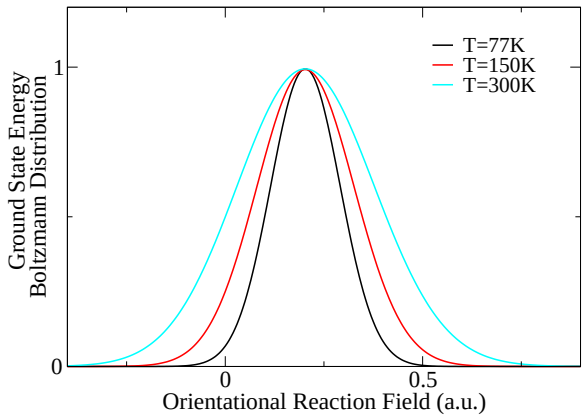

Figure 2.10: *Calculated normalized Boltzmann distributions relevant to the ground-state energy of Nile Red in CH_2Cl_2 (parameters reported in Ref. [38]) at different temperatures.*

the reaction field. In our model, thermal fluctuations are described adopting a Boltzmann distribution of the orientational reaction field. As a consequence, inhomogeneous broadening depends on both the solvent polarity and on temperature. At constant polarity, we expect that inhomogeneous broadening decreases dramatically with lowering temperature. In fact, the distribution of the orientational fields becomes narrower, as shown in Figure 2.10. This is the reason why spectra in polar solvents at low temperature show typical characteristics of nonpolar environments, such as resolved vibronic structure and narrow bands, despite the increased polarity of the solvent.

The reduced Stokes shift is instead related to the rigidity of the matrix. In a glassy solvent, relaxation along the solvation coordinate is hindered, so that the solvent cannot rearrange to respond to the electronic distribution of the solute molecule in the excited state. Therefore, in frozen samples the solvent cannot stabilize the excited state, and the 0-0 transition has the same energy in absorption and fluorescence, and the Stokes shift becomes negligible.

Table 2.3: *Experimental data about the thermochromic study of* ***D1****. Wavelenghts correspond to the maximum of excitation and emission spectra. In the last column the Stokes shift is reported.*

T(K)	λ_{exc}/nm	λ_{fluo}/nm	Stokes shift (cm^{-1})
77	435	465	1483
150	416	546	5723
180	411	536	5674
210	407	526	5559
240	403	518	5510
270	400	510	5392
300	398	502	5205

Increasing the temperature to 150K, the solvent becomes liquid. Panels c and d of Figure 2.9 show the excitation and emission spectra, respectively. The increase of the solvent polarity at low temperature justifies the progressive blue shift of both excitation and emission bands observed as temperature increases from 150K to 300K. The increase of temperature is also responsible for the increased inhomogeneous broadening: vibronic transitions become progressively less resolved, and bands broaden.

Further investigations have to be carried out, to understand why the shifts observed in emission spectra as a function of temperature are weaker than those observed in excitation. In fact from data reported in Ref. [38], emission should be more sensitive to solvent polarity than absorption, but here experimental evidences would suggest a different interpretation.

The second subject of study is the dipolar compound **D1** of Section 1.4.1, whose molecular structure is shown in Figure 1.17. This is a largely neutral DA dye ($\rho \sim 0.03$), with a non-solvatochromic absorption band while the fluorescence spectrum strongly responds to the polarity of the solvent. Spectra are shown in Figure 2.11, and Table 2.3 summarizes all

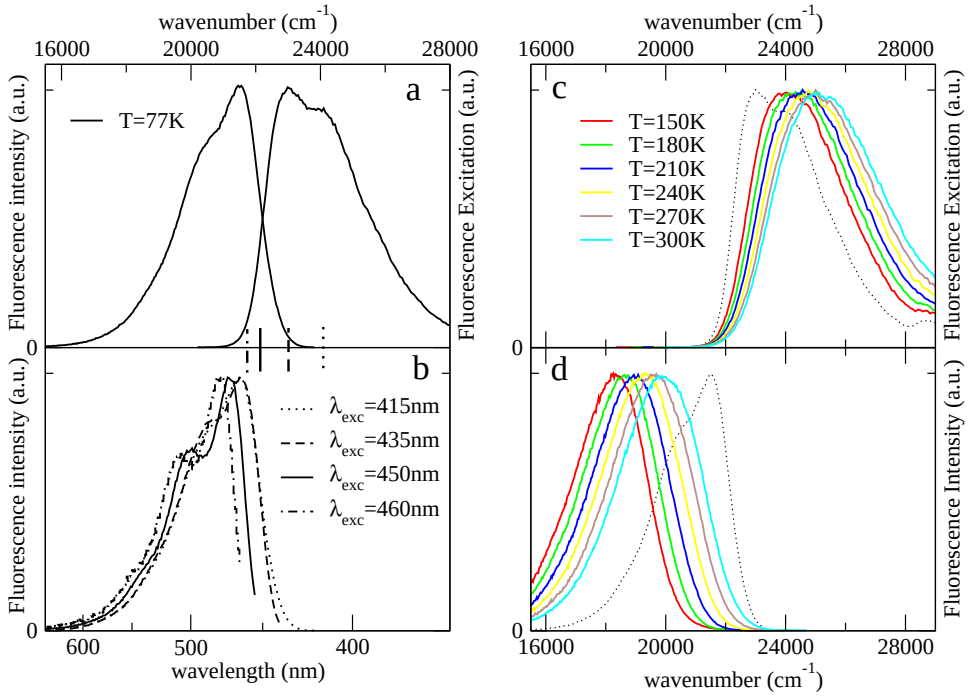

Figure 2.11: *Thermochromic study of* ***D1*** *(the structure of the molecule is sketched in Figure 1.17). Panel a: excitation and emission spectra at 77K in 2Me-THF (glassy solvent). Panel b: emission spectra at 77K collected exciting at different wavelengths; lines in between panel a and b mark the excitation wavelengths. Panel c and d: excitation and emission spectra respectively in 2Me-THF at different temperatures, from 150K to 300K (liquid solvent).*

experimental data. The behavior is similar to that of NR. The vibronic structure in spectra at 77K is resolved, and emission and excitation spectra are almost mirror images. A residual Stokes shift is observed even at 77K. We ascribe this residual Stokes shift to the presence of a slow degree of freedom of the molecule. Slow molecular motions, such as torsional and conformational degrees of freedom, are sources of Stokes shift also at room temperature, as described for chromophore **D1** in Section 1.4.1.

Panel b of Figure 2.11 shows another interesting effect, related to the rigidity of the solvent: the position of emission spectra changes according to the excitation wavelength. As the excitation wavelength moves to the red edge of the excitation band, the emission spectrum is red-shifted. The excitation wavelength selects a particular set of molecules out of the Boltzmann distribution, i.e. the molecules most efficiently absorbing light of that energy. This set of molecules are characterized by a particular environment, i.e. a particular value of the reaction field. This also means that such molecules are characterized by a particular ionicity ρ. When we are dealing with a rigid matrix, the same molecules, with exactly the same environment, will emit, because the relaxation along the solvation coordinate is hindered and energy transfer is suppressed in diluted solutions. Along these lines, the red shift can be easily understood: on the red edge of the excitation band, molecules with higher ρ absorbs, and, as a consequence, they emit at lower energy (see Equation 1.6 and Figure 1.1). This phenomenon, called *energy photoselection*, will be discussed also in Section 2.4 about fluorescence anisotropy. In liquid solvents the situation is different, because, even if the excitation wavelength selects only molecules with a particular environment, after they are promoted to the excited state they relax along the solvation coordinate, and the relaxed excited state is the same, independently of the photoselection in excitation.

When the sample is heated at 150K, the solvent becomes liquid, and a strong red shift of the fluorescence spectrum is observed (panel d of Figure 2.11) because of the relaxation along the solvation coordinate. At 150K,

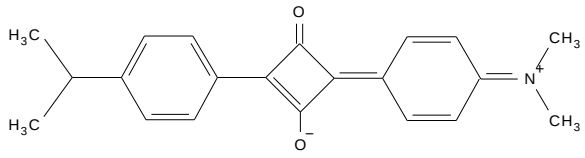

Figure 2.12: *Molecular structure of compound **2a**.*

2Me-THF is a strongly polar solvent, so that the excited state of the solute is strongly stabilized. On the contrary, the excitation spectrum is slightly blue-shifted (panel d of Figure 2.11). Increasing the temperature from 150K to 300K, both emission and excitation spectra move to the blue, and as expected, bands broaden. The behavior of fluorescence spectra is rationalized in terms of the progressive decrease of the polarity of the solvent. The reason why excitation spectra blue-shift with increasing temperature is still not clear, and further investigation is needed to get a deeper insight. In principle, the absorption spectrum (and hence excitation) of **D1** is not sensitive to the polarity of the solvent, as shown in Figure 1.19, where the data about solvatochromism are reported. The refractive index of the solvent plays a role in the position of the bands, but its variation seems to be too low to justify the large observed shift.

Quadrupolar chromophores: evidences of symmetry breaking

In this section, thermochromism of quadrupolar dyes is discussed. Two molecules are investigated, a symmetry-breaking system, compound **1** of Section 1.3.1, and a symmetry-preserving molecule (**2a**, the molecular structure is sketched in Figure 2.12), a squaraine molecule, similar to compound **2** of Section 1.3.1. Compound **1** is a largely neutral dye ($\rho \sim 0.07$), belonging to class I quadrupoles (Figure 1.9). The absorption spectrum of this compound is non solvatochromic, because the ground state in nonpolar. On the other hand, the OPA allowed excited state becomes polar because of symmetry breaking, and as a consequence, fluorescence is strongly solva-

tochromic. **2a** belongs to class II, so that both the ground and the excited states are nonpolar. In this case nor absorption neither fluorescence are affected by the polarity of the solvent.

Spectra at 77K in 2Me-THF (glassy matrix) of both compounds are shown in Figure 2.13. The Stokes shift between the emission and excitation spectra is negligible in both compounds. Moreover, bands are narrower compared to those at room temperature, and the vibronic structure is resolved for compound **1** (in **2a** the vibronic structure is almost absent also at room temperature). The absence of Stokes shift is noteworthy in chromophore **1**. In fact the glassy matrix prevents the polar solvent molecules from reorienting around the solute molecule in the excited state. In other words, the Boltzmann distribution of the solvent reaction field stays fixed to that relevant to the ground state. As a consequence, symmetry-breaking phenomena are hindered in a glassy (or more generally solid) matrix, because the solvent cannot stabilize the polar excited state (for details about symmetry breaking see Sections 1.3 and 1.3.1).

For compound **2a**, the Stokes shift is absent also at room temperature. In fact quadrupolar chromophores belonging to class II have nonpolar ground and excited states, and do not undergo symmetry breaking, so that polar solvation has no effects on spectra. The appearance of vibronic structure in compound **1** as well as the narrow band-shapes for both compounds are related to the weaker effects of inhomogeneous broadening at low temperature, as explained for NR in the previous section.

Interesting effects appear when heating the sample. Top panels of Figure 2.14 show spectra of **1**, while bottom panels are relevant to **2a**. On the left, emission spectra are shown, while right panels show excitation spectra. Table 2.4 summarizes experimental results. Moving from a rigid matrix to a liquid solvent, a different behavior of the two compounds is observed. In fact when the solvent is liquid, symmetry breaking comes into action, but only for compound **1**. From 77K to 150K, a large red shift of the fluorescence band is observed for **1**, confirming symmetry-breaking in the

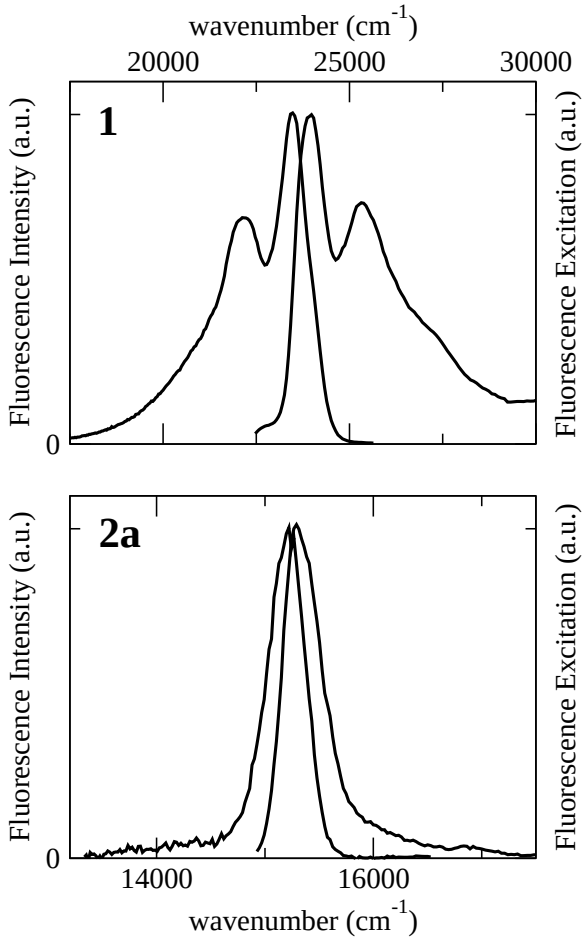

Figure 2.13: *Emission and excitation spectra of compounds **1** and **2a** in 2-MeTHF at 77K (glassy solvent)*

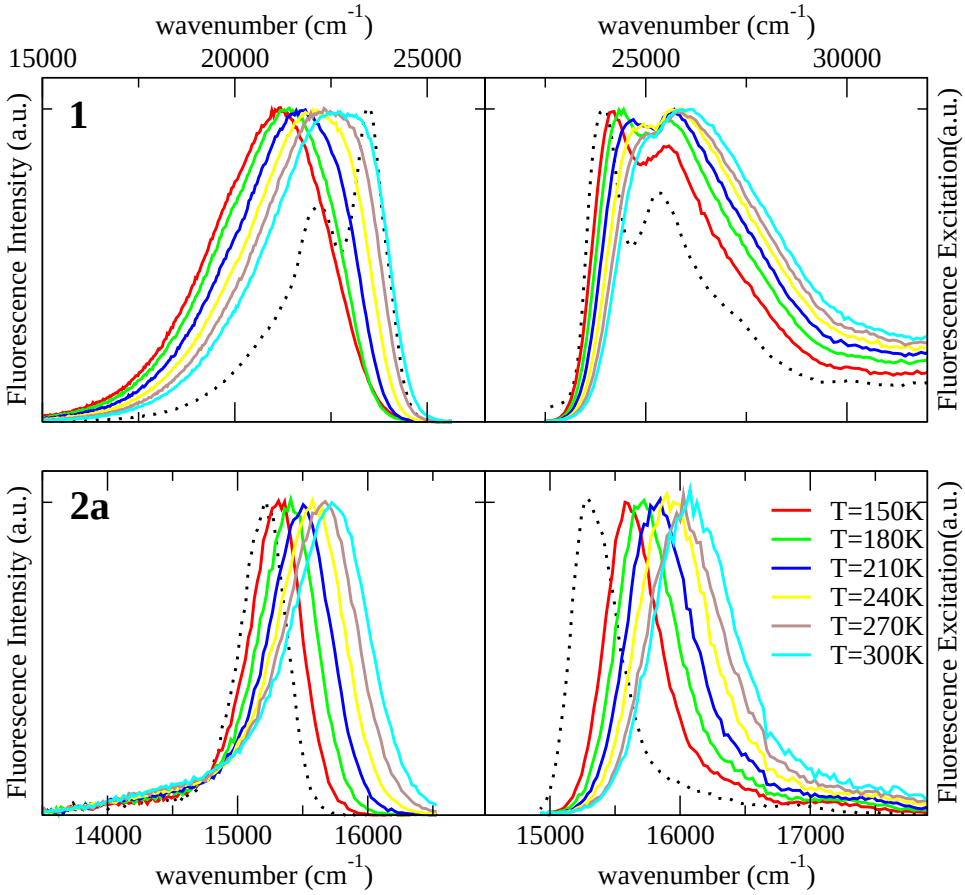

Figure 2.14: *Top panels: emission and excitation spectra of compound* ***1*** *in 2-MeTHF at different temperatures from 150K to 300K (liquid solvent). Bottom panels: emission and excitation spectra of compound* ***2a*** *in 2-MeTHF at different temperatures from 150K to 300K (liquid solvent).*

Table 2.4: *Experimental data about the thermochromic study of **1** and **2a**. Wavelenghts correspond to the maximum of excitation and emission spectra. In the last column the Stokes shift is reported.*

Compound	T(K)	λ_{exc}/nm	λ_{fluo}/nm	Stokes shift (cm^{-1})
1	77	418	426	449
	150	414	472	2968
	180	410	467	2977
	210	390	460	3902
	240	388	452	3649
	270	387	446	3418
	300	384	440	3314
2a	77	654	656	47
	150	641	652	263
	180	637	648	266
	210	632	645	319
	240	628	642	347
	270	625	638	326
	300	622	636	354

excited state. On the other hand, the fluorescence band of **2a** slightly shift to the blue: this different behavior is due to the fact that in **2a** the symmetry is always preserved, so that the solvent has minor effects on the spectra. Increasing further the temperature, the polarity of the solvent lowers, and as a consequence fluorescence spectra of **1** shifts to higher energies. Excitation and emission spectra of **2a** slightly shift to the blue as the temperature increases. The origin of this shift is not clear at present. The increase of the refractive index can cause a blue shift, as observed in the solvatochromic study of a similar compound in Figure 1.12. Anyway, the shifts observed due to temperature are too strong to be ascribed only to the change in the refractive index. The excitation spectra of **1** shift to the blue. In this case there is another effect that can affect the position of the band: the change of the strength of electron-phonon coupling. The increase of temperature leads to a progressive increase of intensity of the 0-1 transition that becomes more intense than the 0-0 transition above 210K.

Octupolar chromophores

The last system discussed is the octupolar chromophore **O1** of Section 1.4.1. We underline that the the dipole **D1**, whose spectra at low temperature were presented before (Figure 1.19), corresponds to one of the arms of **O1**

Figure 2.15 shows emission and excitation spectra at 77K in 2Me-THF, and spectra collected from 150K to 300K at intervals of 30K, while Table 2.5 lists the wavelenghts of the maxima relevant to excitation and emission, and the Stokes shifts. The vibronic structure is resolved at 77K (panel a of Figure 2.15), emission and excitation spectra are almost mirror images and the Stokes-shift is reduced. As for dipolar and quadrupolar dyes, the glassy matrix hinders the relaxation of the solvation coordinate. The residual Stokes-shift, as for the corresponding dipole **D1**, can be ascribed to the presence of a slow vibrational coordinate of the molecule. The reduction of inhomogeneous broadening with lowering the temperature is responsible not only for the narrow and resolved shape of the spectra, but also for the

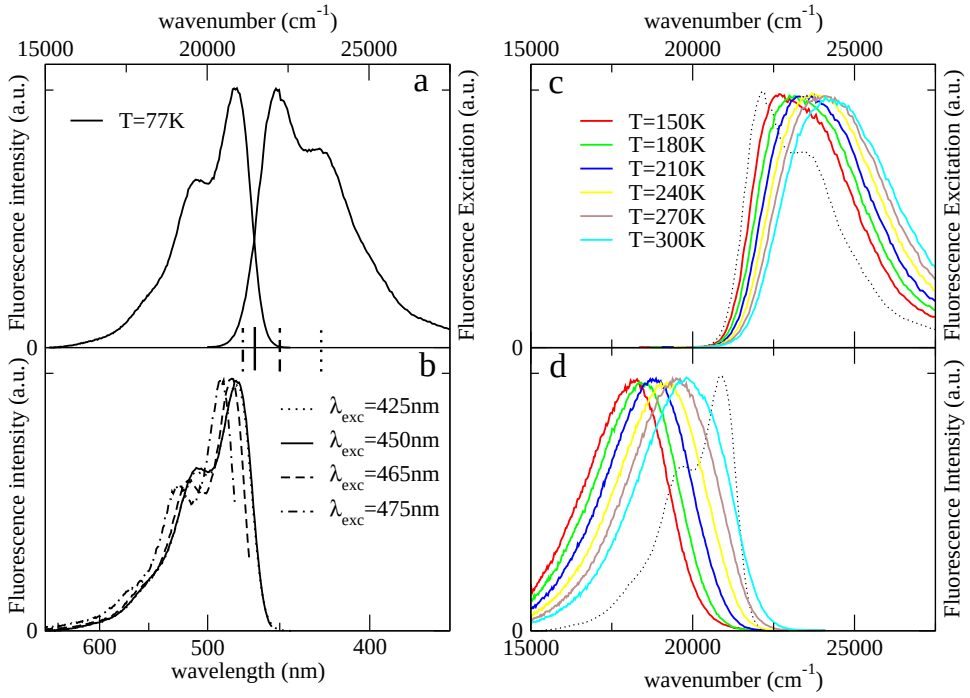

Figure 2.15: *Thermochromic study of* ***O1*** *(the structure of the molecule is sketched in Figure 1.17. Panel a: excitation and emission spectra at 77K in 2Me-THF (glassy solvent). Panel b: emission spectra at 77K collected exciting at different wavelengths; lines in between panel a and b mark the excitation wavelengths. Panel c and d: excitation and emission spectra, respectively, in 2Me-THF at different temperatures, from 150K to 300K (liquid solvent).*

Table 2.5: *Experimental data about the thermochromic study of **O1**. Wavelenghts correspond to the maximum of excitation and emission spectra. In the last column the Stokes shift is reported.*

T(K)	λ_{exc}/nm	λ_{fluo}/nm	Stokes shift (cm^{-1})
77	452	480	1290
150	441	550	4494
180	433	542	4645
210	426	532	4677
240	421	521	4560
270	415	513	4600
300	413	505	4410

red shift of the emission band according to the excitation wavelength, as reported in panel b of Figure 2.15. The reason of this behavior is exactly the same as explained for the corresponding dipole. Since in a rigid matrix only the vibrational relaxation is allowed, while the solvent relaxation is hindered, the molecules selected by the excitation wavelength emit from a state which has the same environment as in the absorption process. A high excitation wavelength selects molecules with high octupolar character, that emit at lower energy, according to equation 1.38.

As discussed in Section 1.4, and shown in the phase-diagram of Figure 1.15, all octupolar chromophores show multistability in the OPA allowed excited state. The symmetry-breaking phenomenon has important consequences on the spectral behavior at low temperature. In fact, increasing the temperature, the solvent becomes liquid, and hence it can induce the symmetry breaking of the system. The behavior of **O1** is similar to that observed for quadrupolar dye **1**, that also shows symmetry breaking. At 150K the solvent is liquid and more polar than at low temperature (Equation 2.19), so that it induces the localization of the excitation in one of the

three arms. As a consequence, the emission spectrum at 150K is strongly red shifted with respect to that at room temperature. Heating the sample, the polarity of the solvent decreases, and, as for all the systems sensitive to polarity, a blue-shift of the emission band is observed. The issue related to the concomitant blue-shift of the excitation band is also evident in this system, and it will be the subject of further investigations.

2.4 Fluorescence anisotropy

Fluorescence anisotropy is a spectroscopic technique based on the principle that upon excitation with polarized light, many samples also emit polarized light. The origin of this phenomenon is related to the presence of transition dipole moments for absorption and emission, which lie along specific molecular axes. In solution, fluorophores are randomly oriented. When exposed to polarized light, molecules with the absorption transition dipole moment oriented along the direction of polarization of the incident light are preferentially excited. Hence, the excited state population is not randomly oriented. Anisotropy measures the change in orientation of the transition dipole moment relevant to emission with respect to absorption.

Depolarization of emission originates from a number of different phenomena. One of the most common reason of depolarization is rotational diffusion. Since anisotropy measures the angular displacement between the absorption and emission transition dipole moments, if the rate of diffusion is faster then the rate of the emission, fluorescence is completely depolarized, and anisotropy is 0. The rate of diffusive motion depends both on the viscosity of the solvent, and on the shape and the dimension of the fluorophore. Small molecules are characterized by a fast diffusion rate. On the contrary, diffusion is hindered in viscous solvents, or in matrices. This is one of the reasons why we were interested in low temperature measurements (presented in the previous Section): glassy matrices are good environments to measure anisotropy of (multi)polar chromophores.

Fluorescence anisotropy finds interesting applications in biochemistry. The timescale of rotational diffusion of biomolecules is comparable to the decay time of many fluorophores. Hence, all factors that alter the rotational correlation time, also affect anisotropy. Fluorescence anisotropy is used for example to quantify protein denaturation, or to study the internal dynamics of proteins. [113]

Our interest in fluorescence anisotropy is related to the possibility to obtain information about the direction of the emission transition dipole moment. This is especially interesting for multibranched systems, where absorption and emission transition dipole moments can be aligned along different directions.

2.4.1 Theory and experimental setup for anisotropy measurements

The experimental setup for fluorescence anisotropy measurements is schematically illustrated in Figure 2.16. The sample is excited with polarized light, and emission is detected through another polarizer. Anisotropy is defined as follows:

$$r = \frac{I_{\parallel} - I_{\perp}}{I_{\parallel} + 2I_{\perp}} \tag{2.20}$$

where $I_{\parallel}$ is the intensity of emission measured when the polarizer before the detector (analyzer) is parallel to the excitation polarizer, while $I_{\perp}$ is the intensity of the emission when the analyzer is perpendicular to the excitation polarizer. Anisotropy is a dimensionless quantity, because the intensity $(I_{\parallel} - I_{\perp})$ is normalized by the total intensity $(I_{\parallel} + 2I_{\perp})$ [113].

The fundamental anisotropy of a sample of molecules in random frozen orientation is given by:

$$r_0 = \frac{2}{5}\left(\frac{3cos^2\beta - 1}{2}\right) \tag{2.21}$$

where β is the angle between transition dipole moments relevant to emission and absorption. The term r_0 is used to refer to anisotropy observed in the

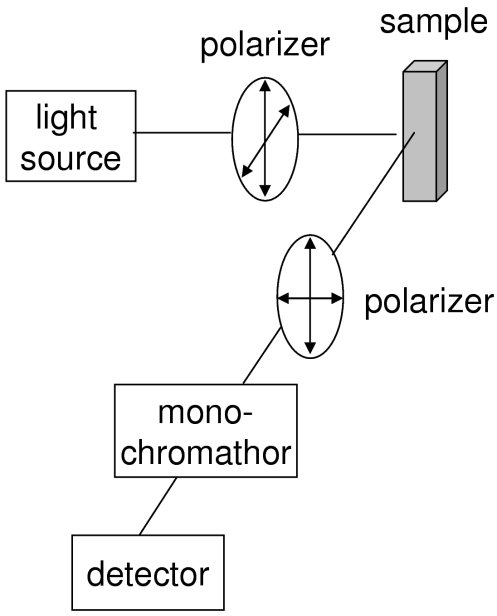

Figure 2.16: *Sketch of experimental setup for anisotropy measurements.*

Table 2.6: *Relationship between the angular displacement of transition moments β and the fundamental anisotropy r_0 for a sample of randomly oriented fluorophores.*

β (deg)	r_0
0	0.4
45	0.1
54.7	0
90	-0.2

absence of other depolarizing process such as rotational diffusion. Equation 2.21 is derived in Ref. [113]. Table 2.6 lists the values of the fundamental anisotropy for different values of β. The maximum value for anisotropy is 0.4, when the absorption and emission transition dipole moments are aligned. Anisotropy is 0 at the magic angle (54.7°), and the lowest value, $r_0 = -0.2$, is obtained when the two dipole moments are perpendicular. Remember that anisotropy is 0 also when some depolarization effect occurs.

Measurements of the fundamental anisotropy r_0 require special conditions. In order to avoid rotational diffusion, the samples are examined in solvents forming transparent glasses upon (fast) cooling (see Table 2.1). Since the matrix is rigid, photoselection plays a main role, as it will be discussed in the next Section. Moreover, solutions must be optically diluted (absorbance < 0.1) to avoid depolarization processes due to internal absorption and subsequent emission of photons, or due to energy transfer.

Two methods are commonly used to measure anisotropy: the L-format method, in which a single emission channel is used, and the T-format where both the parallel and perpendicular components are simultaneously detected, through separate channels [113]. Only the first one is described, corresponding to the setup available in the FluoroMax Instrument.

Assume that the sample is excited with polarized light, and emission is

observed after a monochromator (see Figure 2.16). The monochromator has a different transmission coefficient for vertically and horizontally polarized light, and, as a consequence, the rotation of the polarizer causes a change in the detected intensity even if emission is unpolarized. The G-factor takes into account the sensitivity of the detection system for vertically and horizontally polarized light:

$$G = \frac{I_{HV}}{I_{HH}} \tag{2.22}$$

where I_{HV} is the emission intensity when the excitation wavelength is polarized horizontally (H), while the analizer is polarized vertically (V) and I_{HH} is the emission intensity when both the polarizer and the analizer are horizontal. Consequently, anisotropy is defined as follows:

$$R = \frac{I_{VV} - GI_{VH}}{I_{VV} + 2GI_{VH}} \tag{2.23}$$

The excitation anisotropy spectrum is a plot of anisotropy detected at a fixed wavelength, as a function of the excitation wavelength. According to the Kasha's rule, the lowest singlet state is responsible for emission, independently of excitation. Since the detected wavelength is fixed, the emission dipole moment remains the same. On the other hand, the transition dipole moment relevant to absorption changes for different excited states, so that the anisotropy is different for different absorption bands.

The emission anisotropy spectrum is measured exciting the sample at a fixed wavelength and detecting the emission anisotropy at frequencies covering the whole emission band. The main difference with respect to the excitation anisotropy spectrum, is that in this case only two excited states are involved: the lowest singlet excited state, responsible for emission, and the state that absorbs the excitation wavelength (obviously, they can be the same state). Consequently, the emission anisotropy spectrum is generally a flat line along the whole emission band.

2.4.2 Calculation of anisotropy spectra

Excitation and emission anisotropy spectra of (multi)polar chromophores can be calculated using essential-state models. The models relevant to dipolar, quadrupolar and octupolar dyes were presented in Chapter 1, where they were already applied to calculate absorption and emission spectra. The calculation of anisotropy spectra is not trivial, because the special conditions required for the experimental setup have to be taken into account. In particular two tricky problems have to be considered:

1. Experimental spectra are collected in a glassy matrix at low temperature. This experimental condition has a major consequence related to inhomogeneous broadening. The excitation wavelength preferentially excites a subset of molecules out of the inhomogeneous distribution (those absorbing at the specific wavelength). The same molecules are responsible for emission. Since the matrix is rigid, the relaxation along the solvation coordinate is hindered, and only vibrational relaxation takes place before fluorescence. Therefore the emitting state is specific of the photo-selected molecules. This phenomenon is called *energy photoselection*. We have seen in the previous section that this phenomenon has important consequences also on emission spectra, causing a progressive red shift of the emission band when exciting on the red edge of the absorption band.

2. When exciting with a polarized light beam, molecules with the absorption transition dipole moment oriented along the direction of polarization are preferentially excited. This phenomenon is called *polarization photoselection*. Moreover, since anisotropy is measured in solutions of randomly oriented molecules, an appropriate averaging over all possible orientations has to be performed.

The first problem related to energy photoselection was solved considering the probability of each molecule to absorb the incident monochromatic photons, according to the ground-state energy distribution. Moreover, the

Boltzmann distribution remains the same for the ground state and for the excited state responsible for emission, because solvent relaxation is hindered in the glassy matrix. The relevant Boltzmann distribution is that obtained for the ground state at the glass-transition temperature.

The second problem is related to orientational photoselection. Ref. [114] suggests a very efficient way to calculate the fluorescence intensity for polarized excitation beams, when the sample is randomly oriented in a rigid matrix and is randomly oriented. The following expressions allow to estimate the fluorescence intensity, when the polarizers are parallel ($I_{\parallel}$) or perpendicular ($I_{\perp}$):

$$I_{\parallel} = \frac{|\vec{\mu}_{em}|^2 \cdot |\vec{\mu}_{abs}|^2 + 2(\vec{\mu}_{em} \cdot \vec{\mu}_{abs})^2}{15} \quad (2.24)$$

$$I_{\perp} = \frac{2|\vec{\mu}_{em}|^2 \cdot |\vec{\mu}_{abs}|^2 - (\vec{\mu}_{em} \cdot \vec{\mu}_{abs})^2}{15} \quad (2.25)$$

These two terms have to be weighted separately for the relevant Boltzmann distribution, to take into account the effects related to inhomogeneous broadening. This is a key point: $I_{\parallel}$ and $I_{\perp}$ are the experimental results of two separated measurements, while anisotropy comes from a processing of these data. Hence, the Boltzmann distribution has to be associated to these two terms, and not to the final anisotropy. The previous expressions of Equations 2.24 and 2.25, weighted for the Boltzmann distribution of the ground state, allow to calculate anisotropy using Equation 2.20.

Calculated spectra are discussed and compared with experimental data in the next section.

2.4.3 Experimental spectra and discussion

Anisotropy of dipolar and quadrupolar dyes

We start the discussion of fluorescence anisotropy from Nile Red [NR]. The structure and the spectral characterization at low temperature of NR are reported in Figure 2.9. NR is a dipolar chromophore. The transition in the visible region involves a charge transfer from the electron-donor moiety

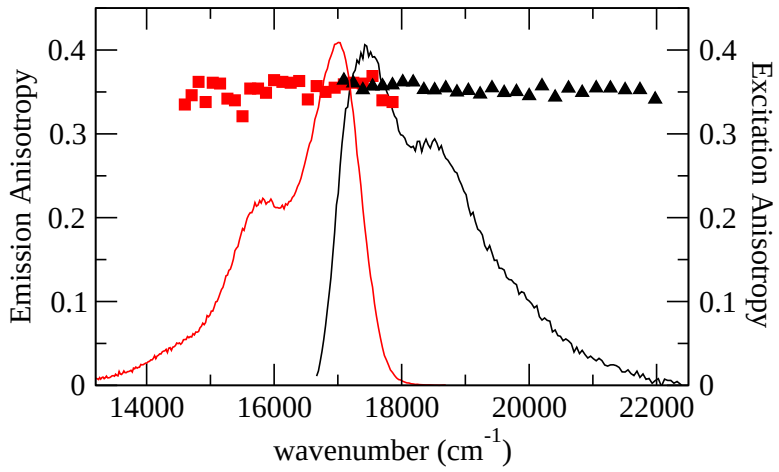

Figure 2.17: *Lines: excitation (black) and emission (red) spectra of NR in 2Me-THF at 77K. Black triangles: excitation anisotropy. Red squares: emission anisotropy. Anisotropy is very close to 0.4, suggesting that transition dipole moments relevant to absorption and fluorescence are almost collinear.*

towards the electron-acceptor moiety. Charge transfer is basically monodimensional, and fluorescence stems from the same charge-transfer state, so that the transition dipole moment relevant to emission is expected to be aligned along the same direction as the absorption dipole moment. Therefore we expect a value for anisotropy close to 0.4 (see Table 2.6). Figure 2.17 shows excitation and emission anisotropy measured in 2-MeTHF at 77K (glassy solvent). As expected, anisotropy is very high, and within excitation and emission bands it oscillates between 0.3 and 0.4. This results confirms that the absorption and fluorescence transition dipole moments are almost collinear.

We expect a high value of anisotropy not only for dipolar dyes, but also for all chromophores showing charge transfer along only one direction [115, 116]. Quadrupolar chromophores presented in Section 1.3 are treated as monodimensional compounds. Figure 2.18 shows emission and

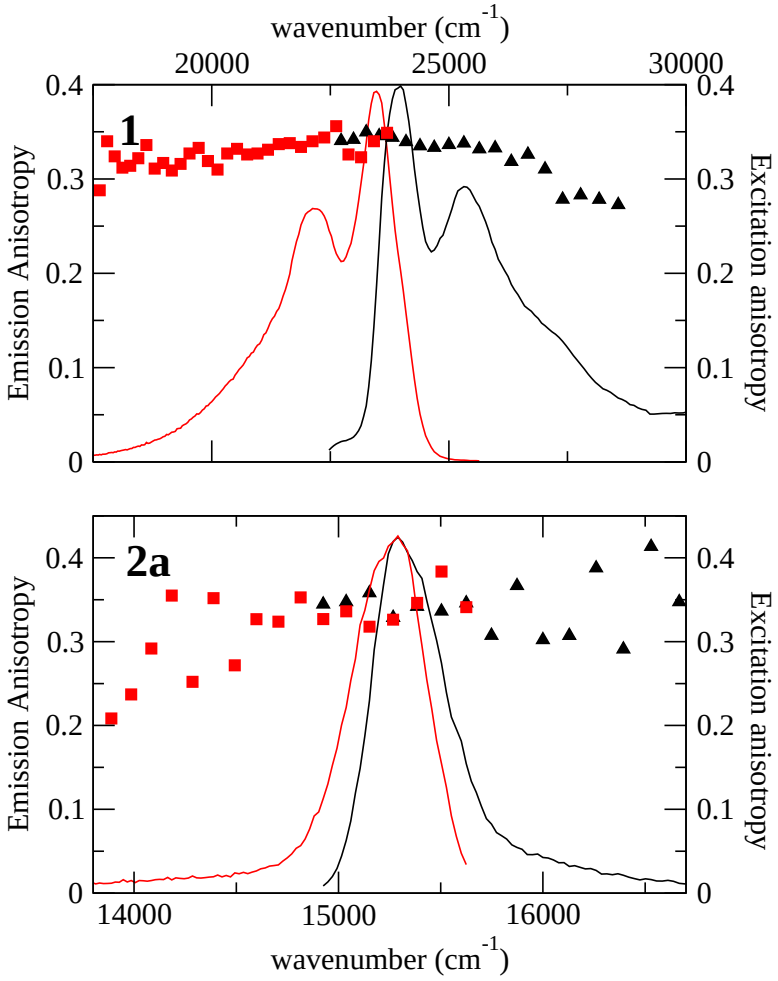

Figure 2.18: *Lines: excitation (black) and emission (red) spectra of a symmetry-breaking quadrupolar compound (top panel) and of a symmetry-preserving compound (bottom panel) in 2Me-THF at 77K. Black triangles: excitation anisotropy. Red squares: emission anisotropy. Anisotropy is higher than to 0.3, so that transition dipole moments relevant to absorption and fluorescence are almost collinear.*

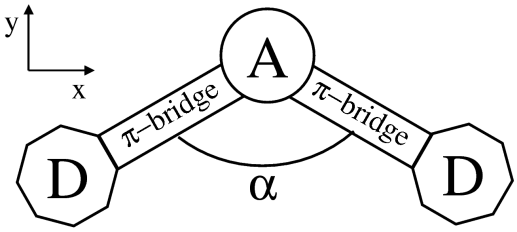

Figure 2.19: *Sketch of a V-shaped quadrupolar dye.*

excitation anisotropy of the quadrupolar dye **1** (Figure 1.10) and of **2a** (Figure 2.12) measured in 2-MeTHF at 77K. Again, absorption and fluorescence involve the same excited state, and the transition is a charge-transfer process, that takes place along the main molecular axis. Both excitation and emission anisotropy are higher than 0.3, confirming that the transition dipole moments relevant to absorption and fluorescence are almost aligned. Symmetry-breaking and symmetry-preserving systems show the same behavior because the molecule is monodimensional, and the excited state reached upon absorption is responsible also for emission. In other words, even if the excitation localizes on one of the two arms of the chromophore, the transition dipole moment relevant to fluorescence is always aligned along the main molecular axis.

The case of a V-shaped quadrupolar dye (Figure 2.19) should show somewhat different behavior. In such systems, the molecule is planar and two different components have to be considered to define the dipole moment operator. In this case, both the $|c\rangle$-state and the $|e\rangle$-state (Equation 1.22) are one-photon allowed, because of the lack of inversion center. In the following, expressions for the transition dipole moments are reported (the reference system is oriented to have the y-axis along the plane of symmetry of the molecule) :

$$\mu_{gc}^{x} = \sqrt{\rho}\mu_0 \sin(\alpha/2), \quad \mu_{gc}^{y} = 0 \tag{2.26}$$

$$\mu_{ge}^{x} = 0, \quad \mu_{ge}^{y} = -\sqrt{\rho(1-\rho)}\mu_0 \cos(\alpha/2) \tag{2.27}$$

where α is the angle between the two arms of the molecules. If we consider the low-energy transition, the relevant dipole moment responsible for absorption is aligned along the x-direction. Since the transitions towards both excited states $|e\rangle$ and $|c\rangle$ are one-photon allowed and the transition dipole moments are perpendicular, we expect a different anisotropy response addressing the $|c\rangle$- or the $|e\rangle$-state. In fact, according to the Kasha's rule, the lowest singlet state is always responsible for fluorescence (in this case the $|c\rangle$-state). When the molecule is excited to the $|e\rangle$-state, we expect a low anisotropy, because absorption and fluorescence transition dipole moments are not aligned. On the contrary anisotropy is expected be high when the excitation wavelength drives the system to the $|c\rangle$-state. We are planning experiments to check these predictions.

Anisotropy of octupolar compounds

Octupolar compounds probably offer the most interesting discussion about fluorescence anisotropy. These compounds are planar and here we adopt the same coordinate system proposed in Section 1.4 and Figure 1.13. Octupolar dyes are described in terms of four electronic states: the ground state $|g\rangle$, the two degenerate states $|c_1\rangle$ and $|c_2\rangle$, and the dark state $|e\rangle$. Equation 1.41 reports the transition dipole moments towards the $|c_1\rangle$ and $|c_2\rangle$ excited states, which are mutually perpendicular. Inhomogeneous broadening removes the degeneracy between the two $|c\rangle$-states. This has important consequences on anisotropy spectra of octupolar compounds. In fact the CT absorption band is given by the superposition of the two transitions relevant to $|c_1\rangle$ and $|c_2\rangle$, that are hardly distinguishable because they have similar energies. On the contrary, anisotropy spectra offer the opportunity to distinguish between the two contributions, because their absorption transition dipole moments are orthogonal.

Experimental anisotropy spectra of compound **O1** (molecular structure shown in Figure 1.17) in 2Me-THF at 77K (glassy solvent) are reported in

Figure 2.20. Excitation anisotropy was detected at different wavelengths, and emission anisotropy was collected for different excitation wavelengths. The behavior is clearly different from that observed for dipolar or quadrupolar compounds. Excitation anisotropy is low on the blue edge of the absorption band, and it increases fast moving the excitation wavelength towards the red edge of the band. It does not depend upon the detecting wavelength. Instead, emission anisotropy strongly depends on the excitation wavelength, while it is barely affected by the emission wavelength. The value of emission anisotropy increases moving the excitation wavelength towards the red edge of the absorption band. Similar results were obtained for a few other octupolar compounds, as reported in Ref. [117, 118] but a clear picture that rationalizes the whole spectral behavior of this class of compounds was still lacking.

Experimental results reported above perfectly agree with the picture about octupolar chromophores presented in Section 1.4. Figure 2.21 reports anisotropy spectra calculated through the essential-state model, adopting the same parameters extracted to calculate linear absorption and emission spectra and two-photon absorption spectra (Table 1.6). The calculated emission spectrum is shifted to the blue with respect to the experimental data. In fact the calculation does not take into account any source of Stokes shift (such as torsional or conformational degrees of freedom), and hence the 0-0 transitions relevant to excitation and emission overlay. Both emission and excitation anisotropy spectra are perfectly recovered by calculation using essential-state models, demonstrating that inhomogeneous broadening is responsible for the unconventional anisotropy spectra of octupolar chromophores. In fact a solution of octupolar dyes in a polar solvent can be described as a collection of dyes each one feeling a slightly different reaction field as dictated by the Boltzmann distribution. Molecules in a vanishing reaction field experience a symmetric environment so that the $|c_1\rangle$ and the $|c_2\rangle$ states stay degenerate. On the opposite, for the molecules experiencing a finite reaction field the $|c_1\rangle$ - $|c_2\rangle$ degeneracy is removed as shown in Figure

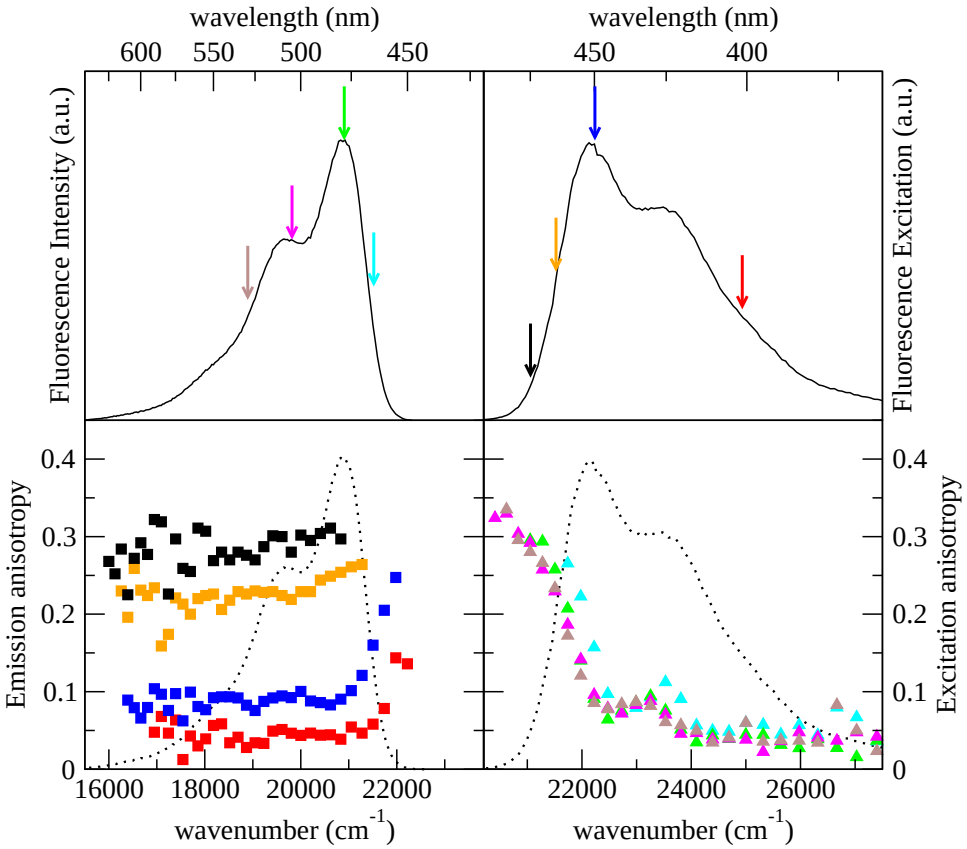

Figure 2.20: *Top Panels: Emission (left) and excitation (right) spectra of* ***O1*** *in 2Me-THF at 77K. Bottom-left panel: emission anisotropy spectra, collected exciting the sample at different wavelengths. Excitation wavelengths are indicated by the arrows on the excitation spectrum (top-right panel). Bottom-right panel: excitation anisotropy collected detecting fluorescence intensity at different wavelengths, indicated by the arrows on the emission spectrum (top-left panel). Emission and excitation spectra (dotted lines) are reported for reference.*

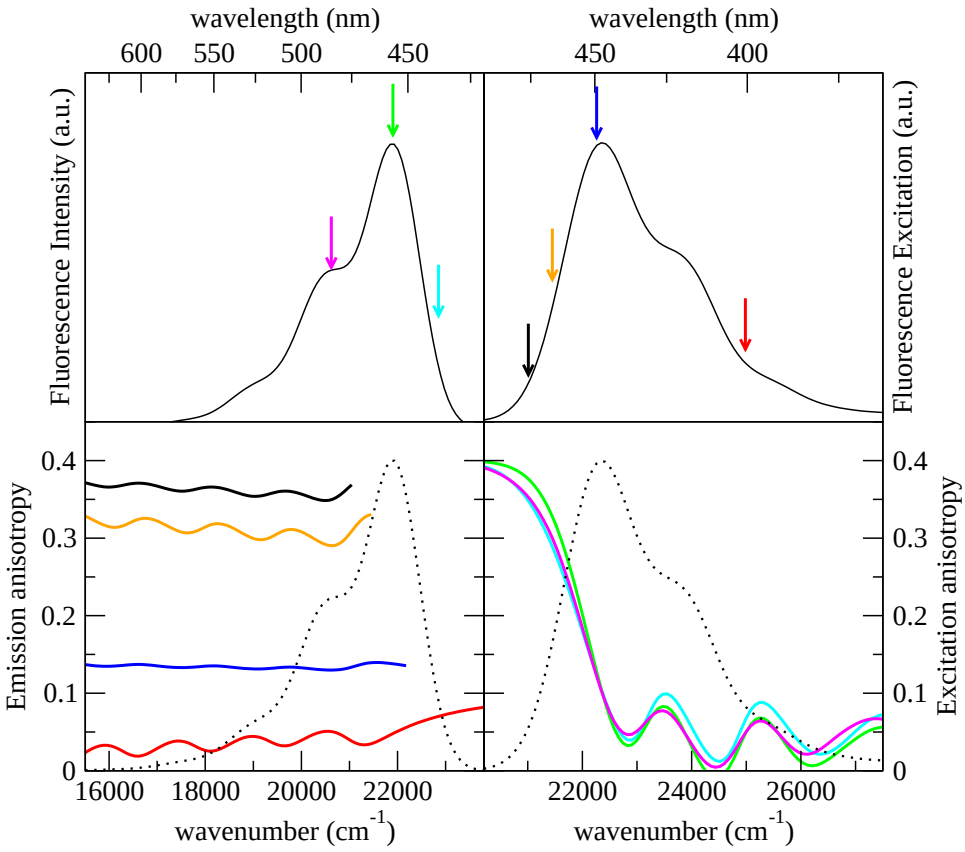

Figure 2.21: *Top Panels: Calculated emission (left) and excitation (right) spectra of* ***O1*** *in 2Me-THF at 90K (glass transition temperature). Bottom-left panel: calculated emission spectra (dotted line) and anisotropy spectra (continuous lines). Excitation wavelengths are indicated by the arrows on the excitation spectrum (top-right panel). Bottom-right panel: calculated excitation anisotropy for the excitation wavelengths indicated by the arrows on the emission spectrum (top-left panel). The excitation wavelengths are shifted to the blue with respect to the experimental ones, to account for the blue-shift of the calculated emission spectrum.*

2.22 (2-MeTHF is a solvent of intermediate polarity, so that inhomogeneous broadening has important effects). The presence of two different states, with a different orientation of the transition dipole moments and a different transition energy, is apparent from the change of excitation anisotropy within the absorption band. On the blue edge of the band, the excitation wavelength is mainly absorbed by the higher energy $|c\rangle$-state, that we identify as $|c_2\rangle$ (Figure 2.22). After absorption, the relaxation process drives the system to the $|c_1\rangle$-state and then emission occurs. In this case anisotropy is low because the transition dipole moment relevant to fluorescence is mainly aligned along the x-direction, while the transition dipole moment relevant to absorption is aligned along the y-direction. When the excitation wavelength moves towards the red edge of the absorption band, the $|c_1\rangle$-state is mainly excited, and the same state emits, so that transition dipole moment are collinear. This corresponds to high anisotropy values.

Excitation anisotropy does not change when the wavelength of detection is changed, because the state responsible for emission is always $|c_1\rangle$. The excellent agreement between experiment and calculation, is a further confirmation that essential-state models are able to rationalize the physics of CT-dyes. The good agreement is due to the appropriate description of inhomogeneous broadening.

Experimental anisotropy was measured also for crystal violet, the octupolar molecule reported in Figure 2.23. Data were collected in propylene glycol at 190K (Figure 2.24), because in 2Me-THF crystal violet shows a very broad emission band, probably due to aggregation effects. Anisotropy spectra show exactly the same behavior as **O1**, both for fluorescence and excitation. These anisotropy spectra confirm that the observed unconventional behavior is a general result in CT-octupolar chromophores dissolved in polar solvents. In fact, also in this case, polar solvation removes the degeneracy between the two $|c\rangle$-states, and as a consequence anisotropy is sensitive to the contributions from the two states $|c_1\rangle$ and $|c_2\rangle$, whose transition dipole moments are perpendicularly oriented. Essential states models reproduce

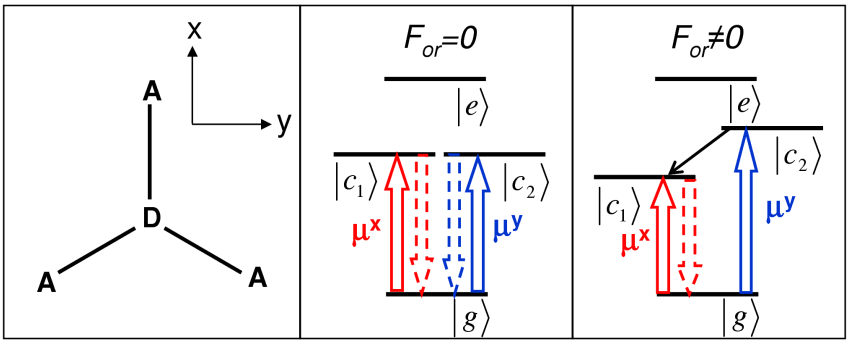

Figure 2.22: *Sketch of the polarization of absorption (full arrows) and fluorescence (dashed arrows) in the absence and in the presence of a reaction field F_{or}, i. e. of inhomogeneous broadening. Transition dipole moments relevant to the two $|c\rangle$-states are polarized perpendicularly. In the absence of a reaction field, corresponding to the case of apolar solvents, the states $|c_1\rangle$ and $|c_2\rangle$ are degenerate, and absorption and fluorescence processes can involve with equal probability both the two $|c\rangle$-states. Anisotropy is expected to be always 0.1, due to the anisotropy sum rule [113]. The case of $F_{or} \neq 0$ characterizes polar solvents due to thermal fluctuations. In these conditions the degeneration of the $|c\rangle$-states is removed. According to the Kasha's rule, only the lowest excited state ($|c_1\rangle$) emits, so that when the system is excited to $|c_2\rangle$ a fast relaxation process occurs, that drives the system towards $|c_1\rangle$. In this case emission is always polarized along the x-direction, while absorption can be polarized along both x- and y-directions. We expect low anisotropy when excitation drives the systems towards $|c_2\rangle$, while anisotropy is high when the system is excited to $|c_1\rangle$.*

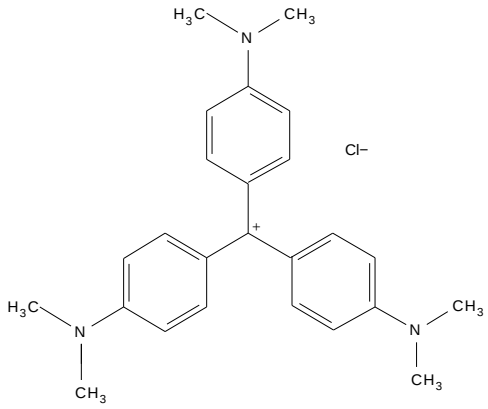

Figure 2.23: *Molecular Structure of crystal violet.*

in a quantitative way anisotropy spectra also of crystal violet (calculated spectra not shown).

To demonstrate that the observed spectral behavior of anisotropy is typical only of octupolar chromophores, we measured excitation and emission anisotropy of **D1** (Figure 1.17), the mono-dimensional arm of the octupolar compound **O1**. For this dipolar system, anisotropy is always around 0.35 (Figure 2.25), independent of the excitation or detection wavelength. In fact, even if inhomogeneous broadening is present (the solvent is always 2Me-THF) it does not affect anisotropy, because emission and absorption involve the same excited state.

We expect a different result for anisotropy of octupolar chromophores in non-polar solvents. In that case the two $|c\rangle$-states are perfectly degenerate, and excitation can involve the $|c_1\rangle$- or the $|c_2\rangle$- state with same probability (cf Figure 2.22). At the same time, fluorescence can stem from both states. Since the observed anisotropy is the average of all possible contributions, we expect a value of excitation and emission anisotropy always equal to 0.1. Experiments to confirm this theoretical predictions are still in progress. The major problem is related to the choice of the solvent: we need an apolar solvent, in which the compound is soluble and that presents a glass transition

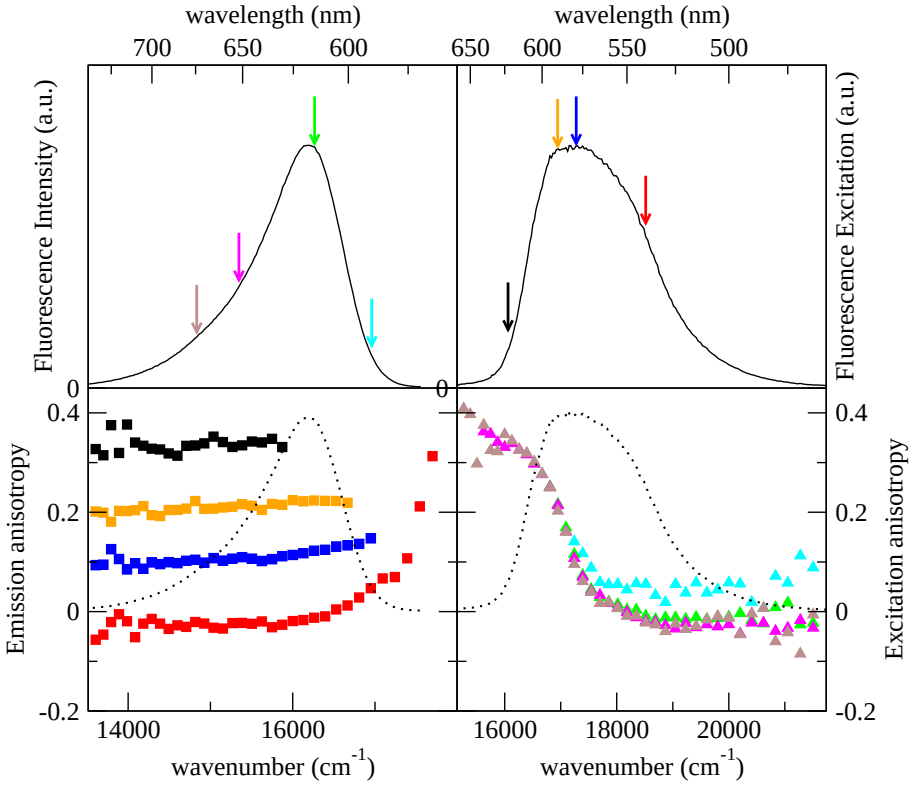

Figure 2.24: *Top Panels: Emission (left) and excitation (right) spectra of crystal violet (Figure 2.23) in propylene glycol at 190K. Bottom-left panel: emission anisotropy spectra, collected exciting the sample at different wavelengths. Excitation wavelengths are indicated by the arrows on the excitation spectrum (top-right panel). Bottom-right panel: excitation anisotropy collected detecting fluorescence intensity at different wavelengths, indicated by the arrows on the emission spectrum (top-left panel)*

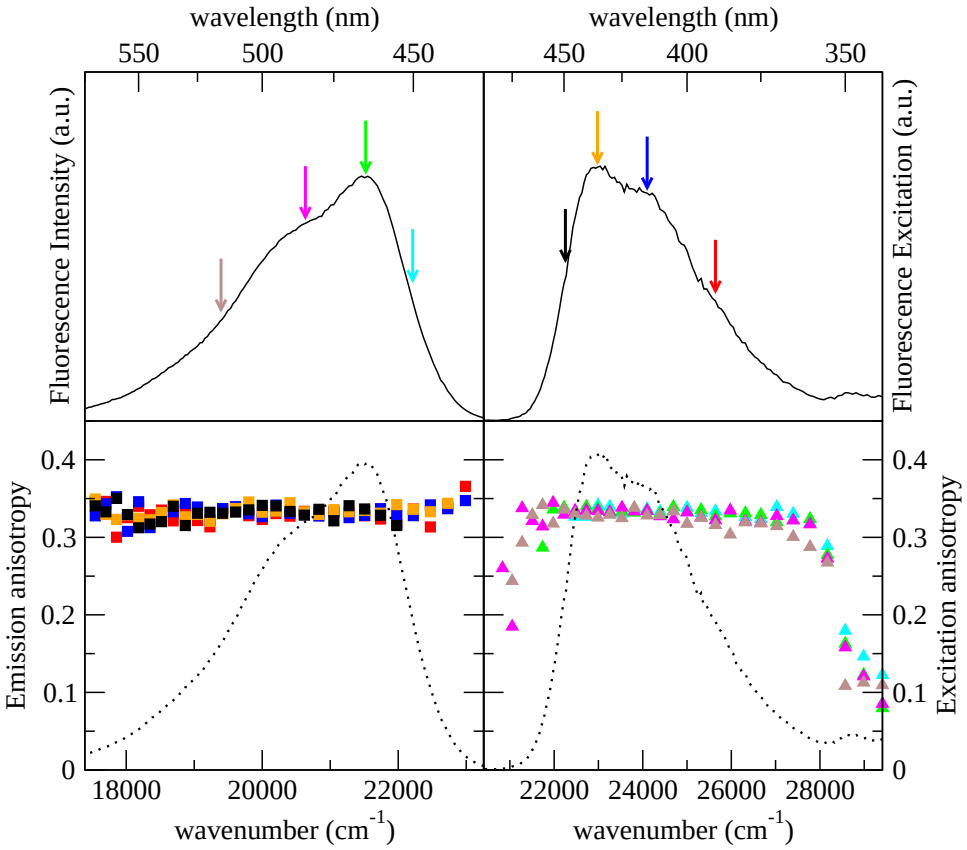

Figure 2.25: *Top Panels: Emission (left) and excitation (right) spectra of* ***D1*** *in 2Me-THF at 77K. Bottom-left panel: emission anisotropy spectra, collected exciting the sample at different wavelengths. Excitation wavelengths are indicated by the arrows on the excitation spectrum (top-right panel). Bottom-right panel: excitation anisotropy collected detecting fluorescence intensity at different wavelengths, indicated by the arrows on the emission spectrum (top-left panel)*

above 77K (vaseline oil seems to be a good candidate).

2.5 Conclusion

In this Chapter electroabsorption, low-temperature fluorescence and fluorescence anisotropy were discussed. Experimental results collected on a few representative chromophores were interpreted based on the developed essential-state models.

In the Section about electroabsorption, we proposed a new approach for the analysis of spectra. We demonstrated that the Liptay approach is not suitable for the analysis of electroabsorption of quadrupolar and octupolar compounds, due to the presence of dark states. On the contrary essential-state models offer an efficient way to calculate electroabsorption spectra, and to retrieve information from them.

Low-temperature absorption and excitation spectra of dipolar, quadrupolar and octupolar chromophores were measured in a range of temperature from 77K to 300K. One of the aims of this work was to setup the experimental technique. In fact, measurements at 77K in glassy solvents are the basis for fluorescence anisotropy spectra. Moreover, we investigated the role of inhomogeneous broadening, and, concerning quadrupoles and octupoles, the related symmetry-breaking phenomena. The results are promising, and further analysis is needed to fully understand the thermochromic behavior of CT dyes.

In the last Section the fluorescence anisotropy technique is presented. Anisotropy spectra allow to investigate the mutual rotation between the transition dipole moments relevant to absorption and fluorescence. In dipolar and quadrupolar dyes the charge-transfer process can be considered mono-dimensional. Hence transition dipole moments relevant to absorption and fluorescence are expected to be collinear. Experimental anisotropy results confirm this prediction. At variance, in planar octupolar dyes interesting effects appear in anisotropy spectra, because of the presence of

the two states whose transition dipole moments are mutually orthogonal. The discussion was focused on polar solvation that is responsible for the removed degeneracy of the $|c_1\rangle$- and $|c_2\rangle$-states, and hence for the peculiar fluorescence anisotropy spectra. Essential-state models reproduce in a quantitative way fluorescence anisotropy spectra, because they properly account for inhomogeneous broadening effects.

Chapter 3

Interacting chromophores: multichromophoric assemblies

3.1 Introduction

Charge-transfer chromophores are largely polarizable molecules and strongly respond to the charge distribution in the local environment [17, 22, 119]. Electrostatic intermolecular interactions are therefore expected to play a major role [43, 44, 47] in systems where several chromophores mutually interact via electrostatic forces, such as molecular crystals [46], films [120], aggregates, or multichromophoric assemblies [45, 48, 121, 122, 123, 124, 125]. One of the most impressive consequences of interchromophore interactions in clusters of dipolar dyes is the occurrence of bistability in crystals of polar chromophores that, predicted a few years ago, [43, 44], has been recently experimentally confirmed [46].

If properly understood, interchromophore interactions offer a powerful tool to design new materials characterized by *collective* and *cooperative* responses. Of interest in this respect is the work done on properly engineered molecules where two or more chromophores are held together by chemical

bonds: linear and nonlinear optical spectra of such multichromophoric assemblies confirmed the importance of electrostatic interactions in linear and nonlinear optical spectra [125, 126, 127, 128].

Essential-state models are useful to describe linear and nonlinear optical properties of multichromophores [22, 43, 47]. In fact, essential-state models can be used to analyze the optical spectra of the isolated chromophore in solution. This analysis yields to the definition of reliable environment-independent parameters for the chromophore at hand. This information is then transferred to multichromophoric assemblies. This bottom-up modeling approach has been successfully adopted to rationalize the spectral behavior of families of interacting systems. Moreover, models can predict the spectral behavior of the interacting systems, providing interesting guidelines to the synthesis.

For a cluster of N chromophores, the Hamiltonian is described as follows:

$$\mathcal{H} = \sum_{i=1}^{N} h_i + \frac{1}{2} \sum_{i,j} H'_{ij} \tag{3.1}$$

where h_i are the Hamiltonians of the isolated chromophores, while H'_{ij} represents the interaction between chromophores i and j. H'_{ij} can be described at different levels of approximation. We assume interactions between chromophores as electrostatic interactions, neglecting any intermolecular overlap: our models apply to systems where interchromophoric distances exceed the Van der Waals distances. Also the charge distributions on interacting chromophores can be modeled according to different approximations. In the simplest approximation, the charge distribution is described by point charges at the D and A location (the so called extended-dipole approach), as shown is Figure 3.1 for the case of two DA (dipolar chromophores). Even if this approximation is fairly rough, it allows to overcome the commonly adopted dipolar approximation. Within the dipolar approximation interactions between chromophores are described in terms of point-dipole interactions. The dipolar approximation is extremely poor in the description of non-dipolar charge distributions (for example for multichromophoric as-

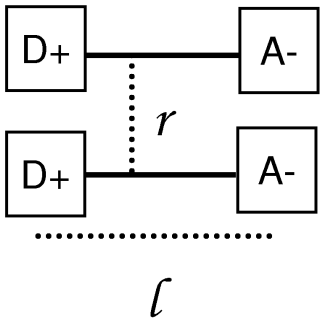

Figure 3.1: *Interchromophore interactions are calculated as electrostatic interactions, assuming that the charge distribution is constituted by point charges. Positive charges correspond to the electron-donor groups, while negative charges correspond to electron-acceptor groups of the zwitterionic basis states.*

semblies of quadrupolar or octupolar molecules). Moreover, the dipolar approximation works well only when the length of the dipoles is negligible with respect to the distance between them.

In this Chapter two dimeric systems (one constituted by two dipolar chromophores and the other by two quadrupolar chromophores) are described in terms of a bottom-up approach, and their optical properties are studied in solution. Moreover a film of dipolar chromophores is also discussed. Essential-state models for the chromophoric units take into account molecular vibrations as well as polar solvation. Modeling electrostatic interchromophore interactions while accounting for the screening by polar solvents is a delicate issue. In the simplest approximation, two different regimes can be considered for screening. The first one corresponds to a static (or quasi static) regime: in this regime the dynamics of screened charges is much slower than all relevant degrees of freedom of the solvent, so that the screening factor is properly described by the static dielectric constant of the solvent. The second regime applies to charges with a characteristics dy-

Table 3.1: *Dielectric constant, refractive index and the ratio between dielectric constant and the squared refractive index of solvents of different polarity.*

Solvent	ϵ^a	n^b	ϵ/n^2
Hexane	1.88	1.375	0.99
Toluene	2.4	1.497	1.07
Tetrahydrofurane	7.6	1.405	3.85
Dichloromethane	9.1	1.424	4.49
Acetonitrile	35.9	1.342	19.9
Dimethyl sulfoxide	46.7	1.479	21.3

^{a} = dielectric constant; ^{b} = refractive index

namics faster than the slow (orientational, vibrational) degrees of freedom of the solvent, but slower than the fast (electronic) degrees of freedom of the solvent. In this regime, typically corresponding to optical frequencies, interactions are screened by the squared refractive index (usually measured at the sodium D line). The difference between the two screening factors is minor in nonpolar solvents (see as an example data in Table 3.1) but is major in polar solvents. It is therefore important to devise methods that distinguish between static interactions, like those that determine the ground-state charge distribution in the chromophore, and dynamic interactions, like the interactions between transition dipole moments. This is possible adopting the so-called best excitonic approach already developed for clusters of dipolar dyes [43, 44, 126] and applied here for the dimer **D** of Figure 3.2. The same approach is exploited here for the first time for dimers of quadrupolar chromophores.

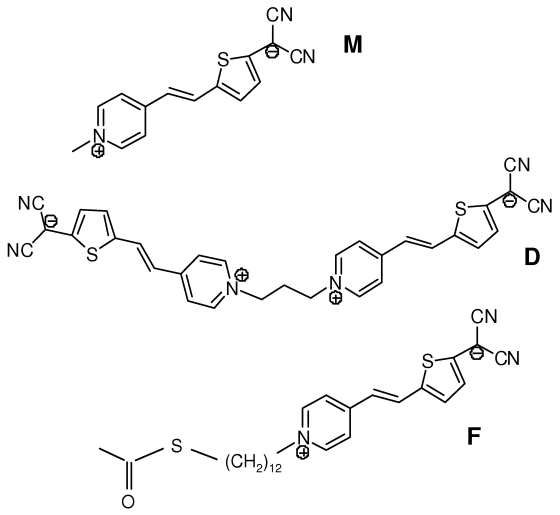

Figure 3.2: *Molecular structures of the dipolar zwitterionic monomer* ***M****, of the corresponding dimer* ***D*** *and of the functionalized chromophore* ***F*** *for the growth of self-assembled films on Au*

3.2 Dimer and film of a zwitterionic dipolar chromophore

In this section we present the experimental and calculated results relevant to a solvated dipolar chromophore, its dimer in solution as well as self-assembled films. The chemical structure of the relevant molecules is shown in Figure 3.2. **M** is a zwitterionic dipolar chromophore: the dicyanomethanide group acts as an electron-acceptor moiety, while the pyridinium ring is the electron-donor group. The dimer, **D**, is constituted by two **M** molecules, linked through the two pyridinium groups by a short alkyl chain, that ensures the absence of conjugation between the two chromophoric units. **F** was used to grow self-assembled films on Au. The chromophoric unit in **F** is the same as **M**, and the functionalization with a S-acetyl group allows the grafting on Au.

In the first part of this Section we describe the spectral behavior of **M** in terms of the two-state model presented in Section 1.2. In the second part, the model for the description of electrostatic interactions is presented and applied to the dimer **D**. A bottom-up approach is followed: the essential-state parameters extracted for the monomer **M** from experimental spectra in solution, are transferred to the dimer **D**, and electrostatic interactions are accounted for. In the last part of the Section, the model for interacting **M** chromophores is extended to rationalize the spectral behavior of self-assembled films grown from **F**.

3.2.1 Optical spectra of M in solution

The monomer **M** of Figure 3.2 is a zwitterionic push-pull chromophore. It was synthesized by the group of Prof. A. Abbotto of University of Milano-Bicocca (Italy), and found interesting applications in the field of second harmonic generation [129].

Because of its zwitterionic nature, **M** is insoluble in non-polar solvents: linear spectra were measured in $CHCl_3$, 2Me-THF and DMSO. The molar

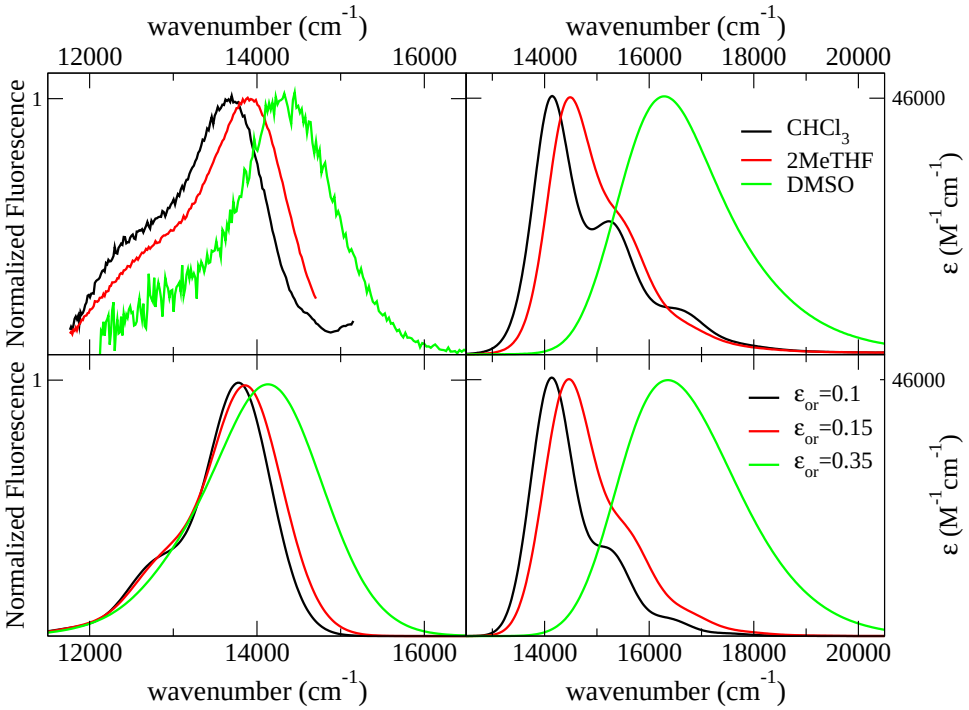

Figure 3.3: *Top panels: on the left, normalized experimental emission of* ***M*** *in solvents of different polarity; on the right, absorption spectra of* ***M*** *in solvents of different polarity, normalized to the molar extinction coefficient measured in DMSO. Bottom panels: Calculated emission (left) and absorption spectra (right) of* ***M****. Absorption spectra are normalized to the value of the molar extinction coefficient calculated in DMSO. The parameters used for calculations are reported in Table 3.3*

Table 3.2: *Spectroscopic data for **M** in solvents of different polarity.*

	λ_{abs} (nm)[a]	λ_{em} (nm)[a]	ϵ ($cm^{-1}M^{-1}$)[a]
$CHCl_3$	707	730	
2Me-THF	690	719	
DMSO	614	700	46100

[a] All data refer to the band maxima

Table 3.3: *The two-state model parameters for **M**.*

η/eV	$\sqrt{2}t$/eV	ϵ_v/eV	ω_v/eV	Γ/eV	μ_0 (D)	ϵ_{or}/eV
-0.26	0.76	0.19	0.13	0.04	23	0.1 ($CHCl_3$)
						0.15 (2MeTHF)
						0.35 (DMSO)

extinction coefficient was measured only in DMSO. Unfortunately emission of **M** is very weak, so that a reliable estimate the fluorescence quantum yield was not possible.

Experimental data are summarized in Table 3.2, and spectra are shown in Figure 3.3. As expected for a zwitterionic dipolar compound, **M** shows a negative solvatochromism both in absorption and fluorescence, i.e. the transition energy increases with the polarity of the solvent (top panels of Figure 3.3). Solvatochromism is more pronounced in absorption than in emission, confirming a highly polar ground state.

The spectral behavior of **M** is rationalized in terms of the two-state model presented in Section 1.2, accounting both for molecular vibrations and polar solvation. Calculated spectra are reported in the bottom panels of Figure 3.3, while Table 3.3 lists the parameters adopted for the modeling. Since the ground state of the molecule is dominated by the charge-separated

state, the energy gap η is set to a negative value, i.e. the D^+A^- state is lower in energy than the neutral DA state. The ground-state polarity is estimated ~ 0.77 in $CHCl_3$ and increases to ~ 0.84 in DMSO. Calculated spectra well describe the experimental solvatochromic behavior and the evolution of the band-shape with the polarity of the medium.

3.2.2 The model for interchromophore electrostatic interactions in solution

Understanding the behavior of multichromophoric assemblies in solution requires a detailed modeling of electrostatic interactions, also accounting for the screening by the surrounding solvent. As discussed above, two regimes can be considered for screening. In the static regime, interactions are screened by the dielectric constant, while in the second regime, typical of optical frequencies, electrostatic interactions are screened by the squared refractive index. To distinguish between static and optical screening, we adopt a step-by-step procedure: first we derive a mean-field Hamiltonian, that describes the ground-state properties of the dimeric unit, and accounts for static screening. Next we introduce excitonic interactions and ultraexcitonic terms, screened by the squared refractive index.

The Mean-Field Approximation

Equation 3.1 describes the Hamiltonian of a chain of interacting molecules. For a dimer constituted of two dipolar chromophores, the Hamiltonian is:

$$\mathcal{H} = h_1 + h_2 + V_{12}\hat{\rho}_1\hat{\rho}_2 \tag{3.2}$$

where $h_{1,2}$ are the Hamiltonians for the isolated molecules, that include the coupling with molecular vibrations and polar solvation, as described in Section 1.2. $\hat{\rho}_1$ and $\hat{\rho}_2$ are the ionicity operators of the chromophores, whose expectation values measure the weight of the zwitterionic state in the ground state, and define the ground state polarity. V_{12} describes electrostatic interactions between the two chromophores in the D^+A^- state. As shown in

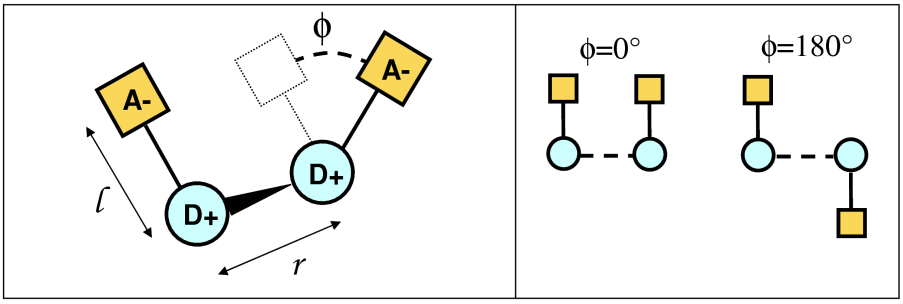

Figure 3.4: *Left panel: schematic view of the dimer geometry, with the definition of geometrical parameters. Right panel: top view of the two special cases* $\phi = 0°$ *and* $\phi = 180°$

Figure 3.4, we represent the zwitterionic form of the chromophore as a rigid rod of length l, with a positive point charge located on the donor site, and a negative point charge located on the acceptor site. To mimic **D** (cf Figure 3.2) the two chromophores are joined through the donor site by a rigid link of length r. Different geometries are defined by varying the angle ϕ from 0° (faced monomeric units) up to 180° (aligned monomeric units pointing in opposite directions). The following expression shows the ϕ dependence of the interaction energy:

$$V_{12} = \frac{14.4}{\epsilon}\left(\frac{1}{r} + \frac{1}{2\sqrt{\left(\frac{r}{2}\right)^2 + \left(l\sin\frac{\phi}{2}\right)^2}} - \frac{2}{\sqrt{r^2 + \left(l\sin\frac{\phi}{2}\right)^2}}\right) \tag{3.3}$$

where r and l are expressed in Å to get the interaction energy in eV. As long as we are interested in ground-state properties, electrostatic interactions are screened by the dielectric constant ϵ.

First we focus the attention on the electronic problem. Hamiltonian 3.2 is easily written and diagonalized on the basis obtained by the direct product of the two basis functions, DA and D^+A^- on each site. The relevant basis states for the dimer are reported in Table 3.4 . The dependence of the

Table 3.4: *Basis set for the dimeric structure*

wavefunctions	charge distribution	energy
Φ_1	$AD - DA$	0
Φ_2	$A^-D^+ - DA$	2η
Φ_3	$AD - D^+A^-$	2η
Φ_4	$A^-D^+ - D^+A^-$	$2\eta + V_{12}$

ground-state properties on the supramolecular arrangement can be described within the mean-field approach. In this picture the problem of interacting chromophores reduces to a single-molecule problem, each molecule experiencing the electric field generated by the other molecule. The mean-field Hamiltonian is:

$$\mathcal{H}_{el}^{mf} = -\sqrt{2}t\hat{\sigma} + 2\eta_{mf}\hat{\rho} \tag{3.4}$$

This mean-field Hamiltonian coincides with the Hamiltonian of the isolated molecule, but the η energy is substituted by an effective energy η_{mf} that accounts for the interaction of each chromophore with the average charge distribution on the other chromophore:

$$2\eta_{mf} = 2\eta + V_{12}\rho_{mf} \tag{3.5}$$

where ρ_{mf} is the mean-field ionicity that describes the charge distribution on each chromophore. The ρ_{mf} value is derived imposing self-consistency. Specifically, we start with a guess for ρ_{mf}, and calculate η_{mf} using Equation 3.5. This η_{mf} value is used to calculate a new estimate of ρ_{mf}, according to Equation 1.3. The procedure is repeated until successive ρ_{mf} values differ less than a predefined precision.

As discussed in Section 1.2, to describe optical properties of a DA chromophore, the two-state model must be extended to account for the coupling to a vibrational coordinate q, and a reaction field F_{or}. These slow coordinates are coupled to the charge distribution in each chromophore as

described in Equations 1.9 and 1.13. The complete mean-field Hamiltonian accounts in an averaged form for the interactions between the two chromophores, and for the coupling to slow (vibrational and environmental) degrees of freedom. This Hamiltonian has the form of 3.4, but with a renormalized η_{mf}:

$$2\eta_{mf} = 2\eta + V_{12}\rho_{mf} - 2\epsilon_v\rho_{mf} - 2\epsilon_{or}\rho_{mf} \tag{3.6}$$

The complete mean-field Hamiltonian is diagonalized, following the same self-consistent procedure described above, to obtain the ground state $|g\rangle$ and the excited state $|c\rangle$, with excitation energy E_c.

The excitonic approximation and the ultraexcitonic terms

The interchromophore interactions that enter the mean-field Hamiltonian apply to static charges and are therefore screened by the static dielectric constant. However, the energies of optical excitations are strongly affected by excitonic interactions, that describe electrostatic interactions between transition dipole moments. Transition dipoles oscillate at optical frequencies, and hence excitonic interactions are screened by the squared refractive index [130, 131, 132, 133].

The excitonic model only accounts for the mixing of states with the same exciton number. To better understand the physics of the system, and to properly account for the different screening in the excitonic picture with respect to the mean-field interactions, we redefine the Hamiltonian in the so-called best excitonic basis [43, 44, 47, 48, 126]. The best excitonic basis functions are the direct product of the mean-field eigenstates $|g\rangle$ and $|c\rangle$ obtained from the diagonalization of the mean-field Hamiltonian for the two monomeric units, as listed in Table 3.5 together with their mean-field energies. Ψ_1 is the direct product of the two ground states of the monomers, and represents the ground state of the dimeric unit. Two states, Ψ_2 and Ψ_3 have a single excitation, while the higher-energy state Ψ_4 has a double excitation.

Table 3.5: *Excitonic Basis set for the dimeric structure.*

wavefunctions	mean-field	energy
Ψ_1	$\|g\rangle\|g\rangle$	0
Ψ_2	$\|g\rangle\|c\rangle$	E_c
Ψ_3	$\|c\rangle\|g\rangle$	E_c
Ψ_4	$\|c\rangle\|c\rangle$	$E_c + E_c$

The electronic mean-field Hamiltonian can be rewritten on the excitonic basis [44, 43, 126]:

$$\mathcal{H}^{el}_{mf} = \hbar\omega_{gc} \sum_{i=1}^{2} \hat{n}_i \tag{3.7}$$

where $\hat{n}_i = \hat{b}_i^+ \hat{b}_i$ counts excitons on the i-th site, while $\hat{b}_i^+$ ($\hat{b}_i$) is the hard-core boson operator that generates (annihilates) an exciton on the i-th site. ω_{gc} is the transition frequency, defined in Equation 1.6, with ρ fixed at the mean-field value. The excitonic Hamiltonian is then obtained by neglecting all off-diagonal elements of the Hamiltonian written on the excitonic basis, with the exception of those connecting degenerate states. The excitonic Hamiltonian reads:

$$\mathcal{H}_{ex} = V_{12} \left[\rho(1-\rho)(\hat{b}_1^+ \hat{b}_2 + \hat{b}_2 \hat{b}_1^+) + (1-2\rho)^2 \hat{n}_1 \hat{n}_2 \right] \tag{3.8}$$

where, in the best excitonic basis $\rho = \rho_{mf}$. The first term is the standard exciton hopping Hamiltonian, and it corresponds to J-type interactions in the standard excitonic model. [131, 134]. The second term accounts for exciton-exciton interactions, and it vanishes for non-dipolar molecules, being proportional to the squared mesomeric dipole moment $(1-2\rho)^2$.

The complete description of electrostatic interactions accounts also for ultraexcitonic terms. The ultra-excitonic Hamiltonian mixes up states with a different number of excitons, and hence it breaks down the mean-field

picture for the ground state:

$$\mathcal{H}_{uex} = V_{12}\left[\rho(1-\rho)(\hat{b}_1\hat{b}_2 + \hat{b}_2^+\hat{b}_1^+) + 2(1-2\rho)\sqrt{\rho(1-\rho)}(\hat{b}_2^+ + \hat{b}_2)\hat{n}_1\right] \tag{3.9}$$

The first term has the same origin as the exciton hopping, and is usually referred as the non-Heitler-London term: it describes the simultaneous (de-)excitation of two molecules. The second term applies only to polar molecules. Ultra-excitonic terms sizably enter in the Hamiltonian of systems with medium-large supramolecular interactions, and give rise to interesting and exotic effects, that cannot be rationalized within the excitonic approximation. One of the most interesting examples is multielectron transfer, induced by absorption of a single photon, in attractive clusters of polar-polarizable chromophores as described in References [43, 44].

The total Hamiltonian of the interacting system reads as follows:

$$\mathcal{H} = \mathcal{H}_{mf} + \mathcal{H}_{ex} + \mathcal{H}_{uex} \tag{3.10}$$

Interactions entering the mean-field Hamiltonian are screened by the dielectric constant, while excitonic and ultraexcitonic terms are screened by the squared refractive index.

The total Hamiltonian, including the coupling with molecular vibrations and polar solvation, reads [121, 126]:

$$\begin{aligned}\mathcal{H} &= \mathcal{H}_{mf} + \mathcal{H}_{ex} + \mathcal{H}_{uex} \\ &- \sqrt{2\epsilon_v}\omega\sum_i\left[\hat{q}_i\hat{\rho}_i + \frac{1}{2}(\omega_v^2\hat{q}_i^2 + \hat{p}_i^2)\right] \\ &- \sum_i F_{or}^i\mu_0\hat{\rho}_i + \frac{(F_{or}^i)^2}{2r_{or}}\end{aligned} \tag{3.11}$$

where $i = 1, 2$ runs over the two chromophoric units. The phononic operators $\hat{q}_i$ and $\hat{p}_i$ are described in Equations 1.10 and 1.11. ϵ_v is the vibrational relaxation energy, while ω is the frequency of the molecular vibration, as described in Section 1.2. $\hat{\rho}_i$ is the ionicity operator relevant to the i-th chromophore, written on the excitonic basis. Two different orientational fields

F^i_{or} are considered, one for each chromophoric unit. The coupled electron-vibrational problem is solved for fixed values of F^i_{or} via a numerically exact diagonalization, and spectra are calculated according to the procedure described in detail in Appendix A.

From the isolated molecule to the dimer: experimental and calculated optical spectra in solution

The dimeric compound **D** was synthesized by the group of Prof. A. Abbotto of University of Milano Bicocca (Italy). Unfortunately, the synthesized compound is not pure (the purification is difficult because of its doubly zwitterionic nature). Anyway, the impurities of the sample do not affect the position and shape of the spectra, while hinder absolute intensity measurements.

Figure 3.5 (top panels) shows the comparison between experimental spectra of dimer **D** and of monomer **M** in DMSO (**D** hardly dissolves in solvents of low and medium polarity). The absorption spectrum of **D** is red-shifted with respect to the absorption spectrum of the monomer by $\sim$450 cm^{-1}. The shift of the emission spectrum is much weaker ($\sim$150 cm^{-1}). The observed shifts of absorption and emission bands in the dimer, even if weak, demonstrate the presence of interchromophore interactions between the two chromophoric units.

The model described in the previous Section to account for screened electrostatic interactions is applied to the calculation of linear spectra of **D**. Following a bottom-up approach, the parameters adopted to describe the monomer **M**, are transferred to the dimer **D** (parameter derived for **M** are listed in Table 3.3). Bottom panel of Figure 3.5 shows calculated spectra for both the monomer **M** and the dimeric unit **D**. To model interchromophore interactions (Figure 3.4), the length of the molecule was set to 10 Å, while the distance between the two chromophoric units is set to 6 Å. The tilt angle ϕ is fixed at 180°. Results from modeling are in good agreement with experimental data: the model reproduces both the sizable red-shift of the absorption band and the weak red-shift of emission.

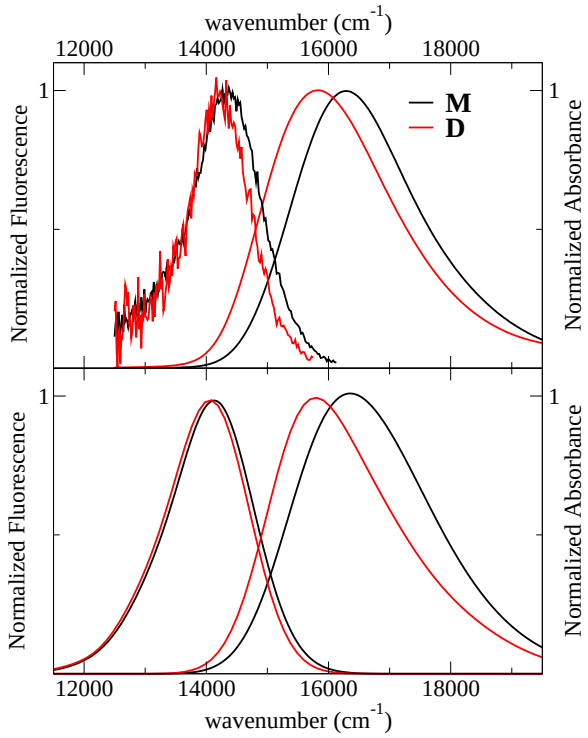

Figure 3.5: *Top panel: experimental absorption and emission spectra of the monomer* ***M*** *and the dimer* ***D*** *in DMSO. Bottom panel: calculated absorption and emission spectra. The parameters adopted to calculate the spectra relevant to the dimer, are the same adopted for the monomer, and are listed in Table 3.3. To calculate the interaction term, the length of the molecule is set to 10*Å*, the distance between molecules to 6*Å*, and the angle between the two molecule to* 180° *(see Figure 3.4).*

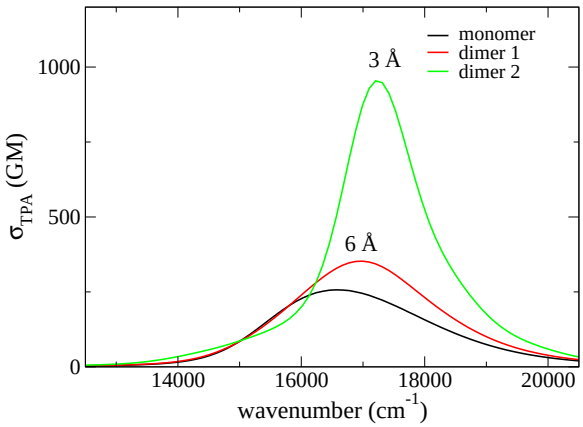

Figure 3.6: *Calculated two-photon absorption spectra for the monomer* ***M*** *and for dimers (for the dimers, intensities are divided by two, to show the response per chromophoric unit) at different distances, in the geometry shown in Figure 3.4 ($\phi = 180°$)*

The model adopted to describe the dimer can also predict nonlinear optical properties of the interacting system. In Figure 3.6 two-photon absorption spectra calculated for the monomer and dimers with different interchromophore distances are reported (intensities are normalized per chromophoric unit). Interactions induce a cooperative behavior: as shown in Figure 3.6, we expect a sizeable increase of the two-photon intensity (per branch) in the dimeric system, especially when the distance between the two chromophores is small. This result is general: attaching two dipolar zwitterionic chromophores from the two donor groups, or equivalently from the acceptor groups, to form a dimeric structure with $\phi \sim 180°$, we always expect an increase of the two-photon response. This is an example of how essential-state models can provide guidelines for the synthesis of engineered multichromophoric systems, optimized for one or more specific responses.

3.2.3 From solvated dye to self-assembled films on gold

Films of **F** were grown by self-assembly on a layer of gold deposited on glass (the S-acetyl group allows the grafting on Au). We briefly describe the procedure followed to grow self-assembled films:

1. The slides of glass, properly cut, were cleaned with the piranha solution (1 : 3, H_2O_2 30% : H_2SO_4 conc). This step is very important to allow a good adhesion of gold on glass. The slides were immersed for 10 minutes into the piranha solution, and then rinsed with ultra pure water and ethanol. The substrates were dried with N_2.

2. Au films were then grown on the glass slides by DC sputtering using an Edwards Sputter Coater S150B sputtering system.

3. A solution of **F** in dimethyl sulfoxide ($\sim$ 1mM) was prepared. We added an excess of NH_4OH to hydrolize the acetyl group and expose the sulfur for assembly on gold.

4. Freshly prepared gold surfaces were immersed for 20 hours into the solution, and stored in the dark.

5. Finally, the glasses were copiously rinsed with ultra pure water and ethanol, to remove molecules not grafted on the surface, and then dried with N_2.

The spectroscopic characterization of molecular monolayers self-assembled on gold is not trivial. Vibrational spectroscopy can provide useful information about the polarity of the chromophores in the film. In fact, the stretching of the cyano groups, in the acceptor part of the dipolar chromophore, are sensitive to the variation of molecular polarity, as described in References [135, 120]. Hence, to investigate the molecular polarity, we measured infrared spectra both on powders of **F** and on films. For films we used the single reflection ATR (attenuated total reflection) technique, using a Germanium semi-sphere. Experimental data are shown in Figure

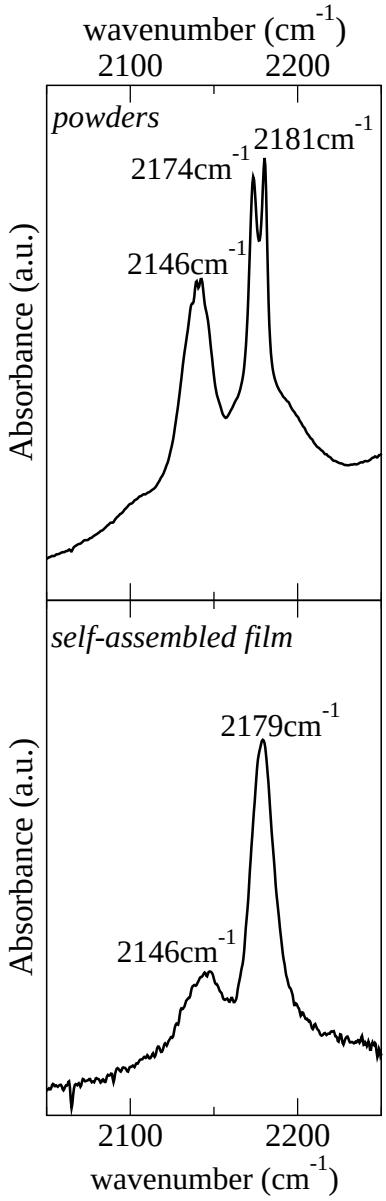

Figure 3.7: *Infrared spectra of the powder of* ***F*** *(top panel) and of its self-assembled film on gold (bottom panel). Only the region corresponding to CN stretching is shown. The CN stretching modes are sensitive to variation of the molecular polarity.*

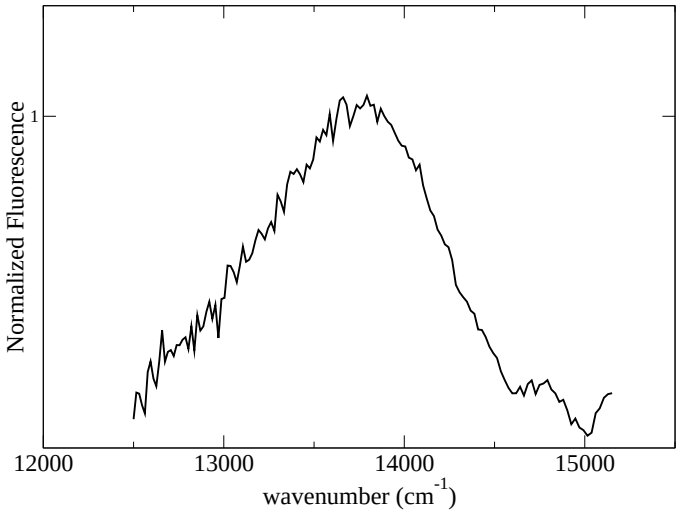

Figure 3.8: *Emission spectrum of the self-assembled film of* ***F*** *on Au.*

3.7: powder and SA films show similar vibrational spectra in the region of the CN-stretching. The comparison of these data with the stretching frequencies reported in References [135, 120], suggests a zwitterionic nature of molecules, both in powders and in the film.

Films were characterized also by electronic spectroscopy. From reflectance measurements we did not get reliable absorption spectra, because of problems related to the thickness of the gold substrate (the control of the thickness of samples is not available in the sputtering system used). Interestingly, fluorescence was detected from films, and the emission spectrum shows a broad band with the maximum located around 13700 cm^{-1} (cf. Figure 3.8). This result is quite surprising: in fact usually emission is quenched when the fluorophore is deposited on a gold substrate. In this case probably the alkyl chain is a good spacer between the gold substrate and the fluorophore, to prevent the fluorescence quenching.

Calculations were performed in order to estimate the tilt angle of molecules and the intermolecular distances in the films. We calculate the ground-state polarity and the fluorescence intensity as a function of the distance

between chromophores and of the tilt angle with respect to the normal to the surface, as shown in the colour maps of Figure 3.9. Thanks to these maps, we can locate a region where chromophores are zwitterionic and fluorescent, as suggested by experimental data.

To keep the computation numerically feasible, we model the film as a squared lattice of 3×3 dipolar molecules [136]. Molecular vibrations are accounted for only to define the mean-field ionicity. In fact explicit non-adiabatic calculations as performed for the dimer are impossible when many molecules with periodic boundary conditions (and hence many vibrational degrees of freedom) are considered. The non-adiabatic basis in fact increases as the n-th power (n=number of molecular vibrations) of the number of phonon states accounted for each degree of freedom. Moreover, the aim of the calculation is to get qualitative results about distances and tilt angle, so that molecular vibrations can be neglected without compromising the result.

Interactions are included accounting for the non-screened Madelung energy, so that we consider an effective distance between molecules, that takes into account the screening factor. In this case the screening problem is not so delicate as in solution. In fact, in an organic solid, the dielectric constant can be always considered of the same order of magnitude as the squared refractive index, so that the same screening factor can be considered for all the interaction terms (mean-field, excitonic and ultraexcitonic). Results are reported in Figure 3.9. The ϕ angle represents the angle from the normal to the surface: for $\phi = 0^\circ$ molecules are perpendicular to the substrate, while for $\phi = 90^\circ$ molecules lie on the substrate. The top panel of Figure 3.9 shows that the molecules in a film are zwitterionic for large values of the ϕ angle, i.e. when interactions between chromophores become attractive, or for large distances. At the same time, the bottom panel of Figure 3.9 indicates that the self-assembled film is sizeably fluorescent only for a large tilt angle from the normal to the surface. The superposition of the two plots, allows to locate the region satisfying the two requirements of zwitterionic chromophores

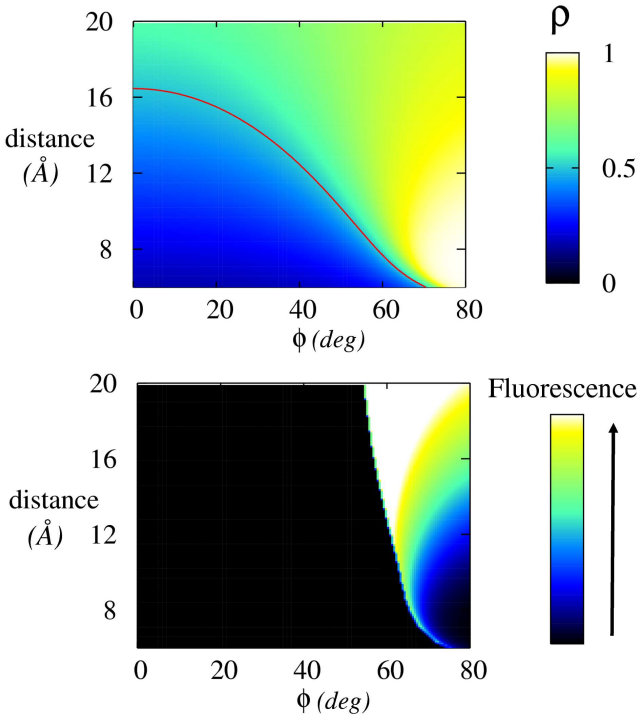

Figure 3.9: *Top panel:* ρ_{mf} *calculated for a 3×3 lattice of* $\boldsymbol{M}$ *as a function of the distance between molecules and of the angle from the normal to the surface (details about the calculation are reported in the text). The red line corresponds to* $\rho_{mf} = 0.5$. *Bottom panel: fluorescence intensity of the 3×3 lattice.*

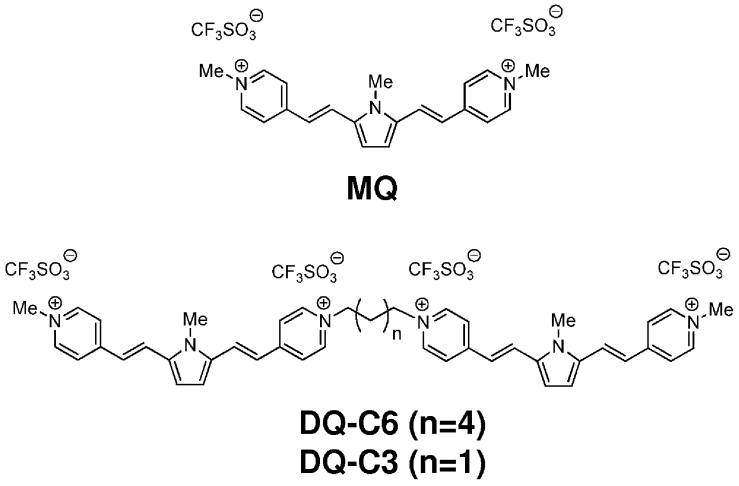

Figure 3.10: *Molecular structures of the model chromophore* ***MQ*** *and of the dimers* ***DQ-C6*** *and* ***DQ-C3****.*

forming a fluorescent film: modeling suggests that chromophores in the film are quite distant and their tilt angle from the normal to the surface is wide.

3.3 Dimers of quadrupolar chromophores

So far, studies on interacting chromophores for NLO have been limited to dipolar dyes. No systematic studies on discrete multichromophoric assemblies of quadrupolar dyes and on their two-photon absorption properties have been reported in the literature. On the other hand, quadrupolar systems are generally fairly efficient two-photon absorbers, so that looking at two-photon absorption of clusters of quadrupolar dyes is interesting [48]. On the basis of these premises, in this Section we extend the discussion of interchromophore interactions to quadrupolar systems and we present a work developed in collaboration with the group of Prof. A. Abbotto of University of Milano-Bicocca, Italy, (that synthesized the molecules) and the group of Prof. C. Ferrante of University of Padova, Italy, (that measured

the two-photon absorption spectra) [48].

MQ (Figure 3.10) has a large two-photon absorption cross section [137, 138, 139] and found interesting applications in cellular imaging [140, 141]. In this quadrupolar dye, the pyrrole group acts as a highly efficient electron-donor group, while the two pyridinium rings act as electron-acceptor groups. Our discussion starts with a detailed analysis of spectral data of **MQ**, for the definition of a reliable essential-state model.

Two dimers of **MQ** have been synthesized (**DQ-C3** and **DQ-C6** in Figure 3.10), where the two **MQ** units are joint by a saturated hydrocarbon chain (that ensure the lack of conjugation between the two units). Since **MQ** bears two positive charges, electrostatic interactions are expected to be important even in the ground state. Moreover, the two molecular arms of each **MQ** unit become nonequivalent in the dimer, and such symmetry lowering may induce important spectroscopic consequences. In the second part of this Section, we describe interchromophore interactions in the dimeric structures. Following a bottom-up approach, we start from the model developed for the monomer **MQ**, and we introduce electrostatic interactions between point charges, properly screened by the solvent.

3.3.1 Optical spectra of MQ: experimental data and modeling

Due to its multisaline nature, **MQ** is poorly soluble in nonpolar solvents. The top panel of Figure 3.11 shows absorption and fluorescence spectra of **MQ** collected in tetrahydrofuran (THF), in dimethyl sulfoxide (DMSO) and in acetonitrile (CH_3CN). We assume that the ion pairs exist as solvated free ions or solvent-separated ion pairs rather than contact ion pairs [142]. Figure 3.12 shows the two-photon absorption (TPA) spectrum collected in DMSO. Table 3.6 summarizes results for DMSO solutions. Appendices B and C report experimental protocols for fluorescence quantum yields and TPA measurements. As expected for quadrupolar chromophores (Section 1.3), the TPA state is located at higher energies than the one-photon ab-

Table 3.6: *Spectroscopic data for* ***MQ***, ***DQ-C6*** *and* ***DQ-C3*** *in DMSO solution.*

	λ_{abs} (nm)^a	λ_{em} (nm)^a	ϵ (cm$^{-1}M^{-1}$)$^{a-c}$	Φ (%)^{c,d}	λ_{TPA} (nm)$^{a-c}$	σ_{TPA} (GM)$^{a-c}$
MQ	522	612	70300	36	410-415	1892
DQ-C6	527	613	68500	35	410-415	1857
DQ-C3	532	615	61500	5.1	410-415	1807

[a] All data refer to band maxima.

[b] One- and two-photon absorption intensities are given per chromophore unit.

[c] Experimental uncertainty does not exceed ±5% for ϵ, ±10% for Φ, ±20% for σ_{TPA}.

[d] Fluorescence quantum yield, obtained using fluorescein in NaOH 0.1M ($\Phi = 0.9$) as a reference compound.

sorption (OPA) state.

Absorbance and fluorescence spectra are shown in the top panel of Figure 3.11: they are marginally affected by the polarity of the solvent, suggesting that both the ground and the excited states of **MQ** are characterized by vanishing dipole moments: **MQ** is classified as a class II quadrupolar dye according to the phase diagram of Figure 1.9 [39]. However, when compared with spectra of typical class II quadrupolar dyes, like the squaraine dye **2** (cf Section 1.3.1, Figure 1.12), spectra in Figure 3.11 show an important Stokes-shift, suggesting that the model proposed in Section 1.3 for optical spectra of quadrupolar dyes must be extended to account for other slow degrees of freedom. The insensitivity of the Stokes shift to the solvent polarity suggests that it is related to some internal degree of freedom, not breaking the molecular symmetry. Further support to the intramolecular nature of the Stokes shift is offered by the thermochromic data, shown in

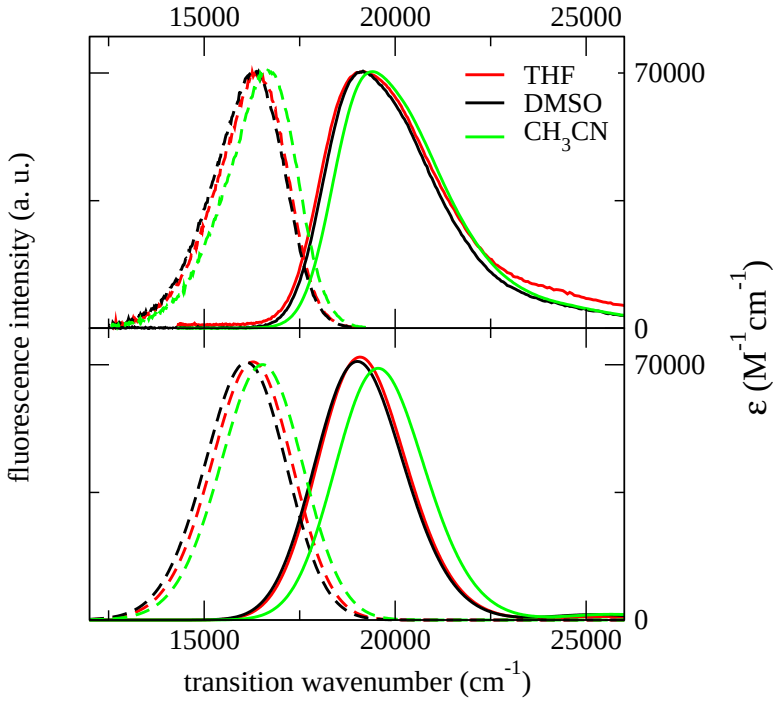

Figure 3.11: *Top panel: absorbance (continuous lines) and fluorescence (dashed lines) spectra of* ***MQ*** *in three solvents of different polarity. Absorption spectra in THF and CH_3CN are normalized to the molar extinction coefficient measured in DMSO. Bottom panel: Calculated absorption and fluorescence spectra (continuous and dashed lines, respectively) of* ***MQ*** *using the model parameters listed in Table 3.7 (THF and DMSO). For CH_3CN we adopt the same model parameters as for DMSO with the exception of* $\eta = 0.99\ eV$.

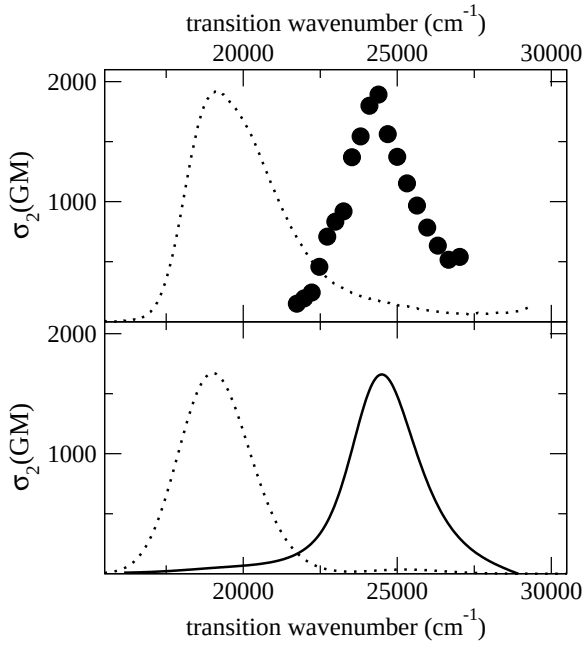

Figure 3.12: *Top panel: Symbols show the experimental TPA spectrum of* ***MQ*** *in DMSO. The dotted line refers to the normalized OPA spectrum of* ***MQ*** *in DMSO. Bottom Panel: Calculated TPA (continuous line) and the normalized OPA spectra (dotted line) of* ***MQ*** *using the model parameters listed in Table 3.7.*

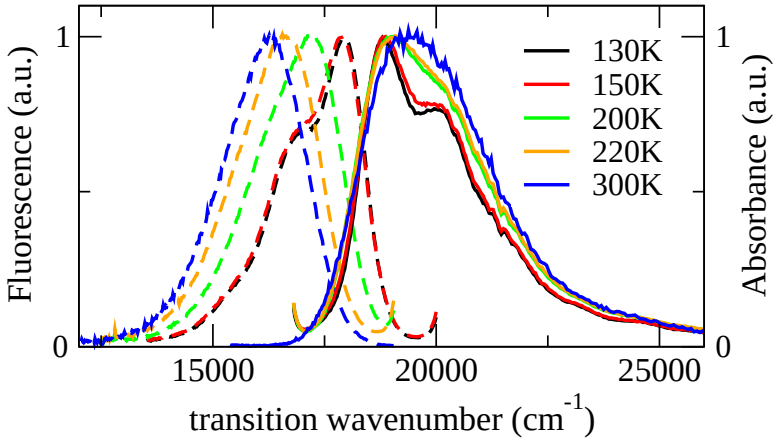

Figure 3.13: *Temperature evolution of fluorescence excitation spectra (continuous lines, proportional to absorption spectra) and emission spectra (dashed lines) of* ***MQ*** *in DMSO*

Figure 3.13. The Stokes shift observed in frozen DMSO solution at 220K (DMSO melts at 292K) is similar to that measured at high temperature and, in the frozen solvent, cannot be ascribed to the reorientation of solvent molecules. A sharp reduction of the Stokes shift is observed at about 150K, where both absorption and fluorescence spectra acquire a well-developed vibronic structure. Optical spectra are only marginally affected by a further decrease of temperature down to 130K. This behavior is consistent with the presence of a slow vibrational or conformational mode whose relaxation at high enough temperature is responsible for the observed Stokes shift as well as for the broadening of optical spectra. At low temperature, this conformational mode is frozen out, resulting in a sharp reduction of both the Stokes shift and of inhomogeneous broadening. With these considerations in mind, we propose here an essential-state model for optical spectra of **MQ** that represents an extension of the model presented in Section 1.3 (cf Ref. [39]) to account for the presence of a conformational degree of freedom [48].

MQ is a doubly charged quadrupolar dye, whose low-energy physics

can be understood accounting for the resonance between the three limiting structures: $AD^+A^+ \leftrightarrow A^+DA^+ \leftrightarrow A^+D^+A$. In the spirit of the essential-state models, these three resonating structures define the minimal basis set to describe electronic properties of **MQ**. The symmetric A^+DA^+ state, ϕ_0, is the lowest-energy state and plays the same role as $|N\rangle$ in neutral quadrupolar dyes (see Equation 1.15). Two degenerate states, ϕ_c and ϕ_s (the rationale for the c and the s lettering will be clear in the next section), correspond to AD^+A^+ and A^+D^+A, respectively, and represent states where an electron is transferred from the central donor toward one of the two lateral acceptor groups. A matrix element $-\sqrt{2}t$ mixes ϕ_0 with either ϕ_c or ϕ_s, to account for electron hopping along each molecular arm. The two degenerate states, ϕ_c and ϕ_s, are separated from ϕ_0 by an energy gap 2η. The electronic Hamiltonian reads:

$$\mathcal{H}_{el} = -\sqrt{2}t(\hat{\sigma}_c + \hat{\sigma}_s) + 2\eta(\hat{\rho}_c + \hat{\rho}_s) \tag{3.12}$$

where

$$\hat{\rho}_c = |AD^+A^+\rangle\langle AD^+A^+| \tag{3.13}$$

$$\hat{\rho}_s = |A^+D^+A\rangle\langle A^+D^+A| \tag{3.14}$$

$$\hat{\sigma}_c = |A^+DA^+\rangle\langle AD^+A^+| + |AD^+A^+\rangle\langle A^+DA^+| \tag{3.15}$$

$$\hat{\sigma}_s = |A^+DA^+\rangle\langle A^+D^+A| + |A^+D^+A\rangle\langle A^+DA^+| \tag{3.16}$$

In principle, the dipole moment of charged species is ill defined; however we take advantage of the symmetric nature of **MQ** and describe its charge distribution in terms of a monopole and a dipole located in the molecular center. Because the monopole is invariant in all basis states, it becomes irrelevant in the discussion of solvation. On the opposite, the dipole moment vanishes in the state ϕ_0 while ϕ_c and ϕ_s have equal and opposite dipole moments of magnitude μ_0. This dipole moment refers to states where an electronic charge is displaced along one of the molecular arms: μ_0 is therefore very large and, following Mulliken [51], we neglect all other matrix elements of the dipole moment operator on the chosen basis. Under this approximation

the dipole moment operator reads:

$$\hat{\mu} = \mu_0(\hat{\rho}_c - \hat{\rho}_s) \tag{3.17}$$

After an electron is transferred from the central donor toward one of the two acceptors, the relevant molecular arm relaxes. To account for this relaxation, we introduce two effective molecular vibrations, q_c and q_s with the same frequency ω_v and the same relaxation energy ϵ_v. q_c and q_s play the same role as q_1 and q_2 of Equation 1.28. Polar solvation enters the model with a reaction field F_{or}, which measures the electric field generated at the solute location by the reorientation of polar solvent molecules. The description of polar solvation is exactly the same proposed for neutral quadrupolar dyes in Section 1.3.

The large and solvent-independent Stokes-shift observed at room temperature, cannot be reproduced unless an additional slow degree of freedom is introduced. The insensitivity of the observed Stokes shift to the solvent polarity suggests that the relevant mode corresponds to a molecular deformation. Therefore, we introduce an effective conformational coordinate Q, with frequency ω_Q and relaxation energy ϵ_Q. The total Hamiltonian reads:

$$\begin{aligned}\mathcal{H} &= \mathcal{H}_{el} - \omega_v\sqrt{2\epsilon_v}q_c\hat{\rho}_c - \omega_v\sqrt{2\epsilon_v}q_s\hat{\rho}_s - \omega_Q\sqrt{2\epsilon_Q}Q(\hat{\rho}_c + \hat{\rho}_s) \\ &\quad -\mu_0 F_{or}(\hat{\rho}_c - \hat{\rho}_s) + \frac{1}{2}(\omega_v^2 q_c^2 + p_c^2) + \frac{1}{2}(\omega_v^2 q_s^2 + p_s^2) \\ &\quad +\frac{1}{2}\omega_Q^2 Q^2 + \frac{\mu_0^2}{4\epsilon_{or}}F_{or}^2\end{aligned} \tag{3.18}$$

where $\mathcal{H}_{el}$ is the electronic Hamiltonian of Equation 3.12, the second and the third terms describe the linear coupling of electrons to molecular vibrations, and the fourth and the fifth terms describe the coupling to the conformational coordinate and to the polar solvation reaction field, respectively. The last four terms describe the harmonic oscillators associated with the four slow degrees of freedom. We explicitly account for the kinetic energy associated with molecular vibrations (p_c and p_s are the conjugated momenta to q_c and q_s, respectively) while the conformational coordinate Q and the

Table 3.7: *The three-state model parameters for **MQ**.*

η/eV	$\sqrt{2}t$/eV	ϵ_v/eV	ω_v/eV	Γ/eV	μ_0 (D)	ϵ_{or}/eV
0.95	0.87	0.15	0.12	0.1	22	0.1 (THF)
						0.25 (DMSO)

solvation reaction field F_{or} are treated in the adiabatic approximation, and the relevant kinetic energy is disregarded.

In the isolated **MQ** unit the two molecular arms are equivalent and it is convenient to define symmetrized basis states, $|Z_\pm\rangle = (\phi_c \pm \phi_s)/\sqrt{2}$ and vibrational coordinates: $|q_\pm\rangle = (q_c \pm q_s)/\sqrt{2}$. Only the symmetric $|Z_+\rangle$ state is mixed to ϕ_0, while $|Z_-\rangle$ stays unmixed. On this basis the electronic Hamiltonian, dependent on slow coordinates, reads:

$$\mathcal{H}_{el}(q_+, q_-, \tilde{Q}, F_{or}) = \begin{pmatrix} 0 & -2t & 0 \\ -2t & 2\eta - \omega_v\sqrt{\epsilon_v}q_+ - \sqrt{\epsilon_Q}\tilde{Q} & -\omega_v\sqrt{\epsilon_v}q_- - \mu_0 F_{or} \\ 0 & -\omega_v\sqrt{\epsilon_v}q_- - \mu_0 F_{or} & 2\eta - \omega_v\sqrt{\epsilon_v}q_+ - \sqrt{\epsilon_Q}\tilde{Q} \end{pmatrix} \quad (3.19)$$

where the renormalized coordinate $\tilde{Q} = \omega_Q Q$ is introduced to eliminate any explicit reference to the conformational frequency, ω_Q, that becomes irrelevant in the adiabatic approximation. Both F_{or} and $\tilde{Q}$ are treated as classical coordinates, while q_+ and q_- are treated exactly, i.e., via a numerical diagonalization of the nonadiabatic Hamiltonian. Spectra are calculated following the procedure described in Appendix A.

Table 3.7 lists the model parameters for **MQ**, chosen to reproduce absorption and fluorescence spectra in THF and DMSO, and its TPA spectra in DMSO. The solvent polarity plays a minor spectroscopic role in **MQ**, resulting in large uncertainties in the ϵ_{or} estimates. Calculated linear and TPA spectra are shown in the bottom panels of Figure 3.11 and Figure 3.12, respectively. The comparison of both linear and two-photon absorption spectra shows a quantitative agreement between experimental and calculated data.

Absorption and fluorescence spectra collected in CH_3CN are slightly blue-shifted with respect to spectra measured in DMSO, in spite of the similar dielectric constant of the two solvents. This anomalous behavior can be ascribed to the different refractive index of the two solvents: the smaller refractive index of CH_3CN suggests a lower stabilization of AD^+A^+ / A^+D^+A states with respect to the other solvent and hence an increased η value [54, 62, 63]. In fact, spectra collected in acetonitrile are very well reproduced using the same model parameters adopted for DMSO (including ϵ_{or}), but a slightly larger $\eta = 0.99$ eV. We did not attempt a detailed analysis of the temperature dependence of spectra collected in DMSO (Figure 3.13). In fact, as explained in Section 2.3, both the solvent dielectric constant and refractive index depend on temperature, so that not only the solvent relaxation energy, but also η should be adjusted at each temperature, leading to an excessive proliferation of model parameters.

3.3.2 Optical spectra of dimers: modeling interchromophore interactions in solution

As expected due to the presence of multiple charges, the solubility of **DQ-C6** and **DQ-C3** dimers is rather poor in common organic solvents. Absorption and fluorescence spectra were successfully collected only in the strongly polar solvent DMSO. The top panel of Figure 3.14 shows experimental absorption and fluorescence spectra of **MQ**, **DQ-C6** and **DQ-C3** in DMSO, while the bottom panel shows the corresponding TPA spectra. Fluorescence and TPA spectra of the dimeric species do not show any significant deviation from monomer spectra, whereas OPA are red-shifted on going from **MQ** to **DQ-C6** and **DQ-C3** as a result of increasing interchromophore interactions.

Understanding this behavior requires a detailed modeling of electrostatic interchromophore interactions, also accounting for the screening from the surrounding solvent. To face this problem, we developed a non-trivial extension of the model presented in Section 3.2.2 for dimers of dipolar chromophores. We adopt the same step-by-step approach: first we derive a

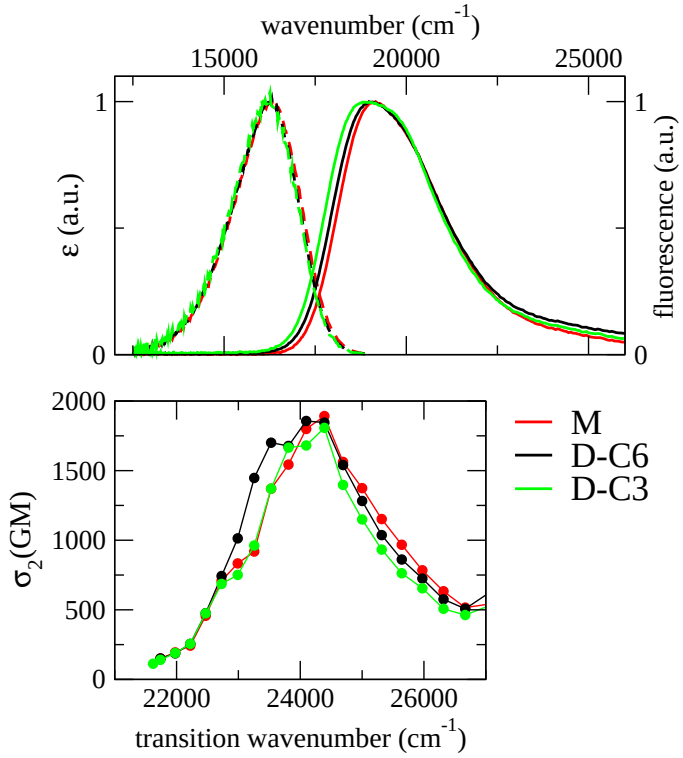

Figure 3.14: *Optical spectra of* ***MQ***, ***DQ-C6*** *and* ***DQ-C3*** *in DMSO. Top panel: absorption and fluorescence spectra are shown as continuous and dashed lines, respectively; all spectra are normalized to 1. Bottom panel: dots report TPA spectra; lines are drawn as guides to the eyes. The x-axis is the wavenumber of the transition, twice the wavenumber of the absorbed photon. The y-axis is the TPA cross section in GM: all data refer to normalized concentrations per monomeric unit.*

Table 3.8: *Basis set for the dimeric structure*

wavefunctions		charge distribution	energy	rescaled energy[a]
Φ_1	$\phi_0\phi_0$	$A^+DA^+ - A^+DA^+$	V_1	0
Φ_2	$\phi_0\phi_c$	$A^+DA^+ - AD^+A^+$	$2\eta + V_2$	$2\eta + v_2$
Φ_3	$\phi_c\phi_0$	$A^+D^+A - A^+DA^+$	$2\eta + V_2$	$2\eta + v_2$
Φ_4	$\phi_0\phi_s$	$A^+DA^+ - A^+D^+A$	$2\eta + V_3$	$2\eta + v_3$
Φ_5	$\phi_s\phi_0$	$AD^+A^+ - A^+DA^+$	$2\eta + V_3$	$2\eta + v_3$
Φ_6	$\phi_c\phi_c$	$A^+D^+A - AD^+A^+$	$2\eta + V_4$	$2\eta + v_4$
Φ_7	$\phi_c\phi_s$	$A^+D^+A - A^+D^+A$	$2\eta + V_5$	$2\eta + v_5$
Φ_8	$\phi_s\phi_c$	$AD^+A^+ - AD^+A^+$	$2\eta + V_5$	$2\eta + v_5$
Φ_9	$\phi_s\phi_s$	$AD^+A^+ - A^+D^+A$	$2\eta + V_6$	$2\eta + v_6$

[a] $v_i = V_i - V_1$

mean-field Hamiltonian for the dimeric species that, describing the ground-state properties, accounts for static screening. Extending the procedure developed and exploited for cluster of dipolar dyes, we then define the excitonic Hamiltonian, that accounts for optical screening.

Ground-state properties: the mean-field approximation

In **DQ-C6** and **DQ-C3** two **MQ** species are joined by a flexible chain through one of the A sites to define an $A^+DA^+ - A^+DA^+$ dimeric unit (Figure 3.10). Accounting for three resonating structures for each chromophore, yields to nine basis states for the dimers (Table 3.8). The two states A^+D^+A and AD^+A^+ of each one of the two chromophores, equivalent for the isolated **MQ** species, become nonequivalent in the dimer. For each **MQ** unit in the dimer we then define the two states AD^+A^+ and A^+D^+A as ϕ_c and ϕ_s depending on the central or side position of the neutral A moiety (the A site in one **MQ**-unit is central when linked to the other chromophore). Electrostatic interchromophore interactions affect the energy of the basis

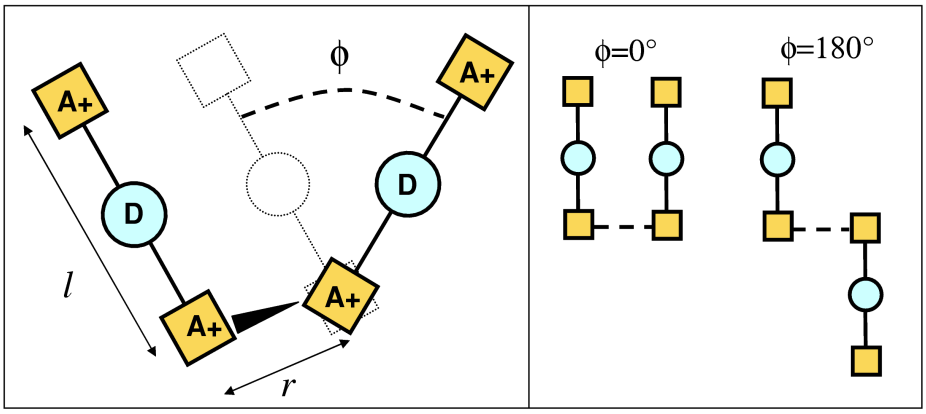

Figure 3.15: *Molecular structures of the model chromophore* ***MQ*** *and of the dimers* ***DQ-C6*** *and* ***DQ-C3***

states, as shown in the last two columns of Table 3.8. Specifically, the V_i energies (or the rescaled $v_i = V_i - V_1$) describe the electrostatic interactions between different charge distributions and can be calculated from the mutual arrangement of the monomers once a specific model is adopted for the charge distribution [17, 43, 44, 47]. As described for dimers of dipolar chromophores in Section 3.2.2, we represent each chromophore as a rigid rod of total length l, where two positive point charges are located, depending on the basis state, either at the two A groups at the extreme sites of the rod and/or at the D group in the middle (Figure 3.15). The two chromophores are connected through the A sites by a link of length r. Finally, different geometries are defined by varying the angle ϕ from 0° (faced **MQ** units) up to 180° (aligned **MQ** units pointing in opposite directions). To simplify the notation, we define the following distances:

$$\begin{aligned} a &= r \\ b &= \sqrt{r^2 + l^2} \\ c &= \sqrt{r^2 + l^2\,(1 - \cos\phi)^2 + l^2 \sin^2\phi} \end{aligned}$$

$$
\begin{aligned}
d &= \sqrt{r^2 + l^2\left(1 - \frac{1}{2}\cos\phi\right)^2 + \frac{l^2}{4}\sin^2\phi} \\
e &= \sqrt{r^2 + \frac{l^2}{4}} \\
f &= \sqrt{r^2 + \frac{l^2}{4}\left(1 - \cos\phi\right)^2 + \frac{l^2}{4}\sin^2\phi}
\end{aligned}
\tag{3.20}
$$

Explicit expressions for v_i energies in Table 3.8 read:

$$
\begin{aligned}
v_2 &= \frac{14.4}{\epsilon}\left(-\frac{1}{a} - \frac{1}{b} + \frac{1}{d} + \frac{1}{e}\right) \\
v_3 &= \frac{14.4}{\epsilon}\left(-\frac{1}{b} - \frac{1}{c} + \frac{1}{d} + \frac{1}{e}\right) \\
v_4 &= \frac{14.4}{\epsilon}\left(-\frac{1}{a} - \frac{2}{b} + \frac{2}{d} + \frac{1}{f}\right) \\
v_5 &= \frac{14.4}{\epsilon}\left(-\frac{1}{a} - \frac{1}{b} - \frac{1}{c} + \frac{1}{d} + \frac{1}{e} + \frac{1}{f}\right) \\
v_6 &= \frac{14.4}{\epsilon}\left(-\frac{2}{b} - \frac{1}{c} + \frac{2}{e} + \frac{1}{f}\right)
\end{aligned}
\tag{3.21}
$$

where distances are expressed in Å to get the v_i energies in eV. Being interested in static properties, v_i interactions are screened by the static dielectric constant ϵ.

The mean-field problem is more complicated than for dipolar chromophores, because, as discussed previously, ϕ_c and ϕ_s are non-equivalent in the dimeric unit, and we have to deal with two order parameters. First, we focus our attention on the electronic problem. The electronic Hamiltonian relevant to the dimeric unit is the sum of the two electronic hamiltonians for each unit and of the terms that describe electrostatic interchromophore interactions:

$$
\begin{aligned}
\mathcal{H}_{el} &= -\sqrt{2}t\sum_i(\hat{\sigma}_c^{(i)} + \hat{\sigma}_s^{(i)}) + (2\eta + v_2)\sum_i \hat{\rho}_c^{(i)} + (2\eta + v_3)\sum_i \hat{\rho}_s^{(i)} + \\
&\quad (v_4 - 2v_2 - 2v_3)\hat{\rho}_c^{(1)}\hat{\rho}_c^{(2)} + (v_6 - 2v_2 - 2v_3)\hat{\rho}_s^{(1)}\hat{\rho}_s^{(2)} + \\
&\quad (v_5 - v_2 - v_3)(\hat{\rho}_c^{(1)}\hat{\rho}_s^{(2)} + \hat{\rho}_s^{(1)}\hat{\rho}_c^{(2)})
\end{aligned}
\tag{3.22}
$$

where the $i = 1, 2$ apex on the $\hat{\sigma}$ and $\hat{\rho}$ operators runs on the two chromophoric units. In the ground state the two molecules are equivalent, so that

$\rho_c = \langle \hat{\rho}_c{}^{(1)} \rangle = \langle \hat{\rho}_c^{(2)} \rangle$ and $\rho_s = \langle \hat{\rho}_s{}^{(1)} \rangle = \langle \hat{\rho}_s^{(2)} \rangle$, where $\langle\rangle$ indicates the ground-state expectation value. We define the deviation operators $\hat{\delta}_{c,s}^{(i)} = \hat{\rho}_{c,s}^{(i)} - \langle \hat{\rho}_{c,s}^{(i)} \rangle$: the mean-field approximation neglects in the above Hamiltonian all nonlinear terms in the deviation operators. In this approximation, the problem reduces to the diagonalization of the Hamiltonian for an isolated chromophore subject to the electrostatic potential generated by the (frozen) charge distribution on the nearby chromophore:

$$\mathcal{H}_{el}^{mf} = -\sqrt{2}t \sum_i (\hat{\sigma}_c^{(i)} + \hat{\sigma}_s^{(i)}) + 2\eta_c \hat{\rho}_c^{(i)} + 2\eta_s \hat{\rho}_s^{(i)} \tag{3.23}$$

The mean-field Hamiltonian coincides with the Hamiltonian of the isolated **MQ** molecules, but the η energy is substituted by effective $\eta_{c,s}$ energies that account for the interaction of each chromophore with the average charge distribution on the nearby chromophore.

The two arms of each **MQ** unit are not equivalent in the dimer and two different η values are associated with the ϕ_c and ϕ_s states as follows:

$$\begin{aligned} 2\eta_c &= 2\eta + v_2 + (v_4 - 2v_2 - 2v_3)\rho_c + (v_5 - v_2 - v_3)\rho_s \\ 2\eta_s &= 2\eta + v_3 + (v_6 - 2v_2 - 2v_3)\rho_s + (v_5 - v_2 - v_3)\rho_c \end{aligned} \tag{3.24}$$

As for dimers of dipolar units, the problem is solved in a self-consistent way, with the requirement that the $\rho_{c,s}$ values entering the mean-field Hamiltonian matrix coincide with the squared coefficients of $\phi_{c,s}$ in the ground-state wavefunction. Specifically, we start with a guess for $\rho_{c,s}$, diagonalize the resulting mean-field Hamiltonian, calculate new estimates for $\rho_{c,s}$ as the squared coefficients of the $\phi_{c,s}$ functions, and repeat the procedure until successive $\rho_{c,s}$ values differ less than a predefined precision (typically set to 10^{-8}).

Each chromophoric unit in the dimer is described in terms of the same model derived for the isolated **MQ** unit. Therefore, we introduce two vibrational coordinates $q_{c,s}^{(i)}$ $(i = 1, 2)$, one conformational coordinate $\tilde{Q}^{(i)}$ and one solvent reaction field $F_{or}^{(i)}$ for each chromophore. We work in the adiabatic approximation, and use the Hellman-Feynman theorem to minimize

the ground-state energy and find the equilibrium positions for the slow coordinates as follows:

$$\begin{aligned}\left(q_{c,s}^{(i)}\right)_{eq} &= \frac{\sqrt{2\epsilon_v}}{\omega_v}\rho_{c,s} \\ \left(\tilde{Q}^{(i)}\right)_{eq} &= \sqrt{2\epsilon_Q}(\rho_c+\rho_s) \\ \left(F_{or}^{(i)}\right)_{eq} &= \frac{2\epsilon_{or}}{\mu_0}(\rho_c-\rho_s)\end{aligned} \tag{3.25}$$

Inserting these equilibrium coordinates into the coupling Hamiltonian in Equation 3.18, we end-up with a complete mean-field Hamiltonian that accounts in an averaged form for the mutual interaction between the two chromophores and for the coupling to vibrational, conformational and environmental degrees of freedom. This Hamiltonian has again the form in Equation 3.23, but with renormalized $\eta_{c,s}$ parameters:

$$\begin{aligned}2\eta_c &= 2\eta + v_2 + (v_4 - 2v_2 - 2v_3)\rho_c + (v_5 - v_2 - v_3)\rho_s - \\ &\quad 2\epsilon_v\rho_c - 2\epsilon_Q(\rho_c+\rho_s) - 2\epsilon_{or}(\rho_c-\rho_s) \\ 2\eta_s &= 2\eta + v_3 + (v_6 - 2v_2 - 2v_3)\rho_s + (v_5 - v_2 - v_3)\rho_c - \\ &\quad 2\epsilon_v\rho_s - 2\epsilon_Q(\rho_c+\rho_s) - 2\epsilon_{or}(\rho_c-\rho_s)\end{aligned} \tag{3.26}$$

The complete mean-field Hamiltonian is diagonalized, following the same self-consistent procedure described above, to get the ground state $|g\rangle$ and the two excited states $|c\rangle$ and $|e\rangle$, with excitation energies E_c and E_e respectively. The large screening of electrostatic interactions in DMSO results in minor effects of interchromophore interactions in the ground-state properties of the dimeric units. In particular, as discussed above, each chromophore in the dimer has a lower symmetry than the isolated **MQ** unit, but the effects of this symmetry lowering are very weak. Figure 3.16 shows the evolution of $\rho_c - \rho_s$ as a function of the intermolecular distance and of the torsion angle calculated in the mean-field approximation for a **DQ** unit in DMSO. We adopt for the **MQ** subunits the same model parameters as obtained in the previous section (Table 3.7), and calculate the electrostatic interchromophore interactions, v_i, setting $l = 8\mathring{\text{A}}$, and accounting for the screening

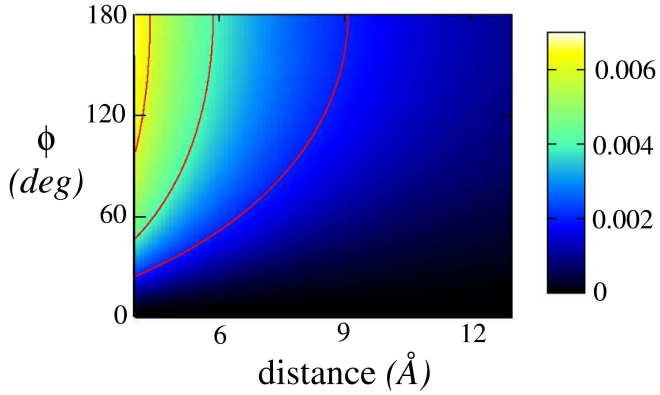

Figure 3.16: *Mean-field results for* ***DQ****. The color map shows* $\rho_c - \rho_s$ *as a function of* r *and* ϕ *(cf. Figure 3.15). Molecular parameters are taken from Table 3.7 and we set* $l = 8$Å*.*

due to the static dielectric constant of DMSO. When the two molecules are faced ($\phi = 0$), the symmetry of the isolated **MQ** unit is preserved, irrespective of the interchromophore distance, and $\rho_c - \rho_s = 0$. Deviations from this limit are observed at small distances and large ϕ angles. However, on an absolute scale, $\rho_c - \rho_s$ stays small, and in fact no hint of symmetry lowering is recognized in optical spectra of either **DQ-C6** or **DQ-C3**.

The excitonic approximation: linear and nonlinear absorption spectra

Here we adopt the same strategy developed for dimers of dipolar chromophores in Section 3.2.2, to single out excitonic interactions, and to screen them with the squared refractive index. According to the literature [43, 44, 47], we define the best excitonic functions Ψ_i, in Table 3.9, as the direct product of the mean field eigenstates $|g\rangle$, $|c\rangle$ and $|e\rangle$ obtained by the self-consistent diagonalization of the mean-field Hamiltonian for the two **MQ** units. Among the basis states we recognize the ground state, Ψ_1, two states

Table 3.9: *Excitonic Basis set for the dimeric structure.*

wavefunctions		mean-field energy
Ψ_1	$\|g\rangle\|g\rangle$	0
Ψ_2	$\|g\rangle\|c\rangle$	E_c
Ψ_3	$\|c\rangle\|g\rangle$	E_c
Ψ_4	$\|g\rangle\|e\rangle$	E_e
Ψ_5	$\|e\rangle\|g\rangle$	E_e
Ψ_6	$\|c\rangle\|c\rangle$	$E_c + E_c$
Ψ_7	$\|c\rangle\|e\rangle$	$E_c + E_e$
Ψ_8	$\|e\rangle\|c\rangle$	$E_c + E_e$
Ψ_9	$\|e\rangle\|e\rangle$	$E_e + E_e$

with a single c excitation (Ψ_2 and Ψ_3), two states with a single e excitation (Ψ_4 and Ψ_5), and states where both molecules are excited (Ψ_{6-9}). The corresponding mean-field energies (third column of Table 3.9) are simply the sum of the mean-field energies relevant to the two chromophores.

For interacting dipolar species (cf Section 3.2.2) the transformation to the best excitonic basis is analytical. For interacting quadrupoles instead we must rely on a numerical transformation. In particular the $|g\rangle$, $|c\rangle$ and $|e\rangle$ states obtained from the diagonalization of the monomer mean-field Hamiltonian, are expressed as linear combinations of the basis states ϕ_0, ϕ_c and ϕ_s on each chromophore, so that the Ψ_i functions are linear combinations of the Φ_i functions. Then a linear transformation allows to rewrite the dimer Hamiltonian from the Φ_i to the Ψ_i basis [48]. If the excitonic approximation works well [17, 22, 43, 44, 130, 131, 132, 133, 134], the off-diagonal elements of the Hamiltonian matrix written on the excitonic basis are small with respect to the excitation energies, and the off-diagonal matrix elements of the Hamiltonian have negligible effects, with the notable exception of those off-diagonal elements mixing up degenerate states (i.e. Ψ_2 and Ψ_3, Ψ_4 and Ψ_5,

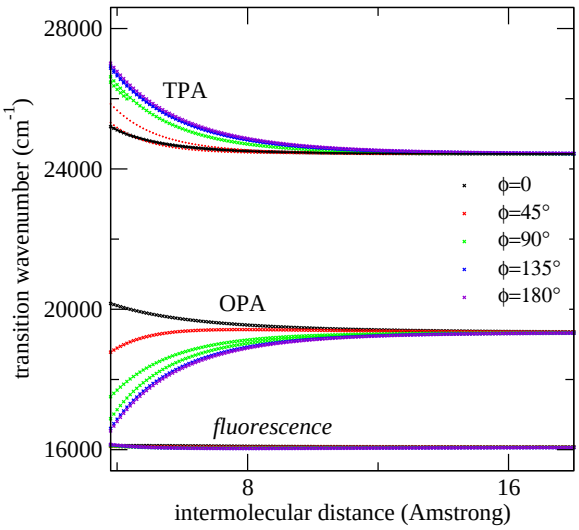

Figure 3.17: *Transition (OPA, TPA and fluorescence) energies calculated in the excitonic model for* ***DQ*** *as a function of the intermolecular distance and for different torsion angles (Figure 3.15). Molecular parameters are taken from Table 3.7, and* $l = 8$Å*. Only the most intense transitions are shown for OPA and TPA spectra. For some* ϕ *values, because of the lowering of the molecular symmetry due to electrostatic interactions, a splitting of the OPA and TPA transitions is observed.*

Ψ_7 and Ψ_8, cf. Table 3.9). This is the case for the dimers **DQ**: we neglect all the ultraexcitonic terms (i.e. all off-diagonal matrix elements mixing up states with different number of excitons), because we have explicitly verified that their contribution marginally affect spectra.

The excitonic Hamiltonian for the dimer is then obtained by neglecting all off-diagonal elements of the Hamiltonian written on the excitonic basis, with the exception of those connecting degenerate states. Moreover, in the residual off-diagonal terms, the contributions arising from electrostatic inter-chromophore interactions is multiplied by a factor ϵ/n^2, to renormalize the excitonic interaction energies for the screening at optical frequencies. The diagonalization of the resulting excitonic Hamiltonian finally leads to the

excited states calculated for all slow coordinates fixed at their equilibrium position obtained in the adiabatic approximation for the ground state. With this information we can calculate vertical OPA and TPA frequencies and intensities. Figure 3.17 collects information on transition energies, calculated for a dimer **DQ** as a function of the interchromophore distance for different angles ϕ. As expected, when the intermolecular distance becomes large (> 12Å) we regain the result for the **MQ** molecule in DMSO, irrespective of the mutual orientation of the chromophores. Sizeable and ϕ-dependent excitonic effects are observed decreasing r below ~ 10Å. Quite interestingly, excitonic interactions affect both OPA and TPA frequencies, a result that points to the failure of the dipolar approximation for electrostatic interactions [43, 44]. We notice that, for $\phi > 0$, interchromophore interactions lower the symmetry of each **MQ** unit; as a result a sizeable splitting of the OPA and TPA bands is observed in some cases (Figure 3.17). The splitting is, however, too small to be recognized in the broad experimental spectra.

Concerning OPA, the transition is red-shifted by interchromophore interactions for all angles, apart from the special case of $\phi = 0°$ (i.e. for faced **MQ** units) where a blue-shift is predicted. This special geometry is unlikely to occur because of electrostatic repulsion (at least when interchromophore distances are small enough to give rise to sizeable interaction). On this basis, data in Figure 3.17 nicely agree with the experimentally observed red shift of the linear absorption band upon decreasing the interchromophore distance. Of course, our model for electrostatic interactions is fairly rough, so that intermolecular distances represent effective values. However, results in Figure 3.17 suggest that for **DQ-C6**, with an approximate interchromophore distance of about 8Å, OPA and TPA spectra are marginally affected by interchromophoric interactions. On the contrary, in **DQ-C3** $r \approx 6$Å and a sizeable red shift $\approx 10 - 20$ nm is predicted in OPA spectra, in good agreement with experimental data (Table 3.6). The smaller red shift expected for TPA spectra is hardly recognized in experimental spectra, mainly due to the intrinsic lower resolution of TPA data (spectral resolution of TPA

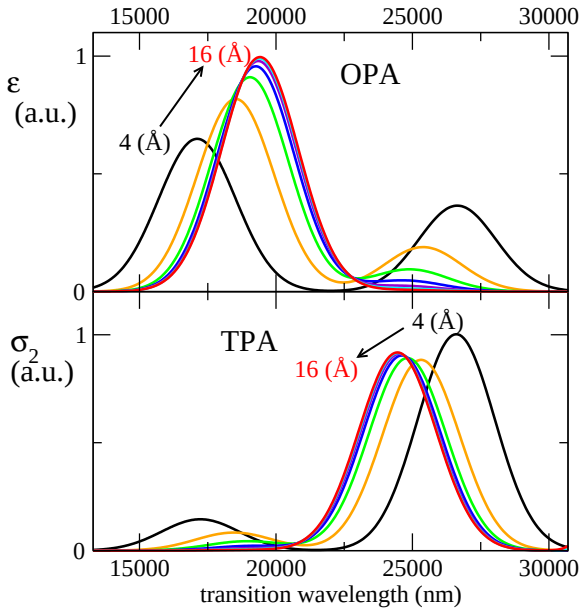

Figure 3.18: *OPA (top) and TPA (bottom) spectra calculated for a dimeric unit with* $\phi = 135°$ *and variable interchromophore distance (from 4 to 16* Å *with 2* Å *steps).*

data is dictated by the spectral width of the Gaussian-shaped excitation pulses produced by the laser). The intensities of the OPA and TPA bands are only marginally affected for distances relevant to the species **DQ-C6** and **DQ-C3**, with just a small decrease of the OPA intensity (as shown in Figure 3.18 for $\phi = 135°$). The detailed calculation of OPA and TPA spectra, including the vibronic structure and accounting for the inhomogeneous broadening from polar solvent, as performed for the dimer of dipolar chromophores in Section 3.2.2 is extremely demanding for the dimeric unit of quadrupolar chromophores. In fact, this would require the diagonalization of the nonadiabatic Hamiltonian for a system with 9 electronic states and 4 vibrational degrees of freedom. With the conservative estimate of 5 vibrational states for each degree of freedom, one should diagonalize (getting all eigenstates and transition dipole moments) a square matrix of dimen-

sion 5625, and calculation should be repeated by exploring the phase space spanned by 4 classical fields (relevant to F^i_{or} and $\tilde{Q}^i$, with $i = 1, 2$), leading to an overwhelmingly big number of calculations. Therefore, we limit attention to vertical transition frequencies and intensities, obtained in the excitonic approximation. To offer some information on the calculated spectral evolution, the two panels of Figure 3.18 describe, as a typical example, the evolution with the interchromophore distance of OPA and TPA spectra for a dimer with $\phi = 135°$, calculated by assigning to each electronic state (as obtained from the diagonalization of the excitonic model) a Gaussian line shape with full-width at half-maximum of 2000cm^{-1}.

Fluorescence spectra: the relaxed excited state

Steady-state fluorescence occurs from the relaxed first excited state. Therefore, the calculation of the fluorescence spectrum requires, as a first step, a mean-field model for the relaxed fluorescent state. The problem is more delicate than the one described for the ground state. In fact the first excited state of the dimeric unit corresponds to a state where only one out of the two chromophores is excited, whereas the ground state is unique. To account for the nonequivalence of the two molecular units, we have developed a mean-field model based on four order parameters, and specifically, $\rho_c^{(1)} = \langle\hat{\rho}_c^{(1)}\rangle$, $\rho_s^{(1)} = \langle\hat{\rho}_s^{(1)}\rangle$, for the first chromophore (chromophore 1), and the two corresponding parameters for the second chromophore (chromophore 2). In the mean-field approximation, the dimer Hamiltonian splits in two Hamiltonians, $\mathcal{H}^{mf}_{(i)}$, relevant to each **MQ** unit. Each one of these Hamiltonians has exactly the same form as the mean field Hamiltonian in Equation 3.23:

$$\begin{aligned}\mathcal{H}^{mf-fluo}_{(1)} &= -\sqrt{2}t(\hat{\sigma}_c^{(1)} + \hat{\sigma}_s^{(1)}) + 2\eta_c^{(1)}\hat{\rho}_c^{(1)} + 2\eta_s^{(1)}\hat{\rho}_s^{(1)} \\ \mathcal{H}^{mf-fluo}_{(2)} &= -\sqrt{2}t(\hat{\sigma}_c^{(2)} + \hat{\sigma}_s^{(2)}) + 2\eta_c^{(2)}\hat{\rho}_c^{(2)} + 2\eta_s^{(2)}\hat{\rho}_s^{(2)}\end{aligned} \tag{3.27}$$

but a different set of η energies is now defined for each **MQ** unit, as follows:

$$2\eta_c^{(1)} = 2\eta + v_2 + (v_4 - 2v_2 - 2v_3)\rho_c^{(2)} + (v_5 - v_2 - v_3)\rho_s^{(2)} -$$

$$
\begin{aligned}
& 2\epsilon_v\rho_c^{(1)} - 2\epsilon_Q(\rho_c^{(1)} + \rho_s^{(1)}) - 2\epsilon_{or}(\rho_c^{(1)} - \rho_s^{(1)}) \\
2\eta_s^{(1)} &= 2\eta + v_2 + (v_4 - 2v_2 - 2v_3)\rho_s^{(2)} + (v_5 - v_2 - v_3)\rho_c^{(2)} - \\
& 2\epsilon_v\rho_s^{(1)} - 2\epsilon_Q(\rho_c^{(1)} + \rho_s^{(1)}) - 2\epsilon_{or}(\rho_c^{(1)} - \rho_s^{(1)})
\end{aligned}
$$

$$
\begin{aligned}
2\eta_c^{(2)} &= 2\eta + v_2 + (v_4 - 2v_2 - 2v_3)\rho_c^{(1)} + (v_5 - v_2 - v_3)\rho_s^{(1)} - \\
& 2\epsilon_v\rho_c^{(2)} - 2\epsilon_Q(\rho_c^{(2)} + \rho_s^{(2)}) - 2\epsilon_{or}(\rho_c^{(2)} - \rho_s^{(2)}) \\
2\eta_s^{(2)} &= 2\eta + v_2 + (v_4 - 2v_2 - 2v_3)\rho_s^{(1)} + (v_5 - v_2 - v_3)\rho_s^{(1)} - \\
& 2\epsilon_v\rho_s^{(2)} - 2\epsilon_Q(\rho_c^{(2)} + \rho_s^{(2)}) - 2\epsilon_{or}(\rho_c^{(2)} - \rho_s^{(2)}) \qquad (3.28)
\end{aligned}
$$

The effective η energies for each chromophoric unit depend, through electrostatic interactions, on the charge distribution on the nearby chromophore, and through the coupling to slow degrees of freedom, on the charge distribution on the chromophore itself. Of course, being interested in stationary results, the electrostatic interactions in the above equations are screened by static dielectric constants. To solve the mean-field problem, we start with a guess for the four order parameters, diagonalize the two Hamiltonians in Equation 3.27, and recalculate the order parameters as the expectation values of the relevant operators on the ground state for chromophore 1 and on the first excited state for chromophore 2. The new estimates for the order parameters enter the mean-field Hamiltonians in Equation 3.27, and the procedure is repeated until convergence is reached. Figure 3.19 shows results obtained along these lines: in particular the asymmetry, $\rho_c^{(i)} - \rho_s^{(i)}$, calculated for each chromophore ($i = 1, 2$) is shown as a function of r and ϕ. In the proposed approach the excitation is localized (by construction) on chromophore 2, and in fact, the results shown in Figure 3.19 for chromophore 1 are similar to those calculated for the ground state (cf. Figure 3.16). On the opposite, chromophore 2 shows a much larger asymmetry, with $\rho_c^{(2)} - \rho_s^{(2)}$ ranging from 0.25 to 0.45, a result easily rationalized on the basis of the larger polarizability of the chromophore in the excited state.

Once the mean-field solution is obtained, one can proceed to the construction of the excitonic model relevant to fluorescence, along the same lines

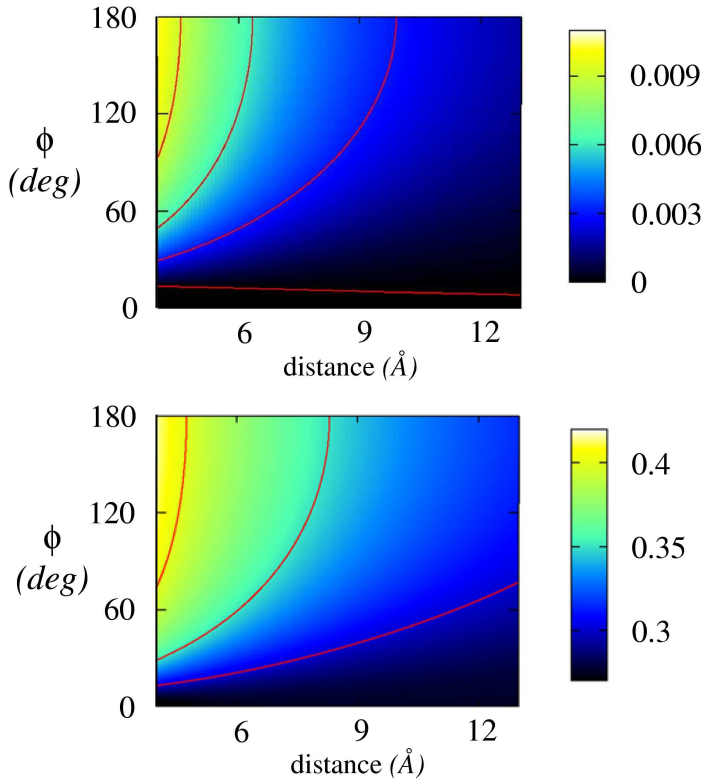

Figure 3.19: *Mean-field results for the fluorescent state. Top and bottom panels show* $\rho_c - \rho_s$ *values obtained for the first and second chromophore, respectively. Molecular parameters are taken from Table 3.7 and we set* $l = 8\mathring{\text{A}}$.

discussed in the previous section. In particular, the total dimer Hamiltonian is rewritten on the relevant excitonic basis, obtained as the direct product of the mean field eigenstates for the first and second chromophore. The excitonic approximation now amounts to neglect all off-diagonal elements that would mix the first excited state, already optimized at the mean-field level, to the other states. All non-neglected matrix element of the transformed matrix coming from electrostatic interactions are then renormalized by ϵ/n^2, to account for screening at optical frequencies. Finally, transition energies and dipole moments are obtained via a numerical diagonalization. In agreement with experimental data, the calculated fluorescence frequency is marginally affected by intermolecular interactions (Figure 3.17), due to the effective localization of the relaxed excited state on one of the two chromophores.

3.4 Conclusion

Interchromophore interactions play a major role in the definition of the properties and behavior of molecular materials. The effects are particularly intriguing in materials for nonlinear optics that are made up by chromophores that, by definition, largely and nonlinearly respond to external stimuli. If properly investigated and rationalized, interchromophore interactions may offer a powerful tool to tune the material response and design efficient and custom-tailored materials [17].

Bottom-up modeling strategies proved very useful to investigate the role of electrostatic interchromophore interactions in materials based on donor-acceptor molecules. These strategies take advantage of the molecular nature of the materials of interest and start from a detailed analysis of optical spectra of isolated chromophores in solution to define reliable essential-state models for the specific chromophores. This information is then used to build models for interacting chromophores in multichromophoric assemblies, films, aggregates and crystals.

When discussing electrostatic interactions in multichromophoric assem-

blies in solution, particular attention must be paid to screening effects by the solvent. Indeed, the dielectric constant of typical organic solvents spans more than one order of magnitude from ≈ 2 for nonpolar solvents up to ≈ 50 for strongly polar solvents. The screening of electrostatic interactions would suggest negligible effects of interchromophore interactions in strongly polar solvents. However it is well-known that excitonic interactions involve transition charge densities and, as such, should be screened by the squared refractive index of the solvent as measured at optical frequencies: the resulting screening constant is rather small (again on the order of 2) and similar for most organic solvents. Discriminating between static and dynamic screening is a tough problem that has been addressed for interacting dipolar chromophores in solution exploiting the analytical transformation toward the excitonic basis. The approach is based on the solution of the mean-field problem for interacting chromophores and the subsequent transformation of the Hamiltonian in the so-called excitonic basis, i.e., the eigenstates of the mean-field Hamiltonian. Adopting the same procedure for interacting quadrupolar (or multipolar) chromophores is nontrivial. First of all, interchromophore interactions in general lower the symmetry of the chromophores so that multiparameter mean-field approaches must be devised. Moreover, the analytical transformation toward the excitonic basis adopted for interacting dipolar DA chromophores does not apply to multipolar dyes and one has to resort to a numerical transformation.

We have adopted a very simple model for electrostatic interactions, based on point charges centered on D and A sites. More refined models can be envisaged, on the basis of more realistic descriptions of the charge distribution in the chromophoric units. However, the proposed approach to account for interchromophore interactions and to discriminate between static and dynamic screening applies quite irrespective of the specific model adopted for electrostatic interactions. In spite of using a fairly simple model for electrostatic interactions, the spectroscopic effects of interchromophore interactions are well accounted for in the proposed model, and we are able

to reproduce spectroscopic data of interacting systems, made up both by dipolar and quadrupolar chromophores.

Chapter 4

Interacting chromophores: energy transfer

4.1 Introduction

In this Chapter we discuss energy transfer process as occurring from an excited molecule (called energy donor $\mathcal{D}$) to a different molecule (called energy acceptor $\mathcal{A}$), according to the following expression:

$$\mathcal{D}^* + \mathcal{A} \rightarrow \mathcal{D} + \mathcal{A}^* \tag{4.1}$$

where $\mathcal{D}/\mathcal{A}$ and $\mathcal{D}^*/\mathcal{A}^*$ are the energy donor/acceptor molecules in the ground and in the excited state, respectively. Energy transfer is possible only if the emission spectrum of $\mathcal{D}$ partially overlaps the absorption spectrum of $\mathcal{A}$, i.e. if the conservation of energy is guaranteed.

Energy transfer is a widespread process in nature: it plays a key role in photosynthesis, allowing for light harvesting and funneling towards the reaction center [12]. Energy transfer also occurs in some species of animals that produce light (bioluminescence) [143]. The scientific community is paying increasing attention to this phenomenon, because of its multifarious and powerful applications in the field of energy storage and energy transport [144, 145, 146, 147]. Recently, the energy-transfer process was exploited to

increase the efficiency of organic solar cells [49], and in organic light-emitting diodes to tune the colour of the emitted light [50].

Energy transfer can follow radiative or non-radiative mechanisms. Radiative transfer corresponds to the absorption by the acceptor $\mathcal{A}$ of a photon emitted by the donor $\mathcal{D}$. This process can only occur when the distance between the molecules is larger than the wavelength of the emitted photon. Radiative transfer does not require any direct interaction between $\mathcal{D}$ and $\mathcal{A}$, but it depends only on the spectral overlap between the emission spectrum of $\mathcal{D}$ and the absorption spectrum of $\mathcal{A}$, and on the concentration. On the contrary, non-radiative transfer implies the transfer of a *virtual photon* between $\mathcal{D}$ and $\mathcal{A}$, and it occurs in the presence of interactions (of different types, depending on the distances as discussed below) between $\mathcal{D}$ and $\mathcal{A}$ [148, 149]. Non-radiative energy transfer also requires spectral overlap between the emission of the donor and the absorption of the acceptor (resonance, Figure 4.1), but only occurs when the intermolecular distances are smaller than the wavelength of the exchanged photon. The term resonance energy transfer (RET) is often used to refer to non-radiative transfer. This Chapter is focused on non-radiative energy transfer, and in particular on the interactions responsible for RET.

It is important to distinguish between different types of interactions responsible for the transfer, according to the distances between $\mathcal{D}$ and $\mathcal{A}$ molecules. At very short distances the interactions arise from intermolecular orbital overlap, and the transfer can occur via an electron exchange (Dexter mechanism) or charge resonance [148, 149]. When the distance between molecules is larger, and intermolecular orbital overlap can be neglected, Coulombic interactions become responsible for RET. At the end of the fifties, Förster proposed a simple model for RET: adopting the dipolar approximation to describe Coulombic intermolecular interactions, he derived an expression that relates the transfer rate to experimentally accessible quantities, allowing for the estimate of the distance between $\mathcal{D}$ and $\mathcal{A}$ from the transfer efficiency [150, 151, 152, 153]. This work represents a milestone

in the field of resonance energy transfer.

In Section 4.2, the Förster approach is described in detail and is applied to investigate the energy transfer process in a trimer constituted by a quadrupolar molecule, working as a donor, and two dipolar chromophores, working as acceptors (Section 4.2.2). This system can find interesting applications in the field of bioimaging. In fact, it allows to exploit the good two-photon absorption properties of the quadrupole and, at the same time, the emission of the dipoles, that, being in the red region of the spectrum, is well-suited for in-vivo applications due to the good penetration into living tissues.

However, the dipolar approximation at the heart of the Förster mechanism becomes inadequate for the description of intermolecular interactions when the distance between the molecules is similar to the molecular size. To overcome this limit, in the second part of this Chapter we propose a different approach to describe the Coulombic interactions responsible for RET. Adopting the same extended-dipole approach used to calculate interactions in multichromophoric systems in Chapter 3, we estimate intermolecular interactions and the transfer rate. First of all, this approach allows to calculate in a more rigorous way intermolecular interactions. Moreover, as described in Section 4.3, relaxing the dipolar approximation opens new channels for energy transfer through dark states.

4.2 Förster resonance energy transfer

The Förster resonance energy transfer is a non-radiative energy-transfer process, that occurs when the distances between donor and acceptor molecules are fairly large (typically 20 - 100 Å). Due to the large distances, interactions responsible for energy transfer are weak. To describe these interactions, Förster adopted the dipolar approximation: the interaction between transition dipole moments of the donor and of the acceptor gives rise to the transfer process [150, 151, 152, 153].

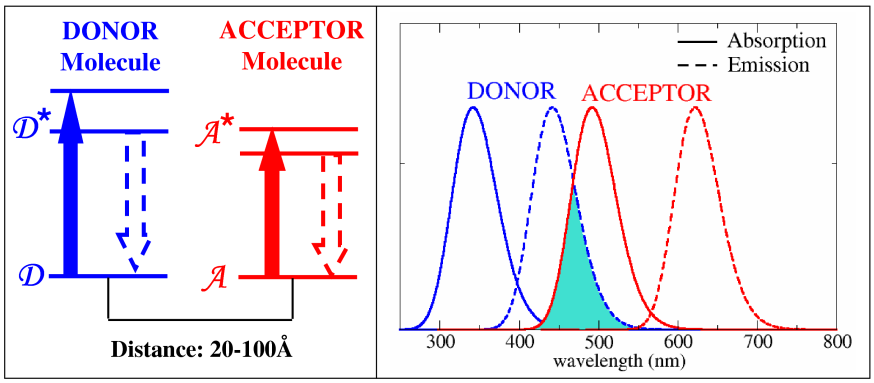

Figure 4.1: *On the left: Energy level scheme of the donor $\mathcal{D}$ and acceptor $\mathcal{A}$ molecule showing resonant energy transfer (the emission of the donor is resonant with the absorption of the acceptor). On the right: Spectral overlap between the emission spectrum of the donor and the absorption spectrum of the acceptor.*

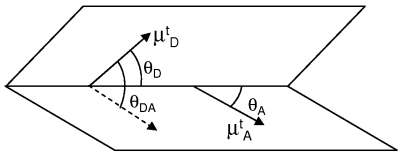

Figure 4.2: *Definition of angles for the calculation of the orientational factor k.*

The Fermi Golden Rule defines the rate of the process:

$$k_{ET} = \frac{2\pi}{\hbar}|\langle\psi^*_{\mathcal{D}}\psi_{\mathcal{A}}|V|\psi_{\mathcal{D}}\psi^*_{\mathcal{A}}\rangle|^2\delta(\tilde{\nu}_{\mathcal{D}} - \tilde{\nu}_{\mathcal{A}}) \tag{4.2}$$

where $\hbar$ is the Planck constant divided by 2π, $\psi_{\mathcal{D}}$ and $\psi_{\mathcal{A}}$ are the ground-state wavefunctions relevant to the donor and the acceptor, respectively, while $\psi^*_{\mathcal{D}}$ and $\psi^*_{\mathcal{A}}$ are the excited-state wavefunctions of the donor and the acceptor, respectively. V describes the interactions responsible for the transfer process, while the second term $\delta(\tilde{\nu}_{\mathcal{D}} - \tilde{\nu}_{\mathcal{A}})$ ensures the energy conservation. This last condition is satisfied when the emission spectrum of the donor overlaps the absorption spectrum of the acceptor, as shown in Figure 4.1. Adopting the dipolar approximation to describe the interaction V, the transfer rate in solution reads:

$$k_{ET} = \frac{2\pi}{\hbar}\left(\frac{\mu^t_{\mathcal{D}}\mu^t_{\mathcal{A}}}{n^2r^3}k\right)^2\delta(\tilde{\nu}_{\mathcal{D}} - \tilde{\nu}_{\mathcal{A}}) \tag{4.3}$$

where $\mu^t_{\mathcal{D}}$ and $\mu^t_{\mathcal{A}}$ are the transition dipole moments relevant to the donor (emission process) and the acceptor (absorption process) respectively. r is the distance between the two molecules. n^2 is the squared refractive index of the solvent, and it is introduced to screen the interaction between the transition dipole moments (for details about screening at optical frequencies, cf Section 3.1).

k is an orientational factor, that accounts for the mutual orientation

Table 4.1: *Orientational factor k^2 for different orientations of the transitions dipole moments.*

Orientation of dipoles	k^2
parallel	1
collinear	4
perpendicular	0
random orientation $\langle k^2 \rangle$	2/3
random orientation $\langle k \rangle^2$	0.476

between the two transition dipole moments [148]:

$$k = \cos\theta_{\mathcal{DA}} - 3\cos\theta_{\mathcal{D}}\cos\theta_{\mathcal{A}} \tag{4.4}$$

Angles $\theta_{\mathcal{D}}$, $\theta_{\mathcal{A}}$ and $\theta_{\mathcal{DA}}$ are defined in Figure 4.2. Table 4.1 reports values of k^2 for different orientations of the dipole moments. If energy transfer is measured in solution, and donor and acceptor molecules are randomly oriented, the orientational factor is averaged over all possible orientations. In particular, the value $k^2 = 2/3$ is obtained by averaging k^2 over all possible orientations ($\langle k^2 \rangle$), i.e. considering that the transition dipole moments of the donor and of the acceptor can explore all possible orientations during the lifetime of the donor in the excited state. This case applies to liquid and non-viscous solvents, in which the diffusive rate of small molecules is very fast. Different is the case of a solute in a rigid matrix, where the molecular diffusion of molecules is hindered. In that case the orientation of transition dipole moments is random, but they are constrained in a fixed position during the emission process. Therefore, the average has to be performed on k (the factor $\langle k \rangle^2$ must then be considered). For random orientation of the molecules, $\langle k \rangle^2 = 0.476$.

The transition dipole moment of the donor $\mu_{\mathcal{D}}^t$ is relevant to the fluorescence process, and can be estimated from the experimental emission spectrum using the following expression [154]:

$$(\mu_{\mathcal{D}}^t)^2 = \frac{3\phi_{\mathcal{D}}^0}{\tau_d^0 64\pi^4 h^2} \int_0^\infty I_{\mathcal{D}}(\tilde{\nu})\tilde{\nu}^3 d\tilde{\nu} \tag{4.5}$$

where h is the Planck constant, $\phi_{\mathcal{D}}^0$ and $\tau_{\mathcal{D}}^0$ are the fluorescence quantum yield and the excited-state lifetime of the donor in the absence of transfer (i.e. in the absence of the acceptor), and $I_{\mathcal{D}}(\tilde{\nu})$ is the fluorescence spectrum of the donor ($\tilde{\nu}$ is the wavenumber in cm^{-1}) normalized to get unit area ($\int_0^\infty I_{\mathcal{D}}(\tilde{\nu})d\tilde{\nu} = 1$).

The transition dipole moment of the acceptor $\mu_{\mathcal{A}}^t$ is relevant to the absorption process, and can be estimated from the experimental absorption spectrum, according to the following expression [154]:

$$(\mu_{\mathcal{A}}^t)^2 = \frac{3hc10^3 ln10}{8\pi^3 N_A} \int_0^\infty \frac{\epsilon_{\mathcal{A}}(\tilde{\nu})}{\tilde{\nu}} d\tilde{\nu} \tag{4.6}$$

where $\epsilon_{\mathcal{A}}(\tilde{\nu})$ is the molar extinction coefficient of the acceptor, c is the speed of light and N_A the Avogadro's number.

From Equations 4.3, 4.5, 4.6, the following expression is obtained, as originally proposed by Förster, [150]:

$$k_{ET} = \frac{9000 ln10}{128\pi^5 N_A n^4} \frac{k^2 \phi_{\mathcal{D}}^0}{\tau_{\mathcal{D}}^0 r^6} \int_0^\infty \frac{\epsilon_{\mathcal{A}}(\tilde{\nu}) I_{\mathcal{D}}(\tilde{\nu})}{\tilde{\nu}^4} d\tilde{\nu} \tag{4.7}$$

According to Equation 4.7, the transfer rate varies with the sixth power of the distance between donor an acceptor.

The Förster radius r_0 is defined as the distance at which transfer and spontaneous decay of the excited donor are equally probable, i.e. $k_{ET} = 1/\tau_{\mathcal{D}}^0$, and is calculated from Equation 4.7:

$$\begin{aligned} r_0 &= \left(\frac{9000 ln10}{128\pi^5 N_A n^4} \frac{k^2 \phi_{\mathcal{D}}^0}{\tau_{\mathcal{D}}^0 r^6} \int_0^\infty \frac{\epsilon_{\mathcal{A}}(\tilde{\nu}) I_{\mathcal{D}}(\tilde{\nu})}{\tilde{\nu}^4} d\tilde{\nu} \right)^{1/6} \\ &= 0.2108 \left(k^2 \phi_{\mathcal{D}}^0 n^{-4} \int_0^\infty I_{\mathcal{D}}(\lambda)\epsilon_{\mathcal{A}}(\lambda)\lambda^4 d\lambda \right)^{1/6} \end{aligned} \tag{4.8}$$

where the second equation is expressed in wavelength (λ). The transfer efficiency is given by:

$$\begin{aligned} \phi_{ET} &= \frac{k_{ET}}{1/\tau_{\mathcal{D}}^{0} + k_{ET}} \\ &= \frac{1}{1 + (r/r_0)^6} \end{aligned} \tag{4.9}$$

4.2.1 Determination of the energy-transfer efficiency

The transfer efficiency can be determined from steady-state or time-resolved measurements. Three steady-state methods can be used [148]:

1. **Decrease in donor fluorescence**. The transfer from the donor to the acceptor causes a decrease of the fluorescence quantum yield of the donor. According to the following expression, the transfer efficiency can be estimated:

$$\phi_{ET} = 1 - \frac{\phi_{\mathcal{D}}}{\phi_{\mathcal{D}}^{0}} \tag{4.10}$$

   where $\phi_{\mathcal{D}}$ and $\phi_{\mathcal{D}}^{0}$ are the fluorescence quantum yield of the donor in the presence and in the absence of the acceptor, respectively.

2. **Comparison between the absorption spectrum and the excitation spectrum.** This method compares the absorption spectrum and the excitation spectrum measured in the presence of transfer. The excitation spectrum is collected detecting only the emission of the acceptor. After normalization of the excitation band of the acceptor to the absorption spectrum, the transfer efficiency is estimated as follows:

$$\phi_{ET} = \frac{I(\lambda_{\mathcal{D}})}{A(\lambda_{\mathcal{D}})} \tag{4.11}$$

   where $I(\lambda_{\mathcal{D}})$ is the intensity of the excitation spectrum within the band relevant to the donor, while $A(\lambda_{\mathcal{D}})$ is the absorbance at the same wavelength. In the case of total transfer, ($\phi_{ET} = 1$), the two spectra coincide.

3. **Enhancement in acceptor fluorescence.** In the presence of energy transfer, the emission of the acceptor increases. The transfer efficiency can be estimated as follows:

$$\phi_{ET} = \frac{\phi_{\mathcal{A}}}{\phi^0_{\mathcal{A}}} - 1 \tag{4.12}$$

where $\phi_{\mathcal{A}}$ and $\phi^0_{\mathcal{A}}$ are the fluorescence quantum yields in presence and in the absence of transfer, respectively.

As far as time-resolved measurements are concerned, the most efficient method to determine the transfer efficiency is based on the decay of the donor fluorescence [148]. Transfer efficiency can be estimated from the average decay times of the donor in the absence and in the presence of the acceptor: $\phi_{ET} = 1 - \frac{\langle \tau_{\mathcal{D}} \rangle}{\langle \tau^0_{\mathcal{D}} \rangle}$.

RET is widely used to determine distances in biomolecules and supramolecular assemblies. After the experimental determination of the transfer efficiency and of the Förster radius (Equation 4.8), the distance between the donor and the acceptor molecule is estimated using Equation 4.9.

4.2.2 Resonance energy transfer in multiphoton absorbing structures

In this Section we present the experimental investigation of RET between the quadrupolar donor **q** and dipolar acceptor **d** shown in Figure 4.3. The molecular system **t** is a trimer constituted by one quadrupole (**q**) in the center and two dipoles (**d**) in peripheral positions, linked by saturated chains, that ensures non-conjugation between the chromophoric systems. The work was developed in collaboration with the group of Prof. Mireille Blanchard-Desce (University of Rennes 1, France) that synthesized the molecules and measured the two-photon responses.

The aim of this work is to exploit the large two-photon absorption cross section of the quadrupole and red-shift the emission through RET between the quadrupole and the dipoles (red emitters) [155, 156, 157, 158]. The idea

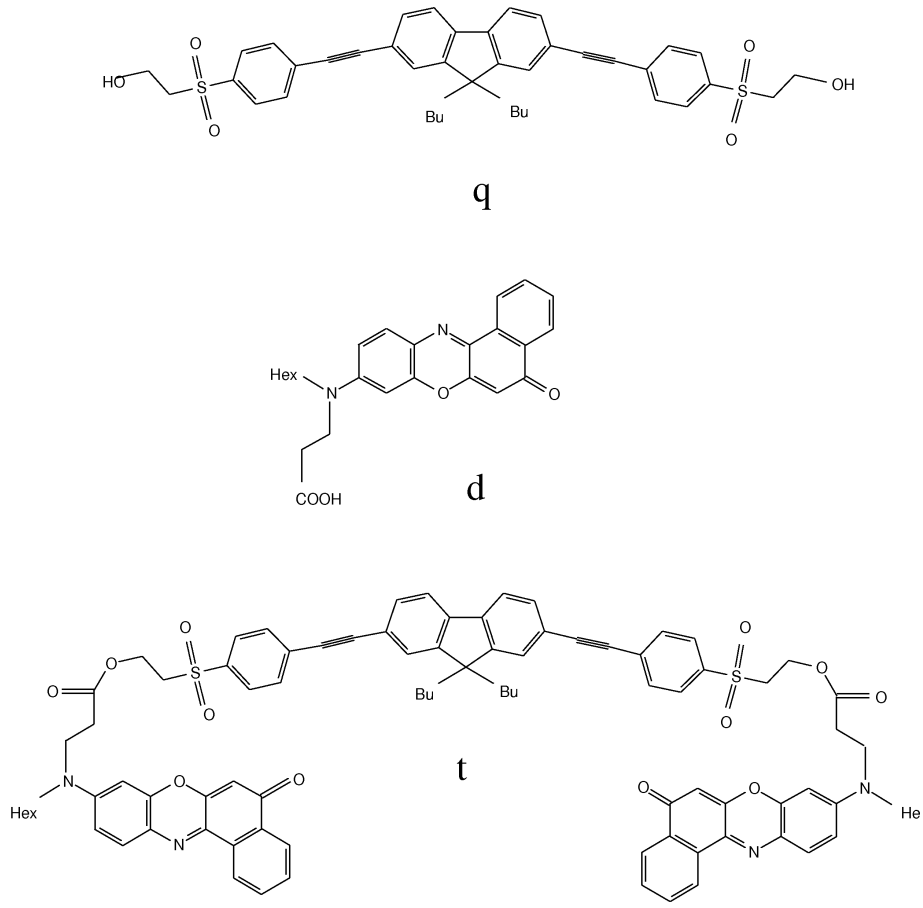

Figure 4.3: *Molecular structures of the quadrupolar compound* ***q****, of the dipolar compound* ***d*** *and of the trimer* ***t****, constituted by one quadrupole in the central core, and two peripheral dipoles.*

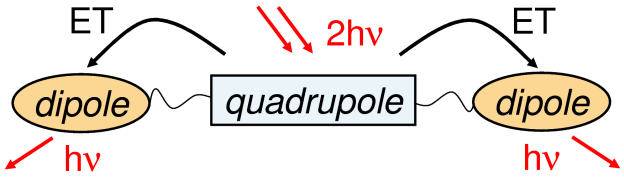

Figure 4.4: *Sketch of the model system* ***t****.*

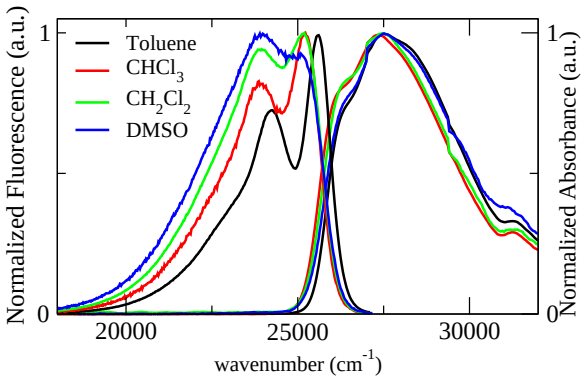

Figure 4.5: *Normalized absorption and fluorescence spectra of* ***q*** *in solvents of different polarity*

is sketched in Figure 4.4. The quadrupolar chromophore is efficiently excited by two-photon absorption. Then the energy is transferred to the two dipolar chromophores, through the RET process described in the previous section. Emission is detected from the dipoles, i.e. in the red region, which is the more interesting with respect to penetration into living tissues (bioimaging applications). Moreover, due to the polarizable nature of charge-transfer dyes, cooperative effects could increase the two-photon response of the system.

The work started with the analysis of electronic spectra of the quadrupolar donor **q** and of the dipolar acceptor **d**. Figure 4.5 shows absorption and emission spectra of **q** in different solvents, and Table 4.2 summarizes the ex-

Table 4.2: *Spectroscopic data for* **q** *in solvents of different polarity.*

Solvent	λ^a_{abs} (nm)	λ^a_{em} (nm)	Stokes Shift (cm^{-1})	ϕ^b	τ^c (ns)	ϵ ($M^{-1}cm^{-1}$)
Toluene	364	390	1832	0.96	0.72	68400
$CHCl_3$	367	397	2059	0.91	0.88	74100
CH_2Cl_2	364	397	2284			
DMSO	363	418	3625			

[a] data referred to the maximum

[b] fluorescence quantum yield, error ±10%

(standard: fluorescein in NaOH 0.1M, $\phi = 0.9$)

[c] excited-state lifetime

perimental results. Absorption spectra of **q** are not sensitive to the polarity of the solvent, as expected for quadrupolar dyes (cf. Section 1.3). Instead the emission spectrum of **q** is slightly solvatochromic, and a red shift of the band is observed when the polarity of the solvent is increased. **q** is a good emitter: the fluorescence quantum yield is higher than 0.9 both in toluene and in chloroform (fluorescence quantum yields were measured following the protocol described in Appendix B).

Apart from the functionalization required for the subsequent esterification with **q**, **d** is the same chromophore as Nile Red, already discussed in Ref. [38] and in Section 2.3.2. The spectra of **d** reported in Figure 4.6 confirm the basic equivalence of the two chromophores.

Since the emission solvatochromism of **q** is comparable to of the absorption solvatochromism of **d**, the spectral overlap between the emission of the donor (**q**) and the absorption of the acceptor (**d**) is barely affected by the solvent polarity. We chose to measure energy transfer in chloroform for solubility reasons. Table 4.4 summarizes the spectral properties of **t** in chloroform. First of all, we notice that the fluorescence quantum yield of

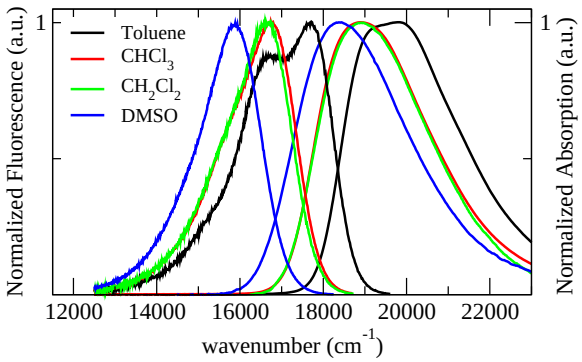

Figure 4.6: *Normalized absorption and fluorescence spectra of* ***d*** *in solvents of different polarity.*

Table 4.3: *Spectroscopic data for* ***d*** *in solvents of different polarity.*

Solvent	λ^a_{abs} (nm)	λ^a_{em} (nm)	Stokes Shift (cm^{-1})	ϕ^b	τ^c (ns)	ϵ ($M^{-1}cm^{-1}$)
Toluene	505	565	2103			25600
$CHCl_3$	530	597	2118	0.85	4.14	30600
CH_2Cl_2	529	602	2292			
DMSO	543	631	2568			

[a] data referred to the maximum

[b] fluorescence quantum yield, error ±10%

(standard: fluorescein in NaOH 0.1M,$\phi = 0.9$)

[c] lifetime of the excited state

Table 4.4: *Spectroscopic data for* ***t*** *in* $CHCl_3$.

Solvent	λ^a_{abs} (nm)	λ^a_{em} (nm)	ϕ^b	ϵ ($M^{-1}cm^{-1}$)
$CHCl_3$	366, 525	366, 597	0.82 (λ_{exc} =525nm)	68900 at 366nm 58900 at 525nm

[a] data referred to the maxima

[b] fluorescence quantum yield

(standard: fluorescein in NaOH 0.1M,$\phi = 0.9$; error $\pm 10\%$)

the dipole in **t**, measured exciting the macromolecule at the maximum of absorption of the dipole itself (to avoid energy transfer), stays very high. Moreover, the maximum of absorption and emission of the dipole and of the quadrupole in **t** are almost in the same position as observed in isolated **q** and **d** chromophores.

Figure 4.7 shows the molar extinction coefficient of **t** in chloroform, compared to the sum of the molar extinction coefficients of **q** and **d** (the latter is multiplied by two, because in the trimer two molecules of **d** are present). We observe that the molar extinction coefficient of **t** is almost additive: only a very weak decrease in the intensity relevant to the absorption of the donor is observed. The amount of the decrease is however less than 10%, within the experimental error.

Figure 4.8 shows the emission spectrum of **t** in chloroform, collected exciting the quadrupolar chromophore, i.e. the donor. The presence of energy transfer is evident: the red emission corresponds to the fluorescence of the **d**-species, i.e. of the energy acceptor. The absorption of the acceptor at the excitation wavelength is negligible, so that the acceptor can be considered as only excited by the transfer of energy from the donor. In the presence of the acceptor, the fluorescence quantum yield of the donor decreases to 0.043. According to the steady-state method 1 presented in the

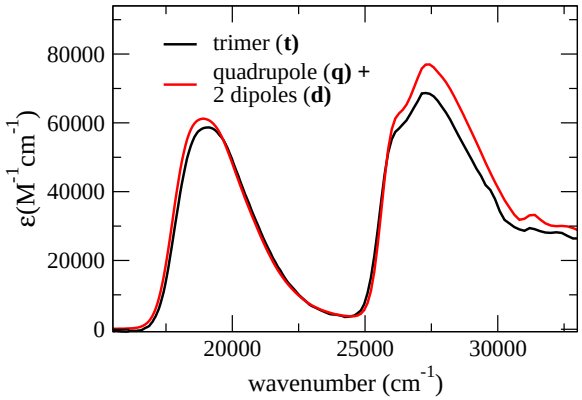

Figure 4.7: *Molar extinction coefficient of* ***t*** *(black line) in* $CHCl_3$ *compared to the sum of molar extinction coefficients of* ***q*** *and* ***d*** *(the latter multiplied by 2).*

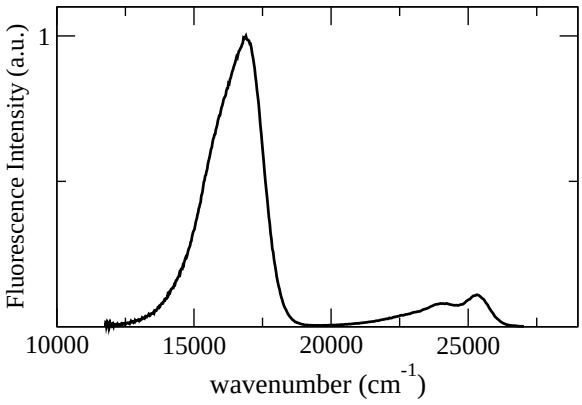

Figure 4.8: *Emission spectrum of* ***t*** *in chloroform collected exciting at the maximum of absorption of the quadrupolar donor. The two bands correspond do the emission of* ***q*** *(at higher energy) and of* ***d*** *(lower-energy band).*

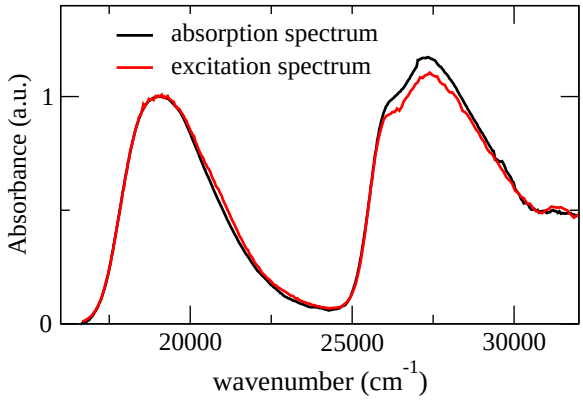

Figure 4.9: *Absorption and excitation spectrum (measured detecting the emission of the donor) of* ***t*** *in chloroform.*

previous section (Equation 4.10), the efficiency of the transfer is 95%. The efficiency of the transfer is estimated also by comparing the excitation spectrum, detected within the emission band relevant to the acceptor, with the absorption spectrum (steady-state method 2), as shown in Figure 4.9. In this way the transfer efficiency is estimated to be 93%. The other methods for the measurement of the transfer efficiency hardly apply to this system. In fact, the fluorescence quantum yield of the acceptor in the presence of the donor is difficult to estimate, because the absorption of the acceptor in the region of the absorption of the donor is very weak. On the other hand, for the time-resolved method, a reliable measurement of the excited-state lifetime of the donor in the presence of the acceptor ($\tau_{\mathcal{D}}$) becomes difficult, because we expect a very low value for $\tau_{\mathcal{D}}$ when the transfer efficiency is high.

The average value for the transfer efficiency, $\phi_{ET} = 0.94$, was considered for the calculation of the transfer rate and for the estimation of the distance between the chromophores. The Förster radius was determined according to Equation 4.8: $r_0 = 36\text{Å}$. The distance between chromophores is estimated

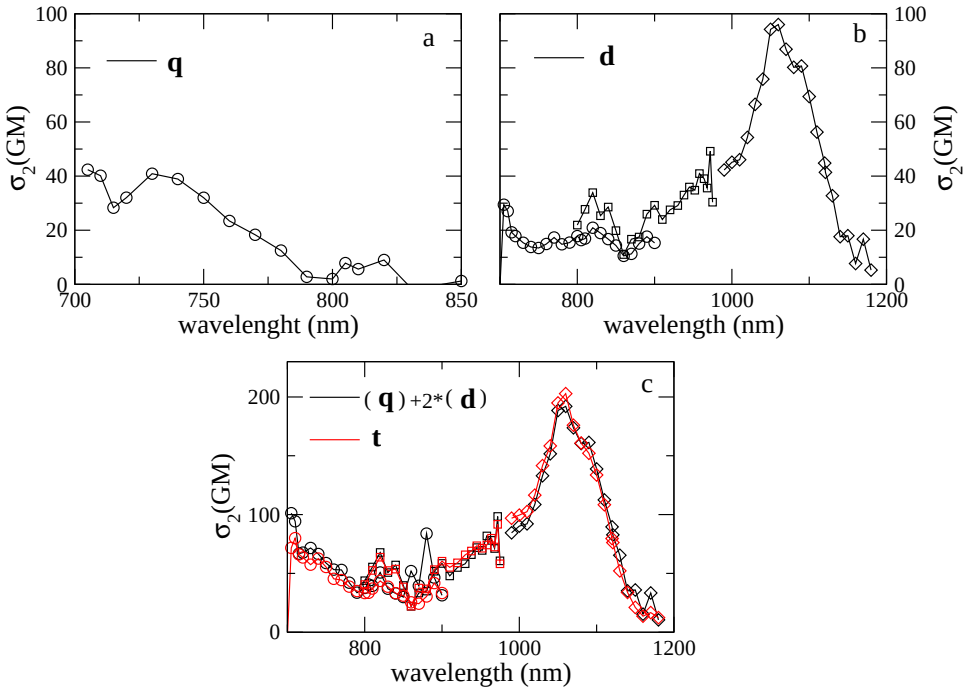

Figure 4.10: *Two-photon absorption spectra of* ***q*** *(panel a),* ***d*** *(panel b) and* ***t*** *(panel c) in chloroform. Panel* ***c*** *also reports the additive response of* ***q*** *and* ***d****. Different symbols refer to different setup for measurement (circle=blue filter; square=red filter; diamond=OPO, cf Appendix C)*

as follows:

$$r = r_0 \left(\frac{1}{\phi_{ET}} - 1 \right)^{1/6} = 23\text{Å} \tag{4.13}$$

The transfer rate is calculated according to Equation 4.7: $k_{ET} = 19.6 \cdot 10^9 \text{s}^{-1}$.

Two-photon absorption cross sections of **q**, **d** and **t** were measured, and experimental data are reported in Figure 4.10. Because of experimental limitations (cf Appendix C), we could detect only a small region of the two-photon absorption band of the quadrupole, and the maximum of the band is not experimentally accessible. On the contrary, the whole two-photon absorption band of the dipole was measured. Panel c compares the two-photon

absorption spectrum of **t** with the sum of the spectra of the monomers: the behavior of **t** is additive, as already observed for linear spectra. The absence of cooperative effects probably comes from the low polarizability of the quadrupole, which makes the molecule almost non-sensitive to the presence of dipolar chromophores and vice versa.

To conclude, in this work we have demonstrated that the pair of molecules **q** and **d** shows a very efficient energy transfer, and that the linkage between them does not alter the good radiative properties of the dipole (the fluorescence quantum yield of the dipole in the trimer, remains high). As a consequence, the possibility to associate the good one- and two-photon absorption properties of the quadrupole to the red emission of the dipole is valid. Interesting perspectives lie in the possibility to substitute the quadrupolar chromophores with a better two-photon absorber, and/or with a more polarizable molecule.

4.3 Beyond the Förster formulation of RET: energy transfer towards dark states

In his pioneering work about RET, Förster adopted the dipolar approximation to describe the interactions between the donor $\mathcal{D}$ and the acceptor $\mathcal{A}$ that give rise to energy transfer. It is well known that the dipolar approximation works well only if the distances between the dipoles is larger than the molecular size. For extended dipoles, lying at short distances, this approximation unavoidably fails. Charge-transfer chromophores are characterized by large transition dipole moments, because the transition involves the transfer of charge from the electron-donor moiety to the electron-acceptor moiety. Moreover, in multichromophoric assemblies, interchromophore distances can be very small, so that the dipolar approximation becomes inadequate to describe interactions responsible for energy transfer.

Here we propose to calculate interactions between the transition charge densities of the donor and acceptor chromophores, relaxing the dipolar ap-

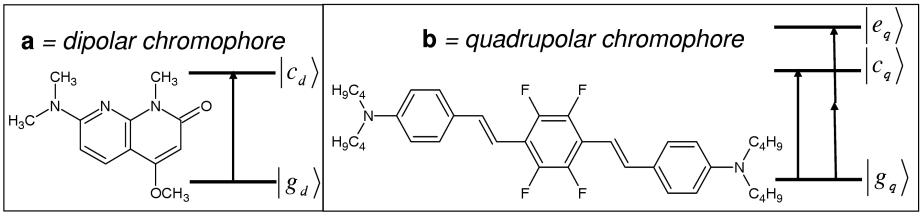

Figure 4.11: *Molecular structures of the dipolar chromophore* ***a*** *and of the quadrupolar chromophore* ***b****. On the left of each structure, the sketch of the electronic states (in an essential state picture) is shown.*

proximation, and adopting the extended-dipole approach, already presented to describe interactions in multichromophoric assemblies. Transition charge densities of charge-transfer dyes are calculated using essential-state models. In this approximation, according to the extended-dipole approach, transition charge densities are described in terms of point charges. As a consequence, the Coulombic interaction between the point-charge distributions, describing the transition charge densities, is responsible for energy transfer. Relaxing the dipolar approximation allows to calculate in a more rigorous way the interaction between molecules, but, even more interestingly, it may open new channels for energy transfer, which are forbidden if the dipolar approximation is adopted [144, 159, 149]. In the next Section the proposed model for the description of energy transfer is applied to the pair of molecules shown in Figure 4.11. The validity of the approach is verified at a theoretical level by comparison with ab-initio calculations. In Section 4.3.2, the same model is adopted to describe energy transfer towards the dark state of the quadrupolar chromophore (i.e. the excited state that is not allowed in one-photon absorption).

4.3.1 Essential-state models for calculation of interactions between transition charge densities

The Fermi Golden rule in Equation 4.2 describes the transfer rate of RET. Instead of adopting the dipolar approximation to describe the interaction between $\mathcal{D}$ and $\mathcal{A}$, we express the interaction term as follows:

$$V = \sum_i \sum_j v_{i,j} \langle \psi^*_{\mathcal{D}} \psi_{\mathcal{A}} | \hat{\rho}_{\mathcal{D},i} \hat{\rho}_{\mathcal{A},j} | \psi_D \psi^*_{\mathcal{A}} \rangle \tag{4.14}$$

where i, j run over the molecular arms of the donor and acceptor molecules. For a dipolar (d) energy donor and a quadrupolar (q) energy acceptor (Figure 4.11), the interaction term reads:

$$V = v_1 \langle \psi^*_d \psi_q | \hat{\rho}_d \hat{\rho}_{q,1} | \psi_d \psi^*_q \rangle + v_2 \langle \psi^*_d \psi_q | \hat{\rho}_d \hat{\rho}_{q,2} | \psi_d \psi^*_q \rangle \tag{4.15}$$

where $\psi_{d/q}$ are the wavefunctions that describe the ground states of the dipolar donor/quadrupolar acceptor, $\psi^*_{d/q}$ are the wavefunctions relevant to the excited state of the donor/acceptor. $\hat{\rho}_d = |D^+A^-\rangle\langle D^+A^-|$ is the ionicity operator, describing the charge distribution of the dipolar energy donor. $\hat{\rho}_{q,1} = |D^+A^-D\rangle\langle D^+A^-D|$ and $\hat{\rho}_{q,2} = |DA^-D^+\rangle\langle DA^-D^+|$ are the ionicity operators relevant to the two arms of the quadrupolar energy acceptor. The integral $\langle \psi_d | \hat{\rho}_d | \psi^*_d \rangle$ defines the transition charge density of the dipolar chromophore, relevant to the transition from the ground state ψ_d to the excited-state ψ^*_d. Similarly, $\langle \psi_q | \hat{\rho}_{q,j} | \psi^*_q \rangle$ defines the transition charge density on the molecular arm j of the quadrupolar energy acceptor relevant to the transition from the ground state ψ_q to the excited-state ψ^*_q. v_1 and v_2 represent the interactions between the point-charge distributions of the zwitterionic basis state $|D^+A^-\rangle$ of the donor and the zwitterionic basis states $|D^+A^-D\rangle$ and $|DA^-D^+\rangle$ of the acceptor, and they depend on the geometry of the system (cf. Figure 4.12). Since we are dealing with transition charge distributions, the optical regime for screening is applied, and the interaction term is screened by the squared refractive index.

The explicit calculation of V is performed on the pair of molecules shown in Figure 4.11. **a** is a dipolar compound and is described in terms of a two-

Table 4.5: *The two-state model electronic parameters for* **a** *and the three state model parameters for* **b**. *Molecular structures of* **a** *and* **b** *are shown in Figure 4.11. The length of molecules is fixed from ab-initio calculations (for* **b** *the value refers to half of the total length of the molecule).*

Molecule	η (eV)	$\sqrt{2}t$ (eV)	length (Å)
a	1.33	1	6.5
b	1.19	0.8	9.5

state model. For the sake of simplicity, we adopt a pure electronic model. The electronic parameters of the model (η and $\sqrt{2}t$) are fixed according to experimental data from literature [160], and are listed in Table 4.5. The transition charge density of a dipolar chromophore is described by the following expression:

$$\rho_d^t = \langle g_d|\hat{\rho}_d|c_d\rangle = \sqrt{\rho_d(1-\rho_d)} \tag{4.16}$$

where $|g_d\rangle$ and $|c_d\rangle$ are the ground and the excited state, respectively, as defined in Equation 1.3, while ρ_d is the ground state polarity of the molecule defined in Equation 1.3. **b** is the quadrupolar chromophore **2** of Reference [39]. The spectral behavior of this molecule was efficiently rationalized in terms of a three-state model. Since we neglect molecular vibrations, the parameters reported in Table 4.5 are renormalized to get the same ground-state polarity as in a non-polar solvent. Two different transition charge densities can be defined for **b**: one relevant to the transition towards the one-photon allowed state $|c_q\rangle$, and the second one relevant to the transition towards the two-photon allowed state $|e_q\rangle$ (which is a dark state, in the sense that it cannot be reached by absorption of a single photon).

We start the discussion considering energy transfer towards the one-photon allowed state $|c_q\rangle$. The ground state $|g_q\rangle$ and the excited state $|c_q\rangle$ read as follow (cf Section 1.3):

$$|g_q\rangle = \sqrt{1-\rho_q}|DAD\rangle + \sqrt{\frac{\rho_q}{2}}(|D^+A^-D\rangle + |DA^-D^+\rangle) \tag{4.17}$$

$$|c_q\rangle = \frac{1}{\sqrt{2}}(|D^+A^-D\rangle - |DA^-D^+\rangle) \tag{4.18}$$

where ρ_q represents the quadrupolar moment of the molecule, as described in Equation 1.24. Two contributions to the transition charge density towards $|c_q\rangle$ can be distinguished, one for each molecular branch:

$$\begin{aligned} \rho^t_{q,1} &= \langle g_q|\hat{\rho}_{q,1}|c_q\rangle = \frac{\sqrt{\rho_q}}{2} \\ \rho^t_{q,2} &= \langle g_q|\hat{\rho}_{q,2}|c_q\rangle = -\frac{\sqrt{\rho_q}}{2} \end{aligned} \tag{4.19}$$

where $\hat{\rho}_{q,(1,2)}$ are the ionicity operators relevant to the two molecular branches. The interaction energy of the two contributions with the transition charge density of the dipolar chromophore can be different according to the geometry of the system.

Left panel of Figure 4.12 shows the geometry that we fixed to evaluate electrostatic interactions between the transition charge densities of the dipole and of the quadrupole, reported in Equation 4.19 and 4.16. In the same Figure distances and lengths are defined. According to this geometry, Coulombic interactions between point charges read:

$$\begin{aligned} V = \alpha \Bigg[& \rho^t_d\rho^t_{q,1}\left(\frac{1}{r} + \frac{1}{\sqrt{(l_q-l_d)^2+r^2}} - \frac{1}{\sqrt{l_q^2+r^2}} - \frac{1}{\sqrt{l_d^2+r^2}}\right) + \\ & \rho^t_d\rho^t_{q,2}\left(\frac{1}{\sqrt{4l_q^2+r^2}} + \frac{1}{\sqrt{(l_q-l_d)^2+r^2}} - \right. \\ & \left. \frac{1}{\sqrt{(2l_q-l_d)^2+r^2}} - \frac{1}{\sqrt{l_q^2+r^2}}\right)\Bigg] \end{aligned} \tag{4.20}$$

where $\alpha = 1437 \cdot 10^{-10}$ to get energy in cm^{-1} when distances are expressed in meters. The expression above allows to calculate the interaction energy as a function of the distance r between chromophores. The black line in right panel of Figure 4.12 plots $V(r)$ (calculation are performed in vacuum, so that the refractive index $n = 1$). This result is compared to the result obtained adopting the dipolar approximation (red line). As expected, the two results coincides at large distances, i.e. when the dipolar approximation

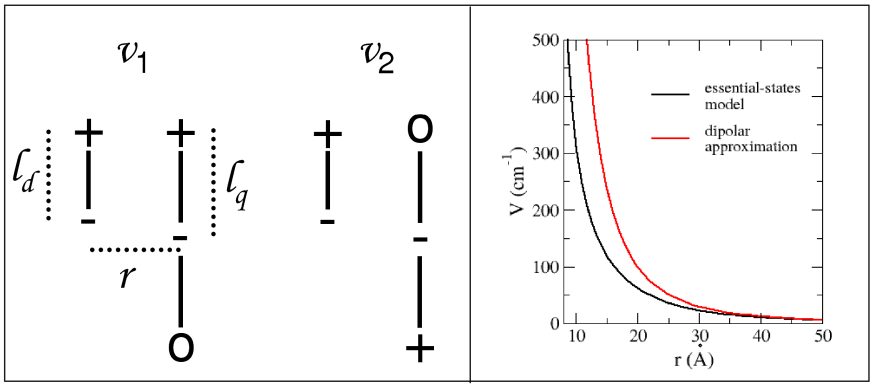

Figure 4.12: *Left panel: definition of the geometrical parameters for the calculation of the interaction energies between the transition charge densities of the dipole* **a** *and of the quadrupole* **b** *shown in Figure 4.11. Right panel: interaction energy (proportional to the transfer rate) calculated according to Equation 4.20, for geometry in the left panel and variable* r*. Results refer to the energy transfer process from the excited state of the donor to the* $|c_q\rangle$ *(optically allowed) state of the quadrupolar dye.*

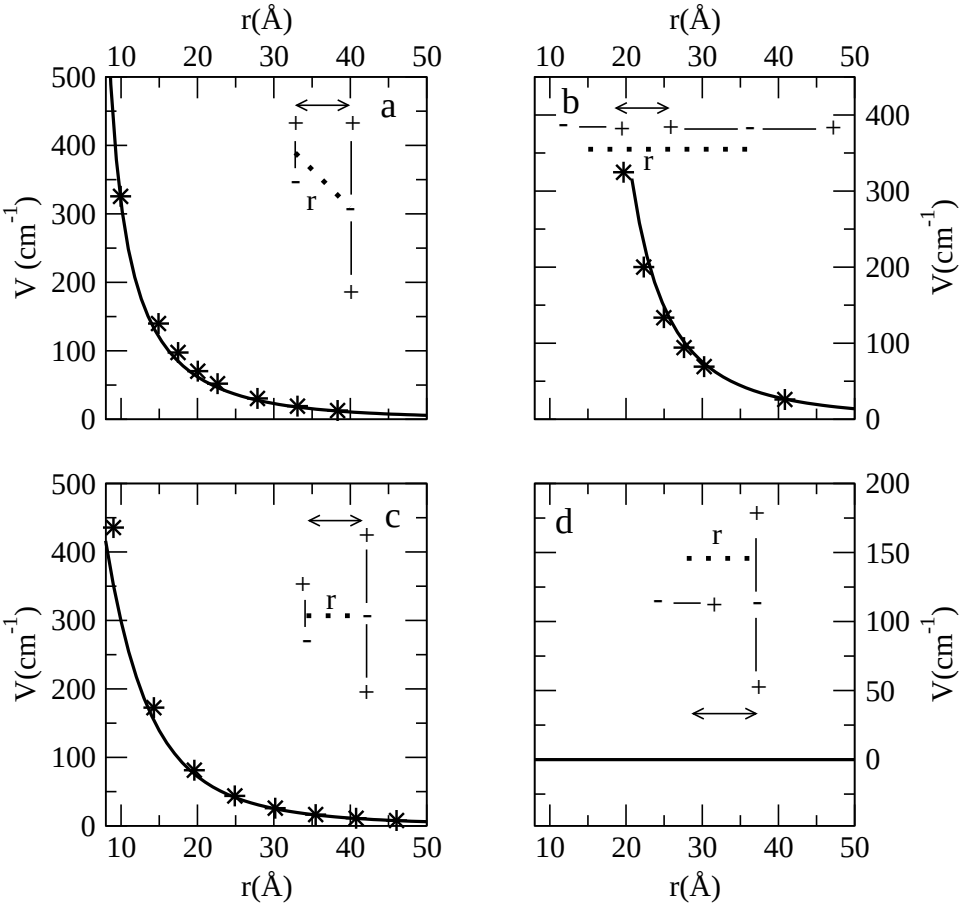

Figure 4.13: *Energy transfer from the excited state of* ***a*** *towards the allowed state of* ***b****. The interaction energy between chromophores is calculated in terms of electrostatic interactions between the transition charge densities. The squared interaction energy is proportional to the transfer rate. Black lines show the result obtained from essential-state models, adopting the molecular parameters listed in Table 4.5 (for the quadrupolar acceptor, the* $|g_q\rangle \rightarrow |c_q\rangle$ *transition is considered), while stars show results of ab-initio calculations (for details about the calculation see text). r is tuned by mutually displacing the two chromophores along the direction of the arrow.*

works well. At short distances the differences between the two results are sizeable, and demonstrate the failure of the dipolar approximation.

In collaboration with the group of Prof. S. Pati from JNCASR in Bangalore (India), the interaction energies evaluated from essential-state models were compared with results obtained through ab-initio calculations. Ab initio molecular orbital calculations have been employed to access the transition densities for individual molecules with Gaussian 03 [161]. The optimized ground state geometry of both molecules in Figure 4.11 were obtained with the B3LYP exchange correlation functional and with 6-31G(d,p) as basis set. The optimization of the excited-state geometry was performed with the configuration interactions with single excitations (CIS) method employing 6-31G(d,p) basis states. The excited state wavefunctions were computed using CIS from a spin-restricted Hartree-Fock reference determinant with 3-21G(d,p) as basis set. The transition densities between the ground and the excited states were generated using the single-CI wavefunctions. Then, the Coulombic coupling matrix elements are calculated following the transition cube formalism by McWeeny [162]:

$$V = \sum_{i,j} \frac{M_{\mathcal{D}}^{i} M_{\mathcal{A}}^{j}}{4\pi\epsilon_0 r_{ij}} \tag{4.21}$$

where $M_{\mathcal{D}}^{i}$ and $M_{\mathcal{A}}^{j}$ are the transition density cube matrix element i and j for the donor and the acceptor at distance r_{ij}.

Results for different geometries are shown in Figure 4.13: black lines are relevant to essential-state models, while stars are the result of ab-initio calculations. The agreement is excellent, and this result confirms the validity and the efficiency of essential-state models for the calculation of inter-chromophore interactions responsible for energy transfer. For the geometry shown in panel d, the interaction energy is zero for symmetry reasons: this geometry is very interesting if we consider the transfer towards the dark $|e_q\rangle$ state, as discussed in the next section.

4.3.2 Energy transfer towards dark states

The interest of energy transfer towards dark states lies on the possibility to open new channels for the transfer process, and as a consequence on the opportunity to make the process more efficient. The energy transfer through dark states can also explain some phenomena observed in the photosynthetic process which cannot be rationalized within the dipolar approximation [163], and some recent observations about systems of interest for organic solar cells [159].

As mentioned above, the dipolar approximation is not suitable for the description of extended dipoles at short distances. Moreover within the dipolar approximation, the energy transfer towards states that are not allowed in one-photon absorption (dark states), is strictly forbidden. In fact, the transition dipole moment of dark states is zero by definition, and hence intermolecular interactions cannot occur in the dipolar approximation. On the contrary, Coulombic interactions between point charges (extended-dipole approach) can be sizeable, and of the same order of magnitude as interactions involving the one-photon allowed state.

The dark state $|e_q\rangle$ written on the non-symmetrized basis, reads:

$$|e_q\rangle = \sqrt{\rho_q}|DAD\rangle + \sqrt{\frac{1-\rho_q}{2}}(|D^+A^-D\rangle + |DA^-D^+\rangle) \tag{4.22}$$

Imposing the same geometry shown in the left panel of Figure 4.12, the interaction energy can be calculated from Equation 4.20, using the following transition charge densities for the quadrupole:

$$\begin{aligned} \rho^t_{q,1} &= \langle g_q|\hat{\rho}_{q,1}|e_q\rangle = \frac{\sqrt{\rho_q(1-\rho_q)}}{2} \\ \rho^t_{q,2} &= \langle g_q|\hat{\rho}_{q,2}|e_q\rangle = \frac{\sqrt{\rho_q(1-\rho_q)}}{2} \end{aligned} \tag{4.23}$$

Figure 4.14 shows the interaction energy of the transition charge density of the dipole with the transition charge density of the quadrupole relevant to the dark state $|e_q\rangle$, for different geometrical arrangements. The squared

interaction energy, according to the Fermi Golden rule, is proportional to the transfer rate of the process. Also in this case we compare results obtained with essential-state models with results obtained with ab-initio calculations (described above). Figure 4.14 shows that the calculated interaction energies are of the same order on magnitude as those obtained considering the one-photon allowed state $|c_q\rangle$, except for the geometry shown in panel c, where interaction is zero by symmetry. Interesting is the case shown in panel d: in this geometry the interaction energy is zero by symmetry if the transfer to $|c_q\rangle$-state is considered. On the contrary, the transfer towards the $|e_q\rangle$-state gives rise to a sizeable interaction energy, on the same order of magnitude of those calculated for the other geometries. Moreover, the results obtained using essential-state models are confirmed by more refined ab-initio calculations. Also in this case, the two approaches give results which are in excellent agreement. This means that the model adopted to describe interactions using the essential-state description is suitable and efficient.

In this section we discussed the interaction energy responsible for energy transfer, and we have shown that, relaxing the dipolar approximation, dark states become available channels for energy transfer, and that their contribution can be as important as that of allowed-states. Of course, according to the Fermi Golden rule in Equation 4.2, energy conservation is required, i.e. the emission of the donor has to overlap the dark transition of the quadrupolar acceptor. The pair of molecules that we have chosen, according to the data from the literature [160], satisfies this requirement: experimental measurements should show energy transfer only through the dark state of the acceptor. The work about energy transfer involving dark states will proceed in several directions: we will verify experimentally this interesting theoretical predictions. First of all, energy transfer will be measured in a concentrated solution of donors $\mathcal{D}$ and $\mathcal{A}$, not directly linked together. The second step involves the synthesis of a properly engineered macromolecule, in which the donor and the acceptor are linked through a

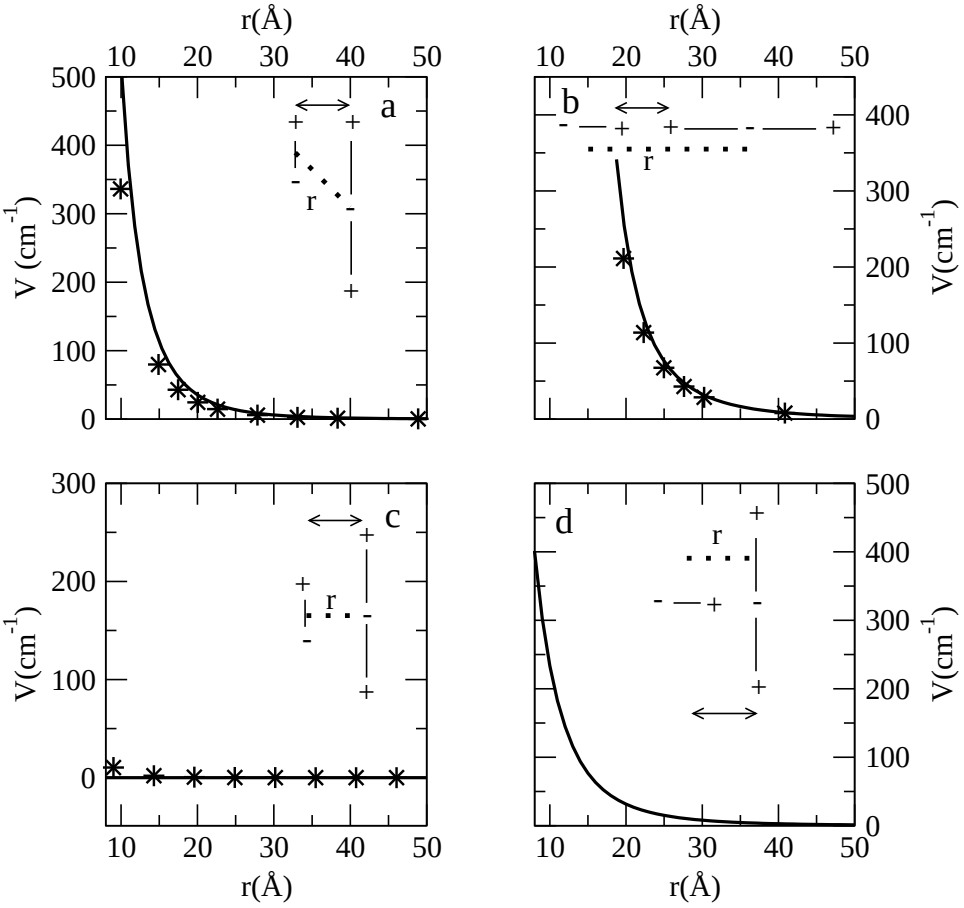

Figure 4.14: *Energy transfer towards dark states: interaction energy between the transition charge density of the dipolar donor molecule and the transition charge density of the quadrupolar acceptor molecule (the transition towards the dark state $|g_q\rangle \rightarrow |e_q\rangle$ is considered). The interaction energy between chromophores is calculated in terms of electrostatic interactions between transition charge densities. The squared interaction energy is proportional to the transfer rate. Black lines show the result obtained from essential-state models, adopting the molecular parameters listed in Table 4.5, while stars show results of ab-initio calculations (for details about the calculation see text). r is tuned by mutually displacing the two molecules along the direction of the arrows.*

non-conjugated connector, as shown in panels d of Figures 4.13 and 4.14. Finally some theoretical effort will be spent in the definition of new computational approaches to calculate the interaction matrix elements in quantum chemical approaches, without the calculation of transition charge densities, and on the development of new expressions for RET not based on the Fermi Golden rule (i.e. relaxing the weak interaction approximation).

4.4 Conclusion

In this Chapter the resonant energy-transfer process between a donor molecule $\mathcal{D}$ and an acceptor molecule $\mathcal{A}$ was discussed. In particular we focused on the intermolecular interactions responsible for energy transfer. In the first part of the Chapter, the Förster approach, based on the dipolar approximation for the description of intermolecular interactions, was presented. This approach is very efficient when transition dipole moments are very small compared to distances. The Förster approach was applied for the analysis of energy-transfer collected on a multi-photon absorbing system, constituted by a quadrupolar central core, and two peripheral dipoles. In this work we demonstrated that the efficiency of the transfer is very high ($> 90\%$), and that it is possible to associate the efficient one- and two-photon absorption properties of the quadrupole to the (red) emission of the dipole.

In the last Section we relaxed the dipolar approximation for the calculation of RET rates. Intermolecular interactions between transition charge densities were described in terms of the same extended-dipole approach described in Chapter 3 to account for interactions in multichromophoric systems, while transition charge densities were calculated using essential-state models presented in Chapter 1. First of all we demonstrated the failure of the dipolar approximation at short interchromophoric distances. More interestingly, we showed that energy transfer can also imply dark states. In particular we calculated the interaction between the transition charge density of a dipolar chromophore and the one-photon forbidden transition charge

density of a quadrupolar chromophore. This interaction, that is strictly zero within the dipolar approximation, is sizeable if the extended-dipole approach is applied, and is on the same order of magnitude of the interaction that we get considering the one-photon allowed transition. Results from essential-state models were confirmed and validated by comparison with ab-initio results. Energy-transfer towards dark states is a very interesting phenomenon, because it opens new channels to increase the efficiency of the process.

Conclusions and perspectives

This thesis presents an extensive study of charge-transfer (CT) dyes, which represent a very interesting class of organic chromophores for advanced applications. The study combines theoretical and experimental work to offer a reliable description of optical properties and spectra of CT chromophores in different environments. CT dyes constitute excellent model systems for investigating charge- and energy-transfer processes, that represent key phenomena in physics, chemistry and biology.

The work started with the description of essential-state models that are at the heart of the theoretical approach that we have developed for CT dyes. CT dyes are made up by electron donor and acceptor groups joint by π-conjugated bridges and their physics is governed by the charge-resonance between donor and acceptor groups. Essential-state models exploit this information and adopt the main resonating structures of each dye as the basis states for the relevant electronic problem. This amounts to an enormous simplification with respect to quantum chemical models for the molecular electronic structure and, quite unavoidably, to the loss of some detail. But we gain in generality: essential-state models are in fact general enough to describe the behavior of classes of chromophores in a unique frame. Moreover, the "easy to manage" electronic Hamiltonians can be extended to account for the coupling to molecular vibrations and polar solvation. The resulting models are far from trivial and allow to rationalize and/or predict important vibrational contributions to nonlinear optical responses, unusual inhomogeneous broadening effects in polar solvents and solvent-induced symmetry

breaking phenomena. The robustness of this theoretical approach is confirmed by the comparison with experimental data on many compounds. In particular, we are able to quantitatively reproduce linear and nonlinear spectra of compounds of different structure and dimensionality.

Essential-state models belong to the large family of semiempirical approaches: model parameters have to be extracted from the comparison with experiment. Explicitly accounting for polar solvation, the molecular model is defined by a handful of solvent-independent parameters that are reliably extracted from the analysis of spectroscopic data. While semiempirical in nature, the predictive power of essential-state models lies in the possibility to calculate low energy spectral properties, including linear and non-linear spectra, for a given chromophore, yielding to a complete description of its photophysics in different environments. The comparison with spectroscopic data is then important to parametrize essential-state models as well as to validate them. On a more general perspective, the analysis of spectral properties of CT dyes is instrumental to deepen our understanding of charge- and energy- transfer processes. Chapter 2 of this thesis was devoted to advanced spectroscopic tools as applied to CT dyes. Specifically we focused attention on the electroabsorption technique, for which we developed detailed models. Moreover, the acquisition of a cryostat allowed us to set up thermochromic as well as fluorescence anisotropy measurements.

The models developed for CT dyes in solution naturally lent themselves to be extended to the description of the same dyes in more complex and challenging environments. Specifically, collective and cooperative phenomena are expected in clusters where different chromophores interact via electrostatic interactions that show up with the enhancement or suppression of nonlinear optical responses, electrostatically-induced bistability, and the exotic phenomenon of multielectron transfer (called in other contexts multiexciton generation). Chapter 3 was devoted to the study of multichromophoric systems. Two families of systems were studied, one based on a zwitterionic DA-chromophore and a second one based on a quadrupolar salt. These ex-

amples allowed to demonstrate the power of the bottom-up approach in this context, and to fully exploit the advantages of essential-state models. In fact the analysis starts from a careful spectroscopic study of the isolated chromophore in solution to extract solvent-independent molecular parameters for the essential-state model. The model proposed to describe two (or more) chromophores interacting via classical electrostatic interactions exploits the same environment-independent molecular parameters. This is possible thanks to the fact that the molecular polarizability is completely and self-consistently taken into account. Apart from proving the effectiveness of bottom-up techniques, our analysis also demonstrated the reliability of models for interchromophore electrostatic interactions based on the extended dipole approximation.

The same electrostatic interactions that are responsible for cooperative and collective phenomena in multichromophoric assemblies drive the phenomenon of energy transfer in heterochromophoric clusters. In the last Chapter of this thesis we presented the first results of a more ambitious project aimed at investigating the energy transfer phenomenon. We were able to prove that the extended-dipole approximation for interchromophore interactions leads to qualitatively different results than the more commonly adopted point-dipole approximation. Specifically, the extended dipole approximation opens new channels for energy transfer through optically dark states, that are strictly forbidden in the point-dipole approximation. In perspective this work opens the possibility to address more fundamental questions: the role of (non-adiabatic) molecular vibrations in energy transfer can in fact be easily investigated in the essential-state picture. Moreover, the role of environment, and more specifically inhomogeneous broadening effects and/or symmetry-breaking effects in polar solvents can be quantitatively addressed. In a more ambitious effort, the engineering of the photonic density of states in photonic crystals and/or in the proximity of plasmonic structures opens new perspectives on energy transfer that can be usefully addressed with the theoretical framework developed here. Finally, the pos-

sibility to relax the approximation of weak coupling, i.e. the development of new expressions for resonance energy transfer not based on the Fermi Golden rule, represents an exciting challenge.

Appendix A

Computational details about the calculation of absorption, fluorescence and two-photon absorption spectra

In this Appendix we describe the procedure for the calculation of linear and nonlinear spectra. Once defined the coupled electron-vibration problem, according to essential-state models presented in Chapter 1 for isolated chromophores and in Chapter 3 for multichromophoric assemblies, the calculation follows the same steps for dipolar, quadrupolar or octupolar chromophores, and for multichromophoric systems.

The orientational i-th components of the reaction field, $F_{or}^{(i)}$, (where i runs on the relevant component of the reaction field: for isolated chromophores, $i = 1$ for linear molecules or $i = 1, 2$ for planar chromophores, while in multichromophoric systems i is the sum of the relevant components for each chromophore) describes a very slow motion that can be treated classically. Therefore, the coupled electron-vibration problem is solved for fixed $F_{or}^{(i)}$ values via a numerically exact diagonalization. Specifically, for each

$F_{or}^{(i)}$, the total Hamiltonian is written on the basis obtained as the direct product of the electronic basis state and the eigenstates of the harmonic oscillator. The vibrational basis is truncated to a number of states large enough as not to affect relevant results (the number of vibrational states, depends on the molecular parameters, and it increases for strong electron-phonon coupling; typical values are 6-10 states). The resulting Hamiltonian matrix is diagonalized numerically to get vibronic eigenstates. A Gaussian bandshape with half-width at half-maximum $\Gamma = \sqrt{2ln2}\sigma$ (cm^{-1}) is assigned to each vibronic transition, so that the molar extinction coefficient (ϵ) and fluorescence spectrum (I) are calculated as function of the wavenumber, $\tilde{\nu}$ (expressed in ($cm^{-}1$)), as follows:

$$\epsilon(\tilde{\nu}) = \frac{10\pi N_A \tilde{\nu}}{3ln10\hbar c\epsilon_0} \frac{1}{\sqrt{2\pi}\sigma} \sum_n \mu_{gn}^2 exp\left[-\frac{1}{2}\left(\frac{\tilde{\nu}_{gn} - \tilde{\nu}}{\sigma}\right)\right] \tag{A.1}$$

$$I(\tilde{\nu}) \propto \tilde{\nu}^3 \frac{1}{\sqrt{2\pi}\sigma} \sum_n \mu_{fn}^2 exp\left[-\frac{1}{2}\left(\frac{\tilde{\nu}_{fn} - \tilde{\nu}}{\sigma}\right)\right] \tag{A.2}$$

In Equation A.1, N_A is the Avogadro number, c is the speed of light, ϵ_0 is the vacuum permittivity, $\tilde{\nu}_{gn}$ and μ_{gn} are the transition wavenumber and dipole moment respectively, for the $g \rightarrow n$ transition from the ground (g) to the generic excited state (n), and summation runs over all (vibronic) excited states. In Equation A.2, referring to fluorescence, $\tilde{\nu}_{fn}$ and μ_{fn} are the transition wavenumber and dipole moment, respectively, for the $f \rightarrow n$ transition from the fluorescent state (f) to the generic lower-energy state (n), and summation runs over all states having lower energy with respect to the fluorescent state, f. The emissive state is selected as the first excited state with a sizeable transition dipole moment from the ground state. The calculation of linear spectra is repeated for different F_{or} values and the total spectra are obtained summing up the contributions at different F_{or} weighted by the relevant Boltzmann population.

The two-photon absorption cross section is calculated according to the following expression [25]:

$$\sigma_2(\omega) = 10^{58} \frac{\hbar\omega^2}{4\epsilon_0^2 c^2} Im\langle\gamma_{ijkl}(-\omega;\omega,\omega,-\omega)\rangle_{IJKL} \tag{A.3}$$

where c is the speed of light, and $\langle\gamma\rangle$ the orientationally averaged second hyperpolarizability ($IJKL$ indices run on the laboratory axis; $ijkl$ run on the axis of the molecular reference system). Tensor elements $\gamma_{ijkl}(-\omega;\omega,\omega,-\omega)$ are given by the following sum-over-states expressions [100]:

$$\begin{aligned}\gamma_{ijkl}(-\omega;\omega,\omega,-\omega) &= \frac{1}{\hbar^3}\sum_{lmn}\left\{\frac{\langle g|\mu_i|l\rangle\langle l|\bar{\mu}_j|m\rangle\langle m|\bar{\mu}_k|n\rangle\langle n|\mu_l|g\rangle}{(\Omega_{lg}-\omega)(\Omega_{mg}-2\omega)(\Omega_{ng}-\omega)}+\right.\\ &\quad \frac{\langle g|\mu_j|l\rangle\langle l|\bar{\mu}_i|m\rangle\langle m|\bar{\mu}_k|n\rangle\langle n|\mu_l|g\rangle}{(\Omega^*_{lg}-\omega)(\Omega_{mg}-2\omega)(\Omega_{ng}-\omega)}+\\ &\quad \frac{\langle g|\mu_i|l\rangle\langle l|\bar{\mu}_j|m\rangle\langle m|\bar{\mu}_l|n\rangle\langle n|\mu_k|g\rangle}{(\Omega_{lg}-\omega)(\Omega_{mg}-2\omega)(\Omega_{ng}-\omega)}+\\ &\quad \left.\frac{\langle g|\mu_j|l\rangle\langle l|\bar{\mu}_i|m\rangle\langle m|\bar{\mu}_l|n\rangle\langle n|\mu_k|g\rangle}{(\Omega^*_{lg}-\omega)(\Omega_{mg}-2\omega)(\Omega_{ng}-\omega)}\right\} \qquad \text{(A.4)}\end{aligned}$$

where only two-photon resonant terms have been retained; g is the ground state and summations run over all vibronic excited states as obtained from the diagonalization; $\Omega_{lg} = \omega_{lg} - i\Gamma_{lg}$ (we set $\Gamma_{lg} = \Gamma$, the width of the Gaussian bandshape defined above, for all transitions) and $\bar{\mu} = \mu - \langle g|\hat{\mu}|g\rangle$.

For linear molecules (dipolar chromophores and linear quadrupolar chromophores), the only tensor element different from zero is the γ_{xxxx} term, where x is the molecular axis. The orientationally-averaged second hyperpolarizability is thus given by $\langle\gamma\rangle_{XXXX} = 1/5\gamma_{xxxx}$. For planar octupolar chromophores (C_3 symmetry), $\langle\gamma\rangle_{XXXX} = 8/15\gamma_{xxxx}$ [101]. As for OPA, the calculation of TPA spectra is repeated for different $F_{or}^{(i)}$ values and the overall spectrum is obtained summing up the TPA spectra weighted by the Boltzmann population.

Appendix B

Measurement of fluorescence quantum yields

By definition, the fluorescence quantum yield, ϕ, represents the portion of excited molecules that deactivate by emitting a fluorescence photon, corresponding to the ratio of the number of emitted photons to the number of absorbed photon per time unit [164]. Fluorescence quantum yield is related to the radiative (k_r) and nonradiative (k_{nr}) rate constants of deactivation by the relationship:

$$\phi = \frac{k_r}{k_r + k_{nr}} \tag{B.1}$$

The measurement of *absolute* quantum yield requires special equipments, such as integrating spheres. For measurements in solution, the *relative* quantum yield is usually determined. The fluorescence efficiency of a sample is related to that of a standard by the equation:

$$\phi_x = \frac{A_s}{A_x}\frac{I_x}{I_s}\frac{n_x^2}{n_s^2}\phi_s \tag{B.2}$$

where x, s refer to the sample and the standard, respectively. A is the absorbance of the solution at the excitation wavelength and accounts for absorbed photons, I is the integrated area of the fluorescence spectrum (in wavelengths) that accounts for emitted photons, and n is the refractive index

of the solvent. To avoid internal filter effects, the solutions of the sample and of the standard must be optically diluted, to have $A < 0.1$.

The integrated area of fluorescence spectra has to be calculated considering the corrected spectra. Gratings, detectors and other spectrometer components have characteristic responses that vary as a function of the wavelength. In a fluorometer, two correction curves have to be accounted for:

1. the correction for the emission channel (grating and detector) allows to get a reliable bandshape of the fluorescence spectrum, and as a consequence a reliable integrated area.

2. the correction relevant to the excitation. The source in a fluorometer is usually a halogen lamp, that emits in the visible range. Of course, the intensity of the lamp depends on the wavelength. For fluorescence quantum yield measurements, if the sample and the standard are excited at different wavelenghts, fluorescence spectra has to be divided by the intensity of the lamp at the excitation wavelength. Moreover, the response of the detector that monitors the intensity of the lamp is a function of the wavelength, so that also its signal has to be corrected.

If not specified, in this work emission spectra were collected exciting the sample at the maximum of the absorption band. Moreover, the standard used for fluorescence quantum yield is Fluorescein in NaOH 0.1M ($\phi_s = 0.9$), excited at 470nm. Its fluorescence quantum yield was tested using different standards, such as Rhodamine101 in EtOH ($\phi_s = 1$) and Quinine Bisulfate in H_2SO_4 0.05M ($\phi_s = 0.56$). Since emission intensity is sensitive to temperature, fluorescence spectra were collected on thermostated solutions, at 23°C, when not differently specified.

The error in the determination of fluorescence quantum yield, adopting the procedure described above, does not exceed ±10%.

Appendix C

Two-photon excited fluorescence

Two-photon absorption is a third-order nonlinear process in which two photons are absorbed simultaneously by the sample (coherent process). This process was predicted by Maria Göppert-Mayer at the end of the twenties and confirmed experimentally in the sixties.

The two-photon absorption cross section data reported in Chapter 1 and 3 were measured using the two-photon excited fluorescence (TPEF) technique. The TPEF technique measures the fluorescence signal induced by the simultaneous absorption of two photons. The two-photon absorption cross section, $\sigma_2(\omega)$, is derived by comparison to a reference compound and by the fluorescence quantum yield (ϕ) of the sample.

Assuming that ϕ is the same when the sample is excited by one or two photons, the fluorescence signal F induced by two-photon absorption is:

$$F \propto cP^2 K \sigma_2 \phi \tag{C.1}$$

where c is the concentration of the active species, P is the incident power, K is the detection efficiency. The detection efficiency is expressed as follows:

$$K = \frac{f}{n^2} \tag{C.2}$$

where f is the correction factor, taking into account the wavelength dispersion of the response function, and n is the refractive index of the medium [25].

The ratio of the function F/P^2 of the sample and the function $(F/P^2)_R$ of a reference compound is proportional to the two-photon absorption cross section σ_2:

$$\frac{F}{P^2}\left(\frac{F}{P^2}\right)_R^{-1} = \frac{cK\sigma_2\phi}{c_R K_R(\sigma_2\phi)_R} \tag{C.3}$$

From Equations C.2 and C.3, the TPEF cross section of the molecule of interest, multiplied by ϕ, is given by the following expression:

$$\sigma_2\phi = (\sigma_2\phi)_R \frac{f_R}{f}\frac{c_R}{c}\frac{n^2}{n_r^2}\frac{F}{P^2}\left(\frac{F}{P^2}\right)^{-1} \tag{C.4}$$

The direct outputs of the measurements are the signals $\frac{F}{P^2}$ of the sample and of the reference compound. The dependence of such signals on P must be constant, i.e. the fluorescence signals must have a quadratic dependence on the incident power. The quadratic dependence of the fluorescence signal on P is always tested for each wavelength, to rule out the occurrence of photodegradation or saturation phenomena [25].

In the CGS system, the TPA cross section has the following units: $\mathrm{cm}^4 \cdot \mathrm{s} \cdot \mathrm{photon}^{-1}$. Practical units commonly adopted are the Göppert-Mayer (GM) defined as: $1\mathrm{GM}=10^{-50} \cdot \mathrm{cm}^4 \cdot \mathrm{s} \cdot \mathrm{photon}^{-1}$ [25].

According to the spectral region, two different reference compounds are used: fluorescein in NaOH 0.1M from 700 to 980nm [79], and styryl 9M in EtOH from 980 to 1200nm [80]. Measurements were performed adopting the experimental protocol proposed by Xu and Webb [79]. From 700 to 980nm an additional control was performed using the known TPEF cross section of Rhodamine B in MeOH.

The excitation source is a Ti:sapphire femtosecond laser system, delivering pulses of ca 150fs duration and 76MHz repetition rate. This laser supplies photons in the 700-980nm spectral range. At University of Rennes 1, to extend the spectral region until 1200nm, an optical parametric oscillator is used (OPO). The incident power on the sample is of the order

of a few mW. The laser beam is focused onto the quartz cell holding the sample. Experimental setup at University of Rennes 1, France, (Prof. M. Blanchard-Desce) collects the fluorescence signal in the backward direction with respect to excitation (epifluorescence geometry). Instead, experimental setup at University of Padova, Italy, (Prof. C. Ferrante) collects the fluorescence signal at 90° with respect to excitation. In both cases, care was taken to avoid reabsorption of the emitted photons (the laser beam was focused close to the proper cell window). In the epifluorescence geometry, a beam splitter is necessary to drive the fluorescence signal towards the detector. In both geometries filters (called in the text blue and red) are introduced before the detecting system to cut the residual laser beam.

Acknowledgements

I wish to express my deep gratitude to my supervisors, Prof. Anna Painelli and Prof. Francesca Terenziani, for their constant presence, guidance and support during this PhD training. I also thank all people of the research team for interesting and useful discussion: Prof. A. Girlando, Prof. M. Masino, Dr. G. D'Avino and Dr. L. Grisanti.

I wish to thank all people I have collaborated with:

- Prof. A. Abbotto of University of Milano-Bicocca (Italy)
- Prof. C. Ferrante of University of Padova (Italy)
- Prof. D. Comoretto of University of Genova (Italy)
- Prof. D. Roberto of University of Milano (Italy)
- Prof. M. Blanchard-Desce of University of Rennes 1 (France), and all people of the UMR 6510
- Prof. S. Pati, Dr. A. Manna and Dr. P. Parida of JNCASR of Bangalore (India)
- Prof. E. Dalcanale and Dr. M. Busi for the support in the growth of self-assembled films on gold

This work was supported by the Italian Ministry for Education, through *PRIN2006031511*. The stage of two months at University of Rennes 1

(France) was financed by the Italo-French University through the *Galileo Programme*. I thank the indian part of the *Indo-Italian Executive Programme of S & T Co-operation 2008-2010*, and the Rector of the University of Parma, Prof. Gino Ferretti, for co-funding the stage at JNCASR of Bangalore (India).

Bibliography

[1] J. R. Heath and M. A. Ratner, Physics Today **56**, 43 (2003)

[2] E. Vogel, Nature Nanotechnologies **2**, 25 (2007)

[3] H. Friend, R. W. Gymer, A. B. Holmes, J. H. Burroghes, R. N. Marks, C. Taliani, D. D. C. Bradley, D. A. Dos Santos, J.-L. Brédas, M. Lögdlund, and W. R. Salaneck, Nature **397**, 121 (1999)

[4] S. K. Sahoo, S. Parveen, and J. J. Panda, Nanomedicine **3**, 20 (2007)

[5] A. Diaspro, G. Chirico, and M. Collini, Q. Rev. Biophys. **38**, 97 (2005)

[6] W. Zhou, S. M. Kuebler, K. L. Braun, T. Yu, J. K. Cammack, C. K. Ober, J. W. Perry, and S. R. Marder, Science **296**, 1106 (2002)

[7] B. H. Cumpston, S. P. Ananthavel, S. Barlow, D. L. Dyer, J. E. Ehrlich, L. L. Erskine, A. A. Heikal, S. M. Kuebler, I. Y. S. Lee, D. McCord-Maughon, J. Q. Qin, H. Rockel, M. Rumi, X. L. Wu, S. R. Marder, and J. W. Perry, Nature **398**, 51 (1999)

[8] C. N. La Fratta, J. T. Fourkas, T. Baldacchini, and R. A. Farrer, Angew. Chem. Int. Ed. **46**, 6238 (2007)

[9] Y. N. Konan, R. Gurny, and E. Alleman, J. Photochem. Photobiol. B **66**, 89 (2002)

[10] P. K. Frederiksen, M. Jorgensen, and P. R. Ogilby, J. Am. Chem. Soc. **123**, 1215 (2001)

[11] T. Breitenbach, M. K. Kuimova, P. Gbur, S. Hatz, N. B. Schack, B. W. Pedersen, J. D. C. Lamber, L. Poulsen, and P. R. Ogilby, Photochem. Photobiol. Sci. **8**, 442 (2009)

[12] V. Sundström, Annu. Rev. Phys. Chem. **59**, 53 (2008)

[13] T. Pulleritis and V. Sundström, Acc. Chem. Res. **29**, 381 (1996)

[14] A. C. Benniston and A. Harriman, Materials Today **11**, 27 (2008)

[15] Z. G. Soos, D. Mukhopadhyay, A. Painelli, and A. Girlando, "Handbook of conducting polymers," (Marcell Dekker, 1998) p. 165

[16] J.-L. Brédas, J. Cornil, D. Beljonne, and F. Meyers, "Handbook of conducting polymers," (Marcell Dekker, 1998) p. 1

[17] A. Painelli and F. Terenziani, "Non-linear optical properties of matter: From molecules to condensed phases," (Springer, 2006) p. 251

[18] S. R. Marder, B. Kippelen, A. K.-J. Jen, and N. Peyghambarian, Nature **388**, 845 (1997)

[19] D. Burland, Chem. Rev. **94**, 1 (1994)

[20] P. N. Prasad and D. J. Williams, *Introduction to nonlinear optical effects in molecules and polymers* (Wiley, 1991)

[21] G. A. Linsday and K. D. Singer, *Exciton in Molecular Crystals* (Americal Chemical Society, ACS Symposium Series 601, 1995)

[22] F. Terenziani, G. D'Avino, and A. Painelli, ChemPhysChem **8**, 2433 (2007)

[23] F. Terenziani, C. Sissa, and A. Painelli, J. Phys. Chem. B **112**, 5079 (2006)

[24] S. Marder, L.-T. Cheng, B. G. Tiemann, A. C. Firedli, M. Blanchard-Desce, J. W. Perry, and J. Skindhøj, Science **263**, 511 (1994)

[25] F. Terenziani, C. Katan, M. Blanchard-Desce, E. Badeva, and S. Tretiak, Adv. Mater. **20**, 4641 (2008)

[26] D. Beljonne, W. Wenseleers, E. Zojer, Z. Shuai, H. Vogel, S. J. K. Pond, J. W. Perry, S. R. Marder, and J.-L. Brédas, Adv. Funct. Mater. **12**, 631 (2002)

[27] D. R. Kanis, M. A. Ratner, and T. J. Marks, Chem. Rev. **94**, 195 (1994)

[28] J. Zyss and I. Ledoux, Chem. Rev. **94**, 77 (1994)

[29] G. S. He, L.-S. Tan, Q. Zheng, and P. N. Prasad, Chem. Rev. **108**, 1245 (2008)

[30] R. M. Metzger, Chem. Rev. **103**, 3803 (2003)

[31] M. Bixon and J. Jortner, Adv. Chem. Phys. **106**, 35 (1999)

[32] A. Nitzan, *Chemical Dynamics in Condensed Phases* (Oxford University Press, 2006)

[33] R. A. Marcus, Rev. Mod. Phys. **65**, 599 (1993)

[34] N. S. Hush, Prog. Inorg. Chem. **8**, 2264 (1967)

[35] N. H. Hush and J. R. Reimers, Chem. Rev. **100**, 775 (2000)

[36] N. S. Hush, Coord. Chem. Rev. **8**, 391 (1985)

[37] C. Reichardt, Chem. Rev. **94**, 2319 (1994)

[38] B. Boldrini, E. Cavalli, F. Terenziani, and A. Painelli, J. Phys. Chem. A **106**, 6286 (2002)

[39] F. Terenziani, A. Painelli, C. Katan, M. Charlot, and M. Blanchard-Desce, J. Am. Chem. Soc. **128**, 15755 (2006)

[40] L. Grisanti, C. Sissa, F. Terenziani, A. Painelli, D. Roberto, F. Tessore, R. Ugo, S. Quici, I. Fortunati, E. Garbin, C. Ferrante, and R. Bozio, Phys. Chem. Chem. Phys. **11**, 9450 (2009)

[41] F. Terenziani, A. Painelli, and D. Comoretto, J. Phys. Chem. A **104**, 11049 (2000)

[42] C. Sissa, F. Terenziani, and A. Painelli, J. Phys. Chem. A **112**, 8697 (2008)

[43] F. Terenziani and A. Painelli, J. Am. Chem. Soc. **125**, 5624 (2003)

[44] F. Terenziani and A. Painelli, Phys. Rev. B **68**, 165405 (2003)

[45] A. Datta, F. Terenziani, and A. Painelli, ChemPhysChem **7**, 2168 (2006)

[46] G. D'Avino, L. Grisanti, J. Guash, I. Ratera, J. Veciana, and A. Painelli, J. Am. Chem. Soc. **130**, 12064 (2008)

[47] G. D'Avino, F. Terenziani, and A. Painelli, J. Phys. Chem B **11**, 25590 (2006)

[48] C. Sissa, F. Terenziani, A. Painelli, A. Abbotto, L. Bellotto, C. Marinzi, E. Garbin, C. Ferrante, and R. Bozio, J. Phys. Chem. B **114**, 882 (2010)

[49] B. E. Hardin, E. T. Hoke, P. B. Armstrong, J.-H. Yum, P. comte, T. Torres, J. M. J. Frechet, M. K. Nazeeruddin, M. Grätzel, and M. D. McGehee, Nature Photonics **3**, 406 (2009)

[50] M. A. Baldo, M. E. Thompson, and S. R. Forrest, Nature **403**, 750 (2000)

[51] R. S. Mulliken, J. Am. Chem. Soc. **74**, 811 (1952)

[52] J. Oudar and D. Chemla, J. Chem. Phys. **66**, 2664 (1977)

[53] A. Painelli, Chem. Phys. Lett. **285**, 352 (1998)

[54] A. Painelli, Chem. Phys. **245**, 185 (1999)

[55] S. Grimme, Rev. Comput. Chem. **20**, 153 (2004)

[56] R. Improta, V. Barone, and F. Santoro, Angew. Chem. Int. Ed. **46**, 405 (2007)

[57] P. Macak, Y. Luo, P. Norman, and H. Agren, J. Chem. Phys. **113**, 7055 (2000)

[58] A. Painelli, L. Del Freo, and F. Terenziani, Chem. Phys. Lett. **346**, 470 (2001)

[59] D. M. Bishop, J. M. Luis, and B. Kirtman, J. Chem. Phys. **116**, 9729 (2002)

[60] L. D. Freo, F. Terenziani, and A. Painelli, J. Chem. Phys. **116**, 755 (2002)

[61] F. Terenziani and A. Painelli, J. Phys. Chem. A **104**, 11041 (2000)

[62] A. Painelli and F. Terenziani, Chem. Phys. Lett. **312**, 211 (1999)

[63] A. Painelli and F. Terenziani, J. Phys. Chem. A **104**, 11041 (2000)

[64] M. Albota, D. Beljonne, J.-L. Brédas, J. E. Ehrlich, J.-Y. Fu, A. A. Heikal, S. E. Hess, T. Kogej, M. D. Levin, S. R. Marder, D. McCord-Maughon, J. W. Pery, H. Röckel, M. Rumi, G. Subramaniam, W. W. Webb, X.-L. Wu, and C. Xu, Science **281**, 1653 (1998)

[65] A. Abbotto, L. Beverina, R. Bozio, A. Facchetti, C. Ferrante, G. A. Pagani, D. Pedron, and R. Signorini, Org. Lett. **4**, 1495 (2002)

[66] B. Strehmel, A. M. Sarker, and H. Detert, ChemPhysChem **4**, 249 (2003)

[67] O. Mongin, L. Porrès, M. Charlot, C. Katan, and M. Blanchard-Desce, Chem. Eur. J. **13**, 1481 (2007)

[68] C. Katan, F. Terenziani, O. Mongin, M. V. Werts, L.Porrès, T. Pons, J. Mertz, S. Tretiak, and M. Blanchard-Desce, J. Phys. Chem. A **109**, 3024 (2005)

[69] S. Webster, J. Fu, A. Padilha, O. V. Przhonska, D. J. Haganand, E. W. Van Stryland, M. V. Bondar, Y. L. Slominsky, and A. D. Kachkovski, Chem. Phys. **348**, 143 (2008)

[70] S. Chung, S. Zheng, T. Odani, L. Beverina, J. Fu, L. A. Padilha, A. Biesso, J. M. Hales, X. Zhan, K.Schmidt, A.Ye, E. Zojer, S. Barlow, D. J. David, E. W. Van Stryland, Z. Shuai, Y. Yi, G. A. Pagani, J.-L. Brédas, J. W. Perry, and S. R. Marder, J. A. Chem. Soc. **128**, 14444 (2008)

[71] L. Beverina, M. Crippa, P. Salice, R. Ruffo, C. Ferrante, I. Fortunati, R. Signorini, C. M. Mari, R. Bozio, A. Facchetti, and G. A. Pagani, Chem. Mater. **20**, 3242 (2008)

[72] J. Fu, L. A. Padilha, D. J. Hagan, E. W. Van Stryland, O. V. Przhonska, M. V. Bondar, Y. L. Slominsky, and A. D. Kachkovski, J. Opt. Soc. Am. B **24**, 67 (2007)

[73] D. Scherer, R. Dorfler, A. Feldner, T. Vogtmann, M. Scwoerer, U. Lawrentz, W. Grahn, and C. Lambert, Chem. Phys. **279**, 179 (2002)

[74] T. G. Goodson III, Acc. Chem. Res. **38**, 99 (2005)

[75] Y. Wang, T. Goodson III, G. S. He, and P. N. Prasad, J. Am. Chem. Soc. **127**, 10128 (2005)

[76] C. Le Drumaguet, O. Mongin, M. H. V. Werts, and M. Blanchard-Desce, Chem. Comm., 2802(2005)

[77] V. L. Floc'h, S. Brasselet, J. Zyss, B. R. Cho, S. H. Lee, S.-J. Jeon, M. Cho, K. S. Min, and M. P. Suh, Adv. Mater. **17**, 196 (2005)

[78] A. Cravino, P. Leriche, O. Alévêque, and J. Roncali, Adv. Mater. **18**, 3033 (2006)

[79] C. Xu and W. W. Webb, J. Opt. Soc. Am. B **13**, 481 (1996)

[80] N. S. Makarov, M. Drobizhev, and A. Rebane, Opt. Express **16**, 4029 (2008)

[81] F. W. Vance, R. D. Williams, and J. T. Hupp, Int. Rev. Phys. Chem **17**, 307 (1998)

[82] G. U. Bublitz and S. G. Boxer, Annu. Rev. Phys. Chem **48**, 213 (1997)

[83] M. Liess, S. Jeglinski, Z. V. Vardeny, M. Ozaki, K. Yoshino, Y. Ding, and T. Barton, Phys. Rev. B **56**, 15712 (1997)

[84] W. Liptay, Angew. Chem., Int. Ed. **8**, 177 (1969)

[85] W. Liptay, "Excited states," (Academic Press, 1974) p. 129

[86] L. L. Premvardhan and L. A. Peteanu, J. Phys. Chem. A **103**, 7506 (1999)

[87] A. Chowdhury, S. A. Locknar, L. L. Premvardhan, and L. A. Peteanu, J. Phys. Chem. A **103**, 9614 (1999)

[88] G. U. Bublitz, W. M. Laidlaw, R. G. Denning, and S. G. Boxer, J. Am. Chem. Soc. **120**, 6068 (1998)

[89] K. A. Walters, Y.-J. Kim, and J. T. Hupp, Inorg. Chem. **41**, 2909 (2002)

[90] L. N. Silverman, P. Kanchanawong, T. P. Treynor, and S. G. Boxer, Philos. Trans. R. Soc. London A **366**, 33 (2008)

[91] A. Sacra, D. J. Norris, C. B. Murray, and M. G. J. Bawendi, J. Chem. Phys. **103**, 5236 (1995)

[92] L. Sebastian and G. Weiser, Phys. Rev. Lett. **46**, 1156 (1981)

[93] A. Horvath, G. Weiser, G. L. Baker, and S. Etemad, Phys. Rev. B **51**, 2751 (1995)

[94] A. Brillante and M. R. Philpott, J. Chem. Phys. **103**, 4019 (1980)

[95] A. Elschner and G. Weiser, Chem. Phys. **98**, 465 (1985)

[96] P. Petelenz, Chem. Phys. **171**, 397 (1993)

[97] M. Slawik and P. Petelenz, J. Chem. Phys. **111**, 7576 (1999)

[98] Z. G. Soos, D. Mukhopadhyay, and M. H. Hennessy, Chem. Phys. **210**, 249 (1996)

[99] C. Sissa, F. Terenziani, and A. Painelli, in *Proceedings of the society of photo-optical instrumentation engineers (SPIE)* (2008) p. C9992

[100] B. J. Orr and J. F. Ward, Mol. Phys. **20**, 513 (1971)

[101] S. J. Cyvin, J. E. Rauch, and J. C. Decius, J. Chem. Phys. **43**, 4083 (1965)

[102] R. Wortmann and D. Bishop, J. Chem. Phys. **108**, 1001 (1998)

[103] C. R. Smith, D. R. Sabatino, and T. J. Praisner, Experiments in fluids **30**, 190 (2001)

[104] M. Seredyuk, A. B. Gaspar, V. Ksenofontov, S. Reiman, Y. Galyametdinov, W. Haase, E. Rentschler, and P. Gütlich, Chem. Mater. **18**, 2513 (2006)

[105] C. F. Zhu and A. B. Wu, Thermochimica Acta **425**, 7 (2005)

[106] F. B. Dias, S. Pollock, G. heley, L.-O. Pålsson, A. Monkman, I. I. Perepichka, I. F. Perepichka, M. Tavasli, and M. R. Bryce, J. Phys. Chem. B **110**, 19329 (2006)

[107] C. M. Brendel, F. B. Dias, T. P. I. Saragi, A. P. Monkman, and J. Salbeck, Phys. Status Solidi A, DOI 10.1002(2009)

[108] G. U. Bublitz and S. G. Boxer, J. Am. Chem. Soc. **120**, 3988 (1998)

[109] R. Richert and A. Wagener, J. Phys. Chem. **95**, 10115 (1991)

[110] Oxford Instruments, *Operator's Handbook OptistatDN* (2006)

[111] Á.Pineiro, P. Brocos, A. Amigo, M. Pintos, R. Bravo, and A. Glines, J. Solution Chem. **31**, 369 (2002)

[112] D. J. Metz and A. Glines, J. Phys. Chem. **71**, 1158 (1967)

[113] J. R. Lakowicz, "Principles of fluorescence spectroscopy," (Kluwer Academic/Plenum Publisher, 2006) Chap. Fluorescence Anisotropy, p. 291

[114] S. S. Andrews, JCE **81**, 877 (2004)

[115] K. D. Belfield, M. V. Bondar, O. D. Kachkovsky, O. V. Przhonska, and S. Yao, Journal of Luminescence **126**, 14 (2007)

[116] K. D. Belfield, M. V. Bondar, J. M. Hales, A. R. Morales, and O. V. Przhonska, Journal of Fluorescence **14**, 3 (2005)

[117] R. Stahl, C. Lambert, C. Kaiser, R. Wortmann, and R. Jakober, Chem. Eur. J. **12**, 2358 (2006)

[118] W. Verbouwe, M. Van der Auweraer, F. C. De Schryver, J. J. Piet, and J. M. Warman, J. Am. Chem. Soc. **120**, 1319 (1998)

[119] A. Painelli, F. Terenziani, and Z. Soos, Theor. Chem. Acc. **117**, 915 (2007)

[120] A. Girlando, C. Sissa, F. Terenziani, A. Painelli, A. Chwialkowska, and G. J. Ashwell, ChemPhysChem **8**, 2195 (2007)

[121] A. Painelli, F. Terenziani, L. Angiolini, T. Benelli, and L. Giorgini, Chem. Eur. J. **11**, 6053 (2005)

[122] K. Liang, M. S. Farahat, J. Perlstein, K.-Y. Law, and D. G. Whitten, J. Am. Chem. Soc. **119**, 830 (1997)

[123] E. Arunkumar, A. Ajayaghosh, and J. Daub, J. Am. Chem. Soc. **127**, 3156 (2005)

[124] Y. Liao, S. Bhattacharjee, K. A. Firestone, B. E. Eichinger, R. Paranji, C. A. Anderson, B. H. Robinson, P. J. Reid, and L. R. Dalton, J. Am. Chem. Soc. **128**, 6847 (2006)

[125] F. Terenziani, S. Ghosh, A.-C. Robin, P. K. Das, and M. Blanchard-Desce, J. Phys. Chem. B **112**, 11498 (2008)

[126] F. Terenziani, M. Morone, S. Gmouh, and M. Blanchard-Desce, ChemPhysChem **7**, 685 (2006)

[127] F. Terenziani, O. Mongin, C. Katan, B. K. G. Bhatthula, and M. Blanchard-Desce, Chem. Eur. J. **12**, 3089 (2006)

[128] A. Facchetti, L. Beverina, M. E. Van der Boom, P. Dutta, G. Evmenenko, A. D. Shukla, C. E. Stern, G. A. Pagani, and T. J. Marks, J. Am. Chem. Soc. **128**, 2142 (2006)

[129] A. Abbotto, S. Bradamante, A. Facchetti, and G. A. Pagani, J. Org. Chem. **62**, 5755 (1997)

[130] D. P. Craig and S. H. Walmsley, *Exciton in Molecular Crystals* (Benjamin, 1968)

[131] A. S. Davydov, *Theory of Molecular Excitons* (Plenum Press, 1971)

[132] M. Pope and C. E. Swenberg, *Electronic Processes in Organic Crystals and Polymers* (Oxford University Press, 1999)

[133] E. A. Silinsh and V. Capek, *Organic Molecular Crystals* (AIP Press, 1994)

[134] V. M. Agranovich and M. D. Galanin, *Electronic Excitation Energy Transfer in Condensed Matter* (North-Holland Publishing Company, 1982)

[135] T. Xu, A. Morris, G. J. Szulczewski, R. R. Amaresh, Y. Gao, S. C. Street, L. D. Kispert, R. M. Metzger, and F. Terenziani, J. Phys. Chem. B **106**, 10743 (2002)

[136] F. Terenziani, A. Painelli, A. Girlando, and R. M. Metzger, J. Phys. Chem. B **108**, 10743 (2004)

[137] A. Abbotto, L. Beverina, R. Bozio, A. Facchetti, C. Ferrante, G. A. Pagani, D. Pedron, and R. Signorini, Org. Lett. **4**, 1495 (2002)

[138] A. Abbotto, L. Beverina, R. Bozio, S. Bradamante, A. Facchetti, C. Ferrante, G. A. Pagani, D. Pedron, and R. Signorini, NATO Sci. Ser. II **100**, 385 (2003)

[139] R. Signorini, C. Ferrante, D. Pedron, M. Zerbetto, E. Cecchetto, M. Slaverio, I. Fortunati, E. Collini, R. Bozio, A. Abbotto, L. Beverina, and G. A. Pagani, J. Phys. Chem. A **112**, 4224 (2008)

[140] A. Abbotto, G. Baldini, L. Beverina, G. Chirico, M. Collini, L. D'Alfonso, A. Diaspro, R. Magrassi, L. Nardo, and G. A. Pagani, Biophys. Chem. **114**, 35 (2005)

[141] S. Versari, A. M. Villa, A. Villa, S. M. Doglia, and G. A. Pagani, J. Biomed. Opt. **11**, 034014 (2006)

[142] V. Gutman, *The Donor-Acceptor Approach to Molecular Interactions* (Plenum Press, 1978)

[143] T. Wilson and J. W. Hastings, Annu. Rev. Cell. Dev. Biol. **14**, 197 (1998)

[144] D. Beljonne, C. Curutchet, G. D. Scholes, and R. J. Silbey, J. Phys. Chem B **113**, 6583 (2009)

[145] G. D. Scholes, Ann. Rev. Phys. Chem. **54**, 57 (2003)

[146] S. Saini, G. Srinivas, and B. Bagchi, J. Phys. Chem. B **113**, 1817 (2009)

[147] M. R. Wasielewki, Chem. Rev. **92**, 435 (1992)

[148] B. Valeur, *Molecular Fluorescence: Principles and Applications* (Wiley-VCH, 2001)

[149] T. Renger, Photosynth Res **102**, 471 (2009)

[150] T. Förster, Ann. Phys. **437**, 55 (1948)

[151] T. Förster, Disc. Far. Soc. **27**, 7 (1959)

[152] T. Förster, Radiation Res. Supp. **2**, 326 (1960)

[153] T. Förster, "Modern quantum chemistry," (Academic Press, 1965) p. 93

[154] S. Saha and A. Samanta, J. Phys. Chem. A **106**, 476 (2002)

[155] D. W. Brousmiche, J. M. Serin, J. M. J. Fréchet, G. S. He, T.-C. Lin, S.-J. Chung, P. N. Prasad, R. Kannan, and L.-S. Tan, J. Phys. Chem. B **108**, 8592 (2004)

[156] M. Kawa and J. M. J. Fréchet, Chem. Mater. **10**, 286 (1998)

[157] D.-L. Jiang and T. Aida, J. Am. Chem. Soc. **120**, 10895 (1998)

[158] Z. Xu and S. Moore, Acta Polym. **45**, 83 (1994)

[159] T. I. Hukka, T. Toivonen, E. Hennebicq, J.-L. Brédas, R. A. J. Janssen, and D. Beljonne, Adv. Mater. **18**, 1301 (2006)

[160] K. S. Lam, D. Lo, and K. H. Wang, Optics Communications **121**, 121 (1995)

[161] M. J. Frisch and et al., "Gaussian 03, Revision C.02," Gaussian, Inc., Wallingford, CT, 2004

[162] R. McWeeny, *Methods of Molecular Quantum Mechanics* (Academic Press, 1992)

[163] J. Herek, N. Fraser, T. Pullerits, P. Martinsson, T. Polívka, H. Scheer, R. Cogdell, and V. Sundström, Biophys. J. **78**, 2590 (2000)

[164] S. Fery-Forgues and D. Lavabre, J. Chem. Ed. **76**, 1260 (1999)

List of Publications

9) C. Sissa, F. Terenziani, A. Painelli, A. Abbotto, L. Bellotto, C. Marinzi, E. Garbin, C. Ferrante, R. Bozio, *Dimers of Quadrupolar Chromophores in Solution: Electrostatic Interections and Optical Spectra*, J. Phys. Chem. B, 114 (2010) 882-893

8) L. Grisanti, C. Sissa, F. Terenziani, A. Painelli, D. Roberto, F. Tessore, R. Ugo, S. Quici, I. Fortunati, E. Garbin, C. Ferrante, R. Bozio, *Enhancing the Efficiency of Two-Photon Absorption by Metal Coordination: Theoretical Evidence of the Role of a Virtual Charge Transfer*, Phys. Chem. Chem. Phys., 11 (2009) 9450-9457

7) C. Sissa, F. Terenziani, A. Painelli, *Electroabsorption spectra of quadrupolar and octupolar dyes in solutions: beyond the Liptay formulation*, J. Phys. Chem. A 112 (2008), 8697-8705

6) A. Abbotto, L. Bellotto, R. Bozio, C. Ferrante, I. Fortunati, E. Garbin, C. Marinzi, A. Painelli, C. Sissa, F. Terenziani, *One- and two-photon absorption and emission properties of heteroaromatic bichromophores*, Proc. SPIE, Int. Soc. Opt. Eng. 6999 (2008)

5) C. Sissa, F. Terenziani, A. Painelli, *Electroabsorption spectra of multipolar chromophores*, Proc. SPIE, Int. Soc. Opt. Eng. 6999 (2008)

4) F. Terenziani, C. Sissa, A. Painelli, *Multipolar dyes for NLO: solvation and aggregation effects*, Proc. SPIE, Int. Soc. Opt. Eng. 6999 (2008)

3) F. Terenziani, C. Sissa, A. Painelli, *Symmetry Breaking in Octupolar Chromphores, Solvatochromism and Electroabsorption*, J. Phys. Chem. B, 112 (2008) 5079-5087

2) S. Elli, A. Magri, E. Venturini, F. Negri, A. Abbotto, L. Bellotto, A. Painelli, C. Sissa, F. Terenziani, *Heteroaromatic Chromophores: Structure, Electric Properties, Condensed Phase and Agregation Effects: a Combined Experimental and Theoretical Study* AIP Conference Proceedings 963 (2007), 703-705

1) A. Girlando, C. Sissa, F. Terenziani, A. Painelli, A. Chwialkowska, G. J. Ashwell, *In Situ Spectroscopic Characterization of Rectifying Molecular Monolayers Self-Assembled on Gold*, ChemPhysChem 8 (2007) 2195-2201